ELUCIDATING GLYCOPOLYCATION STRUCTURE-FUNCTION RELATIONSHIPS FOR IMPROVED GENE THERAPY

A THESIS

SUBMITTED TO THE FACULTY OF

UNIVERSITY OF MINNESOTA

BY

HALEY PHILLIPS

IN PARTIAL FULFILLMENT OF THE REQUIREMENTS

FOR THE DEGREE OF

DOCTOR OF PHILOSOPHY

THERESA M. REINEKE

JUNE 2017

Acknowledgements

The author would like to thank fellow coauthors for contributing work to this and other publications. She would also like to thank Theresa Reineke for her leadership, the members of the committee for their time and guidance, and the funding sources for supporting this work.

The author would like to thank Dr. Mallory Cortez, Dr. Zachary Tolstyka, Dr. Jeff Ting, Dr. Dustin Sprouse, William Boyle, Molly Dalsin, Victoria Szlag, and Anatolii Purchel for their support both in and out of the lab. She would also like to acknowledge the help of Dr. Nilesh Ingle, Dr. Haibo Li, Dr. Yaoying Wu, Leon Lillie, Seyoung Jung, Yogesh Dhande, Bryan Hall, Craig Van Bruggen, Yaming Jiang, Zhe Tan, and Joseph Hexum for immeasurably valuable training, assistance, and discussions.

The gene delivery projects were partially funded by the National Institutes of Health (NIH) Director's New Innovator Award Program (DP2OD006669-01), the University of Minnesota MRSEC under the Award Number DMR-0819885, the Camille and Henry Dreyfus Foundation, the Office of the Director, National Institutes of Health of the National Institutes of Health under Award Number S10OD011952, and NIH grants 1R01DK082516 and P01HD32652. The content is solely the responsibility of the authors and does not necessarily represent the official views of the National Institutes of Health. The authors would also like to

thank the Fairview Hospital Special Coagulation Clinic and the University Genomics Core at the University of Minnesota for research support. We would also like to acknowledge work done using the IVIS Spectrum in vivo imaging system at the University of Minnesota – University Imaging centers, http://uic.umn.edu. All animal studies were performed under the IACUC Protocol #1202A09921 (PI: Hackett).

The thermoset film project was partially funded by the National Science Foundation (NSF) under the Center for Sustainable Polymers, CHE-1413862. Part of this work was carried out in the College of Science and Engineering Characterization Facility, University of Minnesota, which has received capital equipment funding from the NSF through the UMN MRSEC program under Award Number DMR-1420013. The authors would also like to acknowledge work done using the Nikon confocal system at the University of Minnesota – University Imaging centers, http://uic.umn.edu.

Dedication

This thesis is dedicated to my parents, whose love and belief in me never wavered.

And to Zach, who reminds me to love and believe in myself.

Abstract

The gene therapy field is devoted to treating disease by adding, altering, or inhibiting gene expression. This type of therapy holds great promise for the treatment and even cure of monogenic diseases such as cystic fibrosis, Duchenne muscular dystrophy, hemophilia A and B, and epidermolysis bullosa. To produce therapeutic effect, nucleic acids must be delivered and expressed in cells of interest. Deoxyribonucleic acids (DNA) and ribonucleic acids (RNA) in many forms can be delivered using viral or non-viral vehicles. Viral vectors provide efficient DNA delivery; however, packaging limitations and occasional safety issues such as immune responses are major issues. In contrast, non-viral vectors are cheaper and easier to mass produce and can package any length of nucleic acid; however, non-viral vectors struggle to deliver genetic cargo at therapeutically beneficial levels.

Polymers with the ability to condense and protect genetic material make promising non-viral vectors. They are relatively easy to produce compared to viral vehicles, can safely package various plasmid sizes, and have shown significant uptake in a wide variety of human cell lines. Cationic polymers complex with the negatively charged phosphodiester backbone of DNA or RNA, forming inter-polyelectrolyte complexes termed polyplexes. Herein, we explore using experiments *in vitro*, *ex vivo*, and *in vivo* to probe the structure-function relationships dictating polyplex gene delivery and other glycomaterial applications.

Table of Contents

List of Tables

List of Figures

CHAPTER 1: ELUCIDATING GLYCOPOLYCATION STRUCTURE-FUNCTION RELATIONSHIPS FOR IMPROVED GENE THERAPY

Synopsis

Gene therapy is a field devoted to the treatment of disease by adding, altering, or inhibiting gene expression. In contrast, non-viral polymeric gene delivery vehicles can package any length of nucleic acid; however, delivery of non-viral vectors into cells is generally very difficult to achieve at levels that have therapeutic efficacy. This chapter discusses gene delivery hurdles and how strategic polymer design builds vehicle functionality to overcome those hurdles. Additionally, it makes and argument for the benefits of using a combination of *in vitro, ex vivo*, and *in vivo* studies to probe the structure-function relationships dictating polyplex gene delivery and other glycomaterial applications.

1.1 BACKGROUND

1.1.1 Polymer Nucleic Acid Delivery Vehicles

Gene therapy is a field devoted to the treatment of disease by adding, altering, or inhibiting gene expression.[1] This type of therapy holds great promise for the treatment and even cure of monogenic diseases such as cystic fibrosis, Duchenne muscular dystrophy, hemophilia A and B, and epidermolysis bullosa.[2-13] To produce the therapeutic effect, nucleic acids must be delivered and expressed in cells of interest. Deoxyribonucleic acids (DNA) or ribonucleic acids (RNA) in many forms can be delivered using viral or non-viral vehicles. Viral vectors provide efficient DNA delivery;[14-16] however, packaging limitations, occasional safety issues such as immune responses, and the high costs associated with mass production of clinical-grade viruses for treating large patient populations are major issues.[17, 18] In contrast, non-viral vectors can package any length of nucleic acid; however, delivery of non-viral vectors into cells is generally very difficult to achieve at levels that have therapeutic efficacy.[19]

Polymers with the ability to condense and protect genetic material offer a promising delivery alternative to viral vectors. They are relatively easy to produce compared to viral vehicles, can safely package various plasmid sizes, and have shown significant uptake in a wide variety of human cell lines.[4, 17, 18, 20-22] Cationic polymers complex with the negatively charged phosphodiester backbone of DNA

or RNA, forming inter-polyelectrolyte complexes termed polyplexes. Typically, polyplexes contain an excess of polymer, which yields a complex that has a net positive charge. A net positive charge has been shown to aid cellular uptake in cell culture,[23] which makes cationic polyplexes promising vehicles for cell-based gene therapy. However, cationic surface charge can also cause toxicity.[24, 25] Not all diseases can be treated with cell therapy (which is directly editing cells in culture, then transplanting them back into the body), so another desirable delivery method is to inject vehicles into the bloodstreams for systemic nucleic acid delivery. However, when previous studies introduced positively charged polyplexes into the blood stream, they aggregated with various negatively charged blood serum proteins in a process called opsonization.[26] Opsonization prevents gene delivery by not only hindering polyplex cellular uptake,[27] but also by making polyplexes targets for active removal by the body's mononuclear phagocyte system (also called the reticuloendothelial system).[4, 26, 28] Aggregated polyplexes even proved toxic to the *in vivo* hosts by becoming entrapped in lung capillary beds[4, 27, 29, 30] To combat cytotoxicity and aggregation, non-charged "stealth" polyplex coatings were developed by adding an uncharged hydrophilic block to the cationic polymer. During polyplex formation, it is hypothesized that the hydrophilic block arranges itself around the outside of the polyplex, forming a neutral and steric shell-like barrier around the cationic polyplex core to further

protect the genetic material from degradation by nucleases, decrease cell exposure to positive charge and nonspecific uptake, and prevent polyplex aggregation and premature blood clearance[20, 31] Protein aggregation is not the only issue hindering polyplex gene delivery. There are many intracellular and extracellular hurdles polyplexes must overcome to prove effective gene delivery vehicles.

1.1.2 Gene Delivery Hurdles

The hurdles polymeric gene delivery vehicles encounter depend on the types of nucleic acid being delivered, the end point for delivery, and the administration route.[20] Gene delivery hurdles can be generally divided into two categories: intracellular and extracellular. Intracellular hurdles include obstacles from cellular uptake all the way through the cell to nucleic acid expression. Extracellular hurdles include all barriers between polyplex formulation and cellular uptake.[20] Some extracellular barriers, such as nucleic acid packaging, will apply whether the vehicles are being administered to cells in culture or to whole living organisms. Other hurdles such as the innate immune response and nonspecific tissue capture will vary by administration route and tissue target.

The structure-function relationships that determine the delivery efficiency of polymer vehicles also vary depending on the polymer type. First the intracellular and extracellular delivery hurdles will be described to illustrate the obstacles

polymer gene delivery vehicles face. Then, to limit the scope of this discussion, this section will include a comprehensive description of the structure-function relationships that glycopolymers and their closely related controls, PEG and PEI, have demonstrated in the field thus far.

1.1.2.1 Intracellular Hurdles

Intracellular hurdles include obstacles from cellular uptake all the way through the cell to nucleic acid expression (Figure 1.1). The figure depicts hurdles that a successful nonviral vehicle should overcome. Vehicles should: a) package therapeutic genes, b) protect genetic material in culture media, c) cell uptake (by endocytosis/other), d) escape from endo- or lysosomal degradation, e) traffic to nucleus, f) release DNA, g) permit gene expression, h) degrade. Most polyplexes are actively taken up by cells through endocytosis.[4, 20] The first intracellular hurdle gene delivery vehicles encounter is cellular uptake. Endocytosis is an energy dependent process where the cell membrane invaginates to take up extracellular material into vesicles of about 0.05 to 0.1 μm in diameter.[4, 32] There are three types of endocytosis: micropinocytosis, phagocytosis, and receptor-mediated endocytosis.[4] Receptor-mediated uptake (also known as clathrin-mediated endocytosis, which the most common protein found coating receptor-mediated uptake vesicles)[32] can be triggered by including one of a variety of ligands on the vehicle. Common ligands for eukaryotic cells

are cholesterol, transferrin, insulin and other protein hormones, and glycoproteins with terminal glucose, galactose, and mannose.[32] Phagocytosis is used by specialized cells such as monocytes, macrophages, and neutrophils to take up foreign particles for digestion and elimination.[33] Therefore, phagocytosis is generally not a preferred route of polyplex uptake. Micropinocytosis is similar to phagocytosis in that it is a non-receptor-mediated route for taking up material to be digested, but it takes up larger particles in 0.02 to 5 µm diameter vesicles.[4, 34] Most polyplexes are taken up via a receptor-dependent route.[4, 35]

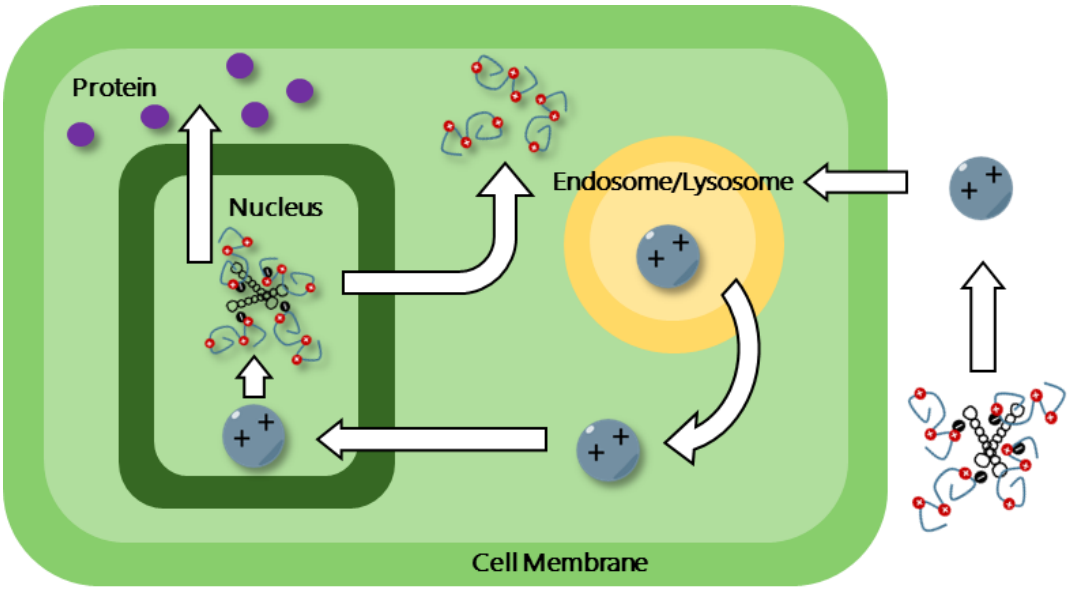

Figure 1.1. Scheme of possible cellular transfection route. Anionic DNA plasmids are red. Cationic polymers block copolymers are green and purple. Purple cationic spheres represent complexed plasmids and polymers. See text for descriptions of parts (a)-(h).

Once polyplexes are endocytosed into the cell, they are destined for digestion by the lysosome unless they can escape the endosome in time. There are several proposed endosomal escape theories. The most popular theory is the pH-buffering effect (also known as the proton sponge effect) in which agents with a high buffering capacity and the ability to swell upon protonation rupture the endosome. A second proposed mechanism is to form endosomal membrane pores using cationic amphiphilic peptides to stress the lipid bilayer.[36] Another

escape option is destabilize the membrane not by pore formation but by fusion to the cellular membrane. This fusion is driven by fusogenic peptides, such as haemagglutinin from the influenza viral coat, that undergo conformational changes when triggered by an environmental change such as a drop in pH.[36] Finally, a fourth possible mechanism is membrane disruption by a multitude of protein, peptide, or chemical endosomal membrane disruption agents.[36] The difficulty in adapting one of the last three methods to aid polyplex uptake is that the process of disrupting the endosome can be toxic to the cell or patient.[36-38] Therefore, it would be ideal to use polymer delivery vehicles that can buffer the endosome without adding a potentially toxic escape agent. Polyethyleneimine (PEI) is one such polymer that has demonstrated a strong ability to buffer and escape endosomes, however, it is also widely known that PEI can be toxic.[38] This toxicity limits its application *in vivo*, but its effectiveness and commercial availability make it a high standard by which to compare novel polymer vehicle structures.

The remaining intracellular hurdles are less well studied than endosomal escape, but no less crucial to gene delivery success. At some point, the nucleic acid cargo must be released from the vehicle in order for it to be expressed.[20, 39] Additionally, DNA must be trafficked to the nucleus and most RNA (such as short interfering or messenger RNA) must end up in the cytosol.[20, 40, 41] Finally, if

genome engineering is desired, the nucleic material can be inserted into the cell genome to be constitutively expressed over time, even in daughter cells.[42, 43] Genome engineering is not always necessary for a therapeutic treatment, but it is often the only permanent cure for many genetic diseases.[19, 42]

Many in-depth studies have been conducted to tease out what structure-function relationships will lead to better endosomal escape, cargo release, and nuclear localization.[20, 24, 40, 44] Genome engineers specialize in developing new genome engineering systems and understanding exactly how they work once they get inside the nucleus.[42, 45-47] What remained less clear at the initiation of the studies documented herein was what polymer structure-function relationships existed for clearing extracellular hurdles, particularly for systemic delivery by cationic glycopolyplexes via the bloodstream.[48]

1.1.2.2 Extracellular Hurdles

Extracellular hurdles occur from the time of polyplex formation until cell uptake begins (Figure 1.2). The foremost purpose of any gene delivery vehicle is to package and protect nucleic acid cargo from degradation by nucleases. It must compact the material, especially large DNA plasmids, down to a size where endocytosis can occur, generally from 25 to 500 nm in diameter (with 25-50 nm seen as the ideal endocytosis size).[49, 50] Most cationic delivery vehicles can accomplish the task, but it can be difficult to maintain a small diameter in the salt

and serum solutions typically used for cell culture.[31] This stability becomes increasingly important in more complex environments such as the blood stream, lymphatic ducts, gastrointestinal tract, or lung fluid.[51] From here on, the extracellular obstacles vary widely based on administration route and tissue target. For our purposes, we will limit the discussion to systemic delivery hurdles for vehicles administered intravenously.

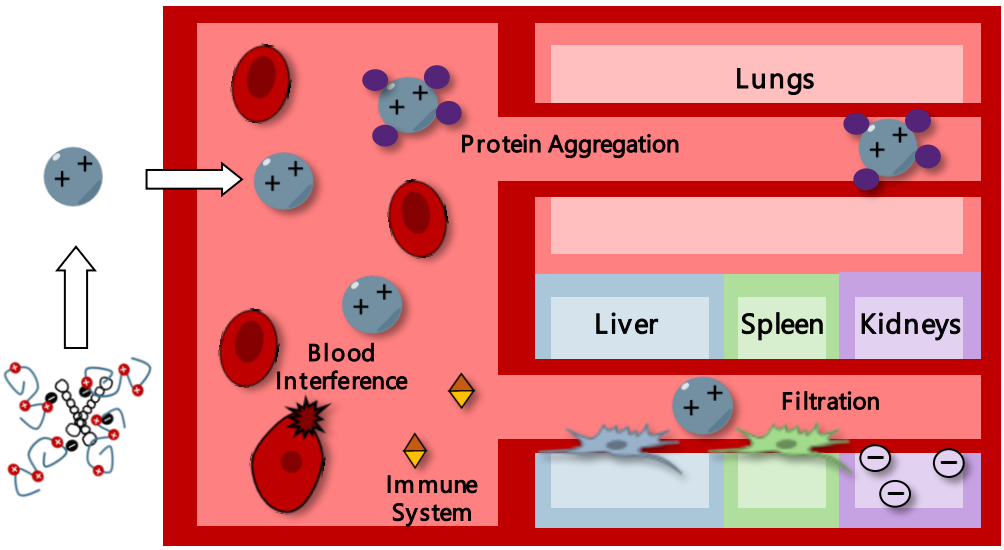

Figure 1.2. Scheme of extracellular hurdles for systemic delivery. Several key interactions and filtration organs are labeled.

Intravenous injection is a simple method for obtaining systemic exposure of a therapeutic drug or material. In humans, it takes only from 10-25 s for computerized tomography (CT) contrast medium to complete one full circulation cycle back to its injection site.[52] In mice, this circulation time drops to only 15 sec.[53] As long as the delivery vehicle remains intact through the needle shear

and remains colloidally stable during circulation, it stands a good chance of reaching even the smallest capillary beds within minutes. For example water soluble single-walled nanotubes from 200-500 nm in length successfully distribute to the liver, lungs, muscle, and kidneys of mice in about 15 seconds.[54] Once in the bloodstream, polyplexes must remain colloidally stable to remain in circulation long enough to passively reach the intended tissue. This colloidal function is determined by the chain length of the hydrophilic polymer block, cationic block charge density, and the hydrophilic:polycation ratio use in the polyplex formulation.[4, 30] Additionally, it is almost always desired to reach a specific tissue of interest. Widespread unspecific delivery means less nucleic acid cargo is available to the tissues and cells that need to express the DNA or RNA, and could even lead to negative off target effects such as an immune response.[55] To avoid the off target issues associated with systemic delivery, an injection method was developed to direct materials to the liver and improve hepatocyte (liver cell) uptake. This method, first referred to as hydrodynamic injection by Budker et al.,[56] rapidly injects high volume solutions, thereby creating high pressure in the liver tissue that permeabilizes cell membranes. The method results in high transfection efficiency and gene expression, but cannot be used on mammals outside the rodent family due to high toxicity, so is typically used to generate disease or genome editing models.[57] In fact, hydrodynamic injection

was used in one of the following studies to verify that polyplexes could successfully deliver plasmid DNA (pDNA) for *in vivo* liver expression.[58] When complexed with a cationic trehalose polymer prior to injection, the pDNA was still expressed, and both the pDNA and the polymer vehicle were taken up by hepatocytes.[58] This initial *in vivo* study set the precedent for possible *in vivo* systemic delivery of pDNA to the liver using cationic glycopolyplexes.

Another hurdle polyplexes encountered while still in the blood stream is the immune response. The immune system can be generally divided into adaptive and innate immunity as well as cell- or humorally-mediated immunity.[59] Adaptive immunity is the part of the immune system that 'learns,' or adapts, from exposure and infection. The adaptive branch requires previous exposure to be activated, but the innate system can be activated by some antigens without any prior contact. Previous clinical tragedies have shown how vital it is to thoroughly test both viral and non-viral materials for immune response prior to clinical use.[18, 60] Due to the complexity and flexibility of the immune system, this in-depth preclinical testing should be directed by a specialist, but some simple immune response screens can (and arguably should) be conducted at the early stages of vehicle development.[61] It has been shown that even widely used biocompatible polymers such a polyethylene glycol (PEG) can induce humoral immune reactions during the first injection, which creates antibodies against the polyplex

vehicles.[62] These antibodies rapidly clear any future injections, rendering the treatment useless.[1, 63] In other cases, nonviral nanocapsule vehicles coated in PEG activated complement protein *in vitro*,[64] which could lead to complement activation-related pseudoallergy (CARPA).[65] CARPA is a potentially lethal immune response where symptoms such as skin rash, rise in pulmonary arterial pressure, and other hematological changes resemble those cause by an allergic reaction, but the exact mechanism underlying the symptoms differs from a true allergic reaction.[65] Not only can the delivery vehicle trigger an immune response, but so can the genetic cargo it carries.[66, 67]

As mentioned previously, nonspecific tissue capture is another obstacle which gene delivery vehicles must avoid to preserve bioavailability for the tissues and cells of therapeutic intent. Aside from hydrodynamic injection, there are several other methods for targeting specific tissues. Targeting has previously been achieved by carefully controlling vehicle diameter,[68] coupling vehicles with ligands specific for a cell type such as vitamin A or *N*-acetyl galactose (GalNAc) for hepatocytes,[69, 70] or with antibodies for specific cells.[71] Recently, stimuli-sensitive systems have been developed that respond to pH,[72] temperature,[73] redox environment,[74, 75] and enzyme activity.[76] Targeting is a crucial function to achieve gene delivery at clinically relevant levels, and will be an important function for future glycoplexes to incorporate.[4, 20]

1.1.3 Understanding Polymer Structure-Function Relationships

Strategic polymer design can create delivery vehicles that successfully overcome multiple intracellular and extracellular hurdles such as promoting endocytosis and endosomal escape, trafficking to the nucleus, and gene expression as well as avoiding aggregation, off-target circulation clearance, and immune responses.[20, 49] There is a large body of existing research probing the structure-function of different polymeric delivery systems. The diversity of polymeric systems makes some direct comparisons difficult, but previous work within the class of glycopolymer vehicles offers a wealth of structure-function data to help design polymers to overcome extracellular hurdles for systemic delivery.

1.1.3.1 Polymer Design to Overcome Extracellular Hurdles

The extracellular hurdles discussed above can be generally divided into three categories: aggregation, off-target clearance, and immune response. Polymer vehicles that overcome those hurdles will possess colloidal stability, bioavailability, and nonantigenic functionalities. Each functionality can be achieved in multiple different ways. This section explores how other glycopolymers (and some closely related non-glycopolymers) have achieved these functionalities.

Colloids are noncrystalline large molecules or sub-microscopic materials that homogenously dispersed in a substance from which they cannot settle or be centrifuged out. Cationic polyplexes are colloidal in water, but can aggregate or settle out of solutions with high ionic strength or negatively charged proteins.[77-79] Once common way to promote colloidal stability in salt and serum solutions is to add a hydrophilic, neutral polymer block to the cation polymer.[31, 80, 81] This neutral block can reduce toxicity, immunogenicity, and nonspecific protein absorption by sterically hindering direct cationic exposure to cell membranes and proteins.[82] One vast improvement to the design of these neutral hydrophilic polymer blocks was to add bulk by incorporating biocompatible carbohydrate moieties. This added bulk increased polyplex colloidal stability compared to the more linear P(EG) blocks.[31, 80, 83] It is hypothesized that the bulkier hydrophilic blocks are sterically pushed towards the outside of the polyplexes forming a micelle-like corona that better shields polyplexes and their cargo from protein aggregation and nuclease enzymes that would degrade the pDNA cargo if it were exposed.[31] Colloidal stability is a critical functionality as vehicles that lack this stability have lower bioavailability and can trigger an immune response through polyplex destabilization and protein opsonization (protein aggregation that targets materials for phagocytic clearance).[81, 82]

Polymer vehicles that demonstrate colloidal stability usually have promising bioavailability and nonantigenic properties as well. One generally accepted method for improving bioavailability focuses on improving vehicle circulation time and penetration. For example, PEGylating poly(ethylene imine) (PEI) improved polyplex stability and circulation time *in vivo*, which allowed the polyplexes to avoid lung accumulation and further circulate to other organs, and also lowered the acute toxicity as compared to non-PEGylated PEI polyplexes.[84] However, colloidal stability doesn't always correlate with increased gene expression, and the PEGylated PEI polyplexes showed decreased levels of gene expression compared to non-PEGylated PEI polyplexes despite significantly accumulation in the liver, lungs and spleen.[84] In this case, an increased circulation time correlated with decreased non-specific lung capture and decreased excretion by the kidneys, thereby increasing the vehicle bioavailability during circulation, but it did not promote increased bioavailability at the cellular level. Polymer design strategies other than simply increasing colloidal stability must be applied to increase cellular bioavailability and gene expression.

Another way of increasing bioavailability is to design polyplexes that reach and are retained in a specific tissue, and are even taken up by select cell types in that tissue.[70] Generally acknowledged to be the most difficult functionality to achieve *in vivo*, tissue targeting is important for not only increasing the dose that

target tissues receive, which would make nonviral gene therapy less expensive and more effective, but it also prevents negative off-target effects.[55, 85-90] While many of the same polymer structure motifs that promote colloidal stability also increase bioavailability through increased circulation time, the true “holy grail” of nonviral gene delivery is the ability to deliver the vehicles to specific tissues and cells.[1, 21, 91] The polymer vehicle that increases both colloidal circulation time as well as tissue/cell targeting would almost certainly succeed in a clinical setting.

Before a polymeric gene delivery vehicle could be introduced to human patients, it is necessary to test their immunogenicity, or ability to trigger an immune response. There are two general branches of the innate immune system: the innate and the adaptive systems. Each of those two branches can be further divided into a humorally- or a cell-mediated response. Humorally-mediated responses rely primarily on proteins to help identify and eliminate antigens, while the other response relies primarily on cells to perform the work. Therefore, polymer gene delivery vehicles must avoid activating both cells and proteins involved in the immune response for both the innate and adaptive immune branches. This is a tall order, but some polymer structures have avoided triggering an immune response under some circumstances.[66, 92] The immune system is complex and can vary slightly from person to person. This is yet

another reason that structure-function studies should be conducted in increasingly complex environments using *ex vivo* and *in vivo* studies.[93]

Many polymeric gene delivery vehicles have been designed to promote colloidal stability and increased circulation time *in vivo*,[30, 88] however, the type of structure-functions needed to achieve tissue targeting and non-antigenicity are less clear.[88, 91] The field continues to push for a better understanding of these functionalities, and improving study design could improve vehicle structure-function understanding in more complex environments.

1.1.4 Structure-Function Study Design

To probe polymer structure-function for gene delivery, the study must be designed in such a way that the function results can be related back to a specific aspect of the polymer function. Due to the complexity of both the experimental environments of interest as well as the complexity of the polyplex system, the study was designed to test the same polyplex systems in both complex and simplified environments. Studying novel carbohydrate polymer vehicles *in vitro*, *ex vivo*, and *in vivo* helps identify structure-function trends that hold up in multiple circumstances. Furthermore, the novel glycopolymers will be studied alongside well-understood PEG and PEI controls, helping link the function results to a specific structural aspect of the glycopolymers.

Carbohydrate-based polymers are hydrophilic, nontoxic, and possess many hydroxyl groups for changing chemical and biological functionality.[31, 70] We previously designed carbohydrate-based polymers that overcame intracellular barriers and also demonstrated potential to overcome extracellular barriers.[33] Multiple sugars were modified into monomers for polymerization by Reversible Addition Fragmentation Chain-Transfer (RAFT) to allow controlled polymerization of polymer that could be clearly characterized *in situ*.[31, 94, 95] The polymers were complexed with pDNA expressing various reporter genes such as green fluorescent protein (GFP) and luciferase, and polyplexes were characterized *in vitro, ex vivo*, and *in vivo* (Figure 1.3). In addition to studies on gene delivery vehicles, one *in vitro* study was also conducted on glycomaterials used to make epoxy thermoset films. This additional study illustrates that cross-state screens can efficiently identify important structure-function relationships for many different novel materials.

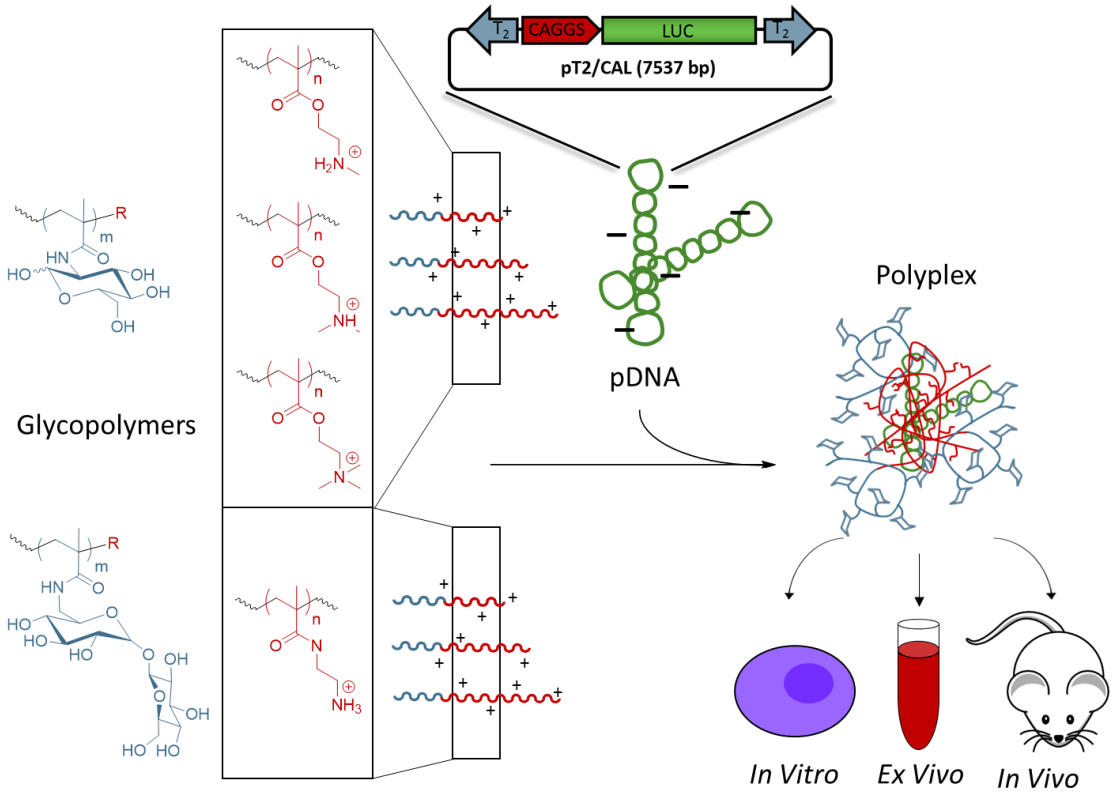

Figure 1.3. Scheme of glycopolyplex study *in vitro*, *ex vivo*, and *in vivo* using glucose- and trehalose-based polymer delivery vehicles complexed with pT2/CAL plasmid DNA (pDNA). Abbreviations in plasmid scheme represent specific sequences discussed in Chapter 3.

1.1.4.1 In Vitro *Structure-Function Studies*

Over the past three decades, *in vitro* studies have been the standard for assessing the toxicity, efficacy, and mechanism of gene delivery vehicles.[20] *In vitro* experiments use cells grown exclusively on culture dishes or other artificial scaffolds. Most *in vitro* experiments are conducted on immortalized (often cancerous) cell lines that are easy to grow and provide relatively reproducible

results. The relatively simplistic cellular environment enabled the field of non-viral gene delivery to answer many important fundamental questions such as how cationic charge affects mitochondrial and cell membrane function,[24, 96] and how polyplex physical characteristics such as charge and colloidal stability affect uptake and gene expression.[31, 80] In addition to these basic screens, cell culture has helped answer more complicated questions such as whether different non-viral vehicles prefer one cell uptake mechanism over another.[35, 41, 97] Cells in culture can be easily observed without disrupting their function, and many studies have used this imaging methods to probe how polyplexes and their cargo are intracellularly trafficked.[40, 98] The practicality and usefulness of cellular assays can hardly be debated, but the simplicity of cell culture limits the application of results. *In vitro* studies alone cannot capture the whole picture.

1.1.4.2 Ex Vivo *Structure-Function Studies*

Instead of immortalized cells cultured exclusively in dishes, *ex vivo* studies use tissues freshly removed from a human or animal donor. This type of study is useful for relating *in vitro* assay results to observations made with materials *in vivo*. The tissue more closely approximates a complete *in vivo* environment, but is easier to manipulate and observe removed from the host. Studies *ex vivo* helped researchers observe polyplex effects on coagulation and hemolysis.[92, 99] Another study found that, although their surface-modified material prevented

protein aggregation, which is a generally accepted mechanism to increase biocompatibility, the surface still induced coagulation upon exposure to whole blood *ex vivo*.[100] One study was prompted after researchers witnessed severe *in vivo* toxicity that suggested issues with coagulation. They used *ex vivo* platelet studies to pinpoint how their poly(amidoamine) dendrimer particles altered platelet morphology and function.[101] This example illustrates that *in vitro, ex vivo*, and *in vivo* studies do not need to be conducted unidirectionally, but that the characterization process can fluidly move between experimental states.

For some applications, *ex vivo* studies are sufficient for characterizing the materials, but for vehicles to be administered directly to patients, it is necessary to push towards *in vivo* preclinical testing.

1.1.4.3 In Vivo *Structure-Function Studies*

The most complicated and arguably the most valuable type of study is conducted *in vivo. In vivo* studies conduct experiments using whole living organisms. The complex environment most closely approximates what the delivery vehicles would encounter in a living patient, but it also makes observing vehicle structure-function characteristics more difficult. Often *in vivo* studies will use complementary *ex vivo* methods such as organ imaging and histology to make more quantitative observation about material distribution.[27] Other times it is possible to measure the gene delivery outcome directly by quantifying protein

production or observing animal host health improvement.[102] Still other methods have been develop to observe vehicle distribution in real time *in vivo*, although they are usually limited to observing carbon nanotubes,[103] heavy metal-based nanoparticles,[104] or fluorescently tagged moities.[105] *In vivo* experiments usually take longer and environmental control is limited, which in turn limits which questions can be answered with these studies. Taken in context with *in vitro* and *ex vivo* results, however, these studies provide a more complete characterization picture than studies from only one category. It was our objective to use all three study-states to identify and characterize the structure-function relationships of cationic glycopolyplex gene delivery vehicles.

1.1.4.4 Thesis Statement and Dissertation Summary

Thesis statement: Studies *in vitro, ex vivo,* and *in vivo* elucidate structure-function relationships characterizing glycopolymer materials for gene delivery and other applications more thoroughly than studies isolated to only one or two of those categories.

Non-viral vehicle design is typically iterative and therefore relies heavily on clear structure-function relationship studies to inform design of the next vehicle generation. It was our hypothesis that using a combination of *in vitro, ex vivo*, and *in vivo* studies would more clearly characterize glycomaterial structure-function than studies isolated to only one or two study categories. Previously, a

multitude of in-depth cell culture studies led to the design of two block copolymer vehicles derived from trehalose and glucose. Chapter 2 in this dissertation characterizes these vehicles *in vitro*, demonstrating that the type of cell culture media can affect polyplex uptake, and that polyplex cell uptake and gene expression don't necessarily correlate. After thorough study in cell culture, Chapter 3 pushes characterization into *ex vivo* and *in vivo* environments, confirming polyplex stability as a key characteristic for hemocompatibility and widespread biodistribution. However, stability against protein aggregation is not sufficient to clear the immune response hurdle. Chapter 4 cycles back to *in vitro* study by characterizing the cytocompatibility and cell proliferation ability of a novel carbohydrate-derived epoxy film, identifying potential antifouling characteristics. Similarly, work included in the appendix uses *in vitro* testing to screen several glycopolyplex vehicles' delivery capacity against immortalized human B cells. Screening vehicles in immortalized non-cancer cells demonstrated that vehicle design fed by *in vitro* data collected from cancer cell lines would not translate to similar results in immortalized cells. These chapters in combination demonstrate that studies from all three experimental states (*in vitro, ex vivo*, and *in vivo*) elucidated new structure-function relationships more clearly than studies from each category would have individually.

CHAPTER 2: CARBOHYDRATE-BASED BLOCK COPOLYCATIONS PROMOTE POLYPLEX STABILIZATION AND *IN VITRO* NUCLEIC ACID DELIVERY

Synopsis

The development and thorough characterization of non-viral delivery agents for gene and genome editing therapies are of high interest to the field of nanomedicine. Indeed, this vehicle class offers the ability to tune chemical architecture/biological activity and readily package nucleic acids of various sizes and morphologies for a variety of applications. Herein, we present the synthesis and characterization polymer vehicles derived from two carbohydrates. Trehalose-based and glucose-based block copolycations were designed to stabilize polyplex formulations for transfection in cell culture. Polymer structure affected polyplex cytotoxicity, cell uptake, and gene expression results. The trehalose-based vehicles provided an additional lyoprotectant property that stabilized polyplexes through several cycles of freeze drying and reconstitution. Lastly, hydrodynamic injections of P(MAT-*b*-AEMA) polyplexes verified that *in vivo* polyplex delivery could lead to gene expression.

1. Li, H.; Cortez, M. A.; Phillips, H. R.; Wu, Y.; Reineke, T. M. *ACS Macro Lett.* **2013**, *2*, 230-235. <http://pubs.acs.org/doi/abs/10.1021/mz300660t>.
2. Tolstyka, Z. P.; Phillips, H.; Cortez, M.; Wu, Y.; Ingle, N. P.; Bell, J. B.; Hackett, P. B.; Reineke, T. M. *ACS Biomat. Sci. Eng.* **2015**, *2*, 43-55. <http://pubs.acs.org/doi/abs/10.1021/acsbiomaterials.5b00312>.

2.1 INTRODUCTION

Gene therapy offers new avenues for the treatment of genetic diseases characterized by deficiency of a protein that can be treated by the delivery of DNA encoding the required polypeptide.[6-13] Viral vectors are often used for DNA delivery;[14-16] however, the most commonly used viruses have limited DNA cargo space and many elicit strong immunological responses. In contrast, non-viral vectors can package any length of nucleic acid; however, delivery of non-viral vectors into cells is generally very difficult to achieve at levels that have therapeutic efficacy.[19]

Cationic polymers that form an inter-polyelectrolyte complex with the negatively charged phosphodiester backbone of DNA or RNA,[106] termed polyplexes, are an attractive choice for non-viral gene delivery agents as their chemical structure, functionality, and molecular weight can be tailored in a controlled fashion. Typically, polyplexes contain an excess of polymer, which yields a complex that has a net positive charge. However, when such polyplexes are introduced into the blood stream they aggregate with various negatively charged proteins, which hinders their ability to penetrate the plasma membranes of cells in tissues.[107] Therefore, non-charged “stealth” coatings such as polyethylene glycol (PEG) have been used to help shield these particles from aggregation.[108] PEGylated complexes generally have decreased immunogenicity

and increased lifetimes in the blood when compared with their unmodified counterparts.[109-17] However, PEG is non-biodegradable and has been implicated in antibody formation,[110] hypersensitivity reactions[111, 112] and accelerated blood clearance upon repeated dosage.[113-115] Accordingly, we have focused on building novel carbohydrate-based polymers to create a hydrophilic polyplex shell as an alternative to PEG. This study presents the first systematic investigation of these glycopolymers *in vivo*.

Previously, we polymerized the glucose-based monomer, 2-deoxy-2-methacrylamido glucopyranose (MAG), to form a block copolymer with *N*-(2-aminoethyl) methacrylamide (AEMA).[116] Tests *in vitro* suggest that the cationic glycopolymers have superior solution stability and lower cell toxicity in cell culture compared to PEI complexes. In addition to glucose, trehalose has also been explored as a PEG alternative.[117] Trehalose is an α-α-linked dimer of glucose that is synthesized by bacteria, fungi, plants, and invertebrate animals[118, 119] and is used by living systems to survive in extreme conditions.[120, 121] Trehalose has long been used as a stabilizing agent in drug formulations such as Herceptin™ and Lucentis™.[122] Step-growth polymers have been synthesized using a modified trehalose as one of the monomers. Polyplexes formed with these polymers displayed lower toxicity, high cellular uptake, and similar gene expression when compared to the commercially available gene delivery polymer

jetPEI.[77, 78, 123] Polytrehalose imparted thermal stability to proteins: lysozyme enzymatic activity was retained upon extreme heating and cooling when polytrehalose was covalently attached.[124] Our lab has reported polyplexes formulated with short interfering RNA (siRNA) and a trehalose block co-polycation 6-methacrylamido-6-deoxy trehalose-*b*-*N*-(2-aminoethyl) methacrylamide [P(MAT-*b*-AEMA)].[117] Polyplexes formulated with P(MAT-*b*-AEMA) polymers displayed high uptake efficiency and powerful gene knockdown in U87 cells.[117]

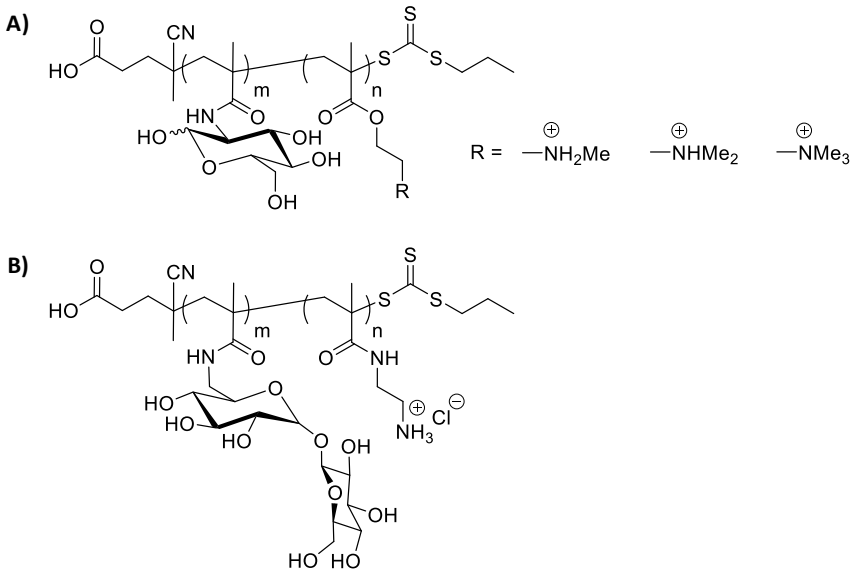

Figure 2.1. Polymer structures for (A) P(MAG_m-b-methacrylate$_n$) and (B) P(EG_m-*b*-$AEMA_n$).

Herein, we investigated the use of P(MAT-*b*-AEMA) and a series of P(MAG-*b*-methacrylate) block copolymers in the formulation of polyplexes containing

plasmid DNA (pDNA) for gene delivery *in vitro* and *in vivo*. Nine poly(2-deoxy-2-methacrylamido glucopyranose)-*b*-poly(polymethacrylate amine) diblock copolycations [P(MAG-*b*-methacrylate)] were synthesized with varied pendant amine methylation (secondary, tertiary, quaternary) to optimize the structure and activity for plasmid DNA delivery,[125] while the P(MAT-*b*-AEMA) polymers kept the same polymer composition and varied only the cationic polymer block length.[58] The plasmids contained either a firefly luciferase or a green fluorescent (GFP) reporter gene under the regulation of a strong synthetic promoter (CAGGS) that is highly active in vertebrate cells.[126] Delivery experiments were first performed in human liver carcinoma (HepG2) cell lines and found to be highly efficacious. The trehalose polymers were then examined for the ability to stabilize polyplex formulations through lyophilization and reconstitution. We reveal that these trehalose-coated polyplexes retain pDNA delivery and gene expression activity after lyophilization and reconstitution, an important metric to improve the consistency of gene delivery and increase shelf life of nanomedicines. We also reveal the first examination of these trehalose block copolycations for *in vivo* pDNA administration. Polyplex formulations were administered to mice using two different injection techniques to observe toxicity, biodistribution, and efficacy of gene delivery *in vivo*. We reveal that these trehalose-coated polyplexes shield the formulations from nonspecific tissue internalization under slow tail vein

infusion, yet also retain stability *in vivo* following rapid hydrodynamic injection, resulting in the promotion of highly specific and excellent gene expression in the mouse liver (compared to jetPEI and pDNA only controls). Indeed, this study demonstrates that trehalose-coated nanomedines offer a new stealth design motif that could provide an alternative to PEGylation for stabilizing formulations for *in vivo* administration.

2.2 EXPERIMENTAL

2.2.1 Materials and Reagents

All reagents were obtained at the highest available purity from Thermo Fisher Scientific, Inc. (Pittsburgh, PA) or Sigma-Aldrich Co. LLC. (St. Louis, MO) and used as received unless noted otherwise. JetPEI was obtained from Polyplus-transfection SA (Illkirch, France). Glycofect was obtained from Techulon, Inc. via donation. 6-Methacrylamido-6-deoxy trehalose (MAT) was synthesized as described previously.[24] Propidium iodide, UltraPureTM Agarose-1000, trypsin, (3-(4,5-dimethylthiazol-2-yl)-2,5-diphenyl tetrazolium bromide (MTT), phosphate-buffered saline (PBS), Minimum Essential Medium with reduced serum (Opti-MEM) and Dulbecco's Modified Eagle Medium (DMEM) were purchased from Life Technologies – Thermo Fisher Scientific (Carlsbad, CA). The pT2/CAL plasmid was prepared as described previously.[35] The Luciferase Assay Kit and cell lysis buffer were obtained from Promega

Corporation (Madison, WI). Bio-Rad DC Protein Assay Reagent A, Reagent B and Reagent S were obtained from Bio-Rad Laboratories, Inc. (Hercules, CA). HepG2 and U87 cells were obtained from the American Type Culture Collection (ATCC) (Manassas, VA). The cells were grown in complete DMEM [supplemented with 10% (v:v) fetal bovine serum and 1% antibiotic-antimycotic solution (containing penicillin, streptomycin, and amphotericin B)] at 37 ºC and 5% CO2 in a humidified incubator.

Monomeric aminoethylmethacrylate (AEMt) was purchased from Polysciences (Warrington, PA). *N*-methyl-aminoethylmethacrylate (MAEMt), *N,N*-dimethyl aminoethylmethacrylate (DMAEMt) and *N,N,N*-trimethylammoniumethylmethacrylate (TMAEMt) was prepared with procedures shown in later chapters. 4-cyano-4-(propylsulfanylthiocarbonyl) sulfanylpentanoic acid (CPP) was synthesized according to a previous procedure.[127] 4,4'-Azobis(4-cyanopentanoic acid) (V-501) was purchased from Aldrich and was crystalized from MeOH prior to use. Methacryloyl chloride was distilled to remove the free radical stabilizer. 2-Deoxy-2-methacrylamido glucopyranose (MAG) was prepared according to a previous publication.[116] All other chemicals were purchased from Aldrich and used without further purification.

Wild-type (WT) C57BL/6J 6wk-old mice were purchased from Jackson Laboratories (Sacramento, CA). All mice were maintained under AAALAC-

accredited (Association for Assessment and Accreditation of Laboratory Animal Care) specific pathogen-free conditions.

2.2.2 Instrumentation

NMR spectra of P(MAT-*b*-AEMA) polymers and components were recorded using a Bruker Avance III HD 500 MHz spectrometer in D2O purchased from Cambridge Isotope Laboratories, Inc. (Andover, MA). NMR data was analyzed using Bruker Top Spin version 3.1. H NMR spectra of P(MAG-*b*-methacrylates) were recorded on a Varian INOVA-300 or Varian INOVA-500 NMR Spectrometer with D_2O or $CHCl_3$-d solvents. UV-Vis data was collected with an Ocean Optics Inc. CUV 1 cm cuvette holder powered by a Mikropack DH-2000 Deuterium/ Halogen open-close TTC lamp, and data was analyzed by Ocean Optics Inc. Basic Acquisition Software.

Size exclusion chromatography (SEC) was conducted using an Agilent 1260 High Performance Liquid Chromatograph running 1.0 wt% acetic acid/0.1 M Na2SO4 as the eluent at a flow rate of 0.4 mL/min. on size exclusion chromatography columns [CATSEC1000 (7 μ, 50×4.6), CATSEC100 (5 μ, 250×4.6), CATSEC300 (5 μ, 250×4.6), and CATSEC1000 (7 μ, 250×4.6)] obtained from Eprogen Inc. (Downers Grove, IL). Signals were acquired using Wyatt HELEOS II light scattering detector (λ = 662 nm), and an Optilab rEX refractometer (λ = 658 nm). SEC trace analysis was performed using Astra VI

software (version 5.3.4.18), Wyatt Technologies (Santa Barbara, CA). The hydrodynamic diameters of the polyplexes were recorded via dynamic light scattering measurements (DLS) with a Malvern Zetasizer Nano ZA. MTT, protein, and luciferase assay plates were analyzed using a Biotek Synergy H1 plate reader (BioTek Instruments, Inc., Winooski, VT). Cy5-uptake was measured on a FACSVerse (Becton Dickinson Biosciences, San Jose, CA) flow cytometer. TEM images were obtained with a FEI Tecnai G2 Spirit BioTWIN (FEI, Hillsboro, OR) transmission electron microscope, operated at 120 kV.

Live animal and animal tissue imaging were performed on an IVIS Spectrum In Vivo Imaging system and data was analyzed with the Living Image software (PerkinElmer Inc., Waltham, MA). RT-qPCR was performed using an Eppendorf Mastercycler (software version 2.2; Eppendorf).

2.2.3 Polymer Synthesis

In the study focused on glucose-based materials, all synthesis and polymer characterization was conducted by Dr. Haibo Li. *N,N*-dimethylaminoethyl methacrylate hydrochloride (DMAEMt) was prepared by treatment of the neutral monomer (11.52 g, 73.28 mmol) with hydrochloride solution (9.5%, 27.40 mL) at 0 ^{o}C, followed by removal of the solvent *in vacuo* and washed by mixed solvent of ethyl acetate and methanol (80:20 v:v) to give 12.07 g product. *N,N,N*-trimethylammonium ethylmethacrylate iodide (TMAEMt) was prepared by

treatment of the *N,N*-dimethylaminoethyl methacrylate (12.39 g, 78.81 mmol) with MeI (5.90 mL, 94.57 mmol) in chloroform (60 mL), followed by removal of the solvent *in vacuo* to give 23.38 g product.

MAEMt was prepared through a three-step reaction (Figure 2.2). First, *2-N*-methyl ethanol was protected by cooling a solution of methyl-2-aminoethanol (7.50 g, 100.12 mmol) in chloroform (50 mL) in an ice bath for 10 minutes. A solution of di-*tert*-butyl dicarbonate (BOC_2O) (21.87 g, 100.12 mmol) in chloroform (50 mL) was added dropwise to the mixture over 30 minutes. The reaction was further stirred at 0 $^{\circ}$C for 1 hour, after which, it was allowed to warm up to room temperature. The solvent was then removed *in vacuo*. After vacuum distillation, 16.29 g of product (93% yield) was obtained. For the second step, a solution of the product obtained from the previous step (BOC protected 2-N-methyl ethanol, 15.73 g, 89.77 mmol) in chloroform (150 mL) was cooled in an ice bath for 10 minutes. Triethyl amine (16.00 mL, 115.07 mmol) was then added to the solution in one portion. After which, methacryloyl chloride (8.92 mL, 92.01 mmol) was added dropwise over 10 minutes. The reaction was allowed to warm up to room temperature and was further stirred overnight. The reaction solution was then washed with water (150 mL) and dried over $MgSO_4$. The desiccant was filtered off and the solution was concentrated *in vacuo*. The final product, BOC protected N-methylaminoethylmethacrylate, was obtained after purification with

column chromatography (with a mobile phase containing 25% ethyl acetate and 75% hexane as the mobile phase (Yield: 16.74 g 74%).

To deprotect, a solution of the product obtained from the previous step (16.16 g, 64.38 mmol) in HCl solution in MeOH (1.25 M, 180 mL) was cooled in ice bath for 1 hour and stirred at room temperature overnight. The solution was then concentrated *in vacuo*. 150 mL ethyl acetate was added to the residue to wash. The ethyl acetate was filtered off and the product was obtained as a white solid, which dried under vacuum to yield a white solid (Yield: 10.86 g, 94%).

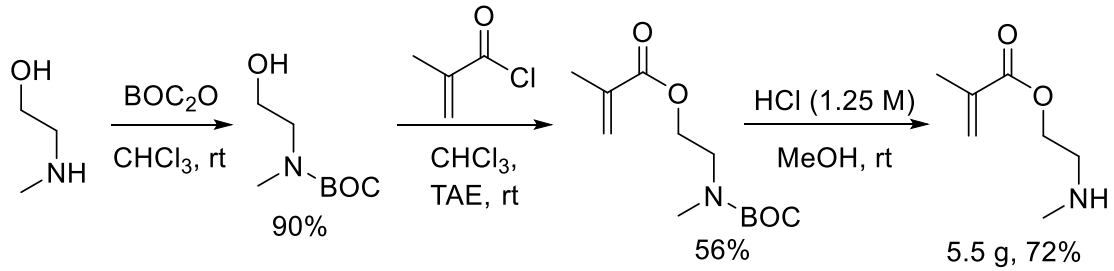

Figure 2.2. Synthesis scheme for methylaminoethylmethacrylate (MAEMT).

The P(MAG) macroCTA was prepared according to a procedure in one of our recent publications.[116] To a 250 mL round bottom flask charged with nitrogen gas, MAG (6.00 g, 24.27 mmol), V501 (5.8 mg, 0.02023 mmol), CPP (56 mg, 0.2023 mmol), acetate buffer (0.1 M, pH =5.2) (72 mL) and ethanol (18 mL) were added and stirred. Nitrogen gas was allowed to purge the solution for 2.5 hours at room temperature. After which, the solution (still under a nitrogen

atmosphere) was heated to 70 ^{o}C and stirred for an additional 280 minutes. The reaction solution was quenched by via rapidly freezing the solution with liquid nitrogen and then exposing the contents to air. The solution was then transferred to dialysis tubing (MWCO 3500) and allowed to dialyze against ultra high purity water for three days (water was changed twice a day. The final solution was then lyophilized to dryness yielding 1.68 g of product. Yield: 28%.

The following is a typical procedure used to prepare the diblock glycopolymers with the various cationic monomers. The PolyMAG macroCTA (0.20 g, 0.01418 mmol), methacrylate chloride monomer (0.278 g, 1.5479 mmol), V501 (0.87 mg, 0.003096 mmol), and acetate buffer (1.0 M, pH=5.2) (2.40 mL) were added to a 5 mL vial charged with nitrogen gas and a mechanical stirring bar. The mixture was stirred to dissolve the reactants and the solution was purged with nitrogen gas for 30 minutes at room temperature. Next, the reaction mixture was heated to 70 ^{o}C, and the reaction was stirred for 26 minutes. The solution was then dialyzed against water for three days and lyophilized to yielding 0.23 g of the final glycopolycation final product.

P(MAT)$_{43}$ was synthesized as previously described.[117] In the study focused on trehalose-based materials, all synthesis and polymer characterization was conducted by Dr. Zachary Tolstyka. Briefly, MAT monomer was polymerized via RAFT in acetate buffer. 4-cyano-4-(propylthiocarbonothioylthio)-pentanoic acid

was dissolved in 645 µL of MeOD and added to the MAT solution, followed by 4,4'-azobis(4-cyanovaleric acid) (V-501) Finally, 861 µL of MeOD was added and oxygen was removed by bubbling nitrogen through the system for 45 min. The flask was heated to 70 °C for 6 h and the reaction was stopped by removing the septum and cooling the reaction mixture on ice. The polymer solution was dialyzed against ultra-pure water (3500 Da MWCO) acidified to pH 4-5 with HCl. After 3 d of dialysis, the polymer solution was freeze dried on a VirTis benchtopK lyophilizer at 62 mT with the condenser at -57.4 °C to yield 454 mg of white solid. See the appendix for an $P(MAT)_{43}$ H NMR spectrum.

Cationic diblock copolymers were synthesized as previously reported.[117] Briefly, $P(MAT)_{43}$ and V-501 were dissolved in 1.0 M acetate buffer (pH = 5.5) and added to a Schlenk tube containing aminoethylmethacrylamide hydrochloride (AEMA). Deoxygenation was achieved via bubbling nitrogen gas for 45 min. The tube was heated to 70 °C. Aliquots (1.25 mL) were removed via syringe at 30 min [P(MAT-*b*-AEMA)-1] and 60 min [P(MAT-*b*-AEMA)-2]. Each aliquot was exposed to air and cooled in liquid nitrogen to stop polymerization. After 90 min [P(MAT-*b*-AEMA)-3], the reaction was halted by septum removal and submerging the Schlenk tube in liquid nitrogen. All three copolymers were dialyzed (3500 Da MWCO) against 0.5 M NaCl solution, followed by 0.1 M NaCl and finally ultra-pure water. All dialysis media were acidified with HCl to pH 4-5.

Polymer solutions were lyophilized as described above to yield white, flocculent powders. All experiments were completed using polymers P(MAT-*b*-AEMA)-1, -2, and -3. Polymer ^{1}H NMR and SEC characterization results can be found in the appendix.

P(MAT-*b*-AEMA)-2 was labeled using an NHS-Cy7 fluorophore by dissolving it in H_2O. Cy7 functionalized with N-hydroxysuccinamide (NHS-Cy7) in DMF was added followed by DMF to target 1 fluorophore/50 amine residues. The mixture was vortexed for 30 s and allowed to proceed at room temperature for 4 h in the dark. The labeled polymer was purified via dialysis (3500 MWCO) against H_2O (acidified to pH ~5.5 with HCl) for 2 days and lyophilized using the same conditions listed before to yield a blue flocculent solid. The extent of Cy7 tagging was quantified measuring the absorbance of a 0.2 mg/ mL of labeled polymer in H2O at 750 nm via UV-Vis (ε = 199000 at 750 nm, Abs = 0.16, Figure 2.3) giving approximately 1 Cy7 fluorophore / 10 polymer chains.

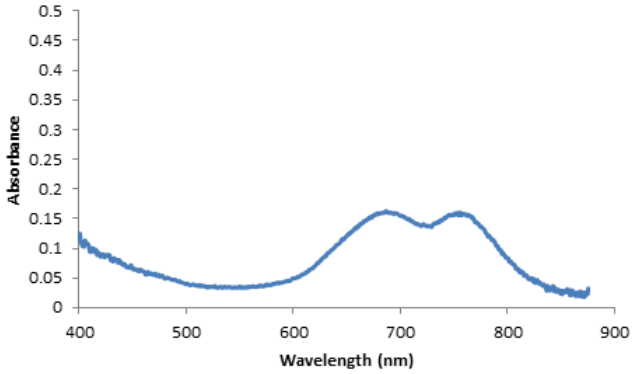

Figure 2.3. Absorbance of P(MAT-b-AEMA)-2-Cy7 in H_2O used to calculate labeling efficiency (~1 Cy7 per 10 polymer chains) from the extinction coefficient for NHS-Cy7 (provided by the manufacturer, Lumiprobe Corp.).

2.2.4 Polyplex Characteristics

Polymer solution at an appropriate concentration in water was added to a 400 µM solution of pDNA in DNase/RNase-free distilled water in an equal volume to yield polyplexes of (nitrogen to phosphate ratios) N/P = 5, 7, 14,15, and 21 at a final concentration of 200 µM pDNA. The nitrogen ratios were calculated based on the concentrations of amines (either pendant from the cationic blocks or within the backbone of jetPEI or Glycofect). The solutions were incubated at 23 °C for 1 h before further use.

2.2.5 Gel Electrophoresis

A gel electrophoresis mobility shift assay was run to determine the minimal amount of polymer needed to achieve complete binding of the pDNA. 10 µL of

each polyplex solution formulated at various N/P ratios were diluted with 10 µL of water to achieve a concentration of 100 µM and were incubated at 25 °C for 1 h to allow polymer-pDNA binding. The polyplex suspensions were run on agarose gels (0.6%) containing 6 µg ethidium bromide at 60 volts for 80 min. Images were obtained using 312 nm UV light.

2.2.6 Dynamic Light Scattering (DLS)

To measure polyplex size in a protein environment over time, DLS experiments were run in DMEM containing 10% FBS. The DLS measurements of all P(MAG-*b*-methacrylate) formulations were collected by Dr. Haibo Li. Polyplexes were formulated at N/P = 7, 14, and 21 in H2O and incubated for 1 h at a concentration of 200 µM pDNA (to allow complexation) before being diluted with DMEM containing 10% FBS by volume. For DLS studies prior to lyophilization, the polyplexes were diluted to a final concentration of 100 µM (T = 0 h). For the post-lyophilization DLS, polyplexes were prepared and lyophilized as previously described, reconstituted with water for 1 hour, then diluted with DMEM with 10% FBS to 133 µM. Size measurements were taken at 25 °C using a 173° detection angle at times of 0 h, 1 h, 2 h, and 4 h.

2.2.7 Transmission Electron Microscopy (TEM) Imaging

3 µL of polyplex solution (formulated with pDNA and polymers P(MAT-*b*-AEMA)-1, -2, or -3) prepared at N/P = 10 were applied to a 300-mesh carbon

coated copper grid (Ted Pella, Inc., Redding, CA). Excess polyplex solution was blotted off with filter paper after 60 s, and 3 µL of 1% uranyl acetate was applied, left for 60 s, then blotted off. The negative staining process was repeated twice more. Images were recorded using an Eagle^{TM} CCD camera (up to 4 mega pixels), and phase contrast was enhanced at 6-12 µm underfocus. Images were saved as TIFF files and polyplex size was analyzed by using ImageJ (see appendix for quantified data). All TEM images were captured by Dr. Yaoying Wu.

2.2.8 Cell Viability Studies

MTT (3-(4, 5-dimethylthiazol-2-yl)-2, 5-diphenyltetrazolium bromide) was used to estimate the cytotoxicity of the polyplexes. HepG2 cells were seeded at 50,000 cells/well in 24-well plates 24 h prior to transfection. Polyplexes were formulated as described previously, then 100 µL polyplex solution was diluted with 200 µL DMEM containing 10% FBS. 300 µL of that mixture was added to each well. The transfection was ended 4 h later by diluting polyplexes with 1 mL of complete DMEM containing 10% FBS. 48 h after polyplexes were added to the cells, 0.5 mg/mL of MTT was added to each well and incubated for 1 h. Cells were lysed using DMSO and 200 µL aliquots were transferred to a 96-well plate for analysis using the plate reader (absorbance was measured at 570 nm). Non-transfected cells were used for normalizing the data.

2.2.9 Cell Uptake Assay

Flow cytometry experiments were performed to examine the cellular uptake of Cy5-labeled pDNA 4 h post-transfection. HepG2 cells were seeded at 300,000 cells/well in 6-well plates 24 h prior to transfection. Polyplexes were prepared as described in the MTT assay protocol, except that the formulation was scaled up from 50,000 cells to 300,000 cells. After 4h, the polyplex media was removed and cells were detached from the plate surface using trypsin, centrifuged to remove polyplexes and trypsin, and then washed twice with PBS. Finally, 1 mL PBS was added and the cellular suspensions were kept on ice. Propidium iodide (1.0 mg/mL, 2.5 µL) was added prior to analysis. Each experiment was performed in triplicate.

2.2.10 Gene Expression Assays

Cells (HepG2) were seeded at 50,000 cells/well in 24-well plates 24 h prior to transfection. Polyplexes were prepared, diluted, and applied to the cells as described in the cytotoxicity section above. After 48 h, the cells were washed with PBS and treated with cell lysis buffer. Aliquots (5 µL) of cell lysate combined with 100 µL luciferase substrate were examined in 96-well plates using a luminometer to determine relative light units (RLUs). Data were measured in triplicate and normalized for the amount of protein in each sample. Sample averages were plotted with error bars representing standard deviations.

2.2.11 Mouse Injections

Appropriate amounts of polyplexes (10 µg or 25 µg of pDNA/dose at desired N/P of polymer) were prepared in a 5% by weight aqueous dextrose solution (D_5W, Hospira, Inc.). For a standard tail vein injection, a 200 µL dose of polyplexes was injected through the tail vein of experimental animals. For hydrodynamic injections, a previously published procedure was used. Briefly, animals to be injected were weighed. A polyplex solution with a volume equivalent to 10% of the weight of the mouse was injected in 3 to 4 s. After injection, animals were placed on a heating pad to recover, then returned to their colony. Mice were either imaged for luciferase transgene expression about 24 and 48 h after transfection or imaged immediately after injection for Cy7 polymer fluorescence. After fluorescence imaging, mice were euthanized and their organs were imaged *ex vivo.*

2.2.12 Mouse Imaging

For luciferase imaging, 100 µL of luciferin substrate solution (28.5 mg/mL) was injected intraperitoneally to each mouse. 3 to 5 min later, mice were imaged for 1 min using a Xenogen Spectrum CCD camera system (Xenogen, Alameda, CA) according to the manufacturer's instructions. Each experiment was performed in triplicate.

After imaging mice for Cy7 fluorescence (data not shown for hydrodynamically injected animals), mice were euthanized by carbon dioxide (CO_2) inhalation, perfused with saline, and selected organs were resected and preserved for analyses. Plasma and tissues were stored at –80 °C. Frozen tissues were homogenized by mortar and pestle, and ~100 mg of each tissue sample was removed for DNA processing. DNA was pulled from the organs using a phenol-chloroform extraction and ethanol precipitation. DNA purity and concentration were determined by using a NanoDrop instrument.

2.2.13 qPCR

DNA samples were normalized to 100 ng/µL. 500 ng of DNA was used with TaqMan Gene Expression Master Mix (Life Technologies – Thermo Fisher Scientific, Carlsbad, CA). TaqMan primers were designed and manufactured by Life Technologies – Thermo Fisher Scientific (Carlsbad, CA), Custom Plus TaqMan Assay, Assay ID – AJ6RNJ4. A standard curve was prepared by serially diluting pT2/CAL plasmid into WT C57BL/6 DNA. Samples were run using the impulse setting. The following conditions were used for the qPCR experiments: 95 °C for 10 min and 40 cycles of 90 °C for 15 s then 60 °C for 1 min. QPCR experiments were performed by Jason Bell.

2.2.14 Statistical Analysis

Statistical analysis was performed using JMP Pro Software (SAS Institute, Cary, NC) through the University of Minnesota Supercomputing Institute.

2.3 RESULTS

2.3.1 Polymer Synthesis and Characterization

Trehalose is a carbohydrate with unique cryo- and lyo-protectant properties, which have prompted the use of this carbohydrate in materials synthesis to both retain and enhance these protective abilities.[117-121, 128] Previously, we have shown that trehalose-containing block copolymers are effective in the formulation of polyplexes and efficient delivery of siRNA.[117] Herein, we sought to examine these trehalose-based polycations for delivery of plasmids to cells in culture and in organs of living animals. Trehalose-based polymers were synthesized via reversible-addition-fragmentation chain-transfer (RAFT) polymerization with a 65:1 monomer: chain-transfer agent (CTA) ratio of 6-methacrylamido-6-deoxy methacrylamido trehalose (MAT) and 4-cyano-4-(propylthiocarbonothioylthio)-pentanoic acid (CPP) with 4,4′-azobis(4-cyanovaleric acid) (V-501) as the initiator to yield P(MAT) with 43 repeats. This 43-repeat unit P(MAT) was used as a macro CTA and chain-extended via RAFT polymerization with 125 equivalents of *N*-(2-aminoethyl) methacrylamide (AEMA) and V-501 as the initiator to yield three cationic block copolymers (Table 2.1),[117] P(MAT-*b*-AEMA)-1 (21 repeats), -2 (44

repeats), and -3 (57 repeats), with each having the same length of MAT block but increasing lengths of the AEMA block.

Table 2.1. Summary of Polymer Molecular Weight and Composition

Polymer	M_n (kDa)	Đ	x DP	y DP
P(MAG$_x$-*b*-MAEMt$_y$)-1	18	1.02	51	30
P(MAG$_x$-*b*-MAEMt$_y$)-2	20	1.02	51	42
P(MAG$_x$-*b*-MAEMt$_y$)-3	27	1.05	51	76
P(MAG$_x$-*b*-DMAEMt$_y$)-1	20	1.02	56	32
P(MAG$_x$-*b*-DMAEMt$_y$)-2	24	1.02	56	53
P(MAG$_x$-*b*-DMAEMt$_y$)-3	28	1.03	56	71
P(MAG$_x$-*b*-TMAEMt$_y$)-1	25	1.29	57	33
P(MAG$_x$-*b*-TMAEMt$_y$)-2	29	1.06	57	48
P(MAG$_x$-*b*-TMAEMt$_y$)-3	36	1.12	57	72
P(MAT$_x$-*b*-AEMA$_y$)-1	20	1.07	43	21
P(MAT$_x$-*b*-AEMA$_y$)-2	23	1.07	43	44
P(MAT$_x$-*b*-AEMA$_y$)-3	25	1.08	43	57

2.3.2 Polyplex Formation and Characterization

These polymers were combined with pDNA encoding for the luciferase reporter gene to form polyplexes. The amount of polymer needed to fully bind the pDNA was first determined via gel electrophoresis. Polymers and pDNA were mixed at nitrogen-to-phosphate (N/P) ratios of 1, 2, 3, 4, 5, and 10, mixed with 1 µL of running buffer and electrophoresed through a 0.6% w/w agarose gel containing ethidium bromide in TAE buffer. The gel was imaged under UV light to confirm binding (Figure 2.4). Anionic plasmid that remains uncomplexed by the

cationic polymer migrates through the gel toward the positively charged anode whereas fully complexed DNA does not. All polymers fully bound the DNA at N/P=5.

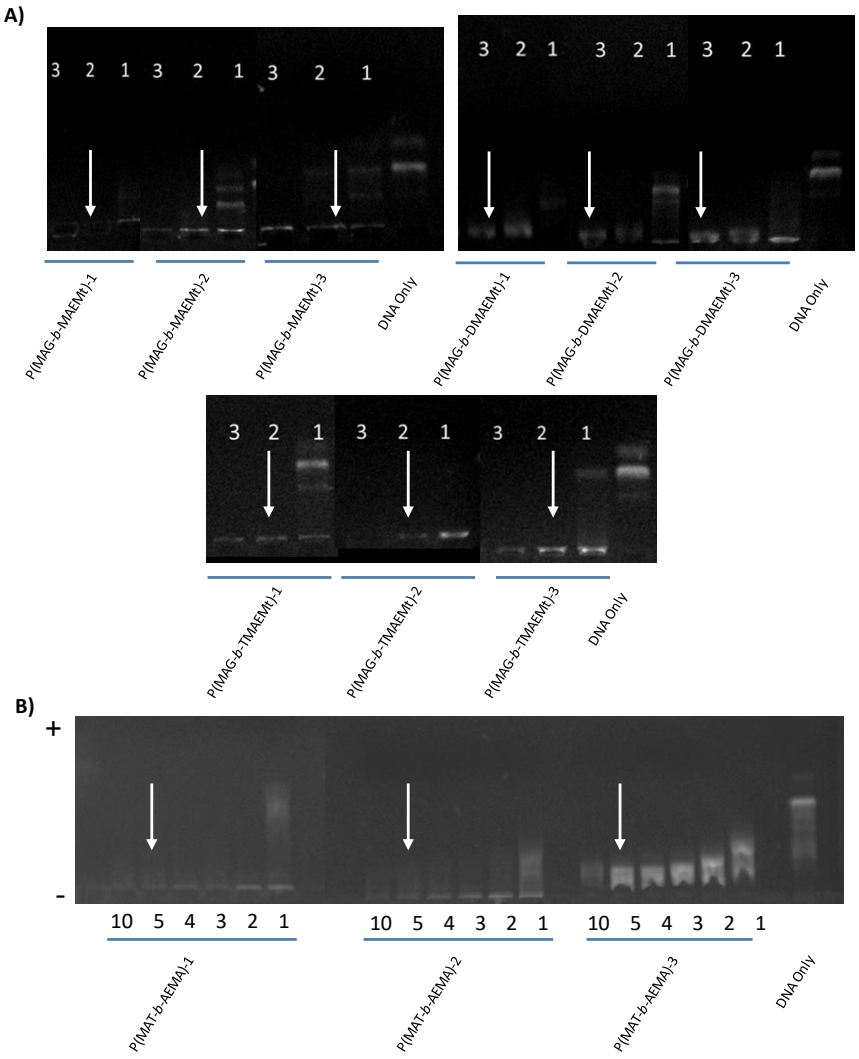

Figure 2.4. Gel electrophoresis shift assay to measure pDNA binding by A) P(MAG-*b*-MAEMT) and B) P(MAT-*b*-AEMA) polymers. All P(MAG-*b*-MAEMT) polymers completely bound pDNA by N/P of 3, while P(MAT-*b*-AEMA) polymers bound pDNA at N/P = 5.

For further studies, each polymer was combined with DNA at three different N/P ratios: 7, 14, and 21, yielding nine polyplex formulations. Polyplex size and stability from aggregation in biological media containing serum (10% by volume fetal bovine serum, FBS) were examined via dynamic light scattering (DLS). We have previously shown that polyplexes formed from this polymer and siRNA have a positive ζ–potential in H_2O. Polyplexes were formulated at 200 μM pDNA and allowed to complex for 1 h at 23 ˚C in water. The polyplexes were then diluted with Dulbecco's Modified Eagle Medium (DMEM) containing 10% by volume fetal bovine serum (FBS) solution to a final concentration of 100 μM in pDNA, and the polyplex size was monitored over 4 h (Figure 2.4). ζ–potential of these polyplexes was not collected as the presence of FBS disrupts the measurement.

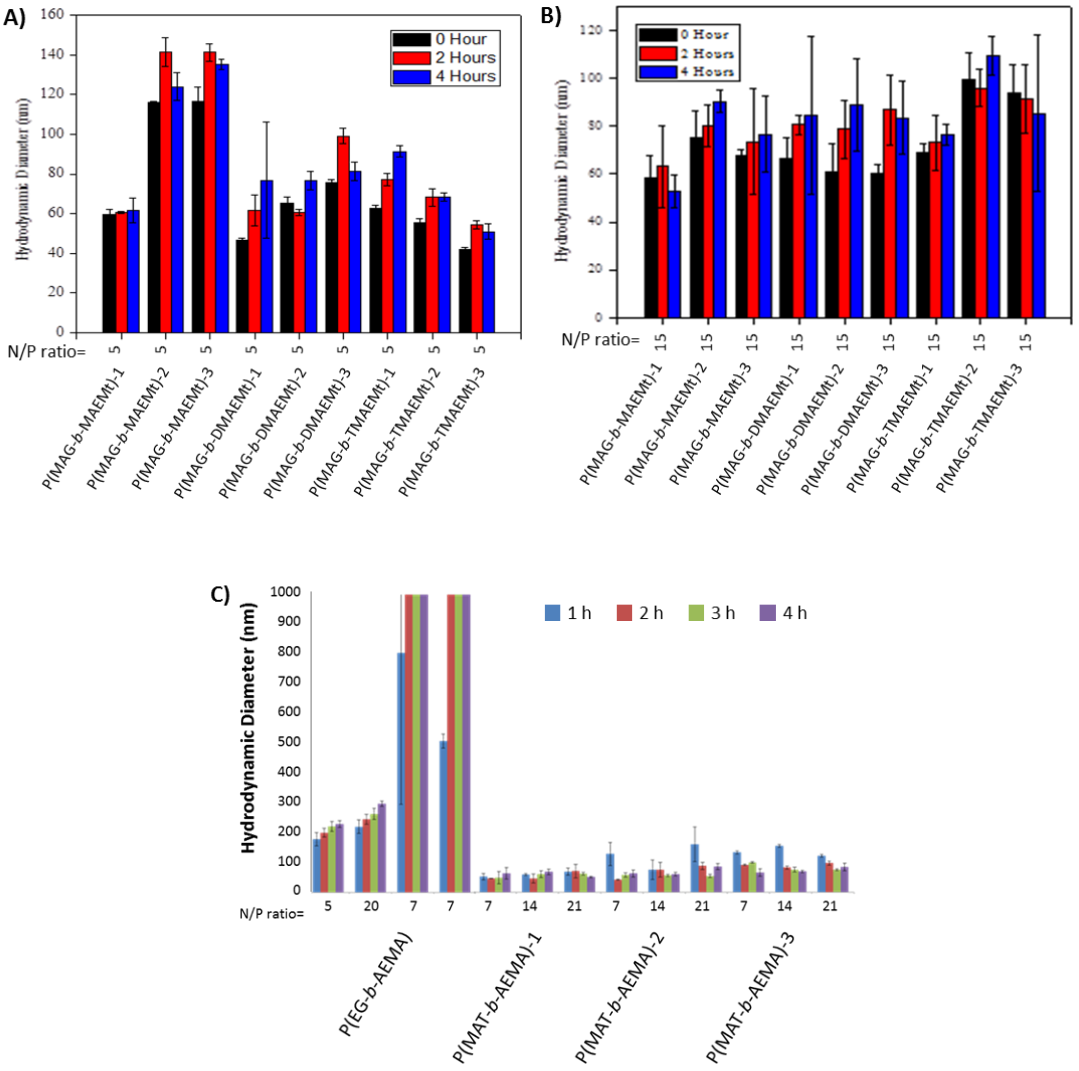

Figure 2.5. Polyplex size monitored by dynamic light scattering (DLS) over time. 0 h measured initial polyplex formulation (at 200 µM pDNA concentration) in water followed by dilution to 100 µM pDNA in A) OptiMEM, B) OptiMEM, or C) DMEM containing 10% FBS from 1 to 4 hours post-dilution. The error bars represent standard deviation of triplicate measurements.

Trehalose polyplex size (~50-100 nm in diameter) remained consistent over the course of this experiment relative to the control polyplexes, jetPEI (N/P=5) and Glycofect (N/P=20), which increased in diameter with time. It is proposed that the jetPEI and Glycofect polyplexes aggregate with amino acids, buffer salts, and FBS proteins found in DMEM, which neutralizes their surface charge and causes aggregation. The trehalose polyplexes neither aggregate nor swell compared to the control complexes. This result mirrors what has been observed previously with carbohydrate-based block-co-polycations: poly 2-deoxy-2-methacrylamido glucopyranose-*b*-*N*-(2-aminoethyl) methacrylamide [P(MAG-*b*-AEMA)] polyplexes formulated with pDNA[116] and P(MAT-*b*-AEMA) polyplexes formulated with siRNA.[117] Polyplexes formed with cationic polymers containing a carbohydrate block are protected from aggregation. The pendant trehalose units of the MAT portion of the block copolymer likely form a shell around the outside of the polymer-pDNA polyplex, providing a highly hydrophilic layer and facilitating steric stabilization of the polyplexes in biological media.

2.3.3 Cell Viability

Examination of the polyplex function was performed on two human cell lines with differing physiological function to assess the general biologic activity of the polyplex formulations. Cell culture studies of polyplex internalization and luciferase gene expression were performed in both HepG2 liver carcinoma and

U87 glioblastoma human cell lines. We chose to examine two cell lines as we have found polyplex behavior to vary substantially in different cell lines. This behavior is difficult to predict and must be determined experimentally. These assays were run in DMEM containing 10% FBS to understand the role of serum in the transfection conditions. First, a colorimetric live-dead cell study was performed to assess the cytotoxicity of polyplexes formed from the P(MAT-*b*-AEMA) and control polymers with pDNA. The 3-(4,5-dimethylthiazol-2-yl)-2,5-diphenyltetrazolium bromide MTT assay is a commonly used viability assay that measures mitochondrial activity.[129] Cells were exposed to polyplexes in DMEM containing 10% FBS for 4 h then incubated for 48 h prior to running an MTT toxicity assay. Survival of each sample was normalized to a negative control of cells that were exposed to neither pDNA nor polymer (Figure 2.6).

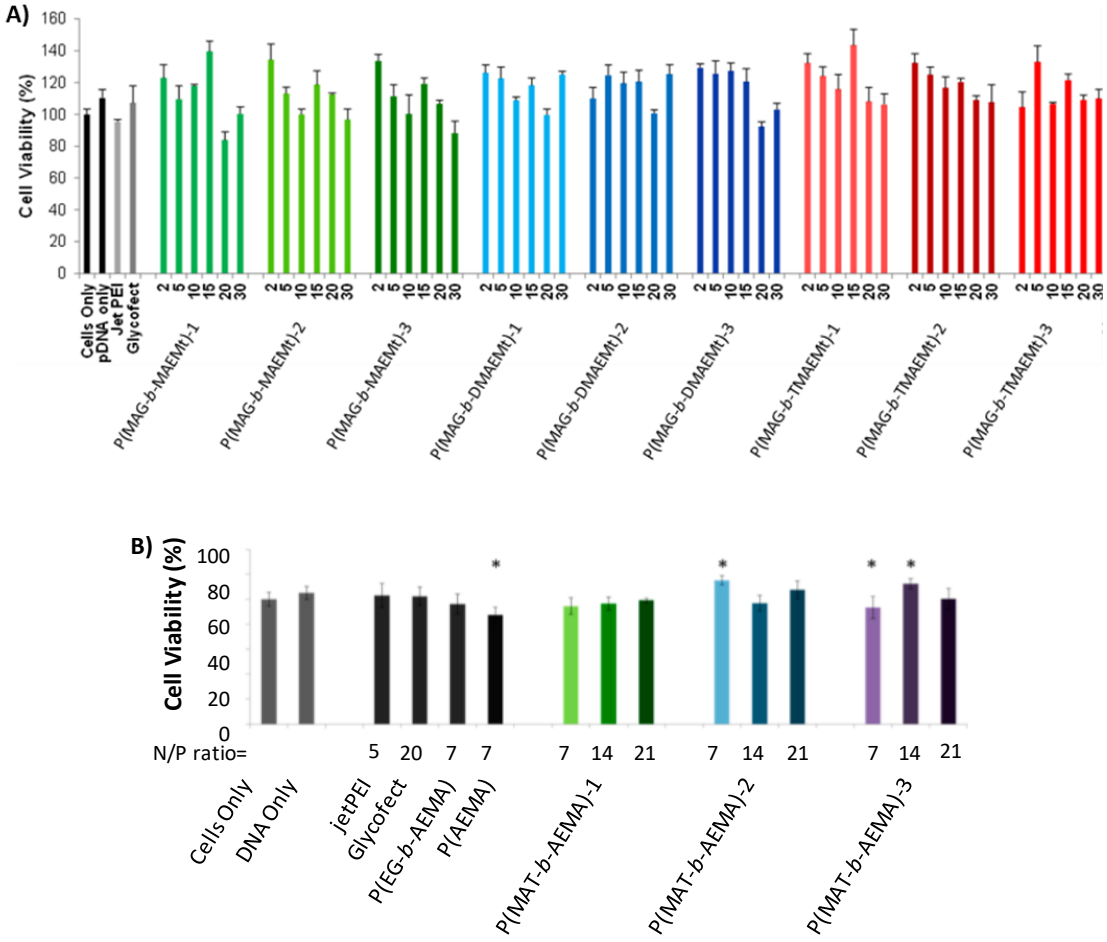

Figure 2.6. Cell viability as measured via MTT assay with HepG2 cells in DMEM + 10% FBS with A) P(MAG-*b*-methacrylate) polymers of varying length and N/P ratio and B) P(MAT-b-AEMA) of increasing length and N/P ratio. Error bars represent the standard deviation from three replicates. All measurements found to be statistically different (Student's t test $p < 0.05$) as compared to cells only are marked with an asterisk.

With HepG2 cells, most samples did not differ in value from the negative control of naïve cells for either the glucose- or trehalose-based polymers. No P(MAG-*b*-MAEMt) sample statistically decreased cell viability below the cells only

control. Only the P(AEMA) and P(MAT-*b*-AEMA)-3 polyplexes formulated at an N/P=7 showed cell survival rates of less than 100%. None of the P(MAT-*b*-AEMA)-1 formulations were found to cause a significant decrease in cell survival when compared to naïve cells grown without polyplexes present via the Student's t-test ($p = 0.05$).[77, 130, 131] Neither jetPEI nor Glycofect were toxic to HepG2 cells. The P(MAT-*b*-AEMA) with shorter AEMA block lengths had equal or higher levels of cell survivability than any of the controls, which also reflects previous work showing the biocompatibility of trehalose polymers.[77, 78, 132]

2.3.4 Gene Expression

The effectiveness of polyplex transfection and plasmid cargo uptake was assessed by measuring expression of a luciferase reporter gene. Polyplexes were formed and incubated with cells for 4 h in DMEM containing 10% FBS, followed by an additional incubation period of 48 h to allow for protein expression. Cells were washed, lysed, and the lysate analyzed for luminescence intensity after treatment with luciferin. In Figure 2.7, luminescence was plotted as relative light units (RLUs) per protein (mg) in each sample to normalize for the number of cells in each well, thus negating differences in expression due to cell death. It was observed in Figure 2.7A that an increase in the N/P ratio for most polymers did not show a significant increase in luciferase gene expression. However, the luciferase expression results did show a general trend when

considering the amine type. The transfection efficiency decreased slightly as the amount of methyl groups on the amine increased (secondary > tertiary > quaternary), suggesting that the P(MAEMt)-containing polymers should be further optimized and examined for nucleic acid delivery.

In Figure 2.7B, jetPEI polyplexes yielded the highest levels of luciferase expression and were statistically higher than the other formulations. Therefore, statistical comparison was recorded against the cells only and the P(AEMA) homopolymer controls. Mirroring the cell uptake data, P(MAT-*b*-AEMA)-2 samples had the highest level of expression, with lower expression for the shorter and longer cationic block polymers. This further supports that hypothesis that the amount of cationic charge can help transfection to a point before it starts to hinder uptake and expression.

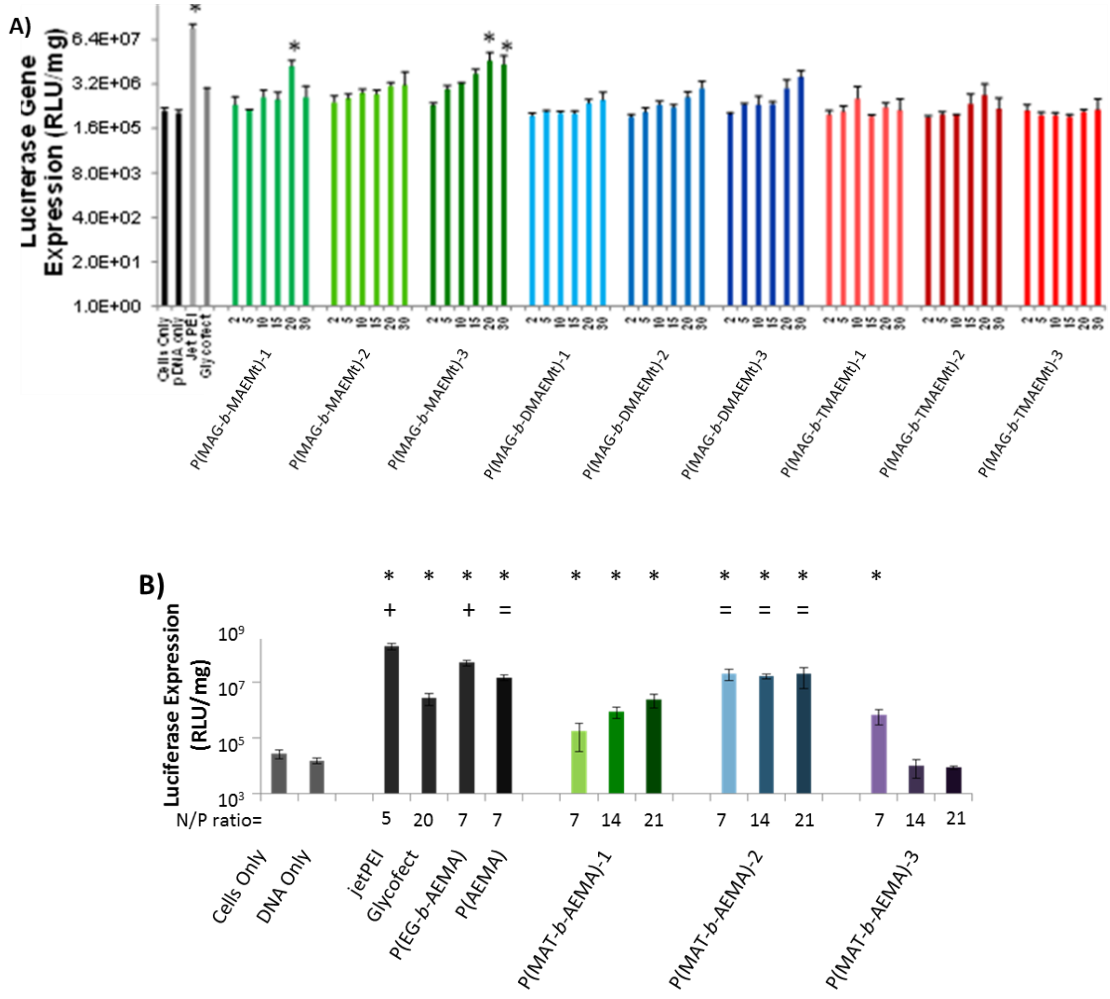

Figure 2.7. Gene expression as measured by the luminescence of HepG2 cell lysate following the addition of luciferin reagent. Cells were transfected using A) P(MAG-*b*-methacrylates) and B) P(MAT-*b*-AEMA) in DMEM + 10% FBS. Data were normalized for cell death. Error bas represent the standard deviation from three replicates. All measurements found to be statistically different (Student's t test $p < 0.05$) as compared to cells only are marked with an *. Samples found to be significantly higher than the positive control p(AEMA) are marked with a +, and samples found to be statistically equivalent to P(AEMA) are marked with an = (Student's t-test $p < 0.05$).

In previous work, we have found that polyplexes formed with glucose-containing P(MAG-*b*-AEMA) exhibited higher transfection efficiency with a shorter length of AEMA when made with siRNA and a longer AEMA block when formulated with plasmid DNA (pDNA).[116] Polyplexes formulated with trehalose-block copolycations, P(MAT-*b*-AEMA) and siRNA also displayed better transfection with a shorter AEMA block than with longer blocks.[117] Among the trehalose polyplex formulations studied herein from N/P=7 to N/P=21, luciferase expression increased 8 fold in HepG2 cells for P(MAT-*b*-AEMA)-1 and decreased with N/P with P(MAT-*b*-AEMA)-3. For P(MAT-*b*-AEMA)-2 polyplexes, luciferase expression was statistically equivalent from N/P = 7 – 21 to expression values from P(AEMA) polyplexes in HepG2 cells. Gene expression with P(MAT-*b*-AEMA)-2 polyplexes was also statistically equivalent to that yielded by P(AEMA) at N/P = 7.

The P(MAT-*b*-AEMA)-2 formulations were the only P(MAT-*b*-AEMA)-based polyplexes to exhibit luciferase expression at the same level as any of the control polymers. This trend was similar to the cellular uptake data, again supporting the hypothesis that AEMA (and therefore positive charge) does aid cellular internalization and expression to a point. However, with a further increase in the N/P ratio, expression values start to decrease. The decrease could be due to two factors: i) prevention of the release and transcription of DNA cargo[116] or ii) by

increasing cell membrane permeability to the point of toxicity.[24, 129] Because luminescence RLUs are normalized to the amount of cell protein in each sample, cytotoxicity is not enough to account for low expression in either cell line. It is more likely that polyplexes with large AEMA blocks and high polymer-to-plasmid ratios have higher charge densities that prevent cargo release and transcription,[116, 133] while complexes with too little AEMA or too small an N/P ratio could prematurely release DNA prior to nuclear entry.[134] We were not as concerned with this latter issue due to the stability of the polyplexes that was observed in the DLS data. It should be noted that differences between some samples are not statistically significant, but the general trend that appears in the uptake assays as well as gene expression studies for both cells lines correlates with previous work in the field.[116, 125, 130, 133]

After the large luciferase screen, a smaller group of P(MAG-*b*-methacrylate) polymers was chosen to further test for transfection efficiency and cellular internalization (*vide infra*) via flow cytometry analysis. This smaller group of polymers was designed to be an orthogonal study to include the three different amine types containing comparable charge block lengths, P(MAG-*b*-MAEMt)-3, P(MAG-*b*-DMAEMt)-3, and P(MAG-*b*-TMAEMt)-3. As the secondary amine derivatives yielded the highest gene expression in the preliminary screen, P(MAG-*b*-MAEMt)-1 and -2 were also included to further investigate the effect of

amine length on transfection efficiency. All additional tests were performed by formulating the polyplexes at an N/P ratio of 15. To further probe transfection efficiency in a quantitative manner, green fluorescent protein (GFP) was used as the reporter gene and analyzed using flow cytometry (P(MAT-*b*-AEMA) was not tested using the GFP method). In DMEM containing 10% (by volume) fetal bovine serum, transfection efficiency decreased as methyl substitution of the amine increased (Figure 2.8, horizontal striped bars), which agreed with the luciferase expression data. When examining the effect of amine length (Figure 2.8, green bars), P(MAG-*b*-MAEMT)-1 and -2 showed similar transfection efficiency, while the longest of that polymer series, P(MAG-*b*-MAEMT)-3, exhibited significantly lower GFP expression (p value < 0.05) than the shorter polymers.

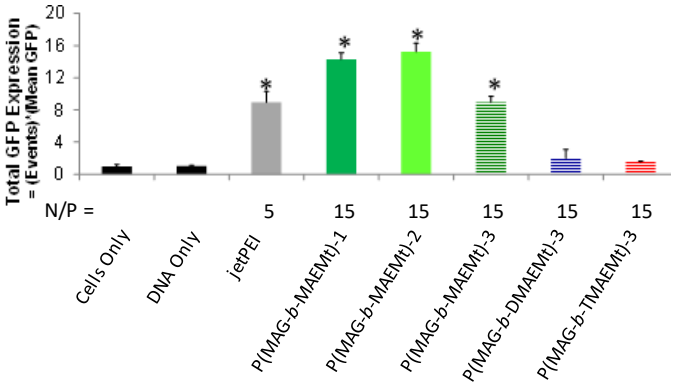

Figure 2.8. Total GFP fluorescence (number of events measured multiplied by mean GFP fluorescence intensity) of HepG2 cells analyzed by flow cytometry. Cells were transfected using P(MAG-*b*-methacrylate) polymers in DMEM + 10% FBS. Error bas represent the standard deviation from three replicates. All measurements found to be statistically different (Student's t test $p < 0.05$) as compared to cells only are marked with an asterisk.

2.3.5 Cell Uptake

To quantify the amount of plasmid cargo taken up by cells, pDNA was fluorescently labeled with cyanine 5 (Cy5) prior to transfection. Polyplexes were formulated and exposed to the cells as previously described for the MTT assay. After transfection, cells were washed, collected, and centrifuged to concentrate the cells in solution and analyzed via flow cytometry. After the first run, 2.5 µL of propidium iodide (PI) was added to the remaining samples in each tube and left to sit for 30 min at room temperature prior to re-analysis. Cells positive for PI were assumed to be dead or dying and were removed from gating. Data were plotted as a percentage of live cells positive for Cy5 (Figure 2.9).

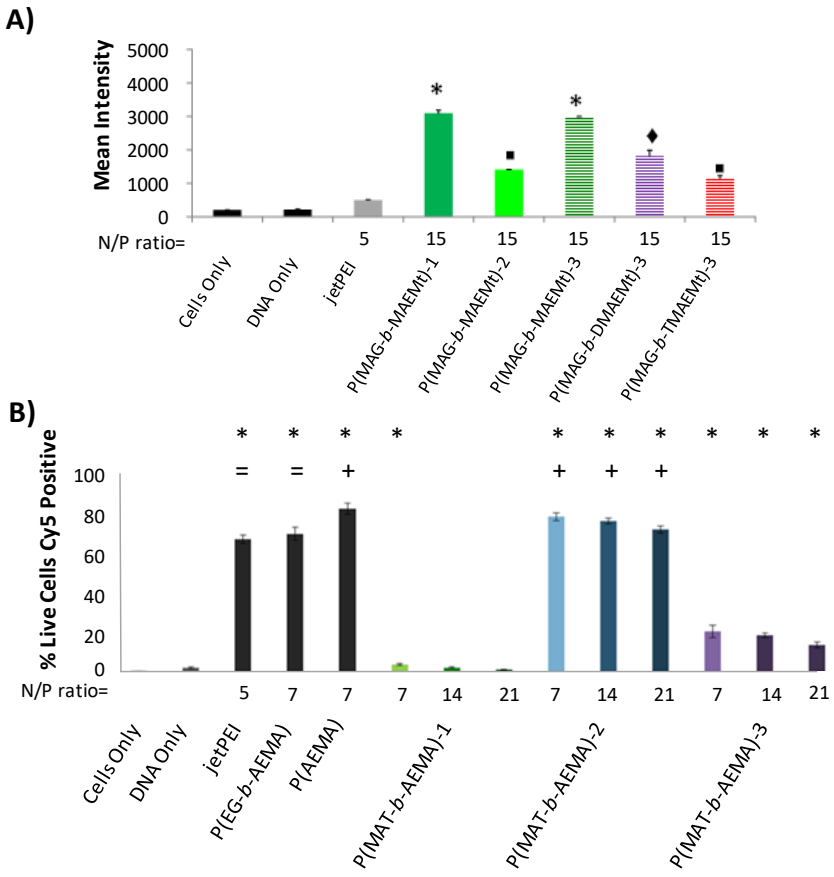

Figure 2.9. Flow cytometry analysis of pDNA-Cy5 cargo carried by A) P(MAG-*b*-methacrylates) and B) P(MAT-*b*-AEMA) into HepG2 cells. Cells were transfected using A) P(MAG-*b*-methacrylate) polymers and B) P(MAT-*b*-AEMA) in DMEM + 10% FBS. Error bas represent the standard deviation from three replicates. All measurements found to be statistically different (Student's t test $p<0.05$) as compared to cells only are marked with an *. Samples found to be significantly higher than the positive control jetPEI are marked with a +, and samples found to be statistically equivalent to jetPEI are marked with an = (according to Student's t-test with $p < 0.05$).

For the cellular internalization results, all samples were statistically compared to the negative control cells exposed to non-complexed pDNA. For

uptake of P(MAG-*b*-methacrylate) polyplexes (Figure 2.9A), P(MAG-*b*-MAEMt)-1 and -3 showed the highest uptake, while P(MAG-*b*-MAEMt)-2 uptake levels tapered off to about the same uptake as P(MAG-*b*-DMAEMt)-3 and P(MAG-*b*-TMAEMt)-3. P(MAG-*b*-TMAEMt)-3 showed the lowest Cy5 intensity among the polymers, but still showed significantly higher Cy5 intensity than both cells only and jetPEI. Although jetPEI usually demonstrates relatively high cell uptake, it is known that the presence of serum hampers jetPEI cell uptake.[125] This illustrates that polyplex interactions with transfection media plays an important role in gene delivery.

In Figure 2.9B, all but one polyplex formulation had higher Cy5 percentages than DNA alone, with P(AEMA) having the highest uptake, followed by P(MAT-*b*-AEMA)-2, then P(EG-*b*-AEMA) and jetPEI. P(MAT-*b*-AEMA)-2 at all three N/P ratios tested had the highest level of polyplex uptake when compared to the other trehalose block-co-polycations formulations (and were statistically superior to the positive control jetPEI in HepG2 cells), which correlates with the high gene expression seen in Figure 2.11 (*vide infra*). P(MAT-*b*-AEMA)-1 and -3 polyplexes have lower uptake compared with either P(MAT-*b*-AEMA)-2 with some formulations barely exceeding background levels. This trend suggests that more positive charge promotes uptake to a point, then begins to limit uptake. While it was expected that P(AEMA) polyplexes would have very high uptake due to its

high amount of positive charge, it was also predicted to be the most toxic. Surprisingly, we did not observe any effects of cell death with P(AEMA) polyplexes (at N/P = 7) and thus, this did not impact uptake values. Also, it should be noted that both P(MAT-*b*-AEMA)-2 and- 3 polyplex formulations at N/P=7 had cell uptake comparable to that of P(EG-*b*-AEMA).[116, 125]

2.3.6 Lyoprotectant Properties

To examine the polyplex formulations further, transmission electron microscopy (TEM) was used to image the formulations before and after lyophilization. Each of the polymers [P(MAT-*b*-AEMA)-1, -2, or -3] were mixed and allowed to complex with pDNA at N/P=10 in water for 1 h at 23 ˚C, then the sample was divided into two portions. The unlyophilized portions were imaged by TEM immediately (Figure 2.10a-c), and the lyophilized samples were imaged after reconstitution and resuspension (Figure 2.10d-f). For comparison, TEM images of P(MAG-*b*-MAEMt)-3 and P(MAG-*b*-DMAEMt)-3 both at N/P=15 are shown in Figure 2.10g-h.[83] Image analysis was used to quantify the polyplexes in the TEM images (Figure 7.21, Appendix). In addition, the lyophilized polyplexes hydrodynamic diameters were measured by DLS after one round of lyophilization (Figure 7.22A, Appendix) as well as an additional second round of lyophilization (Figure 7.22B, Appendix).

No significant size or shape differences were observed between the fresh polyplexes and those reconstituted following lyophilization. We have recently reported that polyplexes formed with P(MAT-*b*-AEMA) and siRNA maintained size and biological activity following lyophilization and resuspension. The particles appear slightly smaller in the TEM images than via DLS, likely due to a combination of dehydration of the particles during TEM sample preparation[135] and the preference of the negative stain for the highly-charged core of the particle.[136]

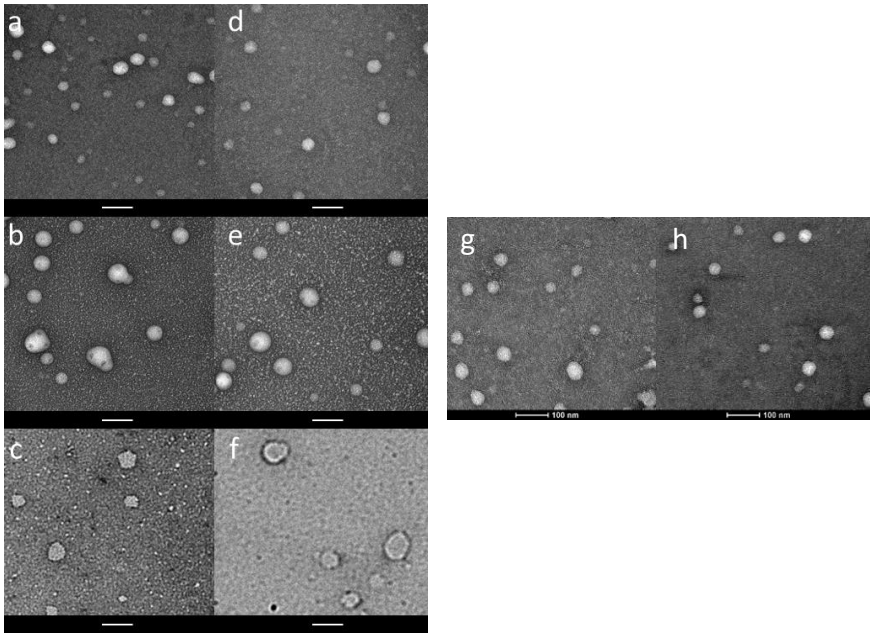

Figure 2.10. TEM images of polyplexes formulated with P(MAT-*b*-AEMA)-1 (a and d), -2 (b and e), and -3 (c and f), respectively, at N/P=10, as well as P(MAG-*b*-MAEMt)-3 (g) and P(MAG-*b*-DMAEMt)-3 (h) polyplexes at N/P=15. Polyplexes from (a, b, c) were imaged prior to lyophilization, with images (d-f) taken after lyophilization and reconstitution to original concentration in water. Polyplex samples (g-h) were prepared as usual in water with no lyophilization. Samples were negatively stained with uranyl acetate and all scale bars represent 100 nm.

Luciferase expression assays were completed as previously described except the assay was performed on U87 cells instead of HepG2 cells. The expression for each lyophilized polyplex sample was normalized to samples made with the same polymer that had not been lyophilized. Figure 2.11 shows this data as a percentage of gene expression retained for each round of lyophilization.

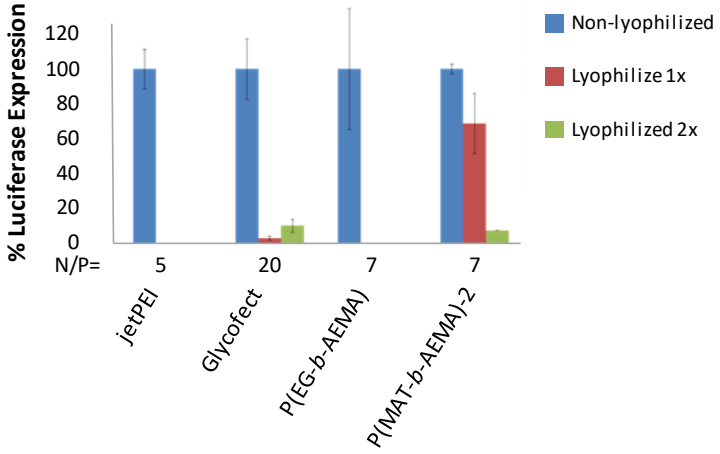

Figure 2.11. Luciferase expression in U87 cells following transfection with lyophilized polyplexes. Luciferase expression from lyophilized samples was normalized to the expression data from non-lyophilized polyplexes for each polymer. Error bars mark the standard deviation from triplicate measurements.

Following a single round of lyophilization and reconstitution, only the two polymers containing a sugar moiety, P(MAT-*b*-AEMA)-2 and Glycofect, retained any ability to transfect U87 cells. P(MAT-*b*-AEMA)-2 exhibited expression equal to 69% of its initial level while Glycofect was reduced to 4%. It is hypothesized that the P(MAT-*b*-AEMA) polyplexes form a core-shell structure with the trehalose-containing block coating the external surface of the polyplex, aiding polyplex stability during the lyophilization process. Neither Glycofect nor jetPEI polyplexes contain stabilization layers leaving these formulations susceptible to aggregation via the lyophilization procedure. Interestingly, the P(EG-*b*-AEMA) was expected to have a similar polyplex structure (containing a hydrophilic PEG

shell coating) to the P(MAT-*b*-AEMA)-2, however it did not retain transfection capability following lyophilization. The trehalose blocks appear to impart a unique protective property to polyplexes for potential lyophilization and storage.

2.3.7 In Vivo

Polyplexes formed from P(MAT-*b*-AEMA)-2 and pDNA had the highest level of gene expression in cultured cells *in vitro* and low toxicity at the three tested N/P ratios; these promising properties led to the selection and examination of this formulation *in vivo.* Murine studies with P(MAT-*b*-AEMA)-2 were explored for delivering luciferase-encoding pDNA with C57 black 6 (C57BL/6) mice. Tail vein injection was used to probe for biodistribution, toxicity, and transfection of the polyplexes in a living organism.

Mice treated via standard tail vein injections were administered with one of four polyplex formulations in 5% dextrose (D_5W, Figure 2.12) and a fifth control sample of D_5W only. Importantly, with all formulations, all mice survived to the 48 h endpoint of the study with no noticeable health deterioration. All mice were active and showed no signs of lethargy nor ill health effects after being dosed with up to 490 μg of polymer per mouse (the equivalent of 19.6 mg/kg of polymer/mouse). Following tail vein injection, the mice were then injected peritoneally with luciferin at 24 and 48 h after polyplex injection and imaged using a bioluminescence Xenogen Spectrum CCD camera system (data not shown).

Luciferase gene expression could not be detected either 24 or 48 h after the infusion of polymers. Following the 48 h imaging, all mice were euthanized and the heart, liver, lung, spleen, kidneys, and brain were harvested for analysis by qPCR to determine biodistribution of the pDNA cargo (Figure 2.12).[137] QPCR analysis of the DNA extracted from those tissues revealed a nearly uniform distribution of genetic material throughout the organs. On a per-cell basis, pDNA was found at a range of 1.1 - 10 plasmid copies per cell in each organ (values less than or equal to 1.0 copies/cell cannot be resolved from the background). Hydrodynamic injection of 25 µg of pDNA, discussed in further detail below, typically achieves delivery of ~100 plasmids per cell in the liver, leading to significant gene expression.[138, 139] The lower level of genetic material delivered to each of these organs following tail vein injection was insufficient to achieve observable gene expression.

Multiple cyanine fluorophores, including Cy7, have been used successfully to tag DNA cargos for *in vivo* imaging.[140-142] Using cyanine-3 labeled siRNA, Davis and coworkers have shown that tail vein-injected polyplexes begin urinary clearance within six min.[142] Here, to determine if the polymer and pDNA reached the tissues with similar distributions (indicative of intact polyplexes), P(MAT-*b*-AEMA)-2 was fluorescently labeled with Cy7 via amine-NHS coupling chemistry. Polyplexes were then formulated with P(MAT-*b*-AEMA)-2-Cy7 polymer and 25 µg

of pDNA at an N/P=7 and administered to mice via tail vein injections. Animals were imaged 15 min post-injection, euthanized, and the organs were harvested and imaged (Figure 2.12).

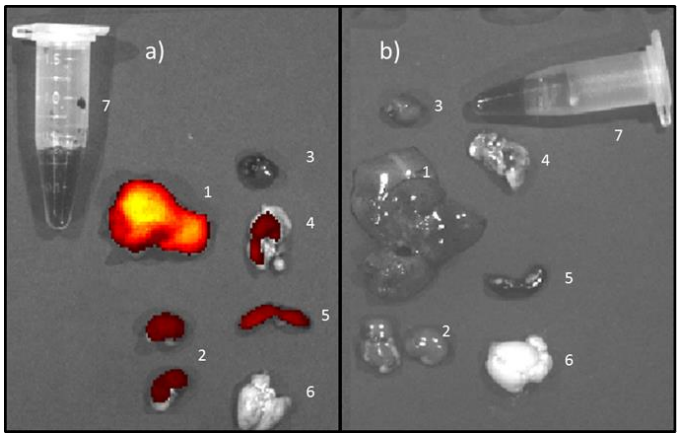

Tail Vein Injection Details					DNA in Organ (Average Plasmid Copies/Cell)					
	Polymer Dose (mg)	DNA Dose (µg)	N/P	Number of Mice	Liver	Brain	Spleen	Heart	Kidney	Lung
pMAT-co-AEMA 2	200.0	10	7	3	0.01	0.8	1.0	0.7	0.5	0.9
	390.0	10	14	3	0.80	0.9	0.3	0.8	0.1	2.9
	590.0	10	21	3	0.10	0.9	1.3	2.0	0.6	6.5
	490.0	25	7	3	1.60	0.9	0.5	1.0	0.1	1.1
5% Wt Dextrose Solution	-	-	-	2	0.2	0.1	0.1	0.2	0.1	1.0

Figure 2.12. Representative fluorescence images of organs harvested from a) a mouse injected via the tail vein with P(MAT-*b*-AEMA)-2-Cy7 polyplexes and b) a naïve mouse measured with a Xenogen Spectrum CCD camera system. Excised tissues: 1, liver; 2, kidney; 3, heart; 4, lung; 5, spleen; 6, brain; 7, blood. Part c) shows the injection parameters and calculates the average number of delivered pDNA copies per genome equivalent (i.e. per cell) as measured by qPCR of DNA from the imaged organs.

Fluorescence was observed in the liver, spleen, kidneys, and lungs of the mice injected with the P(MAT-*b*-AEMA)-2-Cy7 (Figure 2.12). Fluorescence was not observed in the blood, indicating that the polymers/polyplexes had fully cleared the blood stream (at the detectable level). As expected, the organs from the naïve mouse also did not show fluorescence, indicating that the fluorescence visualized in the experimental mice arose from the Cy7-labeled polymer and not from background fluorescence from the tissues.

Collectively, these data show that the concentration of plasmid delivered to each organ was insufficient to observe significant gene expression in the mice when delivered through a standard tail vein injection. Thus, a hydrodynamic injection technique was then examined to promote plasmid delivery specifically to the liver, wherein a large volume of DNA solution, typically 2 mL in a 20g mouse, is infused in 4-8 seconds.[139] More than 99% of the gene can be localized to the liver[143] as the high pressure appears to expand the liver endothelium promoting liver cell internalization and gene expression.[143-145] Typically, naked plasmid DNA is used with this injection technique and results in high signals of gene expression, ~ 10^{10}-10^{11} RLUs, in the liver when the firefly luciferase gene is placed behind a strong promoter such as the hybrid b-actin/cytomegalovirus (CAGGS) synthetic promoter (Scheme 1). The large volume injected combined with the high pressure has been found to strain the mouse, especially the cardiac

system[146, 147] and the liver; it takes 24 to 48 h for the liver to recover from the injection.[1, 4-5] However, while direct scale up of systemic hydrodynamic injection to larger mammals resulting in sustained transgene expression has yet to be achieved,[148] it may be potentially translatable if the high pressure injection is isolated only to the organ of interest and formulation of DNA into polyplexes could improve delivery and gene expression. For example, Itaka and coworkers were able to perform a hydrodynamic injection directed to skeletal muscle by injecting into a limb isolated with a tourniquet.[149] DNA delivered as a polyplex formulated from a PEG-poly-L-lysine cationic block copolymer showed increased expression and DNA lifetime in the tissue when compared to similar injections performed with naked pDNA.[149] Nakamura and coworkers performed hydrodynamic injection followed by a luciferase assay on excised liver tissue and found that polyplexes formed with jetPEI yielded higher luminescence than naked pDNA.[150]

Glycofect, jetPEI, and P(MAT-*b*-AEMA)-2 were used to deliver 10 μg of pDNA via hydrodynamic injection and compared to naked pDNA as a control (Figure 2.13e). All mice survived the high-pressure injections. To analyze gene expression, the mice were injected peritoneally with luciferin at 24 and 48 h and imaged with a Xenogen system (Figure 2.13c, d). Interestingly, jetPEI, despite being the most effective delivery vehicle in tissue culture, showed the lowest

level of luciferase expression in the liver of all tested formulations via live-animal imaging. The luminescence level was found to be 2-3 orders of magnitude below that of the naked pDNA. Even when the amount of DNA was more than doubled to 25 µg, the luminescence level was still 1 to 2 orders of magnitude below that of the control. Glycofect was the more effective of the commercially available transfection agents but still performed an order of magnitude below the control. Polyplexes formed with P(MAT-*b*-AEMA)-2 transfected at a higher level than either of the commercially available polymers and maintained the same level of gene expression as the naked pDNA control. Taken together, these results show that P(MAT-*b*-AEMA)-2 polyplexes are capable of delivering DNA that can subsequently be expressed *in vivo* with minor toxicity.

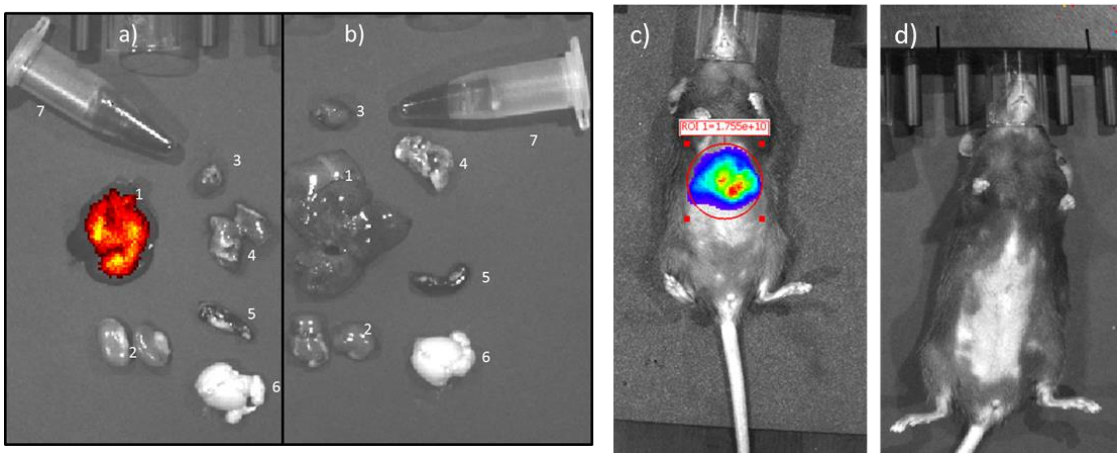

e)

Sample	Formulation	Dose pDNA (µg)	Luminescence 24 h (photons/ s)	Luminescence 48 h (photons/ s)
Glycofect	N/P: 3	10	2.50×10^{9} *	1.39×10^{9} *
jetPEI	N/P: 7	10	3.70×10^{7} *	8.52×10^{7} *
jetPEI	N/P: 3	25	4.53×10^{8} *	1.64×10^{8} *
P(MAT-*b*-AEMA)-2	N/P: 3	10	4.39×10^{10}	2.29×10^{10}
pDNA	N/A	10	3.95×10^{10}	8.93×10^{9}

Figure 2.13. Representative (N = 3) fluorescence images of organs harvested from a) a mouse hydrodynamically injected with P(MAT-*b*-AEMA)-2-Cy7 and b) a naïve mouse measured with a Xenogen Spectrum CCD camera system. Tissues: 1, liver; 2, kidney; 3, heart; 4, lung; 5, spleen; 6, brain; 7, blood. Luminescence mouse images c) after hydrodynamic injection with P(MAT-b-AEMA)-2 and subsequent treatment with luciferin and d) a naive control mouse measured with Xenogen Spectrum CCD camera system. The luminescence images are representative to that observed for N = 3 replicates. Table e) summarizes luminescence data over 48 hours with corresponding polyplex formulation. Luminescence levels were averaged from the values obtained from 3 mice in each data set and are reported in photons/second (s). Samples found to be statistically different (Student's t test) from P(MAT-*b*-AEMA)-2 were marked with an asterisk.

It appears that the majority of the pDNA was delivered to the liver due to the high levels of gene expression observed. Polyplexes were again formed using the Cy7-labeled P(MAT-*b*-AEMA)-2 and injected hydrodynamically for further verification the delivery of intact polyplexes to the liver. Animals were injected, imaged 15 min post-injection, euthanized, and the organs were harvested and imaged (Figure 2.13a,b). The liver was the only organ to show significant fluorescence, indicating that the polyplexes stay intact during the hydrodynamic experiment as polymer and pDNA are localized to the liver and are responsible for yielding high levels of gene expression.

2.4 CONCLUSION

Glucose- and trehalose-containing cationic block copolymers were synthesized and their colloidal stabilization and gene delivery properties were examined in detail *in vitro* and *in vivo*. The block copolymers bound pDNA and remained stable over time even in the presence of serum. Studies in tissue-cultured cells, however, indicated that both the cationic block length and polymer-pDNA ratio are important factors in determining toxicity, cellular uptake, and gene expression.

A comparable series of P(MAG-b-methacrylate) polymers was created to test the degree of pendant amine methylation as well as cationic block length. All polymers maintained a hydrodynamic diameter < 100 nm in serum solution as

well as a low toxicity profile. The P(MAG-*b*-MAEMT) polymers generally exhibited increased delivery efficiency as compared to polymers with more highly substituted amines. The P(MAT-*b*-AEMA) polymers also demonstrated high serum stability, low toxicity, and high levels of luciferase expression. In addition, they were also able to harness the unique property of trehalose as a lyoprotectant upon freeze-drying and resuspension, prompting *in vivo* studies of these formulations.[117]

To test the biodistribution and toxicity of these trehalose-stabilized polyplexes *in vivo* P(MAT-*b*-AEMA)-2 was selected for murine studies. The mice appeared to suffer no ill health effects after being dosed with up to 490 μg of polymer per mouse (the equivalent of 19.6 mg/kg of polymer/mouse). Quantitative PCR studies were conducted to measure the plasmid amount in six major organs. The amount of plasmid present was very low, especially when compared to plasmid levels in the liver following hydrodynamic infusion.[138, 139] The low level of polyplex uptake by all tissues was insufficient to achieve detectable levels of luciferase gene expression. The widespread and roughly equal distribution of the polyplexed plasmid suggested that the trehalose polyplexes were colloidally stable during circulation and offer an excellent design motif for further *in vivo* delivery experiments. To determine the *in vivo* stability of the polyplexes (whether the polymer retained its cargo upon delivery), the

polymer was fluorescently tagged and the mice and their organs were imaged. After 15 min of polyplex circulation, fluorescence was detected in the organs where pDNA was found but not in the blood, which was consistent with results that injected polyplexes are cleared into the urine within 6 min.[142]

A second injection method was then used to bypass extended circulation in the blood as a physical means to target polyplex delivery to a specific tissue. Accordingly, we performed a hydrodynamic infusion to force the majority of polyplexes to the liver,[143-145] which resulted in significant luciferase expression. Indeed, gene expression was comparable to that seen in previous work with diseased mouse models,[144] suggesting that genes coding for therapeutic proteins would also be expressed at high levels when complexed with P(MAT-*b*-AEMA)-2. Due to the large volumes required to perform hydrodynamic injection, it is difficult to expand the use of this delivery technique into higher mammal models.[148-150] Catheters are being explored to localize the high pressure to targeted tissues of interest, yet, it is still difficult to achieve sufficient pressure levels needed to promote successful naked plasmid delivery and gene expression *in vivo*. Polyplexing plasmids could offer a method to reduce the injection volume and pressure needed to maintain significant gene expression. To this end, we show that polyplexing pDNA does not appear to prohibit its delivery/expression through *in vivo* hydrodynamic delivery methods (in fact, higher gene expression was

observed) and shows promise to offer a way to formulate plasmids for direct catheter-based tissue administration. Overall, this work demonstrates the unique properties of trehalose for stabilizing polyplex formulations for lyophilization and delivery *in vivo*, important metrics for advancing new vehicles for clinical gene therapy applications. Additionally, these results illustrate that polyplex structure-function relies not only on how the polymer and pDNA interact, but can also be affected by the solution environment whether *in vitro* or *in vivo*. Future work is aimed at applying these biodistribution and expression methods to further study the P(MAG-*b*-MAEMt) polymers for *in vivo* gene therapy applications as well as to probe how carbohydrate-based block copolymer polyplexes function in the blood stream.

2.4.1 Appendix includes:

Polymer ^{1}H NMR spectra, polymer SEC chromatograms, P(MAG-*b*-methacrylate) kinetic studies, P(MAG-*b*-methacrylate) cell viability, cell uptake, and gene expression studies conducted in OptiMEM, quantitative analysis of TEM images, and DLS of lyophilized P(MAT-*b*-AEMA) polyplexes.

2.4.2 Acknowledgements

The authors of the P(MAG-*b*-MAEMt) publication thank Dr. Nilesh Ingle, Department of Chemistry, University of Minnesota, for consistent support to this work, and the Institute of Technology Characterization Facility, University of

Minnesota, a member of the NSF-funded Materials Research Facilities Network, for assistance in TEM imaging. We also thank the National Institutes of Health (NIH) Director's New Innovator Award Program (DP2OD006669-01) for partial financial support of this project. Also, this work was supported partially by the National Science Foundation through the University of Minnesota MRSEC under the Award Number DMR-0819885.

The majority of the polymer synthesis and film in situ characterization was performed by author Haibo Li, with TEM images contributed by Yaoying Wu. The cell culture work was conducted by Mallory Cortex with assistance from the author of this dissertation.

The authors of the P(MAT-*b*-AEMA) publication acknowledge funding of this project by the NIH Director's New Innovator Program (DP2OD006669) and the Camille and Henry Dreyfus Foundation to TMR. We acknowledge the use of UMN Bruker NMR spectrometers through the following statement: Research reported in this publication was supported by the Office of the Director, National Institutes of Health of the National Institutes of Health under Award Number S10OD011952. We acknowledge the financial support of NIH grants 1R01DK082516 and P01HD32652 to PH. The content is solely the responsibility of the authors and does not necessarily represent the official views of the

National Institutes of Health. All animal studies were performed under the IACUC Protocol #1202A09921 (PI: Hackett).

The majority of the polymer synthesis and film in situ characterization was performed by author Zachary Tolstyka, with contributions by the author of this dissertation. The *in vivo* work was led by Jason Bell with contributions by Zachary Tolstyka, Nilesh Ingle, Mallory Cortez, and the dissertation author. Cell culture was performed by Zachary Tolstyka with heavy contributions by Mallory Cortez and the author of this dissertation.

CHAPTER 3: GLYCOPOLYCATION-DNA POLYPLEXES ARE HEMOCOMPATIBLE, STABLE, AND AVOID NONSPECIFIC ORGAN INTERNALIZATION *IN VIVO*

Synopsis

Gene therapy via genome editing holds great promise for the cure of monogenic diseases; however, nonspecific tissue distribution limits the bioavailability and application of nonviral delivery methods. Herein, we characterize the hemocompatibility and biodistribution of three block copolycations containing a hydrophilic and neutral glucose block chain extended with cationic secondary amines of three lengths, poly(methacrylamido glucopyranose-*block*-2-methylaminoethylmethacrylate) [P(MAG-*b*-MAEMt)-1, -2, -3]. One block copolycation control, P(EG-*b*-MAEMt), and a second homopolymer control, P(MAEMt), were synthesized and the *ex vivo* hemocompatibility and *in vivo* biodistribution of the formulations were examined in detail. The block copolymer vehicles avoided hemolysis, but activated complement protein. *In vivo* distribution results suggest P(MAG-*b*-MAEMt)-2 polyplexes (N/P=5, 15) remained intact during circulation and avoided accumulation in six major organs, while P(EG-*b*-MAEMt) polyplexes were filtered out by mononuclear phagocytic organs. Avoiding non-specific organ capture can improve gene therapy efficacy by increasing genetic cargo bioavailability as well as decreasing expression in undesirable tissues.

This chapter was adapted with permission from the reference below:

1. Phillips, H. R.; Tolstyka, Z. P.; Hall, B. C.; Hackett, P. B.; Reineke, T. M. Glycopolycation-DNA Polyplexes are Hemocompatible, Stable, and Avoid Nonspecific Organ Internalization *In Vivo. In preparation.*

3.1 INTRODUCTION

Genome editing holds great promise for the cure of monogenic diseases such as cystic fibrosis, Duchenne muscular dystrophy, hemophilia A and B, and epidermolysis bullosa.[3-5, 151] However, tissue non-specificity limits the application of genetic therapeutics.[4, 20, 21, 152, 153] Viral vectors provide efficient delivery of genetic cargo. However, packaging limitations, occasional safety issues such as immune response, and the high costs associated with mass production of clinical-grade viruses for treating large patient populations are major issues.[17, 18, 154] Polymers with the ability to condense and protect genetic material offer a promising alternative to viral vectors. They are relatively easy to produce compared to viral vehicles, can safely package various plasmid sizes, and have shown significant uptake in a wide variety of human cell lines.[4, 17, 18, 20-22, 155] Nonviral vehicles, however, generally struggle to deliver therapeutic amounts of genetic material *in vivo* due to various systemic and intracellular transfection barriers.[20]

Colloidal stability is an important delivery vehicle characteristic for preserving cargo bioavailability. Additionally, the vehicle diameters must fall within a range of approximately 50-500 nm to avoid renal filtration and to achieve cellular endocytosis.[49] Vehicles must avoid swelling or aggregation, which can lead to disassembly or precipitation. Swollen vehicles expose their cargo to

nucleases that can digest the genetic payload as well as target the complexes for kidney filtration.[27] Aggregation also enhances trapping of enlarged particles in lung capillary beds.[4, 27, 29, 30] Opsonization, a particular aggregation process with blood serum proteins, also results in particles that are actively removed by the body's mononuclear phagocyte system (also called the reticuloendothelial system).[4, 26, 28]

Strategic polymer design can aid refinement of delivery vehicles that avoid aggregation and contribute other desirable properties such as stable DNA loading and protection, increased circulation time, low cytotoxicity, and high cellular uptake and consequently elevated gene expression.[20, 49] To condense and protect DNA, most polymer vehicles are cationic and bind anionic DNA via electrostatic interactions to form interpolyelectrolyte complexes (polyplexes).[156, 157] When polyplexes are formulated at an N/P ratio (ratio of charged nitrogen to charged phosphate units) greater than 1, there is a net positive charge, which increases association with negatively charged cell membranes and promotes endocytosis.[4] However, this positive charge can also lead to nonspecific protein interactions and aggregation.[2] In addition, higher N/P ratios often lead to increased cellular toxicity.[96, 158] Adding an uncharged hydrophilic block to a polycationic block forms a neutral and steric shell-like barrier around the cationic polyplex core to further protect the genetic material from degradation by

nucleases, decrease cell exposure to positive charge and nonspecific uptake, and prevent polyplex aggregation and premature blood clearance.[20, 31, 159] Through strategic polymer design, we created polyplexes that avoid aggregation, blood interaction, and non-specific tissue uptake.

Polyethylene glycol (PEG) is the most common neutral hydrophilic moiety used to increase polyplex biocompatibility, stability, and circulation time *in vivo.*[160-162] PEG “brushes” as small as 2 kDa can block electrostatic interactions between negatively charged proteins and positively charged surfaces, and attachment of PEG (i.e., PEGylation) to cationic polymers can prevent red blood cell hemolysis and decrease interaction with blood proteins such as fibrinogen and albumin.[161, 163, 164] PEGylation of polymer-DNA complexes generally improves biocompatibility compared to their non-PEGylated counterparts; however, it has made liposomes susceptible to accelerated blood clearance (ABC) after multiple doses.[165-167] The clearance is not likely due to autoantibody activity, but may be a result of either complement activation due to blood serum binding or IgM production against the PEGylated liposomes.[165, 167] Our lab specializes in developing biocompatible carbohydrate-based polymers that form colloidally stable, safe, and effective nonviral gene delivery vehicles.[31, 58, 70, 83, 94]

Carbohydrate-based polymers are often hydrophilic, nontoxic, and possess many hydroxyl groups for changing chemical and biological

functionality.[31, 70] We previously designed carbohydrate-based polymers able to overcome intracellular barriers that have also demonstrated the potential to overcome extracellular barriers[83] and have modified multiple sugars into monomers for Reversible Addition Fragmentation Chain-Transfer (RAFT) polymerization.[31, 94, 95] Gene delivery vehicles composed of poly(methacrylamidoglucopyranose-*block*-2-methylaminoethylmethacrylate) (P(MAG-*b*-MAEMt)) displayed colloidal stability in serum and avoided nonspecific cell interaction with blood *in vitro*.[159] By design, the sugar moieties are pendant to the polymer backbone, offering both hydroxyl groups for further chemical modification, such as the addition of targeting motifs, and accessible carbohydrate groups for cell surface receptor interaction.[70] We chain extended the glucose-based polymers using cationic monomers with secondary, tertiary, or quaternary pendant amines in order to test the effect of the degree of methylation on polyplex cytotoxicity and efficiency of gene delivery.[83] The glucose block, poly(methacrylamido glucopyranose) (P(MAG)), was shown to stabilize polyplexes in cell culture media. Polyplexes made with P(MAG) polymer containing secondary amine moieties, 2-methylaminoethylmethacrylate (P(MAG-*b*-MAEMt)), displayed the highest gene expression in both cell lines, and was selected for further study herein.

To further examine P(MAG-*b*-MAEMt) polyplex biocompatibility in more complex and relevant environments, this study aims to quantify the stability, hemocompatibility, and *in vivo* biodistribution of glycopolycation-DNA complexes in mice. Using P(MAG-*b*-MAEMt) polyplexes with increasing lengths of cationic MAEMt block denoted by a -1, -2, -3 suffix that previously demonstrated serum-stability and gene-delivery capacity, we measured polyplex interactions with blood components and observed the biodistribution of polymer and pDNA cargos in mice after intravenous injection. We were unable to detect any differences in hemocompatibility with varying cationic block length, although P(MAG-*b*-MAEMt)-1, -2, -3 polymer vehicles overall showed superior *ex vivo* hemocompatibility compared to analogous polycations containing PEG-based hydrophilic blocks (Figure 3.1). P(MAG-*b*-MAEMt)-2 polyplexes at N/P=15 also demonstrated stealth properties *in vivo* by avoiding capture by major organs in contrast to P(EG-*b*-MAEMt) polyplexes, which were trapped in the lungs, liver, and kidney (Figure 3.1). The results of this work generally support the importance of hemocompatibility studies and the ability for glucose-based vehicles to widely distribute *in vivo*; thus, offering a useful alternative to PEGylation for improving serum stability and systemic circulation for drug and nucleic acid delivery.

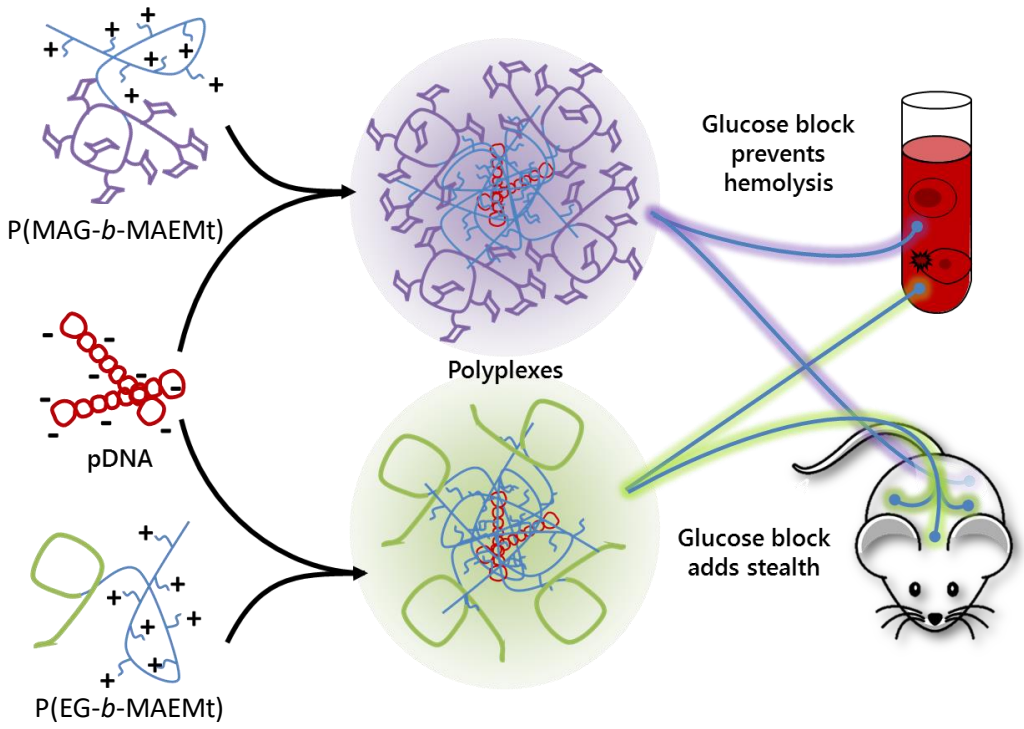

Figure 3.1. P(MAG-*b*-MAEMt) polymers and P(EG-*b*-MAEMt) polymers are complexed with pDNA to form their respective polyplexes. Polyplex blood interaction was tested *ex vivo* and biodistribution patterns were determined *in vivo*. P(EG-*b*-MAEMt) polyplexes at N/P=5 lysed red blood cells and were primarily trapped in the lungs, liver, and kidneys, whereas the P(MAG-*b*-MAEMT)-2 N/P=15 polyplexes did not lyse cells and distributed at low levels to all major organs.

3.2 EXPERIMENTAL

3.2.1 Materials and Methods

All chemicals or reagents were purchased from Sigma Aldrich (St. Louis, MO) unless specified. Cyanine7 NHS ester (Cy7) was purchased from

Lumiprobe (Hallandale Beach, FL). The control polymer jetPEI was purchased from Polyplus Transfection Inc. (Illikirch, France) and Glycofect was donated by Techulon (Blacksburg, VA). Dulbecco's Modified Eagle's Medium (DMEM), fetal bovine serum (FBS), phosphate buffered saline (PBS), and nuclease-free water were purchased from Gibco (Carlsbad, CA), and a sterile 5% dextrose by weight in water (D_5W) solution was purchased through DME Supply Group (Augusta, GA). Agarose powder and 10X tris-acetate-ethylenediaminetetraacetic acid (TAE) gel supplies were obtained from Fisher BioReagents (Hampton, NH). Plasmids (pT2/Cal) were prepared as previously described.[87]

3.2.2 Blood, Biological Reagents, and Animals

Human whole blood with and without 3.2% sodium citrate anticoagulant was purchased from Memorial Blood Centers (St. Paul, MN). Protamine sulfate was obtained from MP Biomedicals (Santa Ana, CA). Partial thromboplastin time-Lupus anticoagulant reagent (PTT-LA), Neoplastin Plus, and 25 mM $CaCl_2$ solution was purchased through Diagnostica Stago (Parsippany, NJ). The MBL oligomer kit (kit no. 029), the MicroVue C4d (kit no. A008) and the MicroVue Bb Plus (kit no. A027) kits were all purchased from Quidel (San Diego, CA), and the preactivated zymosan positive control was obtained through Complement Technology, Inc. (Tyler, TX). Ten week-old C57BL/6 mice were obtained through the National Cancer Institute (NCI, Frederick, MD) and housed in pathogen free

conditions according to the Association for Assessment and Accreditation of Laboratory Animal Care (AAALAC) requirements and fed a normal diet. Mice were handled per the Institutional Animal Care and Use Committee (IACUC) using an Institutional Biosafety Committee (IBC) approved protocol (1202A09921). Lysis buffer was purchased from Qiagen (Hilden, Germany), and proteinase K was obtained through Roche (Basel, Switzerland).

3.2.3 Instrumentation

^{1}H NMR spectra were obtained in D_2O at 23 °C using a Bruker Avance III HD 500 MHz spectrometer from Cambridge Isotope Laboratories, Inc. (Andover, MA), and analyzed the data on Bruker Top Spin 3.1 software. Polymer dispersity was analyzed using size exclusion chromatography (SEC) on an Agilent 1260 High Performance Liquid Chromatography instrument (Santa Clara, CA) with 1.0 wt% acetic acid/0.1 M Na_2SO_4 eluent at a 0.4 mL/min flow rate. The system used Eprogen (Downers Grove, IL) size exclusion columns, [CATSEC1000 (7 μ, 50×4.6), CATSEC100 (5 μ, 250×4.6), CATSEC300 (5 μ, 250×4.6), and CATSEC1000 (7 μ, 250×4.6)], a Wyatt Dawn Heleos-II light scattering module (λ = 662 nm), and an Optilab T-rEX refractometer (λ = 658 nm). Data were analyzed with Wyatt Technologies Astra VI software version 5.3.4.18 (Santa Barbara, CA). Fluorescent polymer tagging was quantified on a CUV 1 cm cuvette holder with a Mikropack DH-2000 Deuterium/Halogen TTC lamp from

Ocean Optics Inc. (Dunedin, FL), and data were analyzed using Ocean Optics Inc. Basic Acquisition Software.

DNA gels were visualized with a Spectroline BI-O-VISION Transilluminator (Westbury, NY) under the UV setting (312 nm) and imaged with a Samsung Galaxy S3 camera phone. Polyplex size over time was determined using a Brookhaven BI-200SM DLS system. The system included a Brookhaven Mini L-30 HeNe laser (637 nm), a Brookhaven BI-NDO detector, a Brookhaven TurboCorr correlator, and a decalin bath.

Hemoglobin absorbance was measured on a BioTek Synergy H1 hybrid plate reader (Winooski, VT) at 380 nm, 415 nm, and 450 nm. Morphology images were captured with differential interference contrast on an EVOS FL digital inverted microscope (Fisher Scientific, Pittsburg, PA), while all animal and tissue imaging was conducted on an IVIS Spectrum with an excitation wavelength of 710 nm, an exposure time of 3 sec, and absorbance wavelength at 780 nm. Images were captured using Living Image software (PerkinElmer Inc., Waltham, MA). Animal tissue was bead milled with a BulletBlender from Laboratory Supply Network, Inc. (Atkinson, NH). Quantitative polymerase chain reaction (qPCR) experiments were performed using an Eppendorf Mastercycler (Hamburg, Germany).

3.2.4 Synthesis and Characterization of Polymers

The MAG and MAEMt monomers and the P(MAG-*b*-MAEMt) polymers were synthesized and characterized previously (Figure 3.2A, new MAEMt monomer 1H NMR in Figure 7.29, Appendix).[83, 95, 168] The P(MAG-*b*-MAEMt)-1, -2, and -3 polymers were synthesized using radical addition-fragmentation chain-transfer (RAFT) polymerization for increasing lengths of time to generate increasing lengths of MAEMt blocks of 31, 42, 76 repeat units. The polymers were dialyzed for 4 days in water (MWCO 3500) and characterized by ^{1}H NMR and size exclusion chromatography with static light scattering analysis.

To synthesize the new P(EG-*b*-MAEMt) control for this study, we first synthesized a PEG chain transfer agent (CTA) by coupling a 2000 Da linear poly(ethylene glycol) methyl ether (mPEG, 4120 mg, 2.05 mmol, 1 eq) to a molecule of 4-cyano-4-(propylsulfanylthiocarbonyl) sulfanylpentanoic acid (CPP, 1130 mg, 4.07 mmol, 2 eq) in the presence of 4-dimethylaminopyridine (DMAP, 263 mg, 2.15 mmol, 1 eq) and N,N'-dicyclohexylcarbodiimide (DIC, 505 mg, 4.0 mmol, 2 eq). The reaction was solvated by 50 mL methylene chloride + 80 mL toluene and run at 0 °C for 12 h, then warmed to room temperature for another 20 h (Figure 3.2B). A crystalline byproduct, was filtered off and the golden yellow product was vacuum dried at 35 °C overnight (yield: 2219 mg, 42.3%).[169] The PEG-CTA was characterized by ^{1}H NMR (see Figure 7.30 Appendix). To chain

extend off the PEG macroCTA, 1 eq CTA (764 mg, 34 mmol) was mixed with 0.1 eq 4,4′-azobis(4-cyanopentanoic acid) (V501, 12.2 mg, 44×10^{-3} mmol) and 56 eq MAEMt monomer (2000 mg, 12 mmol) in 4:1 acetate buffer:ethanol at 70 °C for 14 hours under nitrogen atmosphere (Figure 3.2B-C). The polymer was purified by dialysis (3500 MWCO) in deionized water that was pH adjusted to 5-6 with 12.1 M HCl for 3 days, followed by lyophilization to dryness (yield: 0.9 g, 56%). The light yellow, flakey product was characterized by ^{1}H NMR and SEC (see Figure 7.31 and Figure 7.32, Appendix).

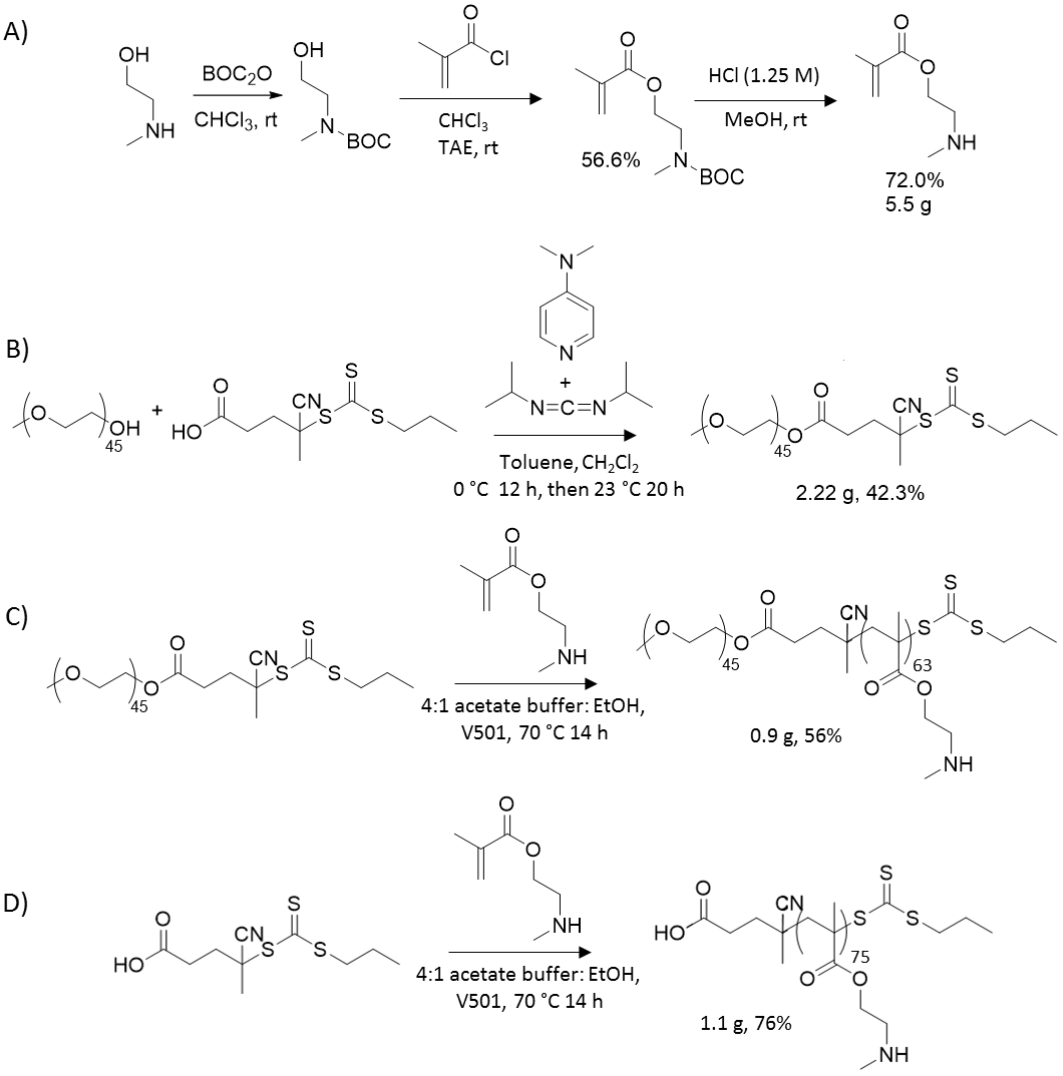

Figure 3.2. Synthesis of (A) MAEMt monomer and (B) PEG macroCTA. Polymerization of (C) P(EG-*b*-MAEMt) and (D) P(MAEMt).

The same reaction conditions used to prepare P(EG-*b*-MAEMt) were used to polymerize the homopolymer control, except that CPP was used in place of the PEG macroCTA (Figure 3.2D). CPP (1 eq.; 30.7 mg, 111 × 10^{-3} mmol) plus

0.1 eq. V501 (4.04 mg, 14.4×10^{-3} mmol) and 56 eq MAEMt monomer (1000 mg, 6.24 mmol) were dissolved in 4:1 acetate buffer:ethanol and reacted at 70 °C for 14 h under nitrogen atmosphere. The polymer was dialyzed (300-500 MWCO) in deionized water adjusted to pH 5-6 with HCl for three days. After dialysis, the product was lyophilized to dryness and characterized by SEC and ^{1}H NMR (Figure 7.32, Appendix).

3.2.5 Fluorescent tagging of Polymers

For *in vivo* studies, P(MAG-*b*-MAEMt)-2 and P(EG-*b*-MAEMt) were fluorescently labeled with a near infrared fluorescent tag, Cyanine7-N-hydroxysuccinamide (Cy7-NHS), via amidation of the NHS ester to a pendant amine. The ratio of Cy7 to MAEMt functionality was 1:50 for both polymers (P(MAG-*b*-MAEMt)-2: 0.00018 mmol Cy7, 0.0098 mmol N^{+}; P(EG-*b*-MAEMt): 0.00070 mmol Cy7, 0.035 mmol N^{+}). The reaction was carried out in a solution containing a 9:1 ratio of 0.1 M sodium acetate buffer to dimethylformamide (DMF). The mixture was vortexed and incubated for 4 h at 23 °C in the dark. The solutions containing the Cy7-labeled polymers were dialyzed exhaustively into DI water (3500 MWCO, pH adjusted to ~5 with 1 M HCl) for 48 h and lyophilized, yielding a blue powder. The degree of labeling with Cy7 was measured by UV-Vis (Ocean Optics, Inc.) absorbance at 750 nm using a solution of 0.2 mg/mL labeled polymer in water (Figure 7.33A, Appendix, P(MAG-*b*-MAEMt-2-Cy7): ε =

199000, A_{750}=0.166; P(EG-*b*-MAEMt)-Cy7: ε = 199000, A_{750}=0.355). Based on the absorbance measurements, the polymers were labeled at an efficiency of 1 Cy7 tag per 12.3 P(MAG-*b*-MAEMt)-2 polymer chains and 1 Cy7 to 9.7 P(EG-*b*-MAEMt) polymer chains. To verify that the fluorescence of the Cy7-tagged polymers is not quenched during polyplex formation, we compared the Cy7 fluorophore absorption of polyplexes to free Cy7-polymer (Figure 7.33B, Appendix).

3.2.6 Polyplex Preparation, Binding, and Size Studies

All polyplexes were formulated with pT2/CAL plasmid DNA (pDNA, 7537 bp) containing the firefly luciferase reporter gene.[170, 171] This plasmid design also included a *Sleeping Beauty* transposon and a CAGGS promoter known to promote high gene expression in vertebrate cells.[171]

To formulate polyplexes, pDNA was diluted to 0.02 μg/μL in D_5W. The overall volume varied based on the sample size needed for each experiment. The polymers were separately diluted with D_5W to the same total volume as the pDNA. However, to achieve the appropriate N/P, which is the molar ratio of ionizable amines to ionizable phosphates in the polyplex system, the concentration of polymer in solution varied according to the polymer molecular weight; the higher the N/P, the higher the concentration of cationic block in solution. P(MAG-*b*-MAEMt)-1, -2, -3 and P(EG-*b*-MAEMt) were each formulated

at N/P=5 and 15. Commercial controls, jetPEI and Glycofect, were formulated at N/P=5 and 20, respectively. Following dilution, polymer and pDNA solutions were filtered separately through a 0.2 μm sterile syringe filter and then polymer solution was added to an equal volume of pDNA solution. Polyplexes were incubated at room temperature for 1 h before use.

P(MAG-*b*-MAEMt)-1, -2, -3 polyplexes showed complete DNA complex formation at N/P=5 according to a previous gel electrophoresis shift assay (results summarized in Figure S4, Supporting Information).[83] This gel-shift assay was performed with the P(EG-*b*-MAEMt) polyplexes as well as the complexes made with the Cy7-tagged polymers using P(MAG-*b*-MAEMt)-2 as a control. A 1.2% agarose gel was prepared by dissolving 1.2 g of agarose in 100 mL of 1x TAE buffer and the solution was heated for 30 minutes. The solution was then removed from the heat and 10 μL of ethidium bromide (EtBr) was mixed into the solution, which was cooled for 5 min. The gel was poured and allowed to solidify for 1 h. While the gel set, polyplex solutions in D_5W were made for: pDNA only, jetPEI N/P=5, Glycofect N/P=20, P(EG-*b*-MAEMt) and P(MAG-*b*-MAEMt)-2 each at N/P= 5 and 15, P(EG-*b*-MAEMt)-Cy7 at N/P=5, and P(MAG-*b*-MAEMt)-2-Cy7 at N/P=5 and 15. The polyplex solutions prepared at 0.02 μg/μL pDNA in D_5W were allowed to complex for 1 h, then 45 μL of each sample was loaded into the

gel. The gel was submerged in 1x TAE buffer and run at 125 mV for 1.5 h and then visualized with the transilluminator (Figure 7.34, Appendix).

For size and stability analysis, polyplexes were made in D_5W solution. EtBr was added to solution and the EtBr fluorescence was measured at 526 nm (Figure 7.35, Appendix). To further assess polyplex stability in the prescence of protein, polyplexes were made in D_5W. After an intitial DLS measurement, phenol red-free Dulbecco's Modified Eagle's Medium (DMEM) containing 10% fetal bovine serum (FBS) by volume (both at room temperature) was added. Polyplex hydrodynamic diameters (HD) were measured by dynamic light scattering (DLS) over 2 h to determine if the polyplex sizes changed in this media.[2,16,19] 200 µL of each sample in D_5W were analyzed for 10 min with a 637 nm laser at 20 mW using 90° backscatter detection, then 400 µL of DMEM/10% FBS was added to the polyplex solution. A measurement was taken 10 min after serum addition, and recorded as t=0. Measurements were repeated once each at 60 and 120 min. The correlation functions were processed into size distribution curves using REPES analysis, and further discussion on data fitting and analysis can be found in the supporting information (Figure 7.36-Figure 7.48, Appendix). Peaks belonging to FBS protein were disregarded, and the polyplex peak in each sample was plotted.

3.2.7 Red Blood Cell Lysis and Morphology Analysis

Whole human blood in 3.2% sodium citrate anticoagulant was used to measure hemolysis. The whole blood was spun on an Eppendorf centrifuge 5810 R at 2400 x *g* for 20 min, and the plasma supernatant was transferred to a 15 mL centrifuge tube and flash frozen for use in the coagulation assays. Once separated from the plasma, red blood cell concentrate (RCC) was either used fresh or stored at 4 °C for up to 30 days.[172] The RCC was washed four times with ~2 mL of PBS at room temperature, then diluted 1:9 in PBS (700 µl RC: 6300 µl PBS). Aliquots (900 µL) of 0.1X RCC were mixed with 100 µL of each polyplex sample in triplicate: jetPEI N/P=5; Glycofect N/P=20; P(EG-*b*-MAEMt) at N/P=5 and 15; and P(MAG-*b*-MAEMt)-1, -2, and -3 each at N/P= 5 and 15. RCC was mixed with 100 µL of D_5W solution as a negative control since D_5W is isotonic with blood *ex vivo*, and one aliquot of 5 µL was added to 495 µL of sterile water as a 100% lysis positive control. All samples were incubated at 37 °C for 1 h. Following centrifugation at 3200 x *g* for 3 min at room temperature, 150 µL of the water sample was pipetted into a clear 96-well plate. 100 µL of each polyplex or D_5W sample was aliquoted and 50 µL of PBS was added. Absorbance was measured on a BioTek Synergy H1 hybrid plate reader at 380 nm, 415 nm, and 450 nm and the hemoglobin (Hb) concentration was calculated using the Harboe

method (Eqn. 1).[172, 173] Eqn. 2 was used to calculate percent hemolysis, and the data were normalized to the 100% lysis control.

$$\textbf{Eqn. 1}\quad Hb\left({}^{g}/_{L}\right) = [(167.2 * A_{415}) - (83.6 * A_{380}) - (83.6 * A_{450})] * \frac{1}{1000} * \frac{1}{dilution\ factor}$$

$$\textbf{Eqn. 2}\quad \%\ Hemolysis = \frac{Supernatant\ Hb\ (g/L)}{Total\ Hb\ (g/L)} * 100$$

To observe changes in red blood cell morphology with polyplex addition, naïve washed RCC was compared to RCC samples incubated with polyplexes. All samples sat for 1 h at 37 ˚C, allowing cells to settle into three layers, and 1.25 µL of cells were drawn from the opaque, cherry-red middle layer, diluted into 3 µL PBS on a glass microscope slide, and topped with a coverslip. All images were collected using the differential interference contrast setting on an EVOS FL digital inverted microscope.

3.2.8 PT and aPTT Coagulation Assays

Platelet poor plasma, hereon referred to as plasma, was separated from whole blood in 3.2% sodium citrate-coated collection tubes following centrifugation at 2400 x *g* for 20 min at room temperature. Plasma was either used immediately or flash frozen in liquid nitrogen and stored at -80 °C for up to 30 days. Polyplex solutions (100 µL) in D_5W were incubated with 900 µL of

plasma for 1 h at 37 °C. D_5W (100 µL) was used as a negative control for both the activated partial thromboplastin time (aPTT) and the prothrombin time (PT) assays. Data from either assay is a measure of the time it took for the sample plasma to coagulate, and is reported in seconds.

To observe coagulation in the aPTT assay, partial thromboplastin time-Lupus anticoagulant reagent (PTT-LA) reagent was prepared following the manufacturer's instructions. 100 µL of reagent was added to 100 µL of plasma sample mixture in a 35 mm Pyrex test tube in triplicate. Plasma incubated with D_5W was the negative control, while the positive control was made by incubating plasma with protamine sulfate (3 mg/mL in PBS). While protamine sulfate is normally used to trigger coagulation, in this case we used it at high concentration to induce coagulation factor dilution, which delays coagulation.[174] The tubes were warmed for 3-4 min in a 37 °C water bath. In a separate tube, 25 mM $CaCl_2$ solution was warmed to 37 °C. Once all samples and reagents equilibrated to 37 °C, 100 µL of warm $CaCl_2$ was added to one sample tube. The bottom of the tube was held in the 37 °C water bath to maintain consistent temperature, briefly lifted and tipped sideways for observation, then resubmerged into the bath. Time was kept from the moment $CaCl_2$ was added until a clot was seen in the tipped solution.

To test whether normal aPTT coagulation time could be restored, we ran a mixing assay where 50% more coagulation factor (via PPP) is added to the system. The original mixture of 100 µL PPP plus sample mixture, 100 µL PTT-LA reagent was divided in half, and 25 µL extra PPP was added to one of the test tubes. In addition, we also tested whether the addition of more contact factor, which is supplied by the PTT-LA reagent as particulate silica, would reduce the coagulation time back to normal range by adding 2x more reagent (50 µL) to the other test tube. 50 µL $CaCl_2$ was added to start coagulation, and clotting times were collected using the tipping method outlined above.

PT was measured using the same manual tube tipping method, but with different reagents. Instead of $CaCl_2$, Neoplastin reagent was prepared per manufacturer instructions, then warmed to 37 °C. Plasma samples were prewarmed in the water bath for 1 min without any additional reagent. To start coagulation, 200 µL of warm neoplastin was added to each sample tube, and PT was measured from time of reagent addition until visible clot formation. D_5W in plasma was again the negative control, but the positive control was made by diluting plasma with 3X the normal amount of neoplastin reagent. This effectively delayed clotting by diluting the protein that forms clots, plasma fibrin, without completely preventing clot formation.

3.2.9 Complement ELISA Assays

To screen the polyplex vehicles against complement activation, polyplexes were formulated in D5W as described before and allowed to incubate on hour at room temperature. Normal human serum was collected from human donors through the Memorial Blood Center (St. Paul, MN) as whole blood in tubes lacking anticoagulant. The blood was allowed to clot at room temperature for 30 min, and the tubes were centrifuged at 1500 g for 10 min. The serum was pipetted off the clot into 15 mL centrifuge tubes. Because it is projected that >10% of the general human population is mannose-binding lectin (MBL) deficient, it was important to weed out serum samples lacking MBL prior to screening MBL activation with our samples.[175] 5 uL of serum from each donor was pre-screened using an MBL oligomer ELISA kit purchased through Quidel, and all donor serum contained normal levels of MBL (data not shown). 10 uL of each polyplex sample was then incubated in 90 uL human serum for 1 h at 37 °C while gently rocking. Two additional control samples were prepared by incubating 90 uL serum with either 10 uL D5W or 10 uL zymosan (10.0 mg/mL). The serum + polyplex samples were then screened for C4 and Bb protein content using the respective ELISA kits (Quidel) following the instructions provided with each kit. The ELISA absorbance values were converted to protein content (ug/mL) and plotted thusly.

3.2.10 In Vivo *Biodistribution Studies*

To observe biodistribution, one of the glucose polymers and the control P(EG-*b*-MAEMt) polymer were fluorescently tagged with Cy7 as described above. These Cy7-tagged polymers formed Cy7-tagged polyplexes with pT2/CAL, which we used to fluorescently image whole mice and in extracted organs. To avoid subjecting the mice to undue stress and hemotoxicity, we tested the P(EG-*b*-MAEMt) control only at N/P=5, as the N/P=15 formulation aggregated in serum and lysed RBCs significantly. Control mice were dosed with D_5W only. For the glucose polymer, we observed that all the polymers regardless of cationic block length behaved similarly with blood components, so we chose the mid-length MAEMt block polymer, P(MAG-*b*-MAEMt)-2 to represent the glucose polymer series. We also knew from previous work that P(MAG-*b*-MAEMt)-2 gave the highest gene expression in HepG2 liver cells *in vitro.*[83]

To perform the biodistribution study, we formed polyplexes in D_5W, allowed them to complex for 1 h at room temperature as before, and injected 200 µL of the formulations into mice tail veins(pDNA concentration= 0.01 µg/µL). After euthanasia by CO_2, all organ imaging was conducted on an IVIS Spectrum with an excitation wavelength of 710 nm, an exposure time of 3 sec, and an absorbance wavelength of 780 nm. Measured fluorescence (Cy7) was expressed as radiant efficiency $(p/cm^2/s/sr)/(\mu W/cm^2)$. Mice were euthanized approximately

30 min post-injection, and blood samples were drawn by cardiac puncture. Mouse vasculatures were then perfused with at least 20 mL of D_5W. Mouse organs were collected, imaged 1 h post-injection, and stored in liquid nitrogen. Fluorescent heat maps were generated using IVIS Living Image Software. All images were simultaneously loaded with the Living Image Browser and regions of interest (ROI), in this case individual organs, isolated via the “Free Draw Method”. Each organ consisted of its own ROI where fluorescence is measured and reported in radiant efficiency/ROI pixel area. Radiant efficiency is defined as the ratio of emission light over excitation light. Plotting the fluorescence using radiant efficiency over ROI pixel area accounts for differences in both sample area and how the imager excitation light interacts with the irregular surface of the samples.

To determine the biological location of the second polyplex component, the pDNA, we purified DNA from mouse organs and measured the amount of cargo plasmid delivered using quantitative polymerase chain reaction (qPCR). First, organs were homogenized using the Next Advance Bullet Blender™ according to an adaptation of the instrument manufacturer’s protocol for liver homogenization. Briefly, we placed the whole organ (or both organs, in the case of the lungs and kidneys) into an Eppendorf tube. Then we added 2-3 large stainless steel beads (1.6 mm diameter), about 20 smaller beads (0.9-2.0 mm

blend), and 500 µL of lysis buffer (Qiagen) and ran the blender for 1 min. To extract the DNA, 20 µL (about 3 µg) of tissue homogenate from each organ sample was placed in a separate microcentrifuge tube with 665 µL lysis buffer and 15 µL proteinase K (Roche) (20 µg/µL) and digested overnight at 55 ºC on an elliptical rocker. DNA was isolated using a phenol chloroform protein extraction followed by ethanol DNA precipitation. Samples in a range of 200 – 1000 ng/µL of DNA were submitted to the University of Minnesota Genomics Core for qPCR analysis. The measurements were conducted using primers luc-F1 (sequence: TGAGTACTTCGAAATGTCCGTTC) and luc-R1 (sequence: GTATTCAGCCCATATCGTTTCAT). The fold increase in pDNA over background tissue readings was plotted.

3.2.11 Statistical Analysis

All values reported are the mean ± the standard deviation of measurements made in triplicate unless noted otherwise. All means were compared to a specified control with the Student's t-test using JMP Pro Software (SAS Institute, Cary, NC) through the University of Minnesota Supercomputing Institute. Results were considered statistically different from the indicated control if $p < 0.05$.

3.3 RESULTS AND DISCUSSION

3.3.1 Polymer Synthesis and Characterization

The MAG and MAEMt monomers and the P(MAG-*b*-MAEMt) polymers were previously synthesized via RAFT polymerization according to our published method.[83] The P(EG-*b*-MAEMt) control polymer was also synthesized via RAFT polymerization by using a PEG_{45}-CTA and chain extending with MAEMt monomers using the same reaction conditions used to make the P(MAG-*b*-MAEMt) polymers. The polymers were characterized via GPC, ^{1}H NMR, and SEC (Figures S1-S4, Supporting Information). Figure 3.3 summarizes the characterization data obtained for the diblock copolymers investigated in this study. P(MAG-*b*-MAEMt) polymers consisted of a constant MAG block length and the length of the MAEMt cationic block was systematically increased from 30 to 76 repeat units.

A)

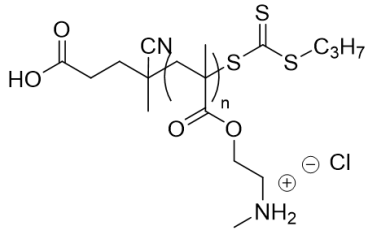

B)

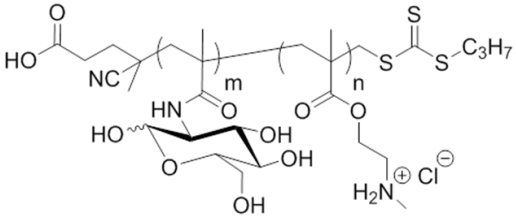

C)

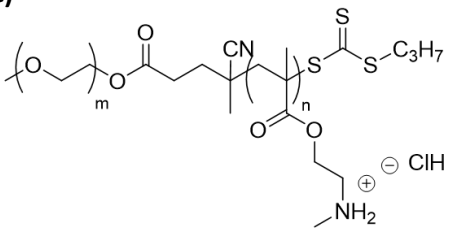

D)

Polymer Abbreviation	m DP	n DP	Mn (kDa)	Đ
P(MAEMt)	0	75	11.7	1.01
P(EG-*b*-MAEMt)	45	63	12.4	1.09
P(MAG-*b*-MAEMt)-1	51	30	18.3	1.02
P(MAG-*b*-MAEMt)-2	51	42	20.4	1.02
P(MAG-*b*-MAEMt)-3	51	76	26.6	1.05

Figure 3.3. Characterization summary for the polymers used in this study. (A) Structure of P(MAEMt$_n$). (B) Polymer structure of P(EG$_m$-*b*-MAEMT$_n$). (C) General structure of all P(MAG$_m$-*b*-MAEMT$_n$) polymers. (D) Polymer block degree of polymerization (DP) values for P(MAG-*b*-MAEMT)-1, -2, -3 and P(MAEMt) were determined using GPC while the P(EG-*b*-MAEMT) block lengths were determined using ^{1}H NMR. M_n and Đ for all polymers were measured by GPC/light scattering.

After Cy7-labeling P(EG-*b*-MAEMt) and P(MAG-*b*-MAEMt)-2, the degree of labeling was assessed by measuring the fluorophore absorbance using UV-Vis (Figure 7.33A, Appendix). The degree of labeling came to 1 Cy7 tag per 12.3 P(MAG-b-MAEMt)-2 polymer chains and 1 Cy7 to 9.7 P(EG-b-MAEMt) polymers. To ensure the polymer complexation process did not quench the Cy7 signal, fluorophore absorbance between free polymer and polyplexes were compared using UV-Vis (Figure 7.33B, Appendix). There was no significant difference in

absorbance between any polyplex formulation and the same concentration of free polymer in D_5W, so polymer complexation does not quench the Cy7 signal.

3.3.2 Polyplex Formation and Characterization

A gel electrophoresis shift assay was performed on all the Cy7-tagged polymers at the N/P ratios used for the animal study as well as the new P(EG-*b*-MAEMt) polymer at both N/P=5 and 15. The P(MAG-b-MAEMt)-1, -2, and -3 binding shift assay was previously published, but P(MAG-b-MAEMt)-2 at N/P=5 and 15, jetPEI N/P=5, Glycofect N/P=20, and pT2/CAL only samples were included as controls.[33] The binding shift assay confirmed that the P(EG-b-MAEMt) polymer as well as P(EG-b-MAEMt)-Cy7 and P(MAG-b-MAEMt)-2-Cy7 completely bound pT2/CAL plasmids even as low as N/P=5 (Figure 7.34, Appendix). The polymers bound pT2/CAL plasmids at both N/P= 5 and 15 ratios and those formulations were used for further characterization.[33] To further assess polyplex binding capability, an ethidium bromide (EtBr) exclusion study was performed (Figure 7.35, Appendix). All polyplexes prevented EtBr from intercalating the pDNA cargo as compared to a D_5W only negative control.

For effective delivery to tissues *in vivo*, polyplexes should maintain a consistent size over time in the presence of serum proteins in the blood and physiological salt concentrations. Polyplex aggregation and opsonization can cause premature clearance from the blood stream, immune response, and/or

cause polyplexes to collect in the lung capillaries.[4, 20, 26-28, 160] Polyplex size was measured in the presence of DMEM/10% FBS solution over 2 hours using DLS (Figure 3.4). Raw DLS traces are shown in Figure 7.36-Figure ***7.48*** included in the Appendix. Both jetPEI and Glycofect, cationic polymers not containing a protective neutral block, were found to aggregate upon incubation in the DMEM + 10% FBS solution. Once protein was introduced to the system, polyplexes made with P(MAEMt) and P(EG-*b*-MAEMt) aggregated at both N/P=5 and 15. In contrast, all polyplexes with a P(MAG) block maintained a relatively consistent hydrodynamic diameter of approximately 125 nm even upon addition of serum. All of the P(MAG-*b*-MAEMt) polyplex formulations were found to be colloidally stable, despite changes in N/P ratio and MAEMt block length, suggesting P(MAG) is able to shield polyplexes from aggregation.[31, 176]

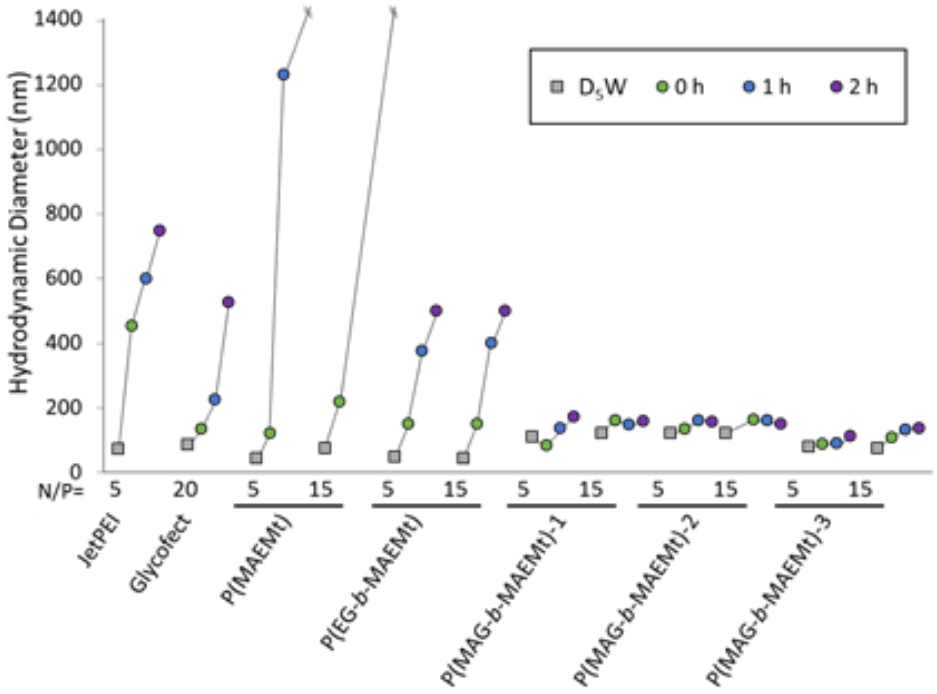

Figure 3.4. Polyplex hydrodynamic diameter in D_5W initially, then in DMEM + 10% FBS over time. The x-axis specifies polyplex polymer and N/P formulation. Peak end points were recorded at t=0, 1, and 2 h after addition of DMEM + 10% FBS to the samples. Each data point represents one ten-minute measurement. Note: The P(MAEMt) N/P=5 measurements at t= 1 and 2 h are of the particles remaining in solution after macroscopic particles settled out (based on visual observation).

3.3.3 Hemolysis and Red Blood Cells Morphology

Red blood cells (RBCs) compose the largest portion of whole blood and act as reliable *in vivo* toxicity indicators.[177] Accordingly, hemolysis and RBC morphology were examined to determine if polyplexes compromised RBC integrity. Polyplexes were formed in D_5W as described above. 100 µL of polyplex

solution in D_5W was incubated with 900 µL 0.1X RCC for 1 h at 37 ºC, and the supernatant from each sample was measured for hemoglobin release, which is proportional to the amount of RBCs lysed.[172, 173] Polyplexes formed with all three P(MAG-*b*-MAEMt) N/P=5 formulations, jetPEI, and Glycofect, did not lyse more cells than the negative control of RBCs incubated with D_5W (Figure 3.5A). The shorter of the three P(MAG-*b*-MAEMt) polymers at N/P=15 also failed to lyse red blood cells, but the polymer with the longest cationic block, P(MAG-*b*-MAEMt)-3, lysed cells at N/P=15. This formulation has the highest ratio of cationic charge:neutral glucose block, and it is known that particles with a net positive charge can disrupt cell membranes.[24, 25] P(EG-*b*-MAEMt) and P(MAEMt) polyplexes at both N/P=5 and 15 demonstrated statistically significant RBC lysis compared to the D_5W negative control.

To observe possible changes in RBC morphology, visual observations were made for all samples diluted into PBS and imaged under a digital microscope (Figure 3.5B, Figure 7.49, Appendix). No significant morphology changes were noticeable, and all cells had a normal disc-like shape with a dark central dimple. No lysed cells were visible using this method.

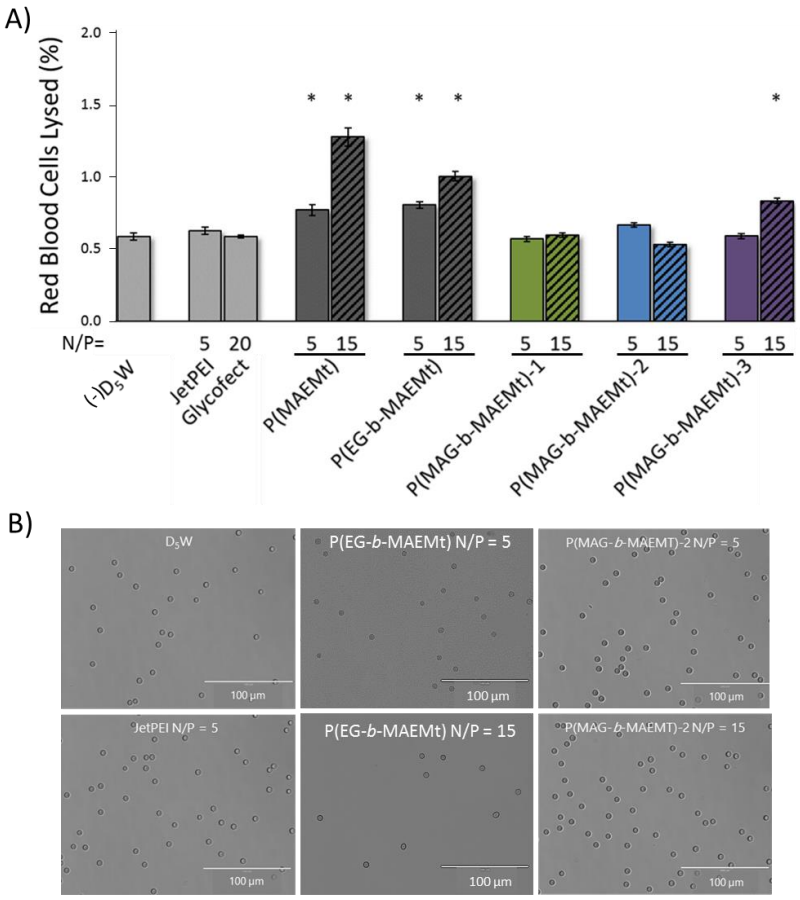

Figure 3.5. RBC lysis and morphology. (A) RBC lysis after one hour of incubation with polyplexes. Hemolysis is proportional to supernatant hemoglobin absorbance and is presented as the percent of RBCs lysed (based on a 100% lysis sample by incubating RBCs in water). Data are the mean of three replicates ± standard deviation with the polymer abbreviation and N/P values on the x-axis. An asterisk indicates a statistical difference between the sample and the D5W negative control according to a Student's t-test with $p < 0.05$. (B) Representative morphology microscopy images of RBCs incubated with select polyplex samples. No distinctive differences in morphology can be seen.

RBC lysis was likely caused by loss of cell membrane integrity after contact with the charged polyplexes, followed by an influx of solution. Neither jetPEI nor Glycofect visually altered RBC morphology or caused lysis, nor did any of the P(MAG-*b*-MAEMt) polymers at either low N/P ratio. Commercially available jetPEI is normally thought to be membrane lytic due to its high density of positive charge. However, Godbey et al. showed that that while free linear PEI polymer can permeabilize membranes, the lytic effect decreases when the polymer is complexed with DNA.[178] In a related study, Lambert and coworkers transfected human neural cells with PEI and confirmed that neural cell electrophysiological function was not affected, and thus the plasma membrane should be intact.[179] While the PEI dose was toxic to cells, this did not coincide with increased membrane permeability. Their lack of observed hemolysis further supports the conclusion that linear PEI did not lyse cell membranes when complexed to DNA at low concentrations. These results combined with the DLS study demonstrate that P(MAG-*b*-MAEMt) polymers do not cause destructive interactions with blood serum or cells at least at lower N/P ratios.

3.3.4 Coagulation

Plasma coagulation is an important blood function that can be altered even by polymers considered biocompatible. Heparin, for instance, is a common polyanion used to prevent coagulation and the formation of blood clots.[180] Other

polymers that are more structurally similar to our glycopolymer diblocks such as poly(amidoamine) (PAMAM) have been found to induce plasma clotting, while nanoparticles with a cationic galactose shell greatly delay coagulation.[92, 99, 101] Furthermore, glycoproteins naturally activate coagulation through two different enzymatic pathways - the partial thromboplastin and the prothrombin pathways.[181] Plasma coagulation was tested following 1 h polyplex incubation to ensure the delivery vehicles did not alter clot formation time. There are two pathways through which plasma may clot, the common, or intrinsic, pathway and the extrinsic pathway. As the pathway names suggest, the extrinsic pathway activates from external trauma that allows blood to escape the vascular system, while trauma internal to the vascular system triggers the intrinsic coagulation pathway through activation of platelets, collagen, and other biomarkers.[181] An aPTT test measures coagulation through the intrinsic pathway, and the PT assay tests the extrinsic pathway. Figure 3.6 compiles clot formation PT and aPTT from plasma incubated with our polyplexes.

The PT for all samples occurred within 12.5-14.5 sec, a normal range by comparison to the D_5W negative control, hence the polyplexes did not affect extrinsic coagulation (Figure 3.6A). In the aPTT assay, all diblock polyplexes at N/P=5 as well as jetPEI and Glycofect polyplexes presented normal coagulation times of about 40.0 sec (Figure 3.6B). Interestingly, the polyplexes made with the

P(MAG-*b*-MAEMt) polymers at N/P=15 significantly delayed coagulation time, while the block copolymer control, P(EG-*b*-MAEMt), did not affect coagulation. The homopolymer, P(MAEMt), likewise did not alter aPTT coagulation. There are several known causes of aPTT delay: antibody production, unfractionated heparin treatment (UFH), coagulation factor deficiency, and contact factor deficiency.[182] Indeed, antibodies are not a factor in these assays as all platelet poor plasma (plasma) samples were prescreened before use to ensure they clotted in a normal time frame. For the same reason, plasma samples that may have been exposed to UFH were not used in these experiments. In this case, depletion of clotting factors in the plasma or depletion of contact factor in the thromboplastin reagent (Neoplastin Plus from Diagnostic Stago) are the two potential causes of coagulation delay. Others have shown that addition of PEG to surfaces that normally trigger coagulation on contact can prevent contact factor activation.[100] It is likely that polyplexes at higher N/P ratios delay coagulation by capturing either coagulation factor from the plasma or the negatively charged contact factor included with the PTT-LA reagent (particulate silica, in this case).

To test this hypothesis, a mixing study was run where key coagulation components were added back to plasma samples showing poor coagulation ability. Plasma samples incubated with block glycopolymers at N/P=15 were split in half, either more plasma or more reagent (containing silica contact factor) was

added to the test tube, and coagulation times were recorded. If the polyplexes depleted coagulation factors or contact factors in the aPTT, the re-addition of that component should return coagulation time to normal. Adding twice as much reagent to the samples decreased coagulation time for all samples, but only the addition of more plasma completely restored a normal aPTT (Figure 7.50, Appendix). This suggests that P(MAG-b-MAEMT) N/P=15 polyplexes deplete both coagulation and contact factors. It should be noted that while the PT and aPTT assays are valuable measures of biomaterial effects on coagulation, these conditions do not exactly mimic *in vivo* conditions, and thus this assay serves as a model system only that should be coupled with further *in vivo* studies (*vide infra*).[100]

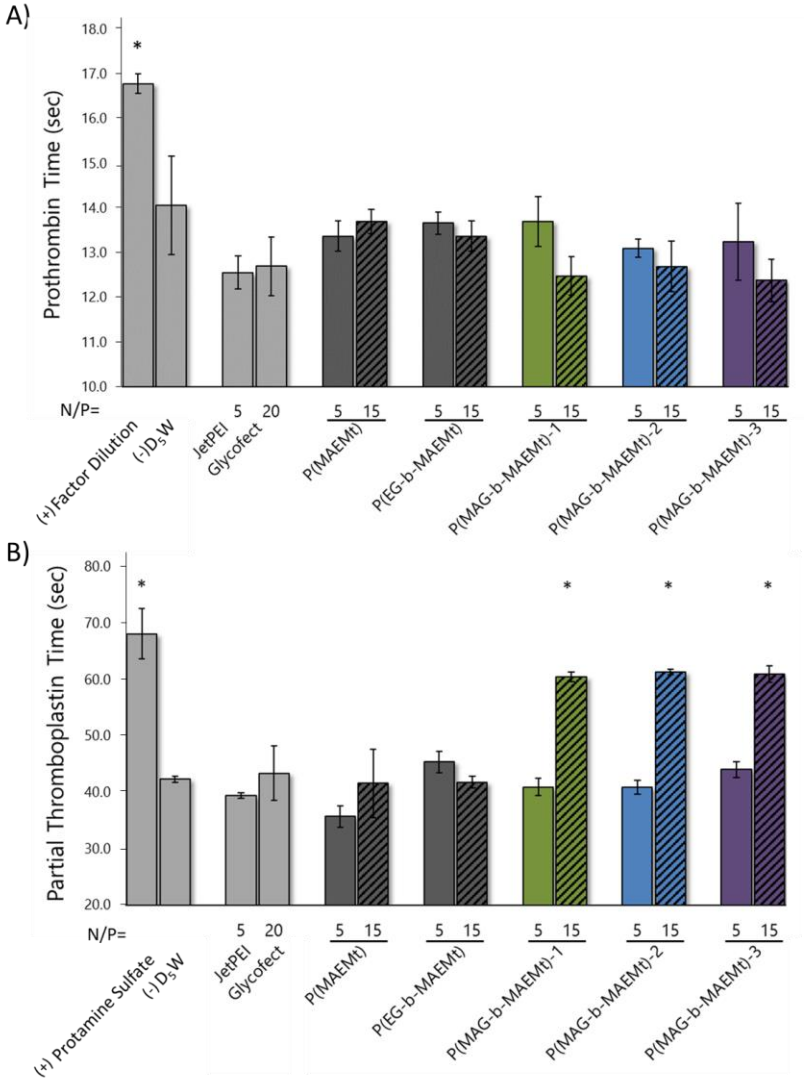

Figure 3.6. Determination of polyplex effects on blood coagulation. (A) The effect of polyplex incubation as a function of N/P ratio (numbers on x-axis) on coagulation through the PT extrinsic pathway. (B) Coagulation time (sec) of blood plasma samples via the aPTT intrinsic pathway after incubation with each polyplex sample for 1 h as a function of N/P ratio (numbers on x-axis). All data are presented as the mean number of seconds ± standard deviation with an asterisk denoting and variation from the negative control according to the Student's t-test with $p < 0.05$.

3.3.5 Complement Activation

The complement system is a form of innate immunity in which complement proteins found in the blood can be activated by contact with foreign material and initiate an enzymatic cascade to remove that material. Complement activation can lead to material rejection, inflammation, antibody mediated injuries, and even cardiovascular distress due to hypersensitivity reactions.[183-185] It is crucial to test whether biomaterials activate complement pathways as a safety measure. Complement activation of the formulations was tested by incubating polyplexes with complement protein found in human serum and then exposed the serum to animal erythrocytes (red blood cells). If complement proteins were activated, they would lyse the red blood cells. Because there are three different pathways through which activation can occur, activation of each pathway was measured separately using experimental conditions unique to each pathway. The results of the complement screen are presented in Figure 3.7.

The three different pathways through which complement activation can occur are the classical pathway (CP), the mannan-binding lectin pathway (MBLP), and the alternative pathway (AP).[186, 187] These pathways converge with the activation of complement component 3 (C3). The CP is typically activated through contact with immune complexes such as immunoglobulins or with lipopolysaccharides.[186, 187] The MBLP can be activated by mannose

polysaccharides displayed in certain patterns.[186] Since it is possible for activation to occur through any pathway, the polyplexes were screened against all three pathways.[188]

CP and MBLP activation initiate through the same processes before diverging to their final forms. Figure 3.7A show the amount of complement component 4d (C4) protein produced by serum incubation with all the polyplex samples as well as a D_5W negative control, and a positive control made by incubating serum with zymosan, a polysaccharide derived from yeast known to activate all three complement pathways.[189, 190] Since C4 protein is common to both the CP and the MBLP, we cannot determine which pathway the polyplex vehicles activate. Future work could repeat the screen using C1q-depleted serum, which would prevent any activation through the CP.[190] If polyplexes still generate C4 protein, then they would be activating the MBLP.

AP activation is known to occur through non-specific covalent binding through nucleophilic groups such as pathogen-associated molecular patterns (PAMPs) normally found on microorganisms to C3.[187] Compared to the D_5W negative control, all tested polyplex formulations significantly activated complement via the AP (Figure 3.7B), although the sample activity levels did not approach the level of complement Bb protein (Bb) produced by the positive control, zymosan. This suggests that complement activation exists on a

spectrum, and that complement activation could be mitigated by cellular and humoral inhibitors *in vivo*.[186] It is known that hydroxyl groups on the surface of biomaterials amplify AP activity.[191] Toda et al. demonstrated that amino groups can only activate the AP indirectly through proteins adsorbed on the material surface.[188] This could be a possible activation mechanism for polyplexes that do not contain –OH groups available for covalent binding to C3 such as jetPEI and P(EG-*b*-MAEMt). Indeed, while the PEG block has an hydroxyl group at the terminus of the polymer, work by Hamad et al. has shown that PEG still activates the AP by binding ficolin protein even if the terminal alcohol is acetylated.[190]

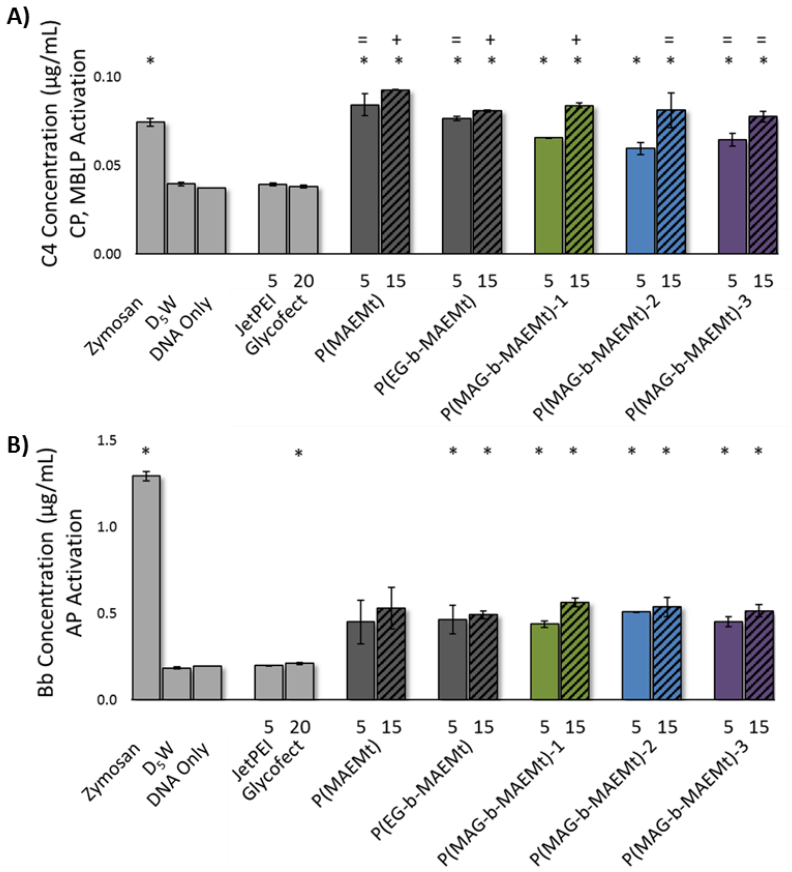

Figure 3.7. Complement activation as assessed using ELISA screens for the production of pathway activation marker proteins. (A) C4 protein is a marker for CP and MBLP activation. Samples that significantly differ from D_5W are marked with an (*). Samples that exceed the positive control, zymosan, are marked with a (+), and samples that statistically equal zymosaon are marked with an (=). (B) Bb protein is an activation marker for the AP. No sample statistically rivaled the positive control, and samples that significantly exceeded the D_5W sample are marked with an (*). Each sample was run in duplicate and the error bars represent the standard deviation. Statistical markers were determined using a Student's t test ($p < 0.05$).

3.3.6 Biodistribution

To understand the biodistribution of polyplexes *in vivo*, P(MAG-*b*-MAEMt)-2 was selected as the most promising formulation due to its stability in biological media and compatibility with human blood. For comparison, the control polymer, P(EG-*b*-MAEMt) was also selected to further understand vehicle stability and compatibility for tail vein administration in mice. Vehicle distribution through the blood is a passive process, so polyplexes must circulate unobstructed through the organism vasculature to reach tissues of interest.[4, 28, 29] During circulation, they must also avoid nonspecific protein aggregation, opsonization, disassembly, or immune system activation.[4, 27, 29, 30, 49, 192] Only after avoiding all these mechanisms the body uses to identify and remove foreign material can the vehicles reach their intended target tissues. Examining every possible polyplex fate is outside the scope of this study, but future studies to further understand the causes of P(MAG-*b*-MAEMt) polyplex distribution and their effect on genetic cargo expression may prove useful. For the current study, vehicle distribution to six major organs were assessed; a lack of polyplex (polymer and pDNA) aggregation in specific organs is a strong indicator of stability, biocompatibility, and stealth nature *in vivo*.

One general strategy for avoiding nonspecific uptake and prolonging circulation, which increases the chance of target tissue uptake, is to incorporate

hydrophilic block copolymers into delivery vehicles.[193-195] The lack of P(MAG-*b*-MAEMt) interaction with blood components suggests the complexes would remain intact during circulation, but because the polymer and genetic cargo are not covalently linked, the biodistribution of both the polymer and pDNA were measured individually. Both P(MAG-*b*-MAEMt)-2 formulations were selected for further study *in vivo* as the mid-length MAEMt block gave the highest gene expression in previous cell studies.[83] P(EG-*b*-MAEMt) at N/P=5 was chosen as the negative polymer control. Both P(MAG-*b*-MAEMt)-2 and P(EG-*b*-MAEMt) polymers were tagged with a Cy7 fluorophore to allow deep tissue imaging in organs, as Cy7 is a near-infrared emitter, and then were complexed with pDNA and injected into mouse tail veins. Following tail vein injection, the mice were imaged for Cy7 fluorescence, and then were euthanized after 30 min. Their major organs were excised and imaged *ex vivo* as a measure of polymer biodistribution and PCR analysis was performed to analyze for the amount of plasmid in the tissues.

Six major organs in addition to blood were collected: the heart, brain, liver, lungs, kidneys, and spleen. Organs were imaged *ex vivo* (Figure 3.8A and Figure 7.51, Appendix), and radiant efficiency was quantified for each organ (Figure 3.8B). Background autofluorescence in the negative control (D_5W only) mice was measured at approximately 5.0×10^8 for all organs (blood was not plotted due to

low fluorescence in all samples). P(EG-*b*-MAEMt) polymers were found at high levels in the liver, which is the most active organs in the mononuclear phagocytosis system.[16] It has been shown that PEGylation using linear molecules of at least 2000 Da help nanoparticles avoid macrophage capture,[26, 196] but it is likely some polyplexes were still captured by macrophages in the liver. P(EG-*b*-MAEMt) polyplexes were also found in the lungs and kidneys, which suggests they were not totally stable against protein opsonization, so they aggregated and were either trapped in the lung capillaries or filtered out by the kidneys.[27, 197]

The fluorescent polymer data shows that P(MAG-*b*-MAEMt)-2 at N/P=5 and 15 distributed evenly in all organs except the liver. P(MAG-*b*-MAEMt)-2 at N/P=15 was the only formulation to successfully avoid capture by any one organ. P(MAG-*b*-MAEMt)-2 N/P=5 distributed in the same way as the higher N/P formulation except with much higher polymer fluorescence in the liver. Although the liver is a mononuclear phagocytosis organ, the lack of signal in the spleen, which is also rich in macrophages, for this polyplex formulation suggests a separate mechanism of capture not solely related to phagocytosis by macrophages.[187] It is possible that the P(MAG-*b*-MAEMt) N/P=5 polyplexes disassociated in the liver and were unable to circulate further, as has been demonstrated with PEGylated polyplexes previously.[197] In fact, increasing the

amount of polymer in the formulation to an N/P ratio of 15 decreases liver uptake to near-background levels. . It is striking that simply increasing the amount of polymer in the formulation leads to a drastically different polyplex distribution pattern. The reason for the specific differences in tissue uptake cannot be fully explained from these data, but is worth further exploration.

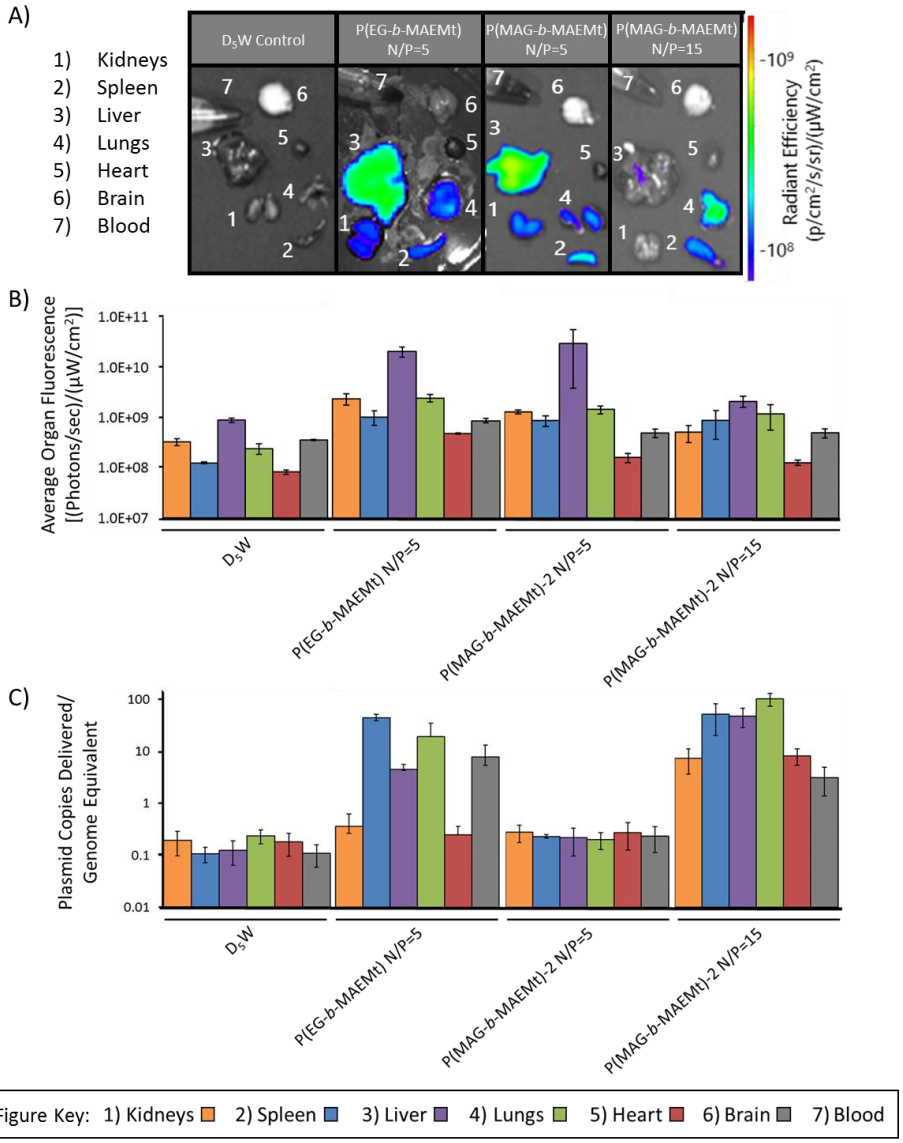

Figure 3.8. Summary of biodistribution data. (A) Representative fluorescent mouse organ images for each sample exhumed at one hour post-injection: 1) kidneys 2) spleen 3) liver 4) lungs 5) brain 6) heart 7) blood. (B) Organ fluorescence in radiance efficiency was plotted by organ and polyplex sample. Each data point is the average of n=5 samples (D_5W samples have an n=3) and error bars represent the standard deviation. (C) DNA was extracted from the harvested organs and analyzed by qPCR. Each data point is the average of an n=5 (D_5W samples have an n=3). The amount of plasmid delivered to each organ was normalized to the amount of genomic background level to normalize for organ mass. Error bars represent the standard deviation.

The amount of genetic material delivered to each organ was measured by qPCR (Figure 3.8C). The relative distribution of pDNA with the P(EG-*b*-MAEMt) and P(MAG-*b*-MAEMt)-2 N/P=5 samples do not correlate with the polymer distribution seen in Figure 5B. Figure 5C shows that with the P(EG-*b*-MAEMT) carrier, high levels of pDNA were found in the spleen and lungs, and moderate levels in the liver. The localization of pDNA in the lungs after delivery by P(EG-*b*-MAEMt) is likely due to polyplexes becoming trapped in the capillaries.[27, 197] With P(MAG-*b*-MAEMt)-2 N/P=5 delivery, there was no pDNA detected in any of the organs. This supports our hypothesis that these polyplexes disassociate in the liver and/or kidneys, leaving the pDNA to be cleared by the kidneys (the pDNA was likely excreted by the urine, but no urine samples were taken to support that theory).[142, 197] The distribution of pDNA with P(MAG-*b*-MAEMt)-2 N/P=15 shows some uptake into all six organs with slightly higher uptake in the liver, spleen, and lungs. To reach all the organs, P(MAG-*b*-MAEMt)-2 N/P=15 must have more stable during circulation than the N/P=5 formulation with the same polymer. This agrees with previous hemocharacterization and DLS data showing P(MAG-*b*-MAEMt)-2 N/P=15 to be stable against protein aggregation and relatively benign in human blood, which are both good functions for promoting stealth circulation *in vivo*.

Together, the data in Figure 5 suggest that P(MAG-*b*-MAEMt)-2 polymer at higher N/P formulations is a useful stealth material to promote pDNA delivery *in vivo*. P(MAG-*b*-MAEMt)-2 N/P=15 appears to be the best polyplex formulation for stable circulation and avoiding organ capture. Further studies are necessary to better understand these distribution patterns and the glycopolyplex physiochemical parameters necessary to achieve desired biodistribution, particularly for future targeting endeavors.

3.4 CONCLUSION

In this work, the contribution of a hydrophilic glucose block to the hemocompatibility and biodistribution pattern of the cationic polymer gene delivery vehicles *ex vivo* and *in vivo* was assessed. The glucose block copolycations, P(MAG-*b*-MAEMt)-1, -2, and -3, formed polyplex formulations with pDNA that were colloidally stable from aggregation in physiological salt and serum conditions as determined by DLS. P(MAEMt) and P(EG-*b*-MAEMt) were synthesized as controls, and unlike the glucose systems, aggregated (according to DLS measurements) under the same physiological salt and serum conditions. P(MAG-*b*-MAEMt)-1, -2, and -3 polyplex samples were exposed to human blood and did not cause red blood cell lysis (except for P(MAG-*b*-MAEMt) N/P=15) nor a visible effect on cell morphology, indicating formulation hemocompatibility. In contrast, the P(MAEMt) and P(EG-*b*-MAEMt) control polyplex formulations lysed

cells even at a lower N/P ratio of 5. Some aPTT coagulation interference was detected for all glucose block copolymers at N/P=15, and all polyplex formulations activated the complement system via the CP/MBLP. Cy7-tagged polyplexes were administered to mice via the tail vein, and biodistribution of the polymer and pDNA was measured by fluorescent imaging and qPCR, respectively. P(MAG-*b*-MAEMt)-2 (N/P=15) polyplexes (polymer and pDNA) avoided capture by any particular organ (low distribution in all organs), while the control vehicles consisting of P(EG-*b*-MAEMt) and P(MAG-*b*-MAEMt)-2 at N/P=5 localized to the spleen, kidneys, lungs. This supports our hypothesis that the lower N/P formulations disassembled in either the liver or kidneys.[142, 197] The P(EG-*b*-MAEMt) pDNA cargo found in the lungs is possibly due to the polyplexes being trapped in the lung capillaries.[4, 27, 29, 30]

Collectively, these results support our hypothesis that P(MAG-*b*-MAEMT)-2 (N/P=15) is a stable, hemocompatible, and stealthy vehicle formulation that avoids nonspecific lung and liver capture and shows promise compared to PEGylated alternatives such as P(EG-*b*-MAEMt). This work increases the understanding of nonviral gene delivery vehicle structure-function relationships and supports that carbohydrate-based blocks offer a more stable and functional alternative for stealth properties than linear PEG derivatives. Indeed, fine-tuning the formulation could allow for passive targeting of these stable formulations to

tumors or the addition of targeting moieties may facilitate tissue delivery specificity. Further work to measure circulation time, the effects of repeated dosing, and the unique distribution patterns of these vehicles is underway.

3.4.1 Appendix includes:

Supplemental synthetic and characterization procedures; ^{1}H NMR spectra, UV-Vis, SEC chromatograms, gel electrophoresis shift assays, dynamic light scattering; additional information about coagulation studies and biodistribution.

3.4.2 Acknowledgements

The authors acknowledge the NIH Director's New Innovator Program (DP2OD006669) and the Camille and Henry Dreyfus Foundation for funding this work. UMN Bruker NMR spectrometer research reported in this publication was supported by the Office of the Director, National Institutes of Health of the National Institutes of Health under Award Number S10OD011952. We also acknowledge the financial support from NIH grants 1R01DK082516 and P01HD32652. The content is solely the responsibility of the authors and does not necessarily represent the official views of the National Institutes of Health. The authors would also like to thank the Fairview Hospital Special Coagulation Clinic and the University Genomics Core at the University of Minnesota for research support. We would also like to acknowledge work done using the IVIS Spectrum

in vivo imaging system at the University of Minnesota – University Imaging centers, http://uic.umn.edu.

The P(MAG-*b*-MAEMt) polymers were previously synthesized and characterized by Dr. Haibo Li. All new material syntheses and characterization as well as all *ex vivo* work was conducted by the author of this dissertation. The *in vivo* study was led by the dissertation author with contributions by Zachary Tolstyka and Bryan Hall.

CHAPTER 4: CARBOHYDRATE-BASED BIOCOMPATIBILE EPOXY RESIN THERMOSETS FOR FIBROBLAST CELL PROLIFERATION

Synopsis

Chapter 4 covers the synthesis and characterization of two new carboxylic acid hardener materials and the polymer thermoset films they form after curing with epoxidized soybean oil. The hardeners, derived from trehalose (TR) and beta-cyclodetrin (CD), were functionalized with heptanoyl chloride (HP) and succinic anhydride (SA) and then homogenously formulated with epoxidized soy bean oil (ESO) in different carboxyl-epoxide ratios. The cured resins were thermally stable up to 300 °C and degraded into water soluble components under basic aqueous conditions. The surfaces of the resulting epoxy polymers films were homogeneous and hydrophilic. Neonatal human dermal fibroblast (HDFn) cell adhesion and proliferation experiments on films made of CD-based epoxy resin with a 50/50 ratio of -COOH/ESO presented comparable biocompatibility to the well-studied poly(DL-lactide-*co*-glycolide) (PLG) copolymer, while TR-based epoxy polymers prevented cell adhesion and growth. The starkly different cell adhesion results and favorable physical characteristics support the further *in situ* and *in vitro* testing of these fully sustainable epoxy polymer materials as potential tissue engineering or antifouling coatings.

1. Zhang, Q.; Phillips, H. R.; Purchel, A.; Reineke, T. M. *In preparation*. **2017**.

4.1 INTRODUCTION

The use of polymeric materials in our daily life is widespread due to their versatile mechanical performance, durability, and ease of processing.[198] Millions of tons of conventional polymers are primarily sourced from the non-renewable and quickly depleting petroleum stock on the earth.[199] What's more, the disposal of those polymer materials after use brings up more severe challenges, such as the ever-growing environmental pollution issue as well as human health concerns.[200-202] To address those severe ecological challenges, sustainably sourced polymers have drawn substantial worldwide interest in recent years.[203-205] Sourcing polymers and their precursors from renewable feedstocks is a safe and strategic approach to fulfill the exponentially increasing demand for polymers and composites while reducing negative environmental impact.[206] Bio-based polymers from natural feedstocks are promising materials with similar and sometimes improved properties. Various bio-based polymers have been prepared from renewable resources, such as bio-based paints from vegetable oils,[207-209] soybean and corn protein-based biopolymers,[210] glucose- and Castor Oil-based polyesters,[211] thermosetting acrylic resins[212] and polyolefins,[213] and cyanate ester resins.[214]

Carbohydrates offer great opportunities to create new renewable polymers because of their sustainability, biodegradability, and natural abundance at low

cost. They are naturally derived and have numerous hydroxyl groups for creating highly functionalized monomers and crosslinked thermosetting polymers.[215, 216] The polymer properties can be adjusted by changing the crosslinking density and chemical compositions.[217] Trehalose and β-cyclodextrin are naturally-occurring carbohydrates obtained by enzymatic fermentation of starch,[218, 219] and they have been used to prepare various polymers with considerable biocompatibility.[220] Recent efforts have been made to crosslink and incorporate trehalose and β-cyclodextrin to exploit their unique properties. Nagashima and coworkers have studied the mechanical strength of an allyl-etherified trehalose-based polymer network formed via thiol-ene photo-polymerization.[221] Trehalose based hydrogels were also prepared by thiol-ene and redox radical polymerization, and the synthesized polymers effectively stabilized a wide variety of enzymes against heat and also controlled protein release behavior.[222-224] Yano et al. has photo-polymerized trehalose-based cinnamoyl esters, and the crosslinked polymer films exhibited high transparency and biocompatibility for fibroblast cell adhesion and proliferation.[225] Crosslinked polymers containing β-cyclodextrin have also been extensively studied for inclusion-recognition applications, such as drug carrier systems and water pollutant adsorbents, making use of the cone-shaped cavities that capture organic molecules.[226, 227] For example, Alsbaiee et al. recently reported a porous β-cyclodextrin-based crosslinked polymer that exhibited

exceptional removal efficiency of organic micropollutants from water with great regeneration ability.[228] β-Cyclodextrin-based hydrogels were formed by free radical polymerization and the gels were able to sustain drug release for several days depending on the cyclodextrin content.[229, 230] More recently, our group has prepared bio-based epoxy thermosets derived from Tr, Cd, succinic anhydride and trimethylolpropane triglycidyl ether, and studied their thermal curing behavior and mechanical properties. The prepared epoxy resins also exhibited excellent lap-shear strength indicating their great promise as renewable high performance epoxy resins.[231] These results imply that both trehalose and β-cyclodextrin are promising components to use in preparing sustainable and biocompatible polymers for various applications.

Due to the crosslinked chemical structure, sustainable thermosetting polymers do not melt when heated and do not dissolve in most solvents, which enables them to maintain their designed properties in various dynamic environments without degrading or breaking down.[232] Hence, there is tremendous interest in studying the biocompatibility of sustainable thermosetting polymer materials that may persist in the environment long after their lifetime use. Bob Langer's research group has prepared various crosslinked and biodegradable elastomers from sustainable sebacic acid and polyols including glycerol, xylitol, sorbitol, and mannitol, and the prepared polymer implants

displayed similar *in vitro* and *in vivo* biocompatibility to the well-studied poly(DL-lactide-co-glycolide) (PLG) copolymer.[233-235] More recently, photo-cured trehalose-based polymer films were also reported to promote fibroblast cell proliferation compared to a polystyrene control.[225] Yang et al. has reported new renewable thermosets based on carvone from caraway seeds, and the rubbery polymers exhibited robust mechanical strength.[236] The fibroblast cell adhesion, growth rate, and morphology on the polymer films were superior to PLG copolymers, indicating the material's potential for engineering various soft tissues. More recently, natural sunflower oil-derived thermosets was prepared via thiol-ene Michael addition under mild conditions.[237] The thermosetting polymers were reinforced by the addition of different content of cellulose nanocrystals and the noticeable adsorption of bovine serum albumin indicates their promise biosensors and cell growing supports.

Bio-based soy bean oil is a safe and green alternative chemical feedstock to prepare sustainable thermosets. Besides its long history in food applications, it is the most inexpensive plant oil-based chemical in the world and can be epoxidized in large volumes.[238] Epoxidized soy bean oil has been widely utilized for various applications, such as bio-based plasticizers and stabilizers to improve the toughness of epoxy resins.[239, 240] In this study, we report the synthesis of thermosetting epoxy polymers from renewable starting materials including

trehalose (TR) or β-cyclodextrin (CD), heptanoic acid, succinic anhydride (SA), and epoxidized soybean oil (ESO). We assessed the thermal curing behavior, thermal properties, mechanical performance, degradation, and the cell adhesion and proliferation properties of the resulting thermoset films. The TR-based epoxy thermosets were elastomeric and did not allow HDFn cell adhesion or growth, while the CD-based films were typical plastic materials that promoted HDFn adherence and growth to a level comparable with the PLG copolymer control films. These results implying their potential applications as tissue engineering or antifouling materials.[241-243]

4.2 MATERIALS AND METHODS

4.2.1 Materials

All chemicals and solvents were purchased from Aldrich and used without further purification unless otherwise noted. Anhydrous trehalose (TR) was purchased from Acros Organics. Food grade β-cyclodextrin (CD) was supplied by Wacker Chemie AG. Succinic anhydride (SA) and heptanoyl chloride (HP) was purchased from Alfa Aesar and used without further purification. Epoxidized soy bean oil (ESO) was obtained from Scientific Polymer Products, Inc. and used as received. Poly(DL-lactide-*co*-glycolide) (PLG) copolymer with a lactide/glycolide ratio of 50/50 (with inherent viscosity range of 0.26-0.54, ester terminated) was purchased from LACTEL Absorbable Polymers. Dry dimethylformamide (DMF)

was obtained using an MBRAUN MB solvent purification system manufactured by M. Braun Inert Gas-System GmbH (Garching, Germany) using HPLC grade solvent. The biological reagents Dulbecco's Modified Eagle's Medium (DMEM), fetal bovine serum (FBS), phosphate buffered saline (PBS), OptiMEM, trypsin, nuclease-free sterile water, and penicillin-streptomycin (pen-strep) were purchased from Gibco (Carlsbad, CA). Calcein-AM was purchased through Affymetrix Inc. (Santa Clara, CA). The human dermal neonatal fibroblast cell line (HDFn) and dimethyl sulfoxide (DMSO) were obtained through ATCC (Manassas, VA).

4.2.2 Instrumentation

^{1}H NMR spectroscopy experiments were performed on a Bruker Avance III HD 500 spectrometer at 500 MHz. FT-IR spectra were obtained using a Bruker Alpha Platinum ATR spectrometer. TGA was performed on a TA Instruments Q500 at a heating rate of 10 °C min^{-1} under a nitrogen flow of 60 mL min^{-1} in a temperature range from 25 to 520 °C. *Differential scanning calorimetry (DSC)* measurements were carried out using a TA Instruments Discovery DSC under a nitrogen atmosphere. T_g values were determined on the second heating at a heating rate of 10 °C min^{-1}. The curing behavior was measured by DSC at heating rates of 2, 5, 10 and 20 °C min^{-1}. Tensile testing was performed using a Minimat Tensile Tester on samples with a dog bone geometry (typical gauge

dimensions 14 × 1.30 × 1.20 mm or 14 x 3.0 x 0.50 mm) with a free crosshead rate of 5 mm min^{-1}. The dynamic mechanical analysis of the cure samples was conducted on a TA Instruments ARES-G2 rheometer with a rectangular torsion geometry with a temperature range of -80 - 150 °C or a frequency range of 0.1 - 100 Hz. Scanning Electron Microscopy (SEM) images were taken using Hitachi S-900 field emission gun SEM. All samples were placed on a carbon tape on the SEM sample stubs (Ted Pella, Inc.) and sputter-coated with a conductive layer of platinum (~5 nm) using Denton DV-502A high vacuum deposition system. Imaging operations were performed using long working distances (10-20 mm) from a sample to the backscattering detector with Autrata modified YAG crystal, and at 5.0 kV of accelerating voltage. Cells were imaged with a Nikon A1RMP multiphoton confocal system connected to a Nikon FN1 microscope with a Plan Apo LWD 25x water-immersion, NA 1.1 objective (Melville, NY). The calcein images were excited at 488 nm and saved as a .TIFF file and exported to ImageJ where they were converted to 8-bit and analyzed for surface area and circularity. Analysis was limited to only isolated cells not in physical contact with any other cells. Cell counts were obtained on a FACSVerse flow cytometer and software from BD Biosciences (San Jose, CA) with a laser excitation wavelength of 488 nm. Data were analyzed via the FlowJo software program (Ashland, OR).

4.2.3 Hardener Synthesis

4.2.3.1 Synthesis of trehalose-based hardener (TR4HP3SA)

In a 250 mL round bottom flask, anhydrous TR (7.04 g, 20.6 mmol) was stirred in 150 mL of anhydrous DMF at 90 °C until completely dissolved to give a clear solution. The resulting solution was cooled in an ice bath, and pyridine (22.0 mL) and DMAP (0.500 g, 4.09 mmol) were added into the solution. Then heptanoyl chloride (H, 12.7 mL, 82.0 mmol) was added slowly to the mixture and the resulting solution was stirred for 48 h at room temperature. After SA (16.5 g, 165 mmol) was added, the resulting solution was heated to 90 °C and stirred for another 48 h. The flask was taken out of the oil bath, and ~300 mL of ethyl acetate was added to dissolve the product. The resulting mixture was transferred to a 1 L separatory funnel, and extracted with 2 M HCl with brine (1 x 400 mL, 2 x 100 mL) and deionized water (3 x 50 mL). The ethyl acetate layer was dried with anhydrous sodium sulfate and concentrated using a rotoavap system. The resulting viscous liquid was dissolved in 100 mL of $CHCl_3$ followed by addition of 5 mL of deionized water and stirred for another 24 h. The resulting mixture was washed with brine (6 x 50 mL) in a separatory funnel to remove all succinic acid. The organic layer was dried with anhydrous sodium sulfate and concentrated on rotavap. The resulting viscous liquid was re-dissolved in ~40 mL of $CHCl_3$ and precipitated into ~ 1.1 L of pentane. The desired product was collected and dried

under high vacuum as a light yellow viscous liquid, 37.5 g, 89.7%. ^{1}H NMR ($CDCl_3$, 500 MHz) δ_{ppm}: 5.72-4.81 (m, 7H), 4.56-3.43 (m, 7H), 2.85-2.47 (m, 12H), 2.47-2.12 (m, 8H), 1.81-1.49 (m, 8H), 1.51-1.13 (m, 24H), 1.09-0.69 (m, 12H).

4.2.3.2 Synthesis of β-cyclodextrin-based hardener (CD6HP8SA)

In a similar manner to the preparation of TR4HP3SA, anhydrous CD (8.80 g, 7.75 mmol) was dissolved in 100 mL of anhydrous DMF at 90 °C and the resulting solution was cooled in an ice bath. After pyridine (26.3 mL) and DMAP (0.500 g, 4.09 mmol) were added, heptanoyl chloride (H, 8.40 mL, 54.3 mmol) was slowly added dropwise and the resulting solution was stirred for 41 h at room temperature. Then the reaction mixture was stirred at 90 °C for another 48 h after addition of SA (21.7 g, 217 mmol). After cooled to room temperature and addition of ethyl acetate (~400 mL), the resulting mixture was extracted with 2 M HCl with brine (1 x 400 mL, 2 x 100 mL) and deionized water (3 x 50 mL). The organic layer was dried with anhydrous sodium sulfate and concentrated on rotavap, and the resulting viscos liquid was stirred in a mixture of $CHCl_3$ (100 mL) and deionized water (5 mL) for 24 h. The organic layer mixture was extracted with brine (3 x 50 mL), dried with anhydrous sodium sulfate and concentrated on rotavap. The resulting viscous liquid was re-dissolved in $CHCl_3$ and precipitated into pentane to provide the desired product as a white solid, 20.1 g, 72.3%. ^{1}H

NMR (acetone-d_6, 500 MHz) δ_{ppm}: 5.94-3.24 (m, 49H), 3.24-1.98 (m, 32H from C$\underline{H}_2$ of SA groups, 12H from COC$\underline{H}_2$ of H group, 5H from DMF residual), 1.81-1.47 (m, 12H), 1.38-1.15 (m, 36H), 1.09-0.57 (m, 18H).

4.2.4 Resin Formulation and Tensile Bar Preparation

The synthesized hardeners were mixed with epoxidized soy bean oil (ESO, assuming 5 epoxide groups per molecule) in different molar ratios of -COOH/epoxide (40/60, 50/50, and 60/40) by solvent blending. Briefly, accurately weighted hardeners and ESO were dissolved in acetone and stirred in a 20 mL scintillation glass vial followed by the removal of acetone on a rotovap system at 30 °C. The resulting epoxy resins were dried under high vacuum as either viscous liquids or solids and stored in a freezer for later use. The thermal curing of the resins was conducted following two methods based on the physical form of the formulated resins. (1) The viscous liquid epoxy resins of TR4HP3SA/ESO were transferred into rubber silicone mold that contained a dog-bone shape, and then dried under high vacuum for 12 h at room temperature. Then, the epoxy resins were pre-cured at ~110 °C for 2h and post-cured at ~165 °C for 3 h for further mechanical testing. (2) The solid epoxy resins of CD6HP8SA/ESO were loaded into a stainless steel mold with a dog-bone shape and cured at ~165 °C for 2 h in a hot press under a pressure of 3000 psi.

4.2.5 Hydrolytic Degradation

To study the hydrolytic degradation of the epoxy resins, three parallel samples of polymer (~50 mg, dogbone shape) were immersed in the appropriate aqueous solution (5 mL) of deionized (DI) H_2O, 1 M NaOH and 1 M HCl. The polymers were allowed to sit undisturbed at room temperature, and periodically removed, blotted dry, weighed, and re-immersed in the same solution.

4.2.6 Swelling Ration and Gel Fraction

Three parallel samples of cured polymers (~50-70 mg, dogbone shape) were weighed (m1) and immersed into 5 mL of THF (48 h) to remove the solubilized fraction. The wet weight (m_2) of the polymer samples was recorded for the swelling ratio calculation. After the wet samples were completely dried at 50 °C under high vacuum for 24 h, the dry weight (m_3) of polymer samples was recorded for the gel fraction calculation. The swelling ratio and gel fraction were calculated according equation (3) and (4).

$$\text{Swelling ratio} = m_2/m_1 \quad (3)$$

$$\text{Gel fraction} = m_3/m_1 \quad (4)$$

4.2.7 In Vitro *Biocompatibility*

Glass Petri dishes (40 mm diameter, washed with concentrated sulfuric acid, DI water, acetone and CH_2Cl_2) were coated with a CH_2Cl_2 solution (1.5%) of the prepared epoxy resins (40 mg), and the Petri dishes were dried under high vacuum for 12h at room temperature after evaporation of the solvent in air. The coated dishes were transferred into a vacuum oven, and the epoxy resins were pre-cured at ~110 °C for 2 h and post-cured at ~165 °C for 3 h under nitrogen atmosphere. The PLG control dishes was coated with CH_2Cl_2 solution (1%) of PLG (25 mg), and the solvent was evaporated overnight in air before drying under high vacuum at room temperature.

To sterilize the dishes prior to cell seeding, the dishes were lightly sprayed inside and out with 75% ethanol in water solution and left to air dry film side up for 10 min inside the biohood under UV light. Each dish containing the film was then filled with 4 mL of DMEM + 10% FBS by volume +1% pen-strep solution and left for 2 h in the biohood with the UV light off. After being soaked in DMEM + 10% FBS, the dishes were rinsed 3 times with sterile water and left to air dry for 2 h in the biohood without the presence of UV light. The dishes were stored away from UV light in sealed sterile glass jars.

HDFn cells between passage # 5-15 were diluted to a concentration of 6,000 cells/mL then aliquoted into each dish (24,000 cells per dish into 4 mL

DMEM + 10% FBS + 1% pen-strep total). The dishes were gently rocked a few seconds to evenly distribute cells, then incubated 24 h at 37 °C. The cell media was refreshed every 24 h for all samples. Cells were allowed growing from 1-5 days. One hour before imaging, a calcein-in-OptiMEM solution was made by diluting 1 µL of calcein-AM (1 mg/mL in DMSO) per 1 mL of OptiMEM and warmed to 37 °C in a water bath. The dishes were aspirated to remove old media, washed 3 times with PBS, and filled with 3 mL of the calcein-OptiMEM solution. The dishes were incubated with the calcein at 37 °C for at least 30 min before imaging. After imaging, cells were trypsonized off the films, washed with PBS, re-dispersed in 200 µL of fresh PBS, and analyzed by flow cytometry using the λ=488 nm filter (N=3 for each assay). The cell counts were collected over the course of 20 s.

4.3 RESULTS AND DISCUSSION

4.3.1 Hardener Synthesis

Via a one-pot two-step reaction in dimethylformamide (DMF), the hydroxyl groups of anhydrous TR and CD were first partially esterified in the presence of 4 and 7 equivalents of heptanoyl chloride (HP), respectively. An excess of SA was further applied to functionalize the remaining hydroxyl groups of both TR and CD (Figure 4.1).[231] The two hydrophobic carboxylic acid hardeners, TR4HP3SA and CD6HP8SA, were obtained in about 72% and 89% yields after purification,

respectively. As shown in Figure 7.24 (Appendix) the integration of protons from the trehalose moiety after functionalization (3.4-5.7 ppm) was defined as 14,[231, 244, 245] and the proton integrations of HP (2.47-2.12 ppm) and SA (2.85-2.47 ppm) were ~8 and ~12, respectively, indicating that TR4HP3SA had an average substitution degree of 4 and 3 for HP and SA groups per TR unit. Similarly, hardener CD6HP8SA had an average substitution degree of 6 and 8 for HP and SA groups, respectively, (Figure 7.25 Appendix) per CD unit. Both HP and SA can be obtained from natural feedstock via thermal degradation of castor oil[246, 247] or fermentation of glycerol.[248-251] Therefore, it is reasonable to consider both epoxy resin hardeners to be fully bio-based curing agents.

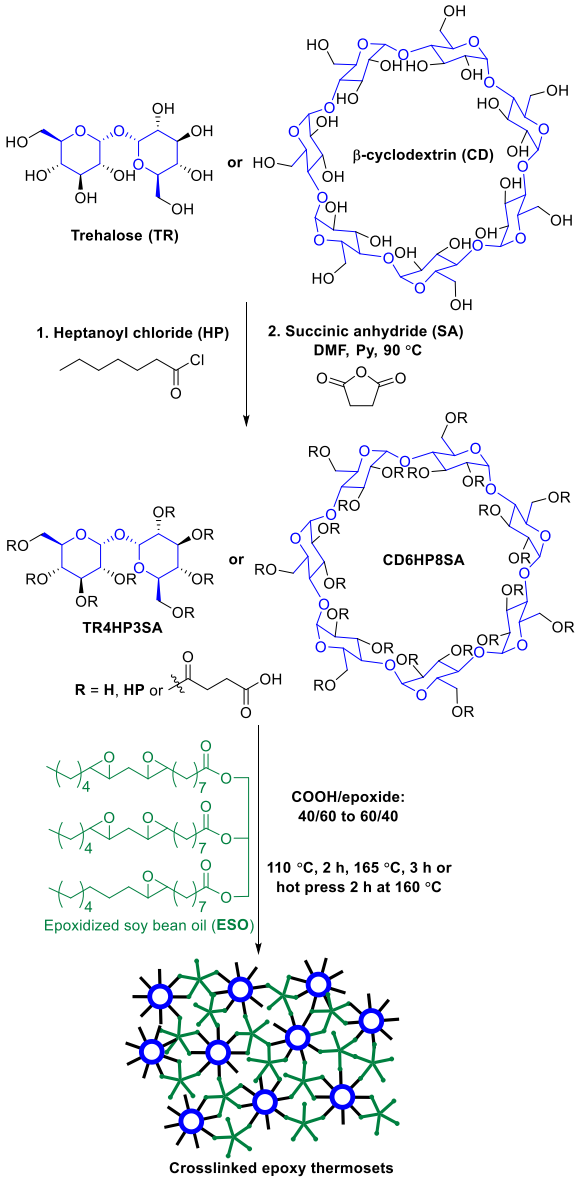

Figure 4.1. Synthesis scheme of sugar-derived epoxy resin hardeners and bio-based thermosets (TR: trehalose; CD: β-cyclodextrin; HP: heptanoyl group SA: succinic anhydride; TR4HP3SA: trehalose based hardener with ~4 HP units and ~3 SA units; CD6HP8SA: β-cyclodextrin hardener with ~6 HP units and ~8 SA units; DMF: dimethyl formaldehyde; Py: pyridine).

4.3.2 Bulk Characterization

The fully bio-based carboxylic acid hardeners, TR4HP3SA and CD6HP8SA, were formulated with plant-based ESO in three -COOH/epoxide ratios (40/60, 50/50, and 60/40) and formed homogenous epoxy resins (Figure 4.2). Differential scanning calorimetry (DSC) was used to monitor the thermal curing behavior and Figure 4.2A shows the DSC curing curves of both two resin systems, TR4HP3SA/ESO and CD6HP8SA/ESO, at 50/50 ratios with a heating rate of 5 °C/min. Both epoxy resin mixtures clearly display a single exothermic peak at around 172.5 and 171.2 °C for TR4HP3SA/ESO and CD6HP8SA/ESO, respectively. The existence of these exothermic peaks indicates the nucleophilic ring opening reaction of the epoxides in ESO by the -COOH groups of the hardeners upon heating. To confirm the crosslinking reactions, Fourier transform infrared (FT-IR) spectra of the monomers and resin mixtures (TR4HP3SA/ESO and CD6HP8SA/ESO at 50/50 ratios) before and after cure are shown in Figure 4.2B. The spectra clearly showed that a shoulder adsorption band at ~1706 cm-1 from the -COOH groups of hardeners, and the epoxide ring peaks at 900-750 cm-1 disappeared after thermal curing. The presence of hydroxyl groups from epoxide ring opening after polymerization is represented by a broad peak at 3450 cm-1. These results indicate the successful crosslinking of epoxides and -COOH groups to form polymers (Figure 7.26 and 7.27 Appendix), and the data agree

well with our previous report.[231] The exotherm peaks of bulk polymerizations from DSC isothermal scans at 165 °C (Figure 7.28, Appendix) disappeared after ~25 min, indicating the fast curing rate for the two epoxy resin systems. Therefore, the formulated epoxy resins were polymerized at ~165-170 °C.

The very small difference between peak temperatures of TR4HP3SA/ESO and CD6HP8SA/ESO under the same conditions (Figure 4.2A and Figure 7.29 in the Appendix), indicate the similar thermal curing reactivity of hardeners TR4HP3SA and CD6HP8SA.[231, 252] This is also supported by determining the activation energy of the thermal curing polymerizations using the peak temperatures at different heating rates of dynamic DSC scans by Kissinger's method.[231, 253] The Kissinger's theory (Kissinger equation) is shown as below:

$$-\ln(q/Tp2) = Ea/RTp - \ln(AR/Ea).$$

The slope of the plot of $-\ln(q/Tp2)$ versus $1/Tp$ can provide us the apparent activation energy, where q is the heating rate of DSC thermal curing scans, Tp is the exothermic peak temperature, Ea is the activation energy, R is the gas constant (8.314 J mol−1 K−1), and A is the pre-exponential factor. As shown in Figure 4.2C, the Ea values of the thermal curing reactions for TR4HP3SA/ESO 50/50 and CD6HP8SA/ESO 50/50 were calculated as 57.1 kJ mol-1 and 54.9 kJ mol^{-1}, respectively, and the close values between the two hardeners demonstrate a similar curing reactivity.

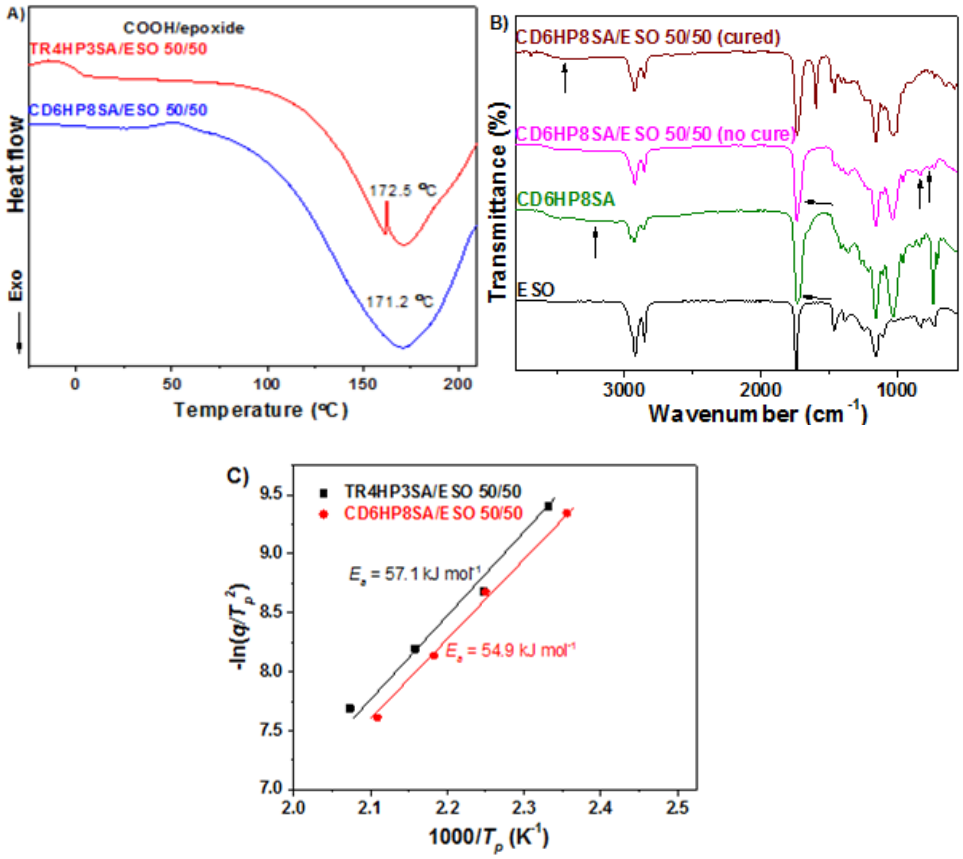

Figure 4.2. DSC curing thermograms of (A) TR4HP3SA/ESO and CD6HP8SA/ESO (50/50) under nitrogen, 5 °C min^{-1}; FT-IR spectra of (B) CD6HP8SA, ESO, CD6HP8SA/ESO (50/50) before and after curing (arrows denote peaks of interest to support crosslinking reaction); (C) linear plot of $-\ln(q/T_p^2)$ versus $1000/T_p$ based on Kissinger's equation.

4.3.3 Thermal Properties

The homogeneous resin mixtures at different -COOH/epoxide ratios were thermally cured, and the thermal properties and thermal stability of the resulting polymers under nitrogen atmosphere were investigated by DSC and

thermogravimetric analysis (TGA). Tuning the mixing ratio of the hardeners and epoxy in the resins can impact the cross-linking reaction and the properties of the resulting polymers. The Tg of each resulting polymer set (Table 4.1 and Figure 4.3B) were very close to each other, ranging from -3 to 3 °C for TR4HP3SA/ESO polymers and from 28 to 36 °C for CD6HP8SA/ESO polymers, and the polymers at 50/50 ratios of -COOH/epoxide exhibited slightly higher Tg for each resin systems. As shown in Table 4.1and Figure 4.3B, the degradation temperatures at 5% weight loss (Td5) of the cured polymers were from ~310 to ~230 °C. This is higher than the Td5 of both hardeners (Figure 7.30, Appendix), indicating the formation of the crosslinked networks within polymers and the higher thermal stability of the polymers. Similar to our previous report,[231] the Td5 dramatically decreased when increasing the ratios of -COOH/epoxide, likely due to the excess hardener -COOH groups with lower thermal stability remaining in the polymers but not participating in the crosslinking reaction, lowering the crosslinking density of the polymers.[254] The swelling ratio and gel fraction of the polymers were tested in tetrahydrofuran (THF) which is a good solvent for hardeners, ESO, and linear polyesters, and the ratios are listed in Table 4.1.

The examined polymers maintained their polymer network upon immersing them in THF for 48 h, revealing that both monomers participated in polymerization and formed crosslinked polymer networks at all -COOH/epoxide

ratios. The CD6HP8SA/ESO resin polymers exhibited much lower swelling ratios and higher gel fractions than those of TR4HP3SA/ESO resins, indicating that the higher structural rigidity and the formation a network with higher crosslinking density for CD6HP8SA/ESO polymers than TR4HP3SA/ESO polymers.[231] The swelling ratios of all polymers increased and their gel fractions decreased when increasing the -COOH/epoxide ratio from 40/60 to 60/40, possibly due to the fact that the excess of epoxide groups at lower -COOH/epoxide ratios could further participate in the crosslinking reaction and result in higher crosslinking density.[231, 254]

Table 4.1. Crosslinked thermoset characterization data.

Polymer	Swell ratio [a]	Gel fraction [a]	T_{d5} [b] (°C)	T_g [c] (°C)
TR4HP3SA/ESO 40/60	2.77±0.119	0.910±0.025	312	-3.0
TR4HP3SA/ESO 50/50	3.49±0.083	0.834±0.019	287	3.1
TR4HP3SA/ESO 60/40	4.34±0.191	0.690±0.015	244	2.8
CD6HP8SA/ESO 40/60	2.06±0.102	0.981±0.009	307	28
CD6HP8SA/ESO 50/50	2.13±0.066	0.979±0.014	285	36
CD6HP8SA/ESO 60/40	2.41±0.111	0.879±0.023	232	33

a Determined by immersing the samples in THF for 48 h, the wet weight was measured for the swelling ratio calculation. The dry weight was measured for the gel fraction calculation after drying the samples at 50 °C under high vacuum. *b* Temperatures at 5% weight loss were determined using TGA. *c* Temperatures were determined by performing DSC at 10 °C min^{-1} under nitrogen.

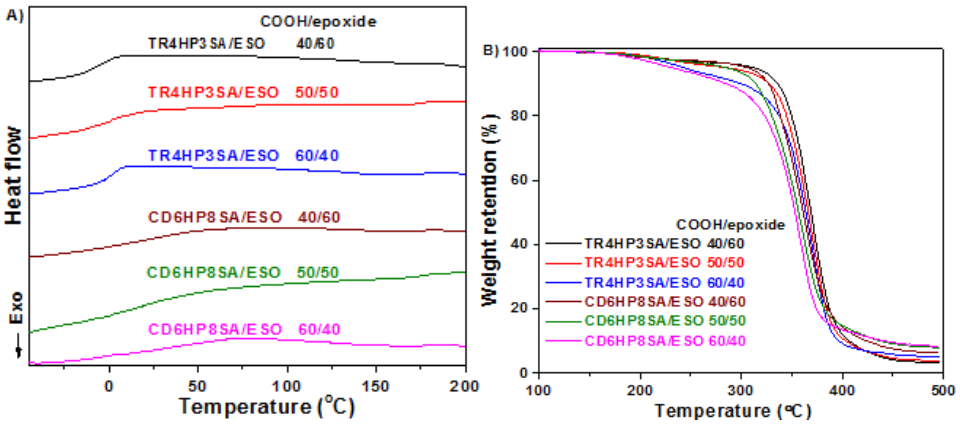

Figure 4.3. (A) DSC thermograms (second heating) and (B) TGA curves for cured TR4HP3SA/ESO and CD6HP8SA/ESO at different ratios with a heating rate of 10 °C min^{-1} under nitrogen.

4.3.4 Tensile Properties

The tensile bars of TR4HP3SA/ESO and CD6HP8SA/ESO at different ratios were prepared and the tensile properties of the polymers were investigated. TR4HP3SA/ESO resins cured as slightly dark yellow tensile bars in a rubber mold after removing residual acetone under high vacuum followed by a pre-curing/post-curing process. And the solid CD6HP8SA/ESO resin mixtures were directly cured as light yellow tensile bars in a hot press for mechanical measurements. As shown in Table 4.2 and Figure 4.4, the thermosetting polymers displayed linear responses at low strains of 50% and 7% for TR4HP3SA/ESO and CD6HP8SA/ESO, respectively. While TR4HP3SA/ESO polymers showed tensile strength of between 0.5 and 1.3 MPa with a strain of 66-186%, cured CD6HP8SA/ESO samples exhibited much a higher tensile

strength of around 10 MPa with a smaller strain of about 40%, probably due to the more rigid structure and higher cross-linking density of the CD hardeners. This is also supported by the fact that all CD6HP8SA/ESO polymers showed very typical plastic deformation in stress-strain curves (Figure 4.4B). Both epoxy resin systems have relatively low Young's moduli of up to ~2.4 and 302 MPa for TR4HP3SA/ESO and CD6HP8SA/ESO polymers, indicating the flexible and soft nature of the epoxy polymers at room temperature. Both tensile strength and Young's moduli of TR4HP3SA/ESO polymers decreased as the ratios of -COOH/epoxide increased from 40/60 to 60/40. However, the tensile strength and Young's moduli of CD6HP8SA/ESO polymers increased and then decreased as the ratios of -COOH/epoxide increased from 40/60 to 60/40, but with less obvious effect on the tensile strength. These results indicate that the chemical structure of the hardeners and epoxy can significantly influence the cross-linking density of the polymers and their mechanical properties.

Table 4.2. Crosslinked thermoset tensile and thermal mechanical characterization.

Polymer	Young's modulus (MPa)[a]	Tensile strength (MPa)[a]	Strain at break (%)[a]	Storage modulus (MPa)[b]
TR4HP3SA/ESO 40/60	2.44	1.3	66.3	1.29
TR4HP3SA/ESO 50/50	0.643	0.71	91.4	0.728
TR4HP3SA/ESO 60/40	0.273	0.46	186	0.472
CD6HP8SA/ESO 40/60	176	10	39.2	224
CD6HP8SA/ESO 50/50	302	11	43.2	374
CD6HP8SA/ESO 60/40	236	9.1	46.5	264

[a] Determined from stress-strain tests and averaged from at least 5 tensile bars. [b] Determined from dynamic mechanical analysis (temperature sweep) at 25 °C with torsion geometry.

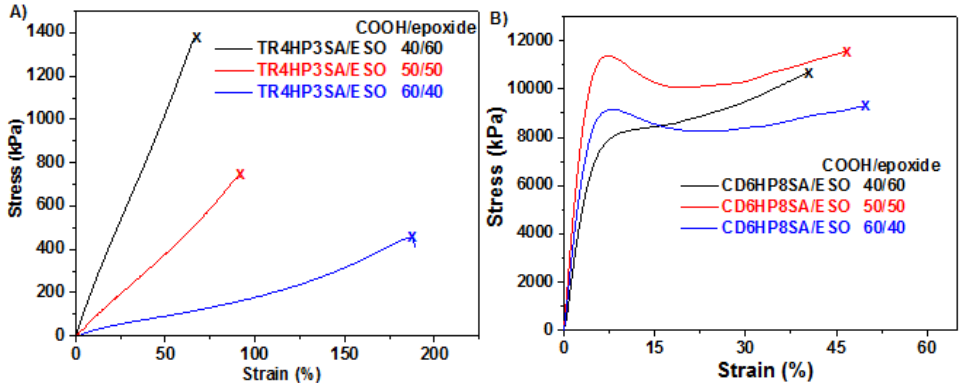

Figure 4.4. Representative stress-strain curves for cured (A) TR4HP3SA/ESO and (B) CD6HP8SA/ESO at different ratios by tensile testing from at least 5 polymer tensile bars.

4.3.5 Dynamic Mechanical Properties

Dynamic mechanic analysis (DMA) experiments of the cured polymers were recorded to study the effect of temperature on their mechanical properties, and the storage moduli of the polymers as a function of temperature are shown in Figure 4.5. All examined epoxy resin polymers were in a glassy state at low temperature (< -20 °C), and their storage moduli were almost constant at ~0.5-0.9 GPa. As the temperature increased, their storage moduli exhibited a noticeable drop (-15 to 32 °C for TR4HP3SA/ESO and 0 to 70 °C CD6HP8SA/ESO polymers) due to the polymer chain relaxation at the glass transition. We observe that CD6HP8SA/ESO polymers had much higher storage moduli than TR4HP3SA/ESO polymers, especially in their rubbery state at elevated temperatures. And the storage moduli drop of CD6HP8SA/ESO epoxy resins was over a range of ~70 °C, which is much slower comparing to a range of only ~45 °C for the TR4HP3SA/ESO resins. This is consistent with our previous discussion that the CD moieties in the CD6HP8SA/ESO polymers enhanced polymer rigidity and cross-linking density which restricted and retarded the polymer chain mobility.[231, 255, 256] The loss factor (tan δ) of epoxy resins (Figure 7.31, Appendix) also showed that the CD6HP8SA/ESO polymers had much broader tan δ peaks and lower tan δ intensity, indicating the presence of a highly cross-linked polymer network.[257] The ratios of -COOH/epoxide did not show

significant effect on the glass transition temperatures of the examined polymers, as indicated by the close peak values of tan δ (Figure 7.31, Appendix), which is consistent with the previous discussion on Tg obtained from DSC experiments (Table 4.1).

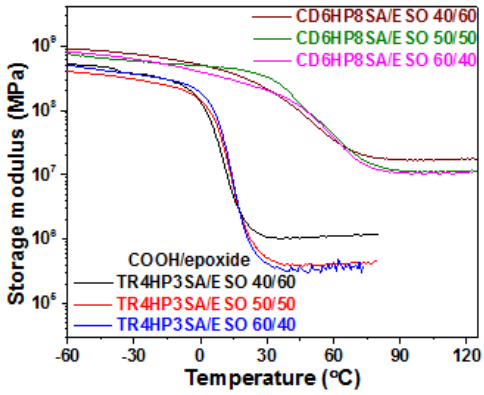

Figure 4.5. Storage modulus versus temperature for the cured TR4HP3SA/ESO and CD6HP8SA/ESO thermosets at different ratios by DMA.

4.3.6 Hydrolytic Degradation

The hydrolytic stability of the cured epoxy resins was measured in neutral, acidic, and basic aqueous environments at room temperature by monitoring the weight loss of the examined polymers over time. As shown in Figure 4.6A and Figure 7.32A (Appendix), the cured TR4HP3SA/ESO and CD6HP8SA/ESO epoxy polymers swelled to different levels after day 1 under neutral aqueous conditions, and there was no further weight loss nor swelling behavior observed over the next 69 days. Similar to the neutral conditions, all epoxy resin polymers only swelled under acidic conditions without any weight loss during the hydrolytic

experiments (Figure 4.6B and Figure 7.32B, Appendix) This is different from our previous report where similar epoxy resin polymers completely degraded to water-soluble components after 50-90 days under acidic conditions.[231] Clearly, the incorporation of hydrophobic HP and ESO moieties greatly enhanced the hydrophobicity of the resulting polymers which hampered their acidic degradation. However, both the solid TR4HP3SA/ESO and CD6HP8SA/ESO polymer samples quickly degraded over a varying time period of 1 hour to 1.5 days in 1 M NaOH as gel mixtures due to the presence of amphiphilic fatty acid salts (Figure 4.6C and Figure 7.32C, Appendix). The polymers with higher -COOH/epoxide ratios degraded much more quickly, probably due to the excess of -COOH groups in the polymer network allowing rapid water penetration to facilitate the hydrolysis under basic conditions. Based on our previous report on monitoring the hydrolytic degradation products of sustainable epoxy polymers using ^{1}H NMR,[231] we anticipate that the degradation products consisted of TR, CD, disodium succinate, and the ring-opened product of ESO (and/or its derivatives of glycerol and salts of fatty acids) which are environmentally benign.

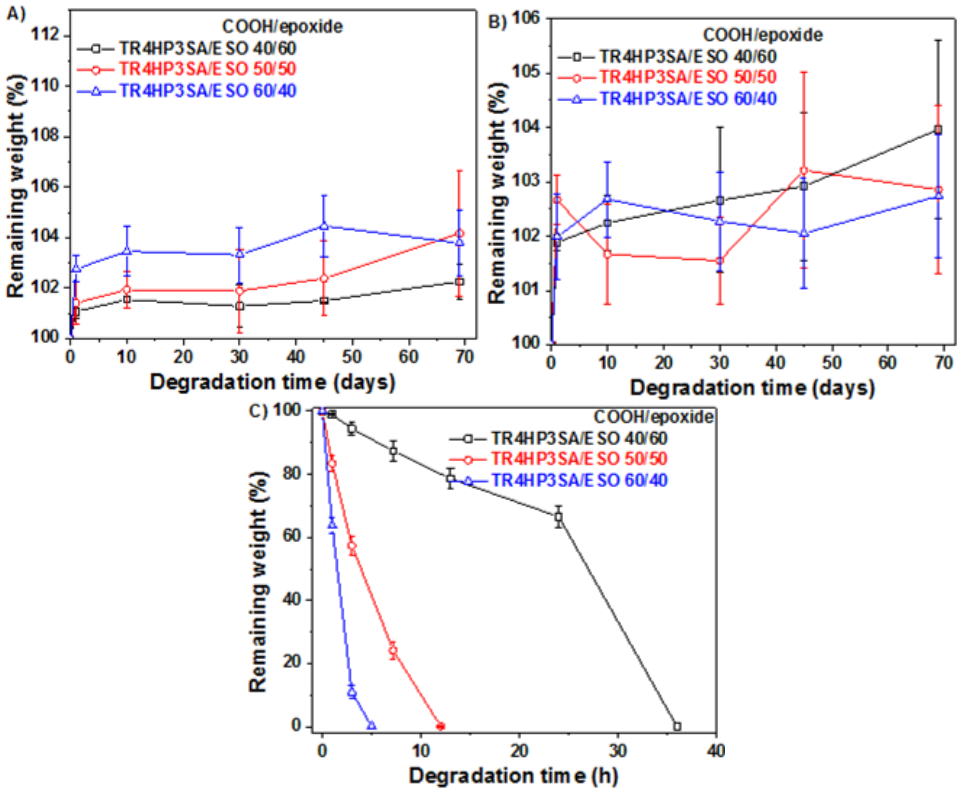

Figure 4.6. Hydrolytic degradation/stability profile of cured TR4HP3SA/ESO at different ratios in (A) water, (B) 1 M HCl, and (C) 1 M NaOH. The error bars represent the standard deviation from the mean of 3 measurements.

4.3.7 Surface Morphology and Wettability

The TR4HP3SA/ESO 50/50 and CD6HP8SA/ESO 50/50 epoxy resin polymer films after thermal curing in glass petri dishes were selected to study their film surface morphology and wettability, which are two factors affecting cell adherence and proliferation.[225, 258, 259] Shown in Figure 4.7 are the SEM surface morphologies of the surfaces of (A) a glass petri dish, (B) a PLG film (a positive control for cell proliferation study), and (C-D) the thermally cured epoxy polymer

films. As shown, the PLG film, the TR4HP3SA/ESO 50/50 film, and the CD6HP8SA/ESO 50/50 film were smooth and homogeneous, and there was no cracking or phase separation observed, showing that the hardeners and soy bean oil were fully miscible during the curing process. The water contact angles of both cured TR4HP3SA/ESO 50/50 and CD6HP8SA/ESO 50/50 polymer films are shown in Figure 4.7, and are compared to a glass substrate and the positive control PLG film. The contact angle of the glass substrate was ~34.7°, and it increased to ~79.1° for PLG film. The contact angles of the TR4HP3SA/ESO 50/50 and CD6HP8SA/ESO 50/50 polymers films were ~84.6° and ~88.6°, respectively. These results show that the examined epoxy resin polymers are more hydrophobic than PLG.

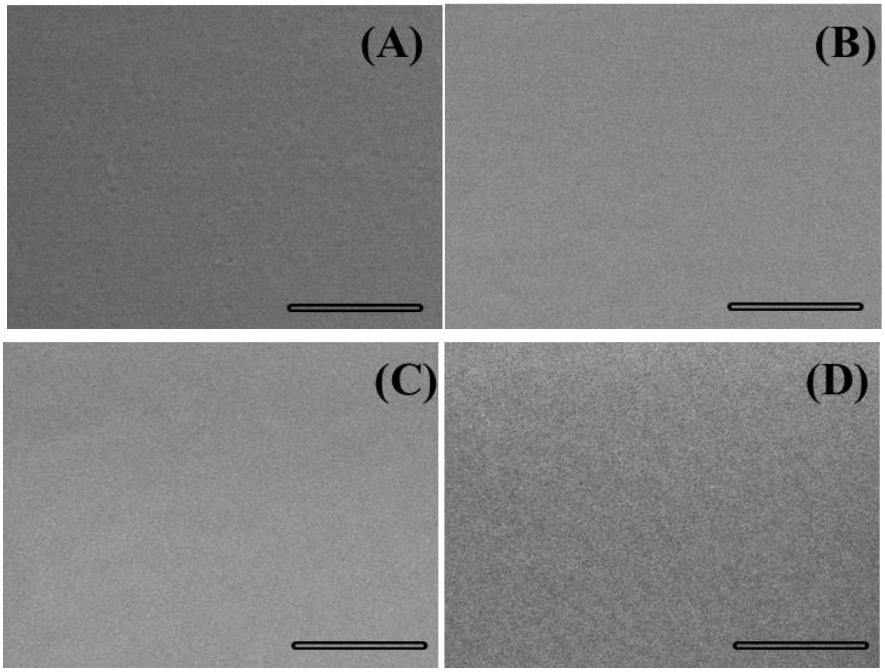

Figure 4.7. SEM images of (A) glass surface, (B) PLG, (C) TR4HP3SA/ESO 50/50 and (D) CD6H8SA/ESO 50/50 (scale bar = 500 nm).

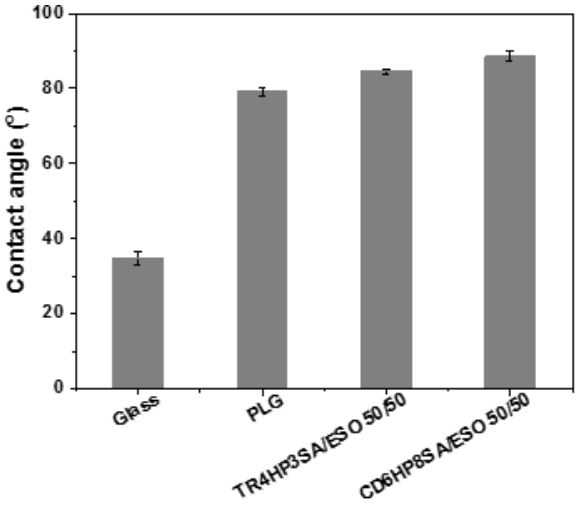

Figure 4.8. Water contact angles of glass surface, PLG, TR4HP3SA/ESO 50/50 and CD7HP8SA/ESO 50/50.

4.3.8 In Vitro *Biocompatibility*

The TR4HP3SA/ESO 50/50 and CD6HP8SA/ESO 50/50 polymer films were prepared in glass petri dishes, and the cell adhesion and proliferation on the polymer film surfaces were investigated and quantified by confocal microscopy and flow cytometry using the human dermal neonatal fibroblast cell line (HDFn). HDFn cells were seeded and cultured on the TR4HP3SA/ESO 50/50 and CD6HP8SA/ESO 50/50 polymer films. HDFn cells were also cultured on PLG films as positive control. Figure 4.8 and Figure 7.33 (Appendix) captured the cell growth characteristics on the polymer films of TR4HP3SA/ESO 50/50, CD6HP8SA/ESO 50/50, and control PLG over a 5-day culture period and the percentage of those cells that are alive (note the drastically different y-axis range when comparing Figure 4.9 and Figure 7.33). As seen in Figure 4.9A, HDFn cells adhered to CD6HP8SA/ESO 50/50 and to control PLG polymer films on day 1, and exponentially proliferated through day 4 and leveled out by day 5. Both CD6HP8SA/ESO 50/50 and control PLG polymer films exhibited high cell viability (Figure 4.9B) as indicated by the high percentage of cells that are alive on each sample. In conjunction, these results demonstrate the low toxicity and similar biocompatibility of the CD6HP8SA/ESO 50/50 polymer compared to that of PLG control copolymer. In contrast, the TR4HP3SA/ESO 50/50 polymer did not allow HDFn cells to adhere or grow on the film surface (Figure 7.33, Appendix). To

probe this lack of adherence, HDFn cells were seeded onto the TR4HP3SA/ESO 50/50 polymer films, and both the supernatant above the film and the adhered cells on the film after 24 h cell culture were collected for cell count analysis by flow cytometry. The film did not allow cells to adhere, nor did many cells survive in the supernatant over the course of 24 h as shown in Figure 7.34 (Appendix). Representative raw flow cytometry data for the cell quantification is shown in Figures 7.35-7.38 (Appendix).

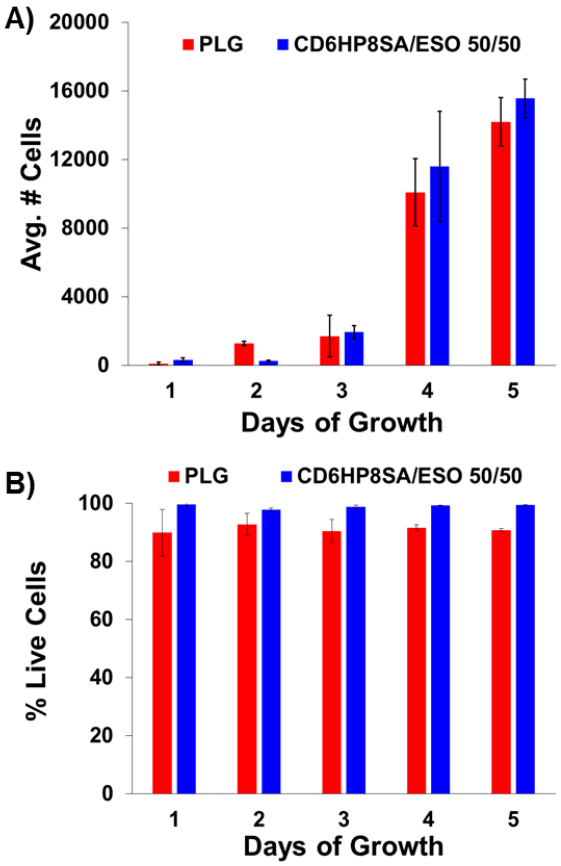

Figure 4.9. (A) Average number of cells and (B) the percentage of those cells that are alive on CD6HP8SA/ESO 50/50 and PLG films at day 1 through day 5 by flow cytometry. N=4 for each assay, and the error bars represent the standard deviation from the mean. No CD6HP8SA/ESO samples were statistically different ($p<0.05$) from the PLG controls according to the Student's t-test.

Currently, there is no data to support that the TR4HP3SA/ESO 50/50 film actively kills cells, and cells may simply be unable to adhere on the surface, which could affect their viability indirectly. As discussed earlier, the surface morphologies and wettability of the TR4HP3SA/ESO 50/50 and CD6HP8SA/ESO

50/50 polymer films did not significantly differ. A preliminary leaching screen study showed that neither polymers is leaching much material as indicated by the very similar gel fractions (by immersing the films in cell culture medium for 150 days) of 94.8±0.5% and 92.0±1.3% for TR4HP3SA/ESO 50/50 and CD6HP8SA/ESO 50/50 polymer films, respectively. Therefore, further studies are needed to explain the cause of their starkly different cell adhesion/proliferation properties.

Quantification of the cell surface area and circularity (Figure 4.10A and B) indicates that cells proliferated and spread on the CD6HP8SA/ESO 50/50 polymer films, and the cells' physical characteristics were comparable to those cultured on the control PLG films. The cellular morphology on CD6HP8SA and the control PLG films from day 1 to day 5 after seeding was visualized with a confocal fluorescence microscope (Figure 4.10C and Figures 7.39-43, Appendix). The cells on the cured CD6HP8SA/ESO 50/50 films showed no significant morphological difference compared to cells on the control PLG, further supporting that CD6HP8SA/ESO 50/50 polymer is at least as biocompatible as that of PLG *in vitro*.

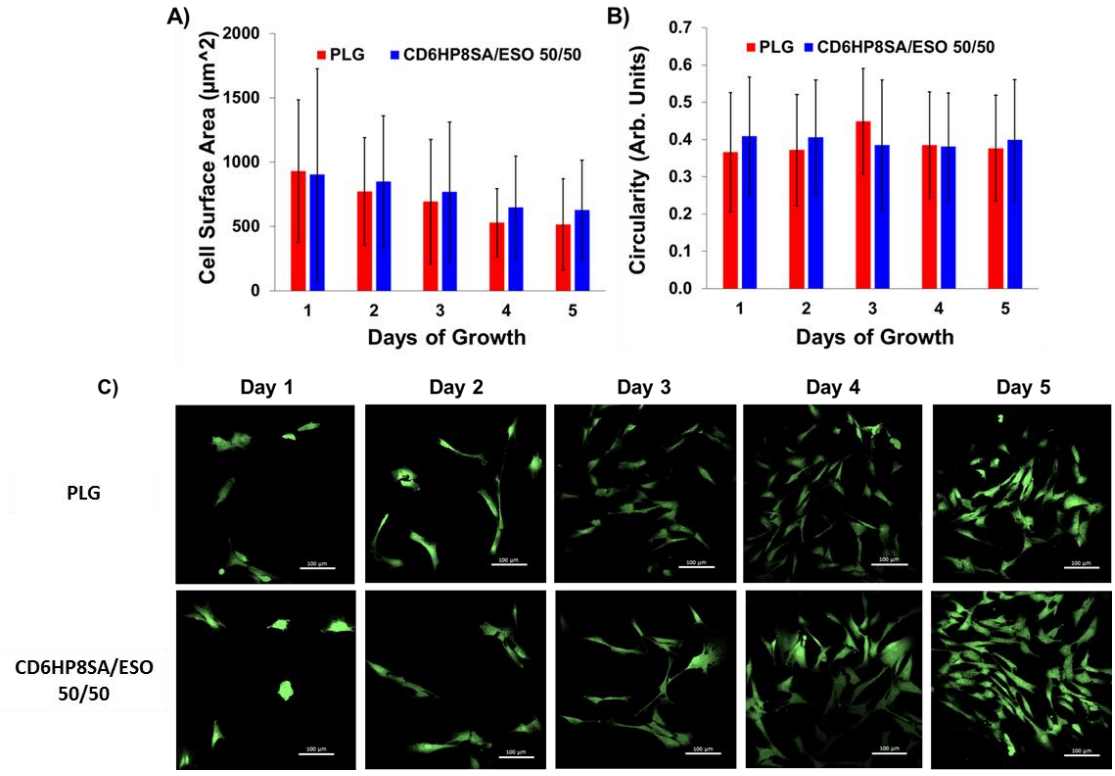

Figure 4.10. (A) Average cell surface area in µm^2, (B) average cell circularity (0-1.0), and (C) confocal micrographs of cells proliferated on the CD6HP8SA/ESO 50/50 and control PLG polymer films at day 1 to day 5 culture. Cell morphology on films were measured by confocal microscopy of the calcein signal in living cells and processed by ImageJ. A minimum of N=80 measurements (maximum N=225) were averaged for each data point, and the error bars represent the standard deviation from the mean. No samples were statistically different ($p < 0.05$) according to the Student's t-test.

4.4 CONCLUSION

We reported the synthesis and characterization of fully sustainable thermosetting epoxy polymers from renewable starting materials including trehalose or β-cyclodextrin, heptanoic acid, succinic anhydride and epoxidized soybean oil. Two new epoxy hardeners were prepared in high yields via a two-

step one-pot reaction, and their thermal curing behavior with ESO was studied. The thermal properties, mechanical performance, hydrolytic degradation under various aqueous environment and the cell adhesion and proliferation properties of the resulting epoxy resin polymers were investigated. DSC experiments indicated that the formulated epoxy resins were thermally cured at ~165 °C and the resulting cured epoxy polymers had thermal stability up to ~300 °C. Both tensile testing and thermal mechanical analysis suggested that *the* TR4HP3SA/ESO 50/50 and CD6HP8SA/ESO 50/50 polymers were soft and flexible materials. The epoxy polymers are quickly degraded to water-soluble components in basic solution but formed gel-like mixtures, and the epoxy resins are resistant to degradation in both acidic and neutral aqueous conditions over a testing period of 69 days. Our results indicate that our TR-based epoxy polymers with ratio of -COOH/epoxide at 50/50 did not allow HDFn cells to adhere and proliferate, suggesting the potential anti-fouling applications of TR-based epoxy polymer film. However, CD-based polymer with a ratio of -COOH/epoxide at 50/50 did promote cell adhesion and growth on the polymer surface, indicating its comparable biocompatibility to PLG control copolymers and its potential use in tissue engineering applications. The drastically different cell adherence properties of TR4HP3SA/ESO and CD6HP8SA/ESO may suggest an interesting mechanism behind the TR4HP3SA polymer's ability to prevent cell growth. More

work is necessary to identify and understand the structure-property functions driving this phenomenon.

4.4.1 Appendix Includes:

^{1}H NMR of the hardeners, DSC, isothemal DSC, TGA, FT-IR, tan δ vs temperature curves, hemolytic degradation profiles, fibroblast cell morphology confocal images, raw cell count data, and flow cytometry gating procedures are included in the Supplementary Information.

4.4.2 Acknowledgements

This work was supported by the NSF under the Center for Sustainable Polymers, CHE-1413862. Part of this work was carried out in the College of Science and Engineering Characterization Facility, University of Minnesota, which has received capital equipment funding from the NSF through the UMN MRSEC program under Award Number DMR-1420013. The authors would also like to acknowledge work done using the Nikon confocal system at the University of Minnesota – University Imaging centers, http://uic.umn.edu.

The majority of the polymer synthesis and film *in situ* characterization was performed by author Quaxuan Zhang, with contributions by Anatolii Purchel. The entirety of the *in vitro* biocompatibility study was performed by the author of this dissertation.

CHAPTER 5: CONCLUSION

5.1 *IN VITRO, EX VIVO*, AND *IN VIVO* STRUCTURE-FUNCTION

5.1.1 Improving Glycopolycation Polyplexes for Systemic Delivery

Future work developing polyplex vehicles for systemic gene delivery should build on the structure-function relationships uncovered through studies *in vitro, ex vivo*, and *in vivo*. *Ex vivo* hemocompatibility and *in vivo* biodistribution supported the hypothesis that colloidal stability was an important polyplex function for achieving systemic delivery. However, complement activation results and the capture of P(MAG-*b*-MAEMt)-2 N/P=5 polymers by the liver indicate that colloidal stability is not sufficient for systemic delivery. While the bulkiness of the P(MAG) block demonstrated superior hemocompatibility compared to the P(EG) block in the hemolysis study, it may also play a role in delaying coagulation. Further protein-binding assays should be done to explore the extent of coagulation factor binding by the glycopolyplexes to determine if they are indeed interacting with those proteins, and if so, could P(MAG-*b*-MAEMt) polymers find a new application the field of anticoagulant medications.

Now that widespread biodistribution has been achieved, it should be possible to add targeting moieties to the P(MAG-*b*-MAEMt) polyplexes such as *N*-acetal galactosamine. Acetylated sugars have been known to activate

complement systems, so any targeting additions should be thoroughly screened for hemocompatibility *ex vivo*.

5.1.2 Continuing B Cell Transfection

Future work for transfecting B cells with non-viral cationic polyplexes should focus on developing or obtaining a satisfactory positive control. B cells of the same line that are genome edited to constitutively express GFP or IDUA protein would improve the quantification of gene expression generated by polyplex transfection. After obtaining a control, future screens could widen the pool to try transfecting other lymphocytes, or even stem cell precursors to B cells. Lastly, it has been shown that B cells endocytosis at different rates based on their age. Syncing the cells and aiming transfection during mitosis stages or even obtaining younger B cells could dramatically increase transfection using the polymers already developed. If that fails, new polymers could be designed with B cell physiology specifically in mind.

5.1.3 Continuing Glycofilm Studies

The trehalose- and β-cyclodextrin-based epoxy films presented similar physical properties upon crosslinking, but had dramatically different biocompatibility profiles. Future work will focus on identifying the structure-function relationships that contribute to those profiles. Initial tests should test both films for possible leachate that may kill cells or alter their physiology. Epoxide

functionality could be shuffled to probe the effects of different functional groups on the cell adhesion levels.

5.2 SUMMARY

Polymers contribute almost limitless chemistry, architecture, and functionality combination possibilities to the field of non-viral gene delivery. Many novel and creative vehicles have been made to overcome the intracellular and extracellular hurdles preventing these vehicles from effectively delivering their genetic payload, but not all vehicle functions are well understood in complex environments. The work discussed herein supports the trend that all polymeric gene delivery vehicles should be screened using a combination of experimental environments in addition to the standard *in situ* and *in vitro* screens. Screens *ex vivo* and *in vivo* supported previous *in vitro* work in highlighting the importance of polyplex colloidal stability, but also identified new structure-function relationships important to achieving system and cellular delivery. In time, *ex vivo* and *in vivo* screening methods will become easier to do, and will simultaneously become standard in the field just as *in vitro* screening methods did. Clarifying structure-function in complex environments will pave the way for more effective vehicles to be developed, and advance the use of safe, effective gene therapy for patients awaiting relief.

CHAPTER 6: BIBLIOGRAPHY

1. Kay, M. A., State-of-the-art gene-based therapies: the road ahead. *Nature Reviews Genetics* **2011,** *12* (5), 316-328.
2. Boudes, P. F., Gene therapy as a new treatment option for inherited monogenic diseases. *European Journal of Internal Medicine* **2014,** *25* (1), 31--36.
3. Hsu, C. Y. M.; Uludağ, H., Nucleic-acid based gene therapeutics: delivery challenges and modular design of nonviral gene carriers and expression cassettes to overcome intracellular barriers for sustained targeted expression. *Journal of Drug Targeting* **2012,** *20* (4), 301-328.
4. Aied, A.; Greiser, U.; Pandit, A.; Wang, W., Polymer gene delivery: overcoming the obstacles. *Drug Discovery Today* **2013,** *18* (21-22), 1090-1098.
5. Vanden Oever, M. J.; Tolar, J., Advances in understanding and treating dystrophic epidermolysis bullosa. *F1000Prime Rep* **2014,** *6*, 31-36.
6. Reid, T.; Galanis, E.; Abbruzzese, J.; Sze, D.; Andrews, J.; Romel, L.; Hatfield, M.; Rubin, J.; Kirn, D., Intra-arterial administration of a replication-selective adenovirus (dl1520) in patients with colorectal carcinoma metastatic to the liver: a phase I trial. *Gene Ther* **2001,** *8* (21), 1618-1626.
7. Roth, J. A.; Cristiano, R. J., Gene therapy for cancer: What have we done and where are we going? *J Natl Cancer I* **1997,** *89* (1), 21-39.
8. Zhang, Y.; Zheng, M. Y.; Kissel, T.; Agarwal, S., Design and Biophysical Characterization of Bioresponsive Degradable Poly(dimethylaminoethyl methacrylate) Based Polymers for In Vitro DNA Transfection. *Biomacromolecules* **2012,** *13* (2), 313-322.
9. Liu, F.; Huang, L., Development of non-viral vectors for systemic gene delivery. *Journal of Controlled Release* **2002,** *78* (1-3), 259-266.
10. Ginn, S. L.; Alexander, I. E.; Edelstein, M. L.; Abedi, M. R.; Wixon, J., Gene therapy clinical trials worldwide to 2012 - an update. *J Gene Med* **2013,** *15* (2), 65-77.
11. Kay, M. A., State-of-the-art gene-based therapies: the road ahead. *Nature reviews. Genetics* **2011,** *12* (5), 316-28.
12. Verma, I. M., Medicine. Gene therapy that works. *Science* **2013,** *341* (6148), 853-5.
13. Wilson, J. M., Genetic diseases, immunology, viruses, and gene therapy. *Hum Gene Ther* **2014,** *25* (4), 257-61.
14. Vorburger, S. A.; Hunt, K. K., Adenoviral gene therapy. *Oncologist* **2002,** *7* (1), 46-59.

15. Yin, H.; Kanasty, R. L.; Eltoukhy, A. A.; Vegas, A. J.; Dorkin, J. R.; Anderson, D. G., Non-viral vectors for gene-based therapy. *Nature reviews. Genetics* **2014,** *15* (8), 541-55.
16. Zhang, Y.; Satterlee, A.; Huang, L., In vivo gene delivery by nonviral vectors: overcoming hurdles? *Mol Ther* **2012,** *20* (7), 1298-304.
17. Walther, W.; Stein, U., Viral vectors for gene transfer: a review of their use in the treatment of human diseases. *Drugs* **2000,** *60* (2), 249-71.
18. Thomas, C. E.; Ehrhardt, A.; Kay, M. A., Progress and problems with the use of viral vectors for gene therapy. *Nat Rev Genet* **2003,** *4* (5), 346-58.
19. Hackett, P. B.; Largaespada, D. A.; Cooper, L. J. N., A Transposon and Transposase System for Human Application. *Mol Ther* **2010,** *18* (4), 674-683.
20. Pack, D. W.; Hoffman, A. S.; Pun, S.; Stayton, P. S., Design and development of polymers for gene delivery. *Nat Rev Drug Discov* **2005,** *4* (7), 581-93.
21. Blanco, E.; Shen, H.; Ferrari, M., Principles of nanoparticle design for overcoming biological barriers to drug delivery. *Nat Biotechnol* **2015,** *33* (9), 941-51.
22. Uchida, E.; Mizuguchi, H.; Ishii-Watabe, A.; Hayakawa, T., Comparison of the efficiency and safety of non-viral vector-mediated gene transfer into a wide range of human cells. *Biol Pharm Bull* **2002,** *25* (7), 891-7.
23. Yue, Z. G.; Wei, W.; Lv, P. P.; Yue, H.; Wang, L. Y.; Su, Z. G.; Ma, G. H., Surface charge affects cellular uptake and intracellular trafficking of chitosan-based nanoparticles. *Biomacromolecules* **2011,** *12* (7), 2440-6.
24. Grandinetti, G.; Smith, A. E.; Reineke, T. M., Membrane and Nuclear Permeabilization by Polymeric pDNA Vehicles: Efficient Method for Gene Delivery or Mechanism of Cytotoxicity? *Molecular Pharmaceutics* **2012,** *9* (3), 523-538.
25. Frohlich, E., The role of surface charge in cellular uptake and cytotoxicity of medical nanoparticles. *Int J Nanomedicine* **2012,** *7*, 5577-91.
26. Shah, N. B.; Vercellotti, G. M.; White, J. G.; Fegan, A.; Wagner, C. R.; Bischof, J. C., Blood-nanoparticle interactions and in vivo biodistribution: impact of surface PEG and ligand properties. *Mol Pharm* **2012,** *9* (8), 2146-55.
27. Deshmukh, M.; Kutscher, H. L.; Gao, D.; Sunil, V. R.; Malaviya, R.; Vayas, K.; Stein, S.; Laskin, J. D.; Laskin, D. L.; Sinko, P. J., Biodistribution and renal clearance of biocompatible lung targeted poly(ethylene glycol) (PEG) nanogel aggregates. *J Control Release* **2012,** *164* (1), 65-73.
28. Ogris, M.; Brunner, S.; Schuller, S.; Kircheis, R.; Wagner, E., PEGylated DNA/transferrin-PEI complexes: reduced interaction with blood components,

extended circulation in blood and potential for systemic gene delivery. *Gene Therapy* **1999,** *6* (4), 595-605.
29. Dash, P. R.; Read, M. L.; Barrett, L. B.; Wolfert, M. A.; Seymour, L. W., Factors affecting blood clearance and in vivo distribution of polyelectrolyte complexes for gene delivery. *Gene Ther* **1999,** *6* (4), 643-50.
30. Alexis, F.; Pridgen, E.; Molnar, L. K.; Farokhzad, O. C., Factors affecting the clearance and biodistribution of polymeric nanoparticles. *Mol Pharm* **2008,** *5* (4), 505-15.
31. Smith, A. E.; Sizovs, A.; Grandinetti, G.; Xue, L.; Reineke, T. M., Diblock glycopolymers promote colloidal stability of polyplexes and effective pDNA and siRNA delivery under physiological salt and serum conditions. *Biomacromolecules* **2011,** *12* (8), 3015-22.
32. Lodish, H.; Berk, A.; Zipursky, S. L.; Matsudaira, P.; Baltimore, D.; Darnell, J., Receptor-Mediated Endocytosis and the Sorting of Internalized Proteins. In *Molecular Cell Biology*, W. H. Freeman: New York, 2000.
33. Dale, D. C.; Boxer, L.; Liles, W. C., The phagocytes: neutrophils and monocytes. *Blood* **2008,** *112* (4), 935-45.
34. Lim, J. P.; Gleeson, P. A., Macropinocytosis: an endocytic pathway for internalising large gulps. *Immunology and Cell Biology* **2011,** *89* (8), 836-843.
35. McLendon, P. M.; Fichter, K. M.; Reineke, T. M., Poly(glycoamidoamine) Vehicles Promote pDNA Uptake through Multiple Routes and Efficient Gene Expression via Caveolae-Mediated Endocytosis. *Molecular Pharmaceutics* **2010,** *7* (3), 738-750.
36. Varkouhi, A. K.; Scholte, M.; Storm, G.; Haisma, H. J., Endosomal escape pathways for delivery of biologicals. *Journal of Controlled Release* **2011,** *151* (3), 220-228.
37. Lönn, P.; Kacsinta, A. D.; Cui, X.-S.; Hamil, A. S.; Kaulich, M.; Gogoi, K.; Dowdy, S. F., Enhancing Endosomal Escape for Intracellular Delivery of Macromolecular Biologic Therapeutics. *Scientific Reports* **2016,** *6*.
38. Dominska, M.; Dykxhoorn, D. M., Breaking down the barriers: siRNA delivery and endosome escape. *Journal of Cell Science* **2010,** *123*, 1183-1189.
39. Liu, Y.; Reineke, T. M., Degradation of Poly(glycoamidoamine) DNA Delivery Vehicles: Polyamide Hydrolysis at Physiological Conditions Promotes DNA Release. *Biomacromolecules* **2010,** *11* (2), 316-325.
40. Fichter, K. M.; Ingle, N. P.; McLendon, P. M.; Reineke, T. M., Polymeric nucleic acid vehicles exploit active interorganelle trafficking mechanisms. *ACS Nano* **2013,** *7* (1), 347-64.

41. Grandinetti, G.; Reineke, T. M., Exploring the Mechanism of Plasmid DNA Nuclear Internalization with Polymer-Based Vehicles. *Molecular Pharmaceutics* **2012,** *9* (8), 2256-2267.
42. Gaj, T.; Gersbach, C. A.; Barbas, C. F., 3rd, ZFN, TALEN, and CRISPR/Cas-based methods for genome engineering. *Trends Biotechnol* **2013,** *31* (7), 397-405.
43. Hackett, P. B., Integrating DNA vectors for gene therapy. *Molecular Therapy* **2007,** *15* (1), 10-12.
44. Reineke, T. M.; Davis, M. E., Structural effects of carbohydrate-containing polycations on gene delivery. 2. Charge center type. *Bioconjugate Chemistry* **2003,** *14* (1), 255-261.
45. Walisko, O.; Jursch, T.; Izsvak, Z.; Ivics, Z., Transposon-Host Cell Interactions in the Regulation of Sleeping Beauty Transposition. In *Transposons and the Dynamic Genome*, Lankenau, D. H.; Volff, J. N., Eds. 2009; Vol. 4, pp 109-132.
46. Mates, L.; Walisko, O.; Schorn, A.; Kaufman, C.; Ivics, Z.; Izsvak, Z., Sleeping beauty: A non-viral vector, capable of gene transfer at efficiencies comparable to integrating viral systems. *Human Gene Therapy* **2007,** *18* (10), 973-973.
47. Maiti, S. N.; Ang, S.; Moriarity, B.; Zhang, J.; Liang, S.; Ossowski, M.; Andrews, K.; Tzeng, K.; Talbot, R.; Torikai, H.; Huls, H.; Kebriaei, P.; Largaespada, D.; Champlin, R.; Hackett, P.; Cooper, L. J. N., A Comprehensive Road Map for Risk Assessment of Sleeping Beauty Transposition Events in T-Cell Immunotherapy. *Molecular Therapy* **2012,** *20*, S179-S179.
48. Barz, M.; Luxenhofer, R.; Zentel, R.; Vicent, M. J., Overcoming the PEG-addiction: well-defined alternatives to PEG, from structure-property relationships to better defined therapeutics. *Polymer Chemistry* **2011,** *2* (9), 1900-1918.
49. Rejman, J.; Oberle, V.; Zuhorn, I. S.; Hoekstra, D., Size-dependent internalization of particles via the pathways of clathrin- and caveolae-mediated endocytosis. *Biochem J* **2004,** *377* (Pt 1), 159-69.
50. Zhang, S.; Li, J.; Lykotrafitis, G.; Bao, G.; Suresh, S., Size-Dependent Endocytosis of Nanoparticles. *Adv Mater* **2009,** *21*, 419-424.
51. Uchegbu, I. F.; Dufes, C.; Kan, P. L.; Schatzlein, A. G., Polymers and Dendrimers for Gene Delivery in Gene Therapy. In *Gene and Cell Therapy, 3rd Ed.*, Templeton, N. S., Ed. Taylor & Francis Group, LLC: Boca Raton, FL, 2009; pp 321-340.

52. Puskas, Z.; Schuierer, G., [Determination of blood circulation time for optimizing contrast medium administration in CT angiography]. *Radiologe* **1996,** *36* (9), 750-7.
53. Debbage, P. L.; Griebel, J.; Ried, M.; Gneiting, T.; DeVries, A.; Hutzler, P., Lectin intravital perfusion studies in tumor-bearing mice: micrometer-resolution, wide-area mapping of microvascular labeling, distinguishing efficiently and inefficiently perfused microregions in the tumor. *J Histochem Cytochem* **1998,** *46* (5), 627-39.
54. Welsher, K.; Sherlock, S. P.; Dai, H., Deep-tissue anatomical imaging of mice using carbon nanotube fluorophores in the second near-infrared window. *Proceedings of the National Academy of Sciences of the United States of America* **2011,** *108* (22), 8943-8948.
55. Jackson, A. L.; Linsley, P. S., Recognizing and avoiding siRNA off-target effects for target identification and therapeutic application. *Nature Reviews Drug Discovery* **2010,** *9* (1), 57-67.
56. Budker, V.; Zhang, G.; Knechtle, S.; Wolff, J. A., Naked DNA delivered intraportally expresses efficiently in hepatocytes. *Gene Ther* **1996,** *3* (7), 593-8.
57. Bonamassa, B.; Hai, L.; Liu, D., Hydrodynamic gene delivery and its applications in pharmaceutical research. *Pharm Res* **2011,** *28* (4), 694-701.
58. Tolstyka, Z. P.; Phillips, H.; Cortez, M.; Wu, Y.; Ingle, N.; Bell, J. B.; Hackett, P. B.; Reineke, T. M., Trehalose-Based Block Copolycations Promote Polyplex Stabilization for Lyophilization and in Vivo pDNA Delivery. **2015**.
59. Kindt, T. J.; Goldsby, R. A.; Osborne, B. A.; Kuby, J., *Immunology, 6th Ed.* W. H. Freeman: New York, 2007; p 574.
60. Schnell, M. A.; Zhang, Y.; Tazelaar, J.; Gao, G. P.; Yu, Q. C.; Qian, R.; Chen, S. J.; Varnavski, A. N.; LeClair, C.; Raper, S. E.; Wilson, J. M., Activation of innate immunity in nonhuman primates following intraportal administration of adenoviral vectors. *Molecular Therapy* **2001,** *3* (5), 708-722.
61. Matz, R. L.; Erickson, B.; Vaidyanathan, S.; Kukowska-Latallo, J. F.; Baker, J. R., Jr.; Orr, B. G.; Holl, M. M. B., Polyplex Exposure Inhibits Cell Cycle, Increases Inflammatory Response, and Can Cause Protein Expression without Cell Division. *Molecular Pharmaceutics* **2013,** *10* (4), 1306-1317.
62. Mima, Y.; Hashimoto, Y.; Shimizu, T.; Kiwada, H.; Ishida, T., Anti-PEG IgM Is a Major Contributor to the Accelerated Blood Clearance of Polyethylene Glycol-Conjugated Protein. *Molecular Pharmaceutics* **2015,** *12* (7), 2429-2435.
63. Saadati, R.; Dadashzadeh, S.; Abbasian, Z.; Soleimanjahi, H., Accelerated Blood Clearance of PEGylated PLGA Nanoparticles Following Repeated

Injections: Effects of Polymer Dose, PEG Coating, and Encapsulated Anticancer Drug. *Pharmaceutical Research* **2013,** *30* (4), 985-995.
64. Mosqueira, V. C.; Legrand, P.; Gulik, A.; Bourdon, O.; Gref, R.; Labarre, D.; Barratt, G., Relationship between complement activation, cellular uptake and surface physicochemical aspects of novel PEG-modified nanocapsules. *Biomaterials* **2001,** *22* (22), 2967-79.
65. Szebeni, J., Complement activation-related pseudoallergy: a stress reaction in blood triggered by nanomedicines and biologicals. *Mol Immunol* **2014,** *61* (2), 163-73.
66. Devoldere, J.; Dewitte, H.; De Smedt, S. C.; Remaut, K., Evading innate immunity in nonviral mRNA delivery: don't shoot the messenger. *Drug Discov Today* **2016,** *21* (1), 11-25.
67. Endmann, A.; Baden, M.; Weisermann, E.; Kapp, K.; Schroff, M.; Kleuss, C.; Wittig, B.; Juhls, C., Immune response induced by a linear DNA vector: Influence of dose, formulation and route of injection. *Vaccine* **2010,** *28* (21), 3642-3649.
68. Meng, H.; Xue, M.; Xia, T.; Ji, Z.; Tarn, D. Y.; Zink, J. I.; Nel, A. E., Use of Size and a Copolymer Design Feature To Improve the Biodistribution and the Enhanced Permeability and Retention Effect of Doxorubicin-Loaded Mesoporous Silica Nanoparticles in a Murine Xenograft Tumor Model. *ACS Nano* **2011,** *5* (5), 4131-4144.
69. Sato, Y.; Murase, K.; Kato, J.; Kobune, M.; Sato, T.; Kawano, Y.; Takimoto, R.; Takada, K.; Miyanishi, K.; Matsunaga, T.; Takayama, T.; Niitsu, Y., Resolution of liver cirrhosis using vitamin A-coupled liposomes to deliver siRNA against a collagen-specific chaperone. *Nat Biotechnol* **2008,** *26* (4), 431-42.
70. Dhande, Y. K.; Wagh, B. S.; Hall, B. C.; Sprouse, D.; Hackett, P. B.; Reineke, T. M., N-Acetylgalactosamine Block-co-Polycations Form Stable Polyplexes with Plasmids and Promote Liver-Targeted Delivery. *Biomacromolecules* **2016,** *17* (3), 830-840.
71. Song, E.; Zhu, P.; Lee, S.-K.; Chowdhury, D.; Kussman, S.; Dykxhoorn, D. M.; Feng, Y.; Palliser, D.; Weiner, D. B.; Shankar, P.; Marasco, W. A.; Lieberman, J., Antibody mediated in vivo delivery of small interfering RNAs via cell-surface receptors. *Nature Biotechnology* **2005,** *23* (6), 709-717.
72. Dong, D. W.; Xiang, B.; Gao, W.; Yang, Z. Z.; Li, J. Q.; Qi, X. R., pH-responsive complexes using prefunctionalized polymers for synchronous delivery of doxorubicin and siRNA to cancer cells. *Biomaterials* **2013,** *34* (20), 4849-59.

73. Kang, H.; Trondoli, A. C.; Zhu, G.; Chen, Y.; Chang, Y.-J.; Liu, H.; Huang, Y.-F.; Zhang, X.; Tan, W., Near-Infrared Light-Responsive Core–Shell Nanogels for Targeted Drug Delivery. *ACS Nano* **2011,** *5* (6), 5094-5099.
74. Kim, S. H.; Jeong, J. H.; Kim, T. I.; Kim, S. W.; Bull, D. A., VEGF siRNA delivery system using arginine-grafted bioreducible poly(disulfide amine). *Mol Pharm* **2009,** *6* (3), 718-26.
75. Musacchio, T.; Vaze, O.; D'Souza, G.; Torchilin, V. P., Effective stabilization and delivery of siRNA: reversible siRNA-phospholipid conjugate in nanosized mixed polymeric micelles. *Bioconjug Chem* **2010,** *21* (8), 1530-6.
76. Zhu, L.; Kate, P.; Torchilin, V. P., Matrix metalloprotease 2-responsive multifunctional liposomal nanocarrier for enhanced tumor targeting. *ACS Nano* **2012,** *6* (4), 3491-8.
77. Srinivasachari, S.; Liu, Y. M.; Prevette, L. E.; Reineke, T. M., Effects of trehalose click polymer length on pDNA complex stability and delivery efficacy. *Biomaterials* **2007,** *28* (18), 2885-2898.
78. Srinivasachari, S.; Liu, Y. M.; Zhang, G. D.; Prevette, L.; Reineke, T. M., Trehalose click polymers inhibit nanoparticle aggregation and promote pDNA delivery in serum. *J Am Chem Soc* **2006,** *128* (25), 8176-8184.
79. Mishra, S.; Webster, P.; Davis, M. E., PEGylation significantly affects cellular uptake and intracellular trafficking of non-viral gene delivery particles. *European Journal of Cell Biology* **2004,** *83* (3), 97-111.
80. Buckwalter, D. J.; Sizovs, A.; Ingle, N. P.; Reineke, T. M., MAG versus PEG: Incorporating a Poly(MAG) Layer to Promote Colloidal Stability of Nucleic Acid/“Click Cluster” Complexes. *ACS Macro Letters* **2012,** *1* (5), 609-613.
81. Tsuchiya, A.; Naritomi, Y.; Kushio, S.; Kang, J. H.; Murata, M.; Hashizume, M.; Mori, T.; Niidome, T.; Katayama, Y., Improvement in the colloidal stability of protein kinase-responsive polyplexes by PEG modification. *Journal of Biomedical Materials Research Part A* **2012,** *100A* (5), 1136-1141.
82. Wattendorf, U.; Merkle, H. P., PEGylation as a tool for the biomedical engineering of surface modified microparticles. *Journal of Pharmaceutical Sciences* **2008,** *97* (11), 4655-4669.
83. Li, H.; Cortez, M. A.; Phillips, H. R.; Wu, Y.; Reineke, T. M., Poly(2 deoxy 2 methacrylamido glucopyranose) b Poly(methacrylate amine)s: Optimization of Diblock Glycopol ycations for Nucleic Acid Delivery. *ACS Macro Lett* **2013,** *2* (3).
84. Merdan, T.; Kunath, K.; Petersen, H.; Bakowsky, U.; Voigt, K. H.; Kopecek, J.; Kissel, T., PEGylation of poly(ethylene imine) affects stability of complexes with plasmid DNA under in vivo conditions in a dose-dependent

manner after intravenous injection into mice. *Bioconjugate Chemistry* **2005,** *16* (4), 785-92.
85. Li, S.-D.; Huang, L., Gene therapy progress and prospects: non-viral gene therapy by systemic delivery. *Gene Therapy* **2006,** *13* (18), 1313-1319.
86. Merkel, O. M.; Beyerle, A.; Beckmann, B.; Zheng, M.; Hartmann, R. K.; Stoger, T.; Kissel, T. H., Polymer-related off-target effects in non-viral siRNA delivery. *Biomaterials* **2011,** *32* (9), 2388–2398.
87. Belur, L. R.; Podetz-Pedersen, K.; Frandsen, J.; McIvor, R. S., Lung-directed gene therapy in mice using the nonviral Sleeping Beauty transposon system. *Nat Protoc* **2007,** *2* (12), 3146-52.
88. Fang, J.; Nakamura, H.; Maeda, H., The EPR effect: Unique features of tumor blood vessels for drug delivery, factors involved, and limitations and augmentation of the effect. *Advanced Drug Delivery Reviews* **2011,** *63* (3), 136-151.
89. Hashida, M.; Nishikawa, M.; Yamashita, F.; Takakura, Y., Cell-specific delivery of genes with glycosylated carriers. *Advanced Drug Delivery Reviews* **2001,** *52* (3), 187-196.
90. Li, K.; Sato, H.; Kim, C. W.; Nakamura, Y.; Zhao, G. X.; Funamoto, D.; Nobori, T.; Kishimura, A.; Mori, T.; Katayama, Y., Tumor accumulation of protein kinase-responsive gene carrier/DNA polyplex stabilized by alkanethiol for intravenous injection. *Journal of Biomaterials Science, Polymer Edition* **2015,** *26* (11).
91. Dufort, S.; Sancey, L.; Coll, J. L., Physico-chemical parameters that govern nanoparticles fate also dictate rules for their molecular evolution. *Advanced Drug Delivery Reviews* **2012,** *64* (2), 179-189.
92. Ahmed, M.; Lai, B. F.; Kizhakkedathu, J. N.; Narain, R., Hyperbranched glycopolymers for blood biocompatibility. *Bioconjug Chem* **2012,** *23* (5), 1050-8.
93. Hunter, A. C.; Moghimi, S. M., Therapeutic synthetic polymers: a game of Russian roulette? *Drug Discovery Today* **2002,** *7* (19), 998-1001.
94. Wu, Y.; Wang, M.; Sprouse, D.; Smith, A. E.; Reineke, T. M., Glucose-Containing Diblock Polycations Exhibit Molecular Weight, Charge, and Cell-Type Dependence for pDNA Delivery. *Biomacromolecules* **2014,** *15* (5), 1716-1726.
95. Sprouse, D.; Reineke, T. M., Investigating the effects of block versus statistical glycopolycations containing primary and tertiary amines for plasmid DNA delivery. *Biomacromolecules* **2014,** *15* (7), 2616-28.
96. Grandinetti, G.; Ingle, N. P.; Reineke, T. M., Interaction of poly(ethylenimine)-DNA polyplexes with mitochondria: implications for a mechanism of cytotoxicity. *Mol Pharm* **2011,** *8* (5), 1709-19.

97. McLendon, P. M.; Buckwalter, D. J.; Davis, E. M.; Reineke, T. M., Interaction of poly(glycoamidoamine) DNA delivery vehicles with cell-surface glycosaminoglycans leads to polyplex internalization in a manner not solely dependent on charge. *Mol Pharm* **2010,** *7* (5), 1757-68.
98. Ingle, N. P.; Xue, L.; Reineke, T. M., Spatiotemporal cellular imaging of polymer-pDNA nanocomplexes affords in situ morphology and trafficking trends. *Mol Pharm* **2013,** *10* (11), 4120-35.
99. Narain, R.; Wang, Y.; Ahmed, M.; Lai, B. F.; Kizhakkedathu, J. N., Blood Components Interactions to Ionic and Nonionic Glyconanogels. *Biomacromolecules* **2015,** *16* (9), 2990-7.
100. Hansson, K. M.; Tosatti, S.; Isaksson, J.; Wettero, J.; Textor, M.; Lindahl, T. L.; Tengvall, P., Whole blood coagulation on protein adsorption-resistant PEG and peptide functionalised PEG-coated titanium surfaces. *Biomaterials* **2005,** *26* (8), 861-72.
101. Jones, C. F.; Campbell, R. A.; Franks, Z.; Gibson, C. C.; Thiagarajan, G.; Vieira-de-Abreu, A.; Sukavaneshvar, S.; Mohammad, S. F.; Li, D. Y.; Ghandehari, H.; Weyrich, A. S.; Brooks, B. D.; Grainger, D. W., Cationic PAMAM dendrimers disrupt key platelet functions. *Mol Pharm* **2012,** *9* (6), 1599-611.
102. Aronovich, E. L.; Hall, B. C.; Bell, J. B.; McIvor, R. S.; Hackett, P. B., Quantification of Alpha-L-Iduronidase Expression Outcomes in Mice Following Sleeping Beauty Transposon-Mediated Gene Therapy. *Molecular Therapy* **2013,** *21*, S172-S173.
103. Biris, A. S.; Galanzha, E. I.; Li, Z.; Mahmood, M.; Xu, Y.; Zharov, V. P., In vivo Raman flow cytometry for real-time detection of carbon nanotube kinetics in lymph, blood, and tissues. *Journal of Biomedical Optics* **2009,** *14* (2).
104. Browning, L. M.; Huang, T.; Xu, X.-H. N., Real-time in vivo imaging of size-dependent transport and toxicity of gold nanoparticles in zebrafish embryos using single nanoparticle plasmonic spectroscopy. *Interface Focus* **2013,** *The Royal Society Publishing* (3), 3.
105. Li, J. L.; Goh, C. C.; Keeble, J. L.; Qin, J. S.; Roediger, B.; Jain, R.; Wang, Y.; Chew, W. K.; Weninger, W.; Ng, L. G., Intravital multiphoton imaging of immune responses in the mouse ear skin. *Nature Protocols* **2012,** *7*, 221-234.
106. Gary, D. J.; Lee, H.; Sharma, R.; Lee, J. S.; Kim, Y.; Cui, Z. Y.; Jia, D.; Bowman, V. D.; Chipman, P. R.; Wan, L.; Zou, Y.; Mao, G. Z.; Park, K.; Herbert, B. S.; Konieczny, S. F.; Won, Y. Y., Influence of Nano-Carrier Architecture on in Vitro siRNA Delivery Performance and in Vivo

Biodistribution: Polyplexes vs Micelleplexes. *Acs Nano* **2011,** *5* (5), 3493-3505.
107. Karmali, P. P.; Simberg, D., Interactions of nanoparticles with plasma proteins: implication on clearance and toxicity of drug delivery systems. *Expert Opinion on Drug Delivery* **2011,** *8* (3), 343-357.
108. Knop, K.; Hoogenboom, R.; Fischer, D.; Schubert, U. S., Poly(ethylene glycol) in Drug Delivery: Pros and Cons as Well as Potential Alternatives. *Angewandte Chemie-International Edition* **2010,** *49* (36), 6288-6308.
109. Caliceti, P.; Veronese, F. M., Pharmacokinetic and biodistribution properties of poly(ethylene glycol)-protein conjugates. *Adv Drug Deliver Rev* **2003,** *55* (10), 1261-1277.
110. Dewachter, P.; Mouton-Faivre, C., Anaphylaxis to macrogol 4000 after a parenteral corticoid injection. *Allergy* **2005,** *60* (5), 705-706.
111. Chanan-Khan, A.; Szebeni, J.; Savay, S.; Liebes, L.; Rafique, N. M.; Alving, C. R.; Muggia, F. M., Complement activation following first exposure to pegylated liposomal doxorubicin (Doxil): possible role in hypersensitivity reactions. *Annals of Oncology* **2003,** *14* (9), 1430-1437.
112. Szebeni, J., Complement activation-related pseudoallergy: A new class of drug-induced acute immune toxicity. *Toxicology* **2005,** *216* (2-3), 106-121.
113. Ishida, T.; Harada, M.; Wang, X. Y.; Ichihara, M.; Irimura, K.; Kiwada, H., Accelerated blood clearance of PEGylated liposomes following preceding liposome injection: Effects of lipid dose and PEG surface-density and chain length of the first-dose liposomes. *Journal of Controlled Release* **2005,** *105* (3), 305-317.
114. Ishida, T.; Kashima, S.; Kiwada, H., The contribution of phagocytic activity of liver macrophages to the accelerated blood clearance (ABC) phenomenon of PEGylated liposomes in rats. *Journal of Controlled Release* **2008,** *126* (2), 162-165.
115. Ishida, T.; Kiwada, H., Accelerated blood clearance (ABC) phenomenon upon repeated injection of PEGylated liposomes. *International Journal of Pharmaceutics* **2008,** *354* (1-2), 56-62.
116. Smith, A. E.; Sizovs, A.; Grandinetti, G.; Xue, L.; Reineke, T. M., Diblock Glycopolymers Promote Colloidal Stability of Polyplexes and Effective pDNA and siRNA Delivery under Physiological Salt and Serum Conditions. *Biomacromolecules* **2011,** *12* (8), 3015-3022.
117. Sizovs, A.; Xue, L.; Tolstyka, Z. P.; Ingle, N. P.; Wu, Y. Y.; Cortez, M.; Reineke, T. M., Poly(trehalose): Sugar-Coated Nanocomplexes Promote Stabilization and Effective Polyplex-Mediated siRNA Delivery. *J Am Chem Soc* **2013,** *135* (41), 15417-15424.

118. Streeter, J. G., Accumulation of Alpha,Alpha-Trehalose by Rhizobium Bacteria and Bacteroids. *J Bacteriol* **1985,** *164* (1), 78-84.
119. Teramoto, N.; Sachinvala, N. D.; Shibata, M., Trehalose and trehalose-based polymers for environmentally benign, biocompatible and bioactive materials. *Molecules* **2008,** *13* (8), 1773-1816.
120. Ramlov, H.; Westh, P., Survival of the Cryptobiotic Eutardigrade Adorybiotus-Coronifer during Cooling to 196-Degrees-C - Effect of Cooling Rate, Trehalose Level, and Short-Term Acclimation. *Cryobiology* **1992,** *29* (1), 125-130.
121. Somme, L., Anhydrobiosis and cold tolerance in tardigrades. *Eur J Entomol* **1996,** *93* (3), 349-357.
122. Ohtake, S.; Wang, Y. J., Trehalose: Current Use and Future Applications. *J Pharm Sci-Us* **2011,** *100* (6), 2020-2053.
123. Anderson, K.; Sizovs, A.; Cortez, M.; Waldron, C.; Haddleton, D. M.; Reineke, T. M., Effects of Trehalose Polycation End-Group Functionalization on Plasmid DNA Uptake and Transfection. *Biomacromolecules* **2012,** *13* (8), 2229-2239.
124. Mancini, R. J.; Lee, J.; Maynard, H. D., Trehalose Glycopolymers for Stabilization of Protein Conjugates to Environmental Stressors. *J Am Chem Soc* **2012,** *134* (20), 8474-8479.
125. Li, H.; Cortez, M. A.; Phillips, H. R.; Wu, Y.; Reineke, T. M., Poly(2-deoxy-2-methacrylamido glucopyranose)-b-Poly(methacrylate amine)s: Optimization of Diblock Glycopolycations for Nucleic Acid Delivery. *Acs Macro Letters* **2013,** *2* (3), 230-235.
126. Podetz-Pedersen, K. M.; Vezys, V.; Somia, N. V.; Russell, S. J.; McIvor, R. S., Cellular immune response against firefly luciferase after sleeping beauty-mediated gene transfer in vivo. *Hum Gene Ther* **2014,** *25* (11), 955-65.
127. Xu, X.; Smith, A. E.; Kirkland, S. E.; McCormick, C. L., Aqueous RAFT Synthesis of pH-Responsive Triblock Copolymer mPEO−PAPMA−PDPAEMA and Formation of Shell Cross-Linked Micelles†. *Macromolecules* **2008,** *41* (22), 8429-8435.
128. Wright, J. C.; Westh, P.; Ramlov, H., Cryptobiosis in Tardigrada. *Biol Rev* **1992,** *67* (1), 1-29.
129. Grandinetti, G.; Ingle, N. P.; Reineke, T. M., Interaction of Poly(ethylenimine)-DNA Polyplexes with Mitochondria: Implications for a Mechanism of Cytotoxicity. *Mol Pharmaceut* **2011,** *8* (5), 1709-1719.
130. Ahmed, M.; Narain, R., The effect of polymer architecture, composition, and molecular weight on the properties of glycopolymer-based non-viral gene delivery systems. *Biomaterials* **2011,** *32* (22), 5279-5290.

131. Lee, C. C.; Liu, Y.; Reineke, T. M., General structure-activity relationship for poly(glycoamidoamine)s: The effect of amine density on cytotoxicity and DNA delivery efficiency. *Bioconjugate Chem* **2008,** *19* (2), 428-440.
132. Reineke, T. M.; Davis, M. E., Structural effects of carbohydrate-containing polycations on gene delivery. 1. Carbohydrate size and its distance from charge centers. *Bioconjugate Chem* **2003,** *14* (1), 247-254.
133. Hwang, S. J.; Bellocq, N. C.; Davis, M. E., Effects of structure of beta-cyclodextrin-containing polymers on gene delivery. *Bioconjugate Chem* **2001,** *12* (2), 280-290.
134. Buckwalter, D. J.; Sizovs, A.; Ingle, N. P.; Reineke, T. M., MAG versus PEG: Incorporating a Poly(MAG) Layer to Promote Colloidal Stability of Nucleic Acid/"Click Cluster" Complexes. *Acs Macro Lett* **2012,** *1* (5), 609-613.
135. Li, X.; Mya, K. Y.; Ni, X. P.; He, C. B.; Leong, K. W.; Li, J., Dynamic and static light scattering studies on self-aggregation behavior of biodegradable amphiphilic poly(ethylene oxide)-poly (R)-3-hydroxybutyrate -poly(ethylene oxide) triblock copolymers in aqueous solution. *Journal of Physical Chemistry B* **2006,** *110* (12), 5920-5926.
136. Nielsen, P. E., Uranyl Photofootprinting. In *DNA-Protein Interactions: Principles and Protocols, Third Edition*, Moss, T.; LeBlanc, B., Eds. 2009; Vol. 543, pp 87-96.
137. VanGuilder, H. D.; Vrana, K. E.; Freeman, W. M., Twenty-five years of quantitative PCR for gene expression analysis. *Biotechniques* **2008,** *44* (5), 619-626.
138. Aronovich, E. L.; Bell, J. B.; Belur, L. R.; Gunther, R.; Koniar, B.; David, C. C.; Schachem, P. A.; Matise, I.; McIvor, R. S.; Whitley, C. B.; Hackett, P. B., Protonged expression of a tysosomat enzyme in mouse tiver after Sleeping Beauty transposon-mediated gene detivery: imptications for non-virat gene therapy of mucopotysaccharidoses. *J Gene Med* **2007,** *9* (5), 403-415.
139. Bell, J. B.; Podetz-Pedersen, K. M.; Aronovich, E. L.; Belur, L. R.; McIvor, R. S.; Hackett, P. B., Preferential delivery of the Sleeping Beauty transposon system to livers of mice by hydrodynamic injection. *Nat Protoc* **2007,** *2* (12), 3153-3165.
140. Cieslewicz, M.; Tang, J. J.; Yu, J. L.; Cao, H.; Zavaljevski, M.; Motoyama, K.; Lieber, A.; Raines, E. W.; Pun, S. H., Targeted delivery of proapoptotic peptides to tumor-associated macrophages improves survival. *P Natl Acad Sci USA* **2013,** *110* (40), 15919-15924.
141. Lin, X.; Zhu, H.; Luo, Z.; Hong, Y.; Zhang, H.; Liu, X.; Ding, H.; Tian, H.; Yang, Z., Near-Infrared Fluorescence Imaging of Non-Hodgkin’s Lymphoma

CD20 Expression Using Cy7-Conjugated Obinutuzumab. *Mol Imaging Biol* **2014**, 1-11.
142. Zuckerman, J. E.; Choi, C. H. J.; Han, H.; Davis, M. E., Polycation-siRNA nanoparticles can disassemble at the kidney glomerular basement membrane. *P Natl Acad Sci USA* **2012,** *109* (8), 3137-3142.
143. Podetz-Pedersen, K. M.; Bell, J. B.; Steele, T. W. J.; Wilber, A.; Shier, W. T.; Belur, L. R.; McIvor, R. S.; Hackett, P. B., Gene Expression in Lung and Liver After Intravenous Infusion of Polyethylenimine Complexes of Sleeping Beauty Transposons. *Hum Gene Ther* **2010,** *21* (2), 210-220.
144. Aronovich, E. L.; Bell, J. B.; Khan, S. A.; Belur, L. R.; Gunther, R.; Koniar, B.; Schachern, P. A.; Parker, J. B.; Carlson, C. S.; Whitley, C. B.; McIvor, R. S.; Gupta, P.; Hackett, P. B., Systemic Correction of Storage Disease in MPS I NOD/SCID Mice Using the Sleeping Beauty Transposon System. *Mol Ther* **2009,** *17* (7), 1136-1144.
145. Aronovich, E. L.; McIvor, R. S.; Hackett, P. B., The Sleeping Beauty transposon system: a non-viral vector for gene therapy. *Hum Mol Genet* **2011,** *20*, R14-R20.
146. Sawyer, G. J.; Dong, X.; Whitehorne, M.; Grehan, A.; Seddon, M.; Shah, A. M.; Zhang, X.; Fabre, J. W., Cardiovascular function following acute volume overload for hydrodynamic gene delivery to the liver. *Gene Ther* **2007,** *14* (16), 1208-1217.
147. Zhang, G.; Gao, X.; Song, Y. K.; Vollmer, R.; Stolz, D. B.; Gasiorowski, J. Z.; Dean, D. A.; Liu, D., Hydroporation as the mechanism of hydrodynamic delivery. *Gene Ther* **2004,** *11* (8), 675-682.
148. Hackett, P. B.; Aronovich, E. L.; Hunter, D.; Urness, M.; Bell, J. B.; Kass, S. J.; Cooper, L. J. N.; McIvor, S., Efficacy and Safety of Sleeping Beauty Transposon-Mediated Gene Transfer in Preclinical Animal Studies. *Curr Gene Ther* **2011,** *11* (5), 341-349.
149. Itaka, K.; Osada, K.; Morii, K.; Kim, P.; Yun, S. H.; Kataoka, K., Polyplex nanomicelle promotes hydrodynamic gene introduction to skeletal muscle. *J Control Release* **2010,** *143* (1), 112-119.
150. Nakamura, S.; Maehara, T.; Watanabe, S.; Ishihara, M.; Sato, M., Improvement of hydrodynamics-based gene transfer of nonviral DNA targeted to murine hepatocytes. *BioMed research international* **2013,** *2013*, 928790.
151. Boudes, P. F., Gene therapy as a new treatment option for inherited monogenic diseases. *Eur J Intern Med* **2014,** *25* (1), 31-6.
152. Ferrari, S.; Geddes, D. M.; Alton, E., Barriers to and new approaches for gene therapy and gene delivery in cystic fibrosis. *Advanced Drug Delivery Reviews* **2002,** *54* (11), 1373-1393.

153. Jones, C. H.; Chen, C. K.; Ravikrishnan, A.; Rane, S.; Pfeifer, B. A., Overcoming nonviral gene delivery barriers: perspective and future. *Mol Pharm* **2013,** *10* (11), 4082-98.
154. Wu, Z.; Yang, H.; Colosi, P., Effect of Genome Size on AAV Vector Packaging. *Molecular Therapy* **2010,** *18* (1), 80-86.
155. Maurisse, R.; De Semir, D.; Emamekhoo, H.; Bedayat, B.; Abdolmohammadi, A.; Parsi, H.; Gruenert, D. C., Comparative transfection of DNA into primary and transformed mammalian cells from different lineages. *Bmc Biotechnology* **2010,** *10*.
156. Katayose, S.; Kataoka, K., Remarkable increase in nuclease resistance of plasmid DNA through supramolecular assembly with poly(ethylene glycol)-poly(L-lysine) block copolymer. *J Pharm Sci* **1998,** *87* (2), 160-3.
157. Ruponen, M.; Yla-Herttuala, S.; Urtti, A., Interactions of polymeric and liposomal gene delivery systems with extracellular glycosaminoglycans: physicochemical and transfection studies. *Biochim Biophys Acta* **1999,** *1415* (2), 331-41.
158. Yue, Z.-G.; Wei, W.; Lv, P.-P.; Yue, H.; Wang, L.-Y.; Su, Z.-G.; Ma, G.-H., Surface Charge Affects Cellular Uptake and Intracellular Trafficking of Chitosan-Based Nanoparticles. *Biomacromolecules* **2011,** *12* (7), 2440-2446.
159. Wang, F.; Bexiga, M. G.; Anguissola, S.; Boya, P.; Simpson, J. C.; Salvati, A.; Dawson, K. A., Time resolved study of cell death mechanisms induced by amine-modified polystyrene nanoparticles. *Nanoscale* **2013,** *5* (22), 10868-76.
160. Nelson, C. E.; Kintzing, J. R.; Hanna, A.; Shannon, J. M.; Gupta, M. K.; Duvall, C. L., Balancing cationic and hydrophobic content of PEGylated siRNA polyplexes enhances endosome escape, stability, blood circulation time, and bioactivity in vivo. *ACS Nano* **2013,** *7* (10), 8870-80.
161. Han, D. K.; Park, K. D.; Ryu, G. H.; Kim, U. Y.; Min, B. G.; Kim, Y. H., Plasma protein adsorption to sulfonated poly(ethylene oxide)-grafted polyurethane surface. *J Biomed Mater Res* **1996,** *30* (1), 23-30.
162. Beletsi, A.; Panagi, Z.; Avgoustakis, K., Biodistribution properties of nanoparticles based on mixtures of PLGA with PLGA-PEG diblock copolymers. *Int J Pharm* **2005,** *298* (1), 233-41.
163. Singh, S.; Papareddy, P.; Morgelin, M.; Schmidtchen, A.; Malmsten, M., Effects of PEGylation on membrane and lipopolysaccharide interactions of host defense peptides. *Biomacromolecules* **2014,** *15* (4), 1337-45.
164. Gon, S.; Fang, B.; Santore, M. M., Interaction of Cationic Proteins and Polypeptides with Biocompatible Cationically-Anchored PEG Brushes. *macromolecules* **2011,** *20* (8161-8168).

165. Dams, E. T.; Laverman, P.; Oyen, W. J.; Storm, G.; Scherphof, G. L.; van Der Meer, J. W.; Corstens, F. H.; Boerman, O. C., Accelerated blood clearance and altered biodistribution of repeated injections of sterically stabilized liposomes. *J Pharmacol Exp Ther* **2000,** *292* (3), 1071-9.
166. Ishida, T.; Maeda, R.; Ichihara, M.; Irimura, K.; Kiwada, H., Accelerated clearance of PEGylated liposomes in rats after repeated injections. *J Control Release* **2003,** *88* (1), 35-42.
167. Wang, X.; Ishida, T.; Kiwada, H., Anti-PEG IgM elicited by injection of liposomes is involved in the enhanced blood clearance of a subsequent dose of PEGylated liposomes. *J Control Release* **2007,** *119* (2), 236-44.
168. Kali, G.; Georgiou, T. K.; Ivan, B.; Patrickios, C. S., Anionic amphiphilic end-linked conetworks by the combination of quasiliving carbocationic and group transfer polymerizations. *Journal of Polymer Science Part A: Polymer Chemistry* **2009,** *47* (17), 4289-4301.
169. Xu, X.; Smith, A. E.; Kirkland, S. E.; McCormick, C. L., Aqueous RAFT Synthesis of pH-Responsive Triblock Copolymer mPEO−PAPMA−PDPAEMA and Formation of Shell Cross-Linked Micelles. *Macromolecules* **2008,** *41* (22), 8429-8435.
170. Aronovich, E. L.; McIvor, R. S.; Hackett, P. B., The Sleeping Beauty transposon system: a non-viral vector for gene therapy. *Hum Mol Genet* **2011,** *20* (R1), R14-20.
171. Belur, L. R.; McIvor, R. S.; Wilber, A., Liver-directed gene therapy using the sleeping beauty transposon system. *Methods Mol Biol* **2008,** *434*, 267-76.
172. Han, V.; Serrano, K.; Devine, D. V., A comparative study of common techniques used to measure haemolysis in stored red cell concentrates. *Vox Sang* **2010,** *98* (2), 116-23.
173. Noe, D. A.; Weedn, V.; Bell, W. R., Direct spectrophotometry of serum hemoglobin: an Allen correction compared with a three-wavelength polychromatic analysis. *Clin Chem* **1984,** *30* (5), 627-30.
174. Darlington, D. N.; Delgado, A. V.; Kheirabadi, B. S.; Fedyk, C. G.; Scherer, M. R.; Pusateri, A. E.; Wade, C. E.; Cap, A. P.; Holcomb, J. B.; Dubick, M. A., Effect of hemodilution on coagulation and recombinant factor VIIa efficacy in human blood in vitro. *J Trauma* **2011,** *71* (5), 1152-63.
175. Thiel, S.; Frederiksen, P. D.; Jensenius, J. C., Clinical manifestations of mannan-binding lectin deficiency. *Mol Immunol* **2006,** *43* (1-2), 86-96.
176. Sizovs, A.; McLendon, P. M.; Srinivasachari, S.; Reineke, T. M., Carbohydrate polymers for nonviral nucleic acid delivery. *Top Curr Chem* **2010,** *296*, 131-90.

177. Liu, Z. H.; Jiao, Y. P.; Wang, T.; Zhang, Y. M.; Xue, W., Interactions between solubilized polymer molecules and blood components. *Journal of Controlled Release* **2012,** *160* (1), 14-24.
178. Godbey, W. T.; Wu, K. K.; Mikos, A. G., Poly(ethylenimine) and its role in gene delivery. *J Control Release* **1999,** *60* (2-3), 149-60.
179. Lambert, R. C.; Maulet, Y.; Dupont, J. L.; Mykita, S.; Craig, P.; Volsen, S.; Feltz, A., Polyethylenimine-mediated DNA transfection of peripheral and central neurons in primary culture: probing Ca2+ channel structure and function with antisense oligonucleotides. *Mol Cell Neurosci* **1996,** *7* (3), 239-46.
180. Hirsh, J.; Oates, J. A.; Wood, A. J. J., Heparin. *The New England Journal of Medicine* **1991,** *324*, 1565-1574.
181. Palta, S.; Saroa, R.; Palta, A., Overview of the coagulation system. *Indian Journal of Anaesthesia* **2014,** *58* (5), 515-523.
182. Chng, W. J.; Sum, C.; Kuperan, P., Causes of isolated prolonged activated partial thromboplastin time in an acute care general hospital. *Singapore Med J* **2005,** *46* (9), 450-6.
183. Tang, L.; Liu, L.; Elwing, H. B., Complement activation and inflammation triggered by model biomaterial surfaces. *J Biomed Mater Res* **1998,** *41* (2), 333-40.
184. Szebeni, J.; Baranyi, L.; Savay, S.; Milosevits, J.; Bunger, R.; Laverman, P.; Metselaar, J. M.; Storm, G.; Chanan-Khan, A.; Liebes, L.; Muggia, F. M.; Cohen, R.; Barenholz, Y.; Alving, C. R., Role of complement activation in hypersensitivity reactions to doxil and hynic PEG liposomes: experimental and clinical studies. *J Liposome Res* **2002,** *12* (1-2), 165-72.
185. Puttarajappa, C.; Shapiro, R.; Tan, H. P., Antibody-mediated rejection in kidney transplantation: a review. *J Transplant* **2012,** *2012*, 193724.
186. Palarasah, Y.; Nielsen, C.; Sprogoe, U.; Christensen, M. L.; Lillevang, S.; Madsen, H. O.; Bygum, A.; Koch, C.; Skjodt, K.; Skjoedt, M. O., Novel assays to assess the functional capacity of the classical, the alternative and the lectin pathways of the complement system. *Clin Exp Immunol* **2011,** *164* (3), 388-95.
187. Fujita, T., Evolution of the lectin–complement pathway and its role in innate immunity. *Nature Reviews Immunology* **2002,** *2* (5), 346--353.
188. Toda, M.; Kitazawa, T.; Hirata, I.; Hirano, Y.; Iwata, H., Complement activation on surfaces carrying amino groups. *Biomaterials* **2008,** *29* (4), 407-17.
189. Smith, M. C.; Pensky, J.; Naff, G. B., Inhibition of zymosan-induced alternative complement pathway activation by concanavalin A. *Infection and Immunity* **1982,** *38* (3), 1279-1284.

190. Hamad, I.; Hunter, A. C.; Szebeni, J.; Moghimi, S. M., Poly(ethylene glycol)s generate complement activation products in human serum through increased alternative pathway turnover and a MASP-2-dependent process. *Mol Immunol* **2008,** *46* (2), 225-32.
191. Arima, Y.; Kawagoe, M.; Toda, M.; Iwata, H., Complement activation by polymers carrying hydroxyl groups. *ACS Appl Mater Interfaces* **2009,** *1* (10), 2400-7.
192. Al-Dosari, M. S.; Gao, X., Nonviral gene delivery: principle, limitations, and recent progress. *AAPS J* **2009,** *11* (4), 671-81.
193. Akhtar, S.; Benter, I., Toxicogenomics of non-viral drug delivery systems for RNAi: Potential impact on siRNA-mediated gene silencing activity and specificity. *Advanced Drug Delivery Reviews* **2007,** *59* (2–3), 164–182.
194. Guerrero-Cazares, H.; Tzeng, S. Y.; Young, N. P.; Abutaleb, A. O.; Quinones-Hinojosa, A.; Green, J. J., Biodegradable polymeric nanoparticles show high efficacy and specificity at DNA delivery to human glioblastoma in vitro and in vivo. *ACS Nano* **2014,** *8* (5), 5141-53.
195. Magalhaes, M.; Farinha, D.; Pedroso de Lima, M. C.; Faneca, H., Increased gene delivery efficiency and specificity of a lipid-based nanosystem incorporating a glycolipid. *Int J Nanomedicine* **2014,** *9*, 4979-89.
196. Photos, P. J.; Bacakova, L.; Discher, B.; Bates, F. S.; Discher, D. E., Polymer vesicles in vivo: correlations with PEG molecular weight. *J Control Release* **2003,** *90* (3), 323-34.
197. Merkel, O. M.; Librizzi, D.; Pfestroff, A.; Schurrat, T.; Buyens, K.; Sanders, N. N.; De Smedt, S. C.; Behe, M.; Kissel, T., Stability of siRNA polyplexes from poly(ethylenimine) and poly(ethylenimine)-g-poly(ethylene glycol) under in vivo conditions: effects on pharmacokinetics and biodistribution measured by Fluorescence Fluctuation Spectroscopy and Single Photon Emission Computed Tomography (SPECT) imaging. *J Control Release* **2009,** *138* (2), 148-59.
198. Rydz, J.; Sikorska, W.; Kyulavska, M.; Christova, D., Polyester-Based (Bio)degradable Polymers as Environmentally Friendly Materials for Sustainable Development. *International Journal of Molecular Sciences* **2014,** *16* (1), 564-596.
199. Hottle, T. A.; Bilec, M. M.; Landis, A. E., Sustainability assessments of bio-based polymers. *Polymer Degradation and Stability* **2013,** *98* (9), 1898–1907.
200. Lligadas, G.; Ronda, J. C.; Galia, M.; Cadiz, V., Renewable polymeric materials from vegetable oils: a perspective. *Materials Today* **2013,** *16*, 373-343.

201. Wang, C.; Kelley, S. S.; Venditti, R. A., Lignin-Based Thermoplastic Materials. *ChemSusChem* **2016,** *9* (8), 770-83.
202. Okada, H.; Tokunaga, T.; Liu, X.; Takayanagi, S.; Matsushima, A.; Shimohigashi, Y., Direct evidence revealing structural elements essential for the high binding ability of bisphenol A to human estrogen-related receptor-gamma. *Environ Health Perspect* **2008,** *116* (1), 32-8.
203. Tschan, M. J.-L.; Brulé, E.; Haquette, P.; Thomas, C. M., Synthesis of biodegradable polymers from renewable resources. *The Royal Society of Chemistry* **2011,** *3*, 836-851.
204. Wang, C.; Venditti, R. A., UV Cross-Linkable Lignin Thermoplastic Graft Copolymers. *American Chemical Society* **2015,** *3*, 1839-1845.
205. Duarah, R.; Karak, N., A starch based sustainable tough hyperbranched epoxy thermoset. *The Royal Society of Chemistry* **2015,** *5*, 64456-64465.
206. Musioł, M. T.; Rydz, J.; Sikorska, W. J.; Rychter, P. R.; Kowalczuk, M. M., A preliminary study of the degradation of
selected commercial packaging materials in compost and aqueous environments. *Polish Journal of Chemical Technology* **2011,** *13*, 55-57.
207. Lu, Y.; Larock, R. C., Novel polymeric materials from vegetable oils and vinyl monomers: preparation, properties, and applications. *ChemSusChem* **2009,** *2* (2), 136-47.
208. Erhan, S. Z., *Industrial Uses of Vegetable Oil*. AOCS Press: Champaign, IL, 2005.
209. Lu, Y.; Larock, R. C., Aqueous Cationic Polyurethane Dispersions from Vegetable Oils. *ChemSusChem* **2010,** *3* (3), 329-333.
210. Grewell, D., Improvement of the mechanical properties of soy protein isolate based plastics through formulation and processing. *International Polymer Processing* **2017,** *22*, 489-496.
211. Shearouse, W. C.; Lillie, L. M.; Reineke, T. M.; Tolman, W. B., Sustainable Polyesters Derived from Glucose and Castor Oil: Building Block Structure Impacts Properties. *American Chemical Society* **2015,** *4*, 284-288.
212. Gallagher, J. J.; Hillmyer, M. A.; Reineke, T. M., Isosorbide-based Polymethacrylates. *American Chemical Society* **2015,** *3*, 662-667.
213. Zhan, M.; Wool, R. P., Biobased composite resins design for electronic materials. *Journal of Applied Polymer Science* **2010,** *118* (6), 3274-3283.
214. Zhan, G.; Zhao, L.; Hu, S.; Gan, W.; Yu, Y.; Tang, X. A., A novel biobased resin-epoxidized soybean oil modified cyanate ester. *Polymer Engineering & Science* **2008,** *48* (7), 1322-1328.
215. Mekonnen, T.; Mussone, P.; Khalil, H.; Bressler, D., Progress in bio-based plastics and plasticizing modifications. *Journal of Materials Chemistry A* **2013,** *1*, 13379-13398.

216. Shin, H.; Olsen, B. D.; Khademhosseini, A., The mechanical properties and cytotoxicity of cell-laden double-network hydrogels based on photocrosslinkable gelatin and gellan gum biomacromolecules. *Biomaterials* **2012,** *33* (11), 3143–3152.
217. Dodiuk, H.; Goodman, S. H., *Handbook of Thermoset Plastics, 3rd ed.* William Andrew Publishing: Westwood, MA, 1999.
218. Schiraldi, C.; Di Lernia, I.; De Rosa, M., Trehalose production: exploiting novel approaches. *Trends Biotechnol* **2002,** *20* (10), 420-5.
219. Biwer, A.; Antranikian, G.; Heinzle, E., Enzymatic production of cyclodextrins. *Appl Microbiol Biotechnol* **2002,** *59* (6), 609-17.
220. Uekama, K.; Hirayama, F.; Irie, T., Cyclodextrin Drug Carrier Systems. *Chem Rev* **1998,** *98* (5), 2045-2076.
221. Nagashima, S.; Shimasaki, T.; Teramoto, N.; Shibata, M., Trehalose-incorporated polymer network by thiol-ene photopolymerization. *Polymer Journal* **2014,** *46*, 728-735.
222. Burek, M.; Czuba, Z. P.; Waskiewicz, S., Novel acid-degradable and thermo-sensitive poly(N-isopropylacrylamide) hydrogels cross-linked by α,α-trehalose diacetals. *Polymer* **2014,** *55* (25), 6460–6470.
223. O'Shea, T. M.; Webber, M. J.; Aimetti, A. A.; Langer, R., Covalent Incorporation of Trehalose within Hydrogels for Enhanced Long-Term Functional Stability and Controlled Release of Biomacromolecules. *Adv Healthc Mater* **2015,** *4* (12), 1802-12.
224. Lee, J.; Ko, J. H.; Lin, E. W.; Wallace, P.; Ruch, F.; Maynard, H. D., Trehalose hydrogels for stabilization of enzymes to heat. *Polym Chem* **2015,** *6* (18), 3443-8.
225. Yano, S.; Teramoto, N.; Miyamoto, R.; Nakajima, E.; Hashimoto, K.; Shibata, M., Fibroblast cell proliferation on photo-cured trehalose cinnamoyl ester thin films. *Journal of Bioactive and Compatible Polymers* **2015,** *30*, 87-98.
226. Tang, S.; Kong, L.; Ou, J.; Liu, Y.; Li, X.; Zou, H., Application of cross-linked beta-cyclodextrin polymer for adsorption of aromatic amino acids. *J Mol Recognit* **2006,** *19* (1), 39-48.
227. Miyamae, K.; Nakahata, M.; Takashima, Y.; Harada, A., Self-Healing, Expansion-Contraction, and Shape-Memory Properties of a Preorganized Supramolecular Hydrogel through Host-Guest Interactions. *Angew Chem Int Ed Engl* **2015,** *54* (31), 8984-7.
228. Alsbaiee, A.; Smith, B. J.; Xiao, L.; Ling, Y.; Helbling, D. E.; Dichtel, W. R., Rapid removal of organic micropollutants from water by a porous beta-cyclodextrin polymer. *Nature* **2015,** *529* (7585), 190-4.

229. dos Santos, J. F.; Couceiro, R.; Concheiro, A.; Torres-Labandeira, J. J.; Alvarez-Lorenzo, C., Poly(hydroxyethyl methacrylate-co-methacrylated-beta-cyclodextrin) hydrogels: synthesis, cytocompatibility, mechanical properties and drug loading/release properties. *Acta Biomater* **2008,** *4* (3), 745-55.
230. Manakker, F. v. d.; Vermonden, T.; Nostrum, C. F. v.; Hennink, W. E., Cyclodextrin-Based Polymeric Materials: Synthesis, Properties, and Pharmaceutical/Biomedical Applications. *Biomacromolecules* **2009,** *10*, 3157-3175.
231. Zhang, Q.; Molenda, M.; Reineke, T. M., Epoxy Resin Thermosets Derived from Trehalose and β-Cyclodextrin. *Macromolecules* **2016,** *49*, 8397-8406.
232. Garrison, T.; Murawski, A.; Quirino, R., Bio-Based Polymers with Potential for Biodegradability. *Polymers* **2016,** *8* (7), 262.
233. Wang, Y.; Ameer, G. A.; Sheppard, B. J.; Langer, R., A tough biodegradable elastomer. *Nat Biotechnol* **2002,** *20* (6), 602-6.
234. Bruggeman, J. P.; de Bruin, B. J.; Bettinger, C. J.; Langer, R., Biodegradable poly(polyol sebacate) polymers. *Biomaterials* **2008,** *29* (36), 4726-35.
235. Bruggeman, J. P.; Bettinger, C. J.; Langer, R., Biodegradable xylitol-based elastomers: in vivo behavior and biocompatibility. *J Biomed Mater Res A* **2010,** *95* (1), 92-104.
236. Yang, J.; Lee, S.; Choi, W. J.; Seo, H.; Kim, P.; Kim, G.-J.; Kim, Y.-W.; Shin, J., Thermoset Elastomers Derived from Carvomenthide. *Biomacromolecules* **2015,** *16*, 246-256.
237. Moreno, M.; Armentano, I.; Fortunati, E.; Mattioli, S.; Torre, L.; Lligadas, G.; Ronda, J. C.; Galià, M.; Cádiz, V., Cellulose nano-biocomposites from high oleic sunflower oil-derived thermosets. *European Polymer Journal* **2016,** *79*, 109–120.
238. Tsujimoto, T.; Takayama, T.; Uyama, H., Biodegradable Shape Memory Polymeric Material from Epoxidized Soybean Oil and Polycaprolactone. *Polymers* **2015,** *7* (10), 2165-2174.
239. Miyagawa, H.; Misra, M.; Drzal, L. T.; Mohanty, A. K., Fracture toughness and impact strength of anhydride-cured biobased epoxy. *Polymer Engineering & Science* **2005,** *45* (4), 487-495.
240. Roudsari, G. M.; Mohanty, A. K.; Misra, M., Study of the Curing Kinetics of Epoxy Resins with Biobased Hardener and Epoxidized Soybean Oil. *ACS Sustainable Chemistry & Engineering* **2014,** *2*, 2111-2116.
241. Gabriel, L. P.; Santos, M. E.; Jardini, A. L.; Bastos, G. N.; Dias, C. G.; Webster, T. J.; Maciel Filho, R., Bio-based polyurethane for tissue engineering applications: How hydroxyapatite nanoparticles influence the

structure, thermal and biological behavior of polyurethane composites. *Nanomedicine* **2017,** *13* (1), 201-208.
242. Bettinger, C. J., Biodegradable elastomers for tissue engineering and cell-biomaterial interactions. *Macromol Biosci* **2011,** *11* (4), 467-82.
243. Holken, I.; Hoppe, M.; Mishra, Y. K.; Gorb, S. N.; Adelung, R.; Baum, M. J., Complex shaped ZnO nano- and microstructure based polymer composites: mechanically stable and environmentally friendly coatings for potential antifouling applications. *Phys Chem Chem Phys* **2016,** *18* (10), 7114-23.
244. Patel, M. K.; Davis, B. G., Flow chemistry kinetic studies reveal reaction conditions for ready access to unsymmetrical trehalose analogues. *Org Biomol Chem* **2010,** *8* (19), 4232-5.
245. Deng, S.; Gangadharmath, U.; Chang, C. W., Sonochemistry: a powerful way of enhancing the efficiency of carbohydrate synthesis. *J Org Chem* **2006,** *71* (14), 5179-85.
246. Dominguez, X. A.; Speron, E.; Slim, J., Castor oil as a starting material for laboratory preparations. *Journal of Chemical Education* **1952,** *29*, 446-448.
247. Borg, P.; Lê, G.; Lebrun, S.; Pées, B., Example of industrial valorisation of derivative products of Castor oil. *Oléagineux, Corps gras, Lipides* **2009,** *16*, 211-214.
248. Jeon, B. S.; Choi, O.; Um, Y.; Sang, B. I., Production of medium-chain carboxylic acids by Megasphaera sp. MH with supplemental electron acceptors. *Biotechnol Biofuels* **2016,** *9*, 129-137.
249. Zhou, Y.; Huang, Y.; Fang, Y.; Tan, T., Selective conversion of castor oil derived ricinoleic acid methyl ester into jet fuel. *Green Chemistry* **2016,** *18*, 5180-5189.
250. Lee, P. C.; Lee, W. G.; Lee, S. Y.; Chang, H. N., Succinic acid production with reduced by-product formation in the fermentation of Anaerobiospirillum succiniciproducens using glycerol as a carbon source. *Biotechnol Bioeng* **2001,** *72* (1), 41-8.
251. Bretz, K., Succinic Acid Production in Fed-Batch Fermentation of Anaerobiospirillum succiniciproducens Using Glycerol as Carbon Source. *Chemical Engineering & Technology* **2015,** *38* (9), 1659-1664.
252. Liu, W. B.; Qiu, Q.; Wang, J.; Huo, Z.; Sun, H., Curing kinetics and properties of epoxy resin–fluorenyl diamine systems. **2008,** *49* (20), 4399–4405.
253. Kissinger, H. E., Variation of peak temperature with heating rate in differential thermal analysis. *Journal of Research of the National Bureau of Standards* **1956,** *57*, 217-227.

254. Hong, J.; Radojčić, D.; Ionescu, M.; Petrović, Z. S.; Eastwood, E., Advanced materials from corn: isosorbide-based epoxy resins. *Polymer Chemistry* **2014,** *5*, 5360-5368.
255. Hazer, B.; Hazer, D. B.; Coban, B., Synthesis of microbial elastomers based on soybean oil. *Journal of Polymer Research* **2010,** *17*, 567-577.
256. Tan, S. G.; Chow, W. S., Thermal properties, curing characteristics and water absorption of soybean oil-based thermoset. *Express Polymer Letters* **2011,** *5*, 480-492.
257. Rials, T. G.; Glasser, W. G., Engineering Plastics from Lignin - IV. Effect of Crosslink Density on Polyurethane Film Properties — Variation in NCO:OH Ratio. *International Journal of the Biology, Chemistry, Physics and Technology of Wood* **2017,** *38* (4), 191-199.
258. Bashur, C. A.; Dahlgren, L. A.; Goldstein, A. S., Effect of fiber diameter and orientation on fibroblast morphology and proliferation on electrospun poly(D,L-lactic-co-glycolic acid) meshes. *Biomaterials* **2006,** *27* (33), 5681-8.
259. Wang, Y. X.; Robertson, J. L.; Spillman, W. B., Jr.; Claus, R. O., Effects of the chemical structure and the surface properties of polymeric biomaterials on their biocompatibility. *Pharm Res* **2004,** *21* (8), 1362-73.
260. Church, H.; Tylee, K.; Cooper, A.; Thornley, M.; Mercer, J.; Wraith, E.; Carr, T.; O'Meara, A.; Wynn, R. F., Biochemical monitoring after haemopoietic stem cell transplant for Hurler syndrome (MPSIH): implications for functional outcome after transplant in metabolic disease. *Bone Marrow Transplant* **2007,** *39* (4), 207-10.
261. Carr, L. R.; Jiang, S., Mediating high levels of gene transfer without cytotoxicity via hydrolytic cationic ester polymers. *Biomaterials* **2010,** *31* (14), 4186-4193.
262. Boyle, W. S.; Senger, K.; Tolar, J.; Reineke, T. M., Heparin Enhances Transfection in Concert with a Trehalose-Based Polycation with Challenging Cell Types. *Biomacromolecules* **2016,** *18* (1), 56-67.

CHAPTER 7: APPENDIX

7.1 ABBREVIATIONS AND ACRONYMS

AEMA	N-(2-aminoethyl) methacrylamide
AP	Alternative pathway
aPTT	Activated partial thromboplastin time
C3	Complement component
C57BL/6J	Wild type black 6 mice
CAGGS	Strong synthetic DNA promoter
CARPA	Complement activation-related pseudoallergy
CD	Cyclodextrin
CP	Classical pathway
CPP	4-cyano-4-(propylsulfanylthiocarbonyl) sulfanylpentanoic acid
CT	Cycle threshold
CTA	Chain transfer agent
Cy5	Cyanine 5
Cy7	Cyanine 7
Đ	Dispersity

D5W	5% by weight aqueous dextrose solution
Da	Daltons
DLS	Dynamic light scattering
DMAEM	N,N-dimethyl aminoethylmethacrylate

t

DMEM	Dulbecco’s Modified Eagle Medium
DMF	Dimethylformamide
DMSO	Dimethyl sulfoxide
DNA	Deoxyribonucleic acids
DSC	Differential scanning calorimetry
ESO	Epoxidized soybean oil
FBS	Fetal bovine serum
FT-IR	Fourier transform infrared
GalNAc	N-acetyl galactose
GFP	Green fluorescent protein
GPC	Gel permeation chromatography
HP	Heptanoyl chloride
HD	Hydrodynamic diameter
HDFn	Neonatal human dermal fibroblasts
HepG2	Human liver carcinoma

Luc	Luciferase
MAEMt	N-methyl aminoethylmethacrylate
MAG	2-deoxy-2-methacrylamido glucopyranose
MAT	6-Methacrylamido-6-deoxy trehalose
MBLP	Mannan-binding lectin pathway
Mn	Number average molecular weight
MWCO	Molecular weight cutoff
MTT	(3-(4,5-dimethylthiazol-2-yl)-2,5-diphenyl tetrazolium bromide
NMR	Nuclear magnetic resonance
N/P	Charged nitrogen to charge phosphate ratio
OptiMEM	Minimum Essential Medium with reduced serum OptiMEM
PAMAM	Polyamidoamine
PAMPs	Pathogen-associated molecular patterns
PBS	Phosphate buffered saline
pDNA	Plasmid DNA
PEI	Polyethyleneimine
PEG	Polyethylene glycol
PI	Propidium iodide

PLG	Poly(DL-lactide-co-glycolide)
pT2/CA	Plasmid DNA with CAGGs promotor

L

PT	Protothrombin time
PTT-LA	Partial thromboplastin time-Lupus anticoagulant reagent
RAFT	Reversible-addition-fragmentation chain-transfer
Rh	Hydrodynamic radius
RLUs	Relative light units
RNA	Ribonucleic acids
RPMI	Roswell Park Memorial Institute cell culture medium
SA	Succinic anhydride
SEC	Size exclusion chromatography
SWNT	Single-walled nanotube
Tg	Thermogravimetry
THF	Tetrahydrofuran
TMAEM	N,N,N-trimethylammoniumethylmethacrylate

t

TR	Trehalose
U87	Human glioblastoma
V501	4,4’-Azobis(4-cyanopentanoic acid)

WT	Wild type
λ	Wavelength
δ	Loss factor

7.2 PRELIMINARY GLYCOPOLYCATION B CELL TRANSFECTION RESULTS

Synopsis

Gene therapy has the potential to improve treatment of MPS I compared to conventional treatment options by altering patients' cells to produce and secrete IDUA over time. To obtain long-term expression of a gene, it must be incorporated into the cell genome. *Sleeping Beauty* (SB) is a non-viral genome engineering system that makes an enzyme to "cut and paste" genes from plasmids DNA into the chromosomes of cells. A major limiting factor for gene integration is the amount of SB plasmid the cells take up. Rather than design and synthesize a new polymer to increase uptake into a specific cell line, a series of glycopolymers previously created in the Reineke Lab were screened for transfection against primary human B cells. These polymers differed in the type of sugar used as well as the amount of charge in the structure, but all four glycopolymers demonstrated biocompatibility and increased gene expression in human cell lines compared to other commercially available cationic polymer controls.

This chapter was adapted with permission from the authors listed below.

a) Haley R. Phillips
b) Craig Van Bruggen
c) Theresa M. Reineke

7.2.1 Introduction

The goal of this proposal is to improve production of a therapeutic protein by cells that can be transplanted into patients as a form of therapy. Cellular uptake of Sleeping Beauty (SB), a genome editing system made of DNA, correlates with increased protein expression. Polymers with carbohydrates, called glycopolymers, have previously increased gene uptake in various human cancer cells, but success varied based on cell and polymer type. Rather than design and synthesize a new polymer to increase uptake into a specific cell line, a series of glycopolymers will be screened for protein production against five blood cell types.

Gene therapy is the treatment of disease by altering gene expression in cells, which is a promising option for autosomal recessive diseases such as mucopolysaccharidosis type I (MPS I). Patients with MPS I lack a functioning α-L-iduronidase (IDUA) enzyme to digest specific chains of sugars, which are generated by all cells as a normal part of the cell life cycle. Accumulation of those sugar chains in cells affects major organs during development and the most severe cases can lead to death. MPS I is currently treated by stem cell transplantation or by repeated enzyme injections. Neither option has fully treated the neurological or skeletal symptoms because both methods are dose-limited by

the amount of cells that can be grafted or the amount of IDUA enzyme that persists in circulation over time.[260]

Gene therapy has the potential to improve treatment of MPS I compared to conventional treatment options by altering patients' cells to produce and secrete IDUA over time. To obtain long-term expression of a gene, it must be incorporated into the cell genome. *Sleeping Beauty* (SB) is a non-viral genome engineering system that makes an enzyme to "cut and paste" genes from plasmids (circular pieces of DNA unassociated with the genome) into the chromosomes of cells.[102] These genes can be expressed for the lifetime of the cell, even after the cell replicates. Both the gene to be incorporated and the gene that codes for the enzyme are located on the same plasmid. Once the plasmid is inside the cell, the cell's own machinery will read the SB gene, make the enzyme, then perform the gene transfer.

A major limiting factor for gene integration is the amount of SB plasmid the cells take up. Cationic polymers are used to increase cellular uptake by shielding the negative charge on DNA, which would be repulsed by the negatively charged membrane of mammalian cells. Polymers with carbohydrates, called glycopolymers, have previously increased gene uptake in various human cancer cells, but success varied based on cell and polymer type.[22, 155] Rather than design and synthesize a new polymer to increase uptake into a specific cell line,

a series of glycopolymers created in the Reineke Lab will be screened for protein production against primary human B cells. These polymers differ in the type of sugar used as well as the amount of charge in the structure, but all four glycopolymers demonstrated biocompatibility and increased gene expression in human cell lines compared to other commercially available cationic polymer controls.[24, 83, 123, 261]

Two short-term specific aims outline how combining polymer chemistry and gene engineering will help achieve the long-term goal of improving MPS I treatment.

Specific aim 1: Screen delivery efficiency of a suite of cationic glycopolymer gene delivery vehicles into an immortalized primary human cell line.

An immortalized primary human B cell line was cultured and transfected *in vitro*. Three cationic glycopolymers were selected for the screen based on previous transfection efficiency in cell culture.[58, 83, 262] P(MAG-*b*-MAEMt)-2, P(MAT-*b*-MAEMt)-2, and $Tr4_{77}$, with and without heparin. Commercial controls Glycofect, JetPEI, Fugene, and Lipofectamine were also screened. The Sleeping Beauty (SB) plasmid coded for green fluorescent protein (GFP), and gene expression was screened directly by measuring GFP production via flow cytometry. Many factors contribute to the production of protein, so polymer SB

complex uptake and cell viability will also be measured according to published methods.[58, 83, 262] However, the most important factor for improving MPS I therapy is long-term production of protein, so polymer-cell combinations that give the highest amount of gene expression over time will be studied further in aim 2.

Specific aim 2: Quantify the expression and chromosomal insertion of the iduronidase gene by delivery with the Sleeping Beauty transposon system into MPS I patient cells using glycopolymers as determined in aim 1.

After initial screening of gene expression with the reporter protein, GFP, in normal human blood cells, the incubations will be repeated on cells from MPS I patients. The amount of patient samples is limited, so the experiment will be repeated using only the cells and polymer combinations that gave the highest gene expression in aim 1. The reporter gene will be replaced with the gene for IDUA, and expression will be determined by quantifying the amount of protein produced both short- and long-term via a fluorimetric assay.[3] Once the long-term production of IDUA has been established by cellular uptake of SB guided by glycopolymers, future work may focus on transplanting those cell populations into MPS I model mice, and finally into human patients awaiting relief.

7.2.2 Experimental

7.2.2.1 Materials

All reagents were obtained at the highest available purity from Thermo Fisher Scientific, Inc. (Pittsburgh, PA) or Sigma-Aldrich Co. LLC. (St. Louis, MO) and used as received unless noted otherwise. A primary human B-Lymphocyte cell line (BLCL) immortalized using an Epstein-barr viral vector was ordered through the Coriell Institute (Camden, NJ). JetPEI was obtained from Polyplus-transfection SA (Illkirch, France). Glycofect was obtained from Techulon, Inc. via donation. Propidium iodide, UltraPureTM Agarose-1000, trypsin, (3-(4,5-dimethylthiazol-2-yl)-2,5-diphenyl tetrazolium bromide (MTT), phosphate-buffered saline (PBS), Minimum Essential Medium with reduced serum (Opti-MEM) and Dulbecco's Modified Eagle Medium (DMEM) were purchased from Life Technologies – Thermo Fisher Scientific (Carlsbad, CA). The pT2/CAL plasmid was prepared as described previously.[35] The Luciferase Assay Kit and cell lysis buffer were obtained from Promega Corporation (Madison, WI). Bio-Rad DC Protein Assay Reagent A, Reagent B and Reagent S were obtained from Bio-Rad Laboratories, Inc. (Hercules, CA). The cells were grown in complete DMEM [supplemented with 10% (v:v) fetal bovine serum and 1% antibiotic-antimycotic solution (containing penicillin, streptomycin, and amphotericin B)] at 37 ºC and 5% CO_2 in a humidified incubator.

All polymers were synthesized previously.[58, 83, 262]

7.2.2.2 Instrumentation

MTT, protein, and luciferase assay plates were analyzed using a Biotek Synergy H1 plate reader (BioTek Instruments, Inc., Winooski, VT). Cy5-uptake was measured on a FACSVerse (Becton Dickinson Biosciences, San Jose, CA) flow cytometer. Cell imaging was performed on an EVOS FL digital inverted microscope (Fisher Scientific, Pittsburg, PA).

7.2.2.3 B Cell Culture and Seeding Methods

B cells are non-adherent and had to be shaken gently during incubation periods. Additionally, this particular cell line preferred to grow at higher cell concentrations than the adherent cancer cell lines typically used in this lab (). Lastly, B cells need non-heat inactivated FBS protein supplementing their cell culture media. DMEM can be used, but it is recommended that RPMI media is used instead. Make a mixture of RPMI + 10%-by-volume FBS with 1%-by-volume penicillin-streptomycin antibiotic like you normally would for adherent cancer cell lines.

To seed cells for an experiment, seed at an initial concentration of 250,000 cells/mL, and leave 1-2 mL working volume in the well to allow the addition of polyplexes and more cell media. This avoids having to take the cells out of the wells, spin them down, and resuspend in fresh media just to feed them during

experiments. The cells will dilute over time, but will remain healthy if not overly diluted at any point.

7.2.2.4 MTT and Luciferase Assay Methods

MTT (3-(4, 5-dimethylthiazol-2-yl)-2, 5-diphenyltetrazolium bromide) was used to estimate the cytotoxicity of the polyplexes. B cells were seeded at 250,000 cells/well in 24-well plates 24 h prior to transfection. Polyplexes were formulated as described previously, then polyplex solution was diluted 2x with either OptiMEM or RPMI containing 10% FBS before dosing cells (overall volumes varied depending on pDNA dose, but pDNA concentration was kept the same). The transfection was ended 4 h later by diluting polyplexes with 1 mL of complete DMEM containing 10% FBS. 48 h after polyplexes were added to the cells, 0.5 mg/mL of MTT was added to each well and incubated for 1 h. Cells were lysed using DMSO and 200 µL aliquots were transferred to a 96-well plate for analysis using the plate reader (absorbance was measured at 570 nm). Non-transfected cells were used for normalizing the data.

For the luciferase assay, B cells were seeded at 250,000 cells/well in 24-well plates 24 h prior to transfection. Polyplexes were prepared, diluted, and applied to the cells as described in the cytotoxicity section above. After 48 h, the cells were washed with PBS and treated with cell lysis buffer. Aliquots (5 µL) of cell lysate combined with 100 µL luciferase substrate were examined in 96-well

plates using a luminometer to determine relative light units (RLUs). Data were measured in triplicate and normalized for the amount of protein in each sample. Sample averages were plotted with error bars representing standard deviations.

7.2.2.5 Flow Cytometry for Uptake and Gene Expression Studies

Flow cytometry experiments were performed to examine the cellular uptake of Cy5-labeled pDNA 1, 4, and 7 h post-transfection in both OptiMEM and RPMI + 10% FBS B cell culture media. B cells were seeded at 250,000 cells/well in 24-well plates 24 h prior to transfection. Polyplexes were prepared as described for the MTT and luciferase assays. After 1, 4, or 7 h, the polyplex media was removed and cells were detached from the plate and washed twice with PBS. Finally, 1 mL PBS was added and the cellular suspensions were kept on ice.

The same flow cytometry procedure was used to measure GFP expression in cells except the post-transfection time was kept at 4 h, and the pDNA dose was varied from 1 to 2 ug pDNA/50,000 cells. The assay was performed in both RPMI + 10% FBS and OptiMEM.

7.2.3 Results

7.2.3.1 Experimental Variables

B lymphocytes are non-adherent and much small than any cells previously studied in this group. Methodological and experimental variables were nailed down first, and are summarized in Table 7.1.

Table 7.1. Summary of experimental variables for B cell transfection.

Variable	Best Result
Cell plating density	250k cells/mL
Post-transfection time	72 h
Transfection time	4 h, 7 h
DNA dose	1 µg/50,000 cells
Polymer, N/P	$Tr4_{77}$, MAG-b-MAEMt-2 (both at N/P=20)
Heparin transfection ($Tr4_{77}$ only)	Unclear
Serum transfection additive	Without FBS

7.2.3.2 Cytotoxicity and Preliminary Gene Expression

Initial MTT and luciferase expression screens were used to test not only cytotoxicity and gene expression, but also to screen experimental variables such as pDNA dose. Figure 7.1 shows the MTT and luciferase expression results while varying the pDNA dose per 50,000 cells. The pDNA concentration was kept at 0.01 ug/uL, so the overall polyplex volume had to increase with dose. No polyplex formation or pDNA dose significantly affected cell viability or luciferase expression.

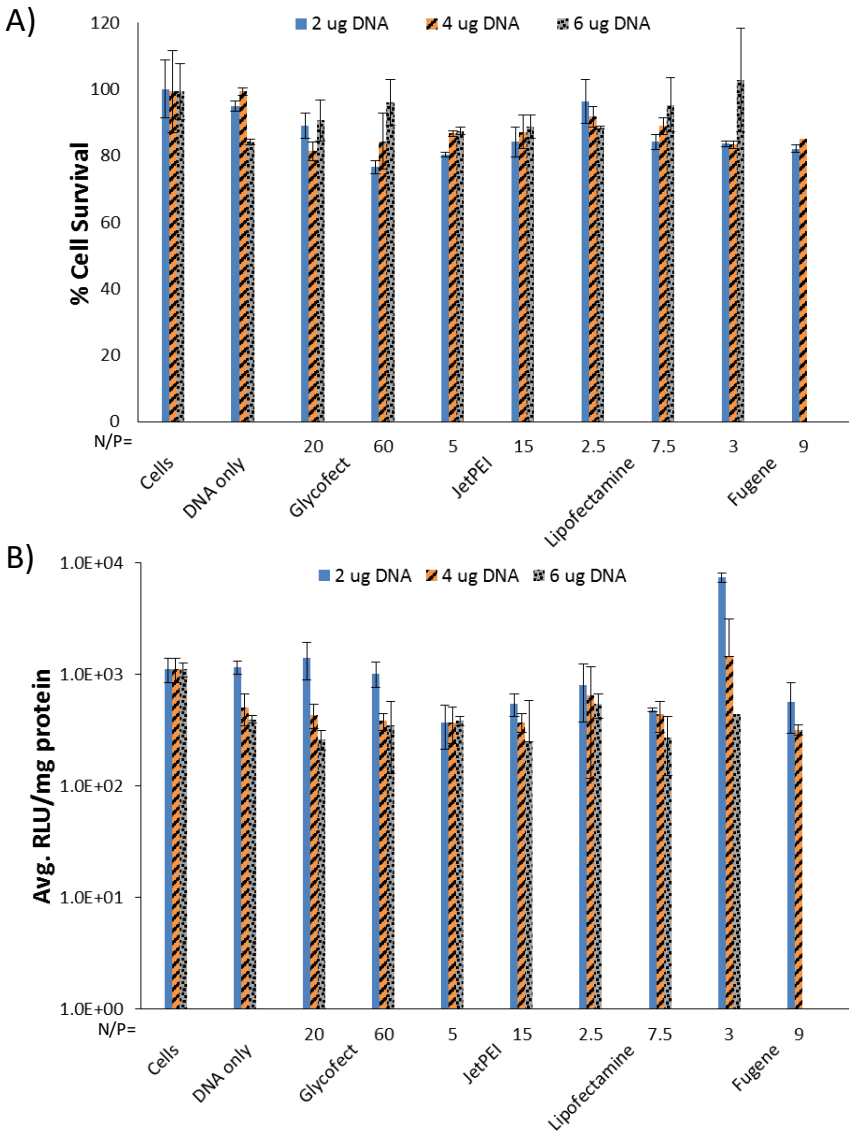

Figure 7.1. Preliminary polymer and pDNA dosing screens. The pDNA was dosed at x µg per every 50,000 B cells, and polyplexes were formulated at the normal pDNA concentration (0.02 ug/mL). Transfections were performed in OptiMEM. (A) Cytotoxicity results from an MTT assay. (B) Luciferase expression normalized to mg protein per sample. No statistics were performed.

7.2.3.3 Cell uptake

Further testing of cellular uptake in cell culture media with and without FBS showed almost no uptake when FBS was present. Uptake in OptiMEM showed a surprising amount of cellular uptake of P(MAG-*b*-MAEMt)-2 at N/P=20 (Figure 7.2).

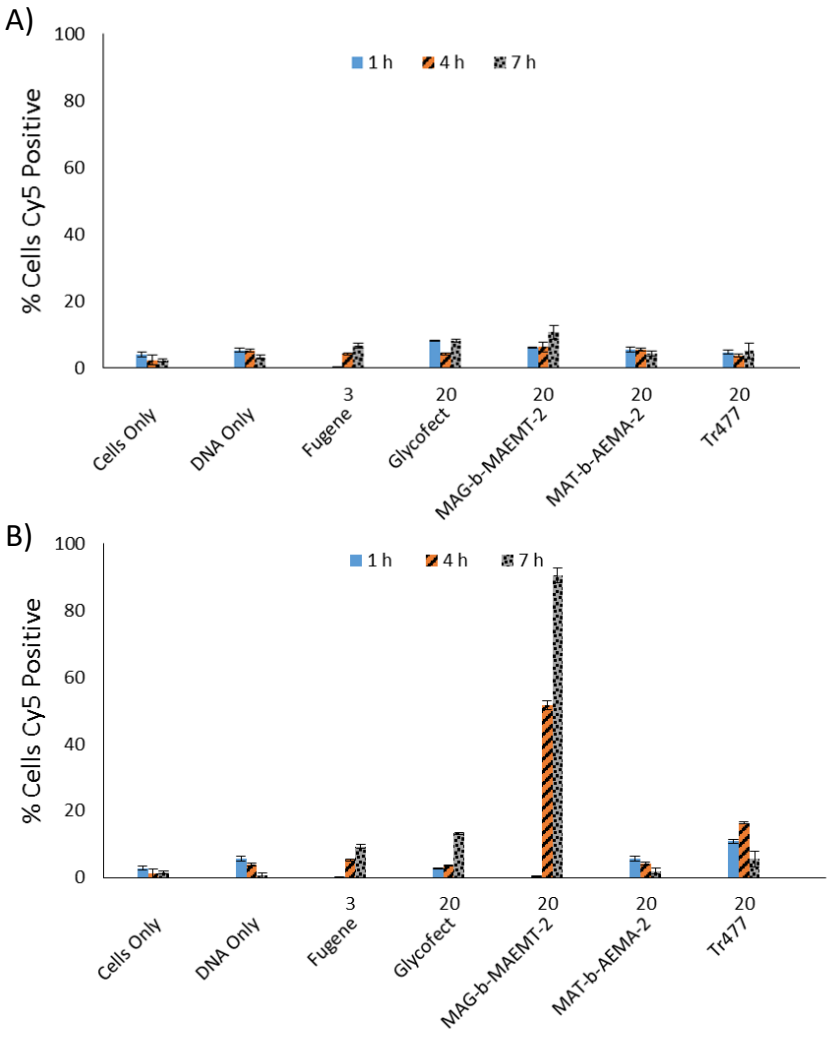

Figure 7.2. Cell uptake results in (A) RPMI + 10% FBS and (B) OptiMEM. The transfection time was varied from 1-7 h, and pDNA was dosed at 0.2 µg/50,000 B cells. No statistics were performed.

7.2.3.4 Quantitative gene expression

To explore whether this uptake would produce quantifiable gene expression, pDNA coding GFP was substituted for the luciferase plasmid and expression was measured by flow cytometry. Figure 7.3 shows expression results when transfected with RPMI + 10% FBS and with OptiMEM. The results surprising seem to contradict the uptake results in that higher levels of gene expression were seen after transfecting in the presence of serum than in OptiMEM. While the overall percentages are low (<5% cells expressing), the results are promising enough to continue screening if a satisfactory positive control can be obtained or created. A good positive control would be the same B cell line genome engineered to constitutively express GFP. Those cells would help flow cytometry gating and data compensation.

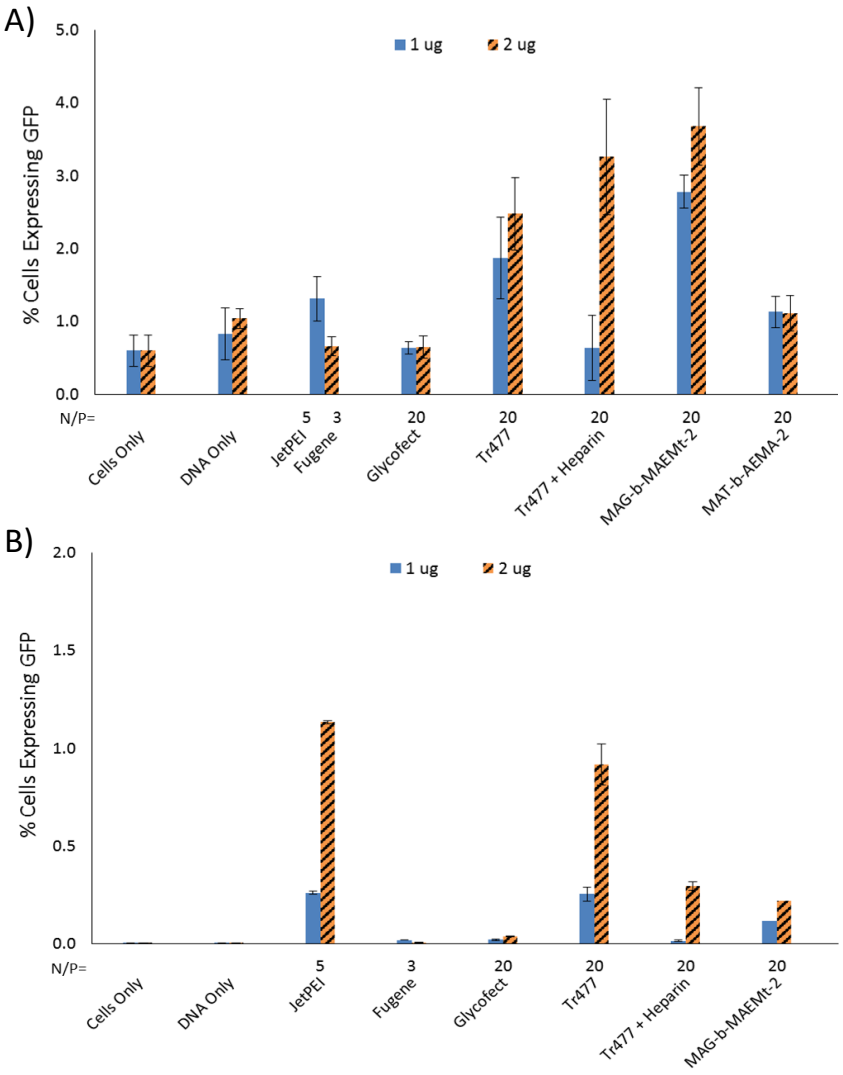

Figure 7.3. GFP expression results with a pDNA dose at x µg/50,000 cells and a 4 h transfection time. Transfection was conducted in (A) RPMI + 10% FBS and (B) OptiMEM. No statistics were performed.

7.2.4 Conclusion

Overall, rather surprising gene expression results were obtained. Transfection in the presence of serum led to higher levels of GFP expression, but lower cell uptake. P(MAG-*b*-MAEMt)-2 was the most promising vehicle, although $Tr4_{77}$ with heparin was also mildly successful at transfecting immortalized primary B cells.

7.2.5 Acknowledgements

The author would like to thank Craig Van Bruggen for assisting with the flow cytometry experiments and Bryan Hall for helping with the IDUA protocol and controls.

7.3 SUPPORTING FIGURES

7.3.1 Chapter 2 Figures

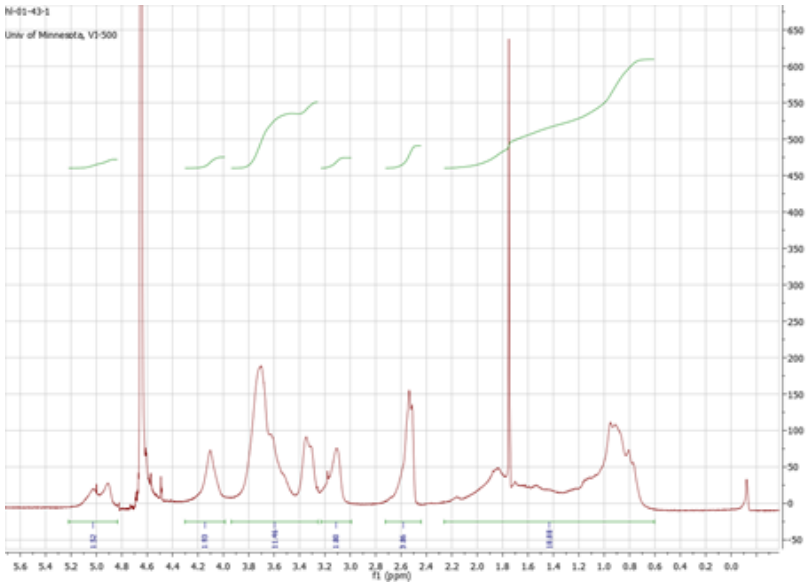

Figure 7.4. NMR spectrum of P(MAG$_{51}$-*b*-PMAEMT$_{30}$).

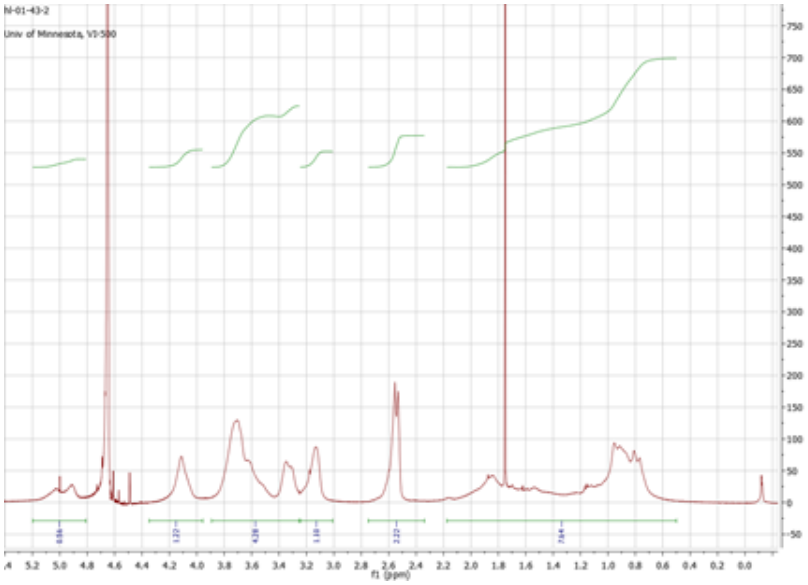

Figure 7.5. NMR spectrum of P(MAG$_{51}$-*b*-PMAEMT$_{42}$).

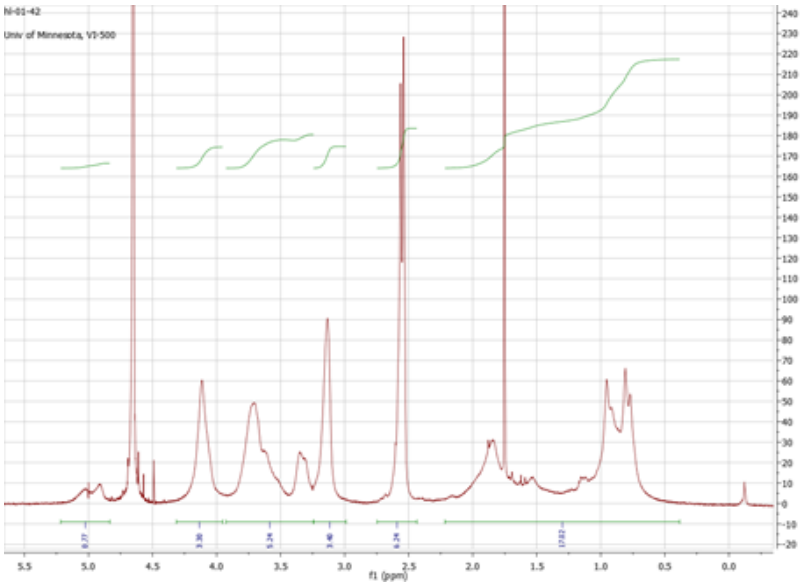

Figure 7.6. NMR spectrum of P(MAG$_{51}$-*b*-PMAEMT$_{76}$).

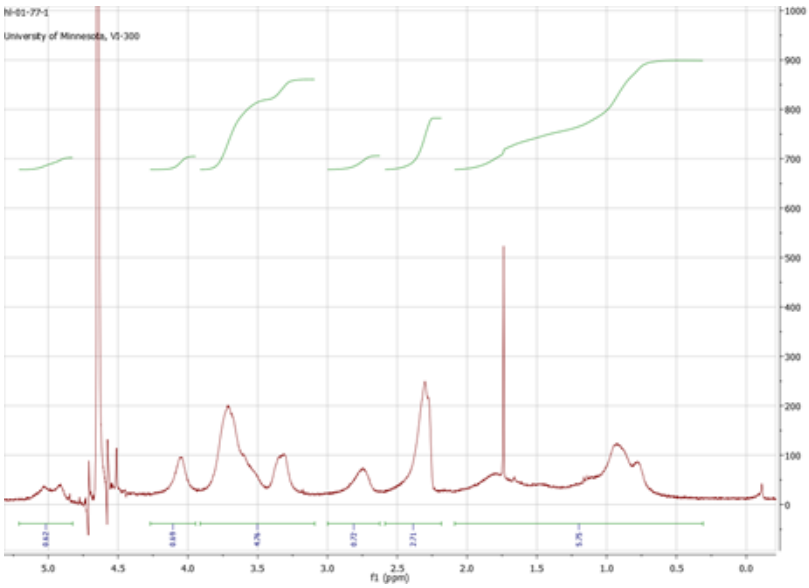

Figure 7.7. NMR spectrum of P(MAG$_{56}$-*b*-PDMAEMT$_{32}$).

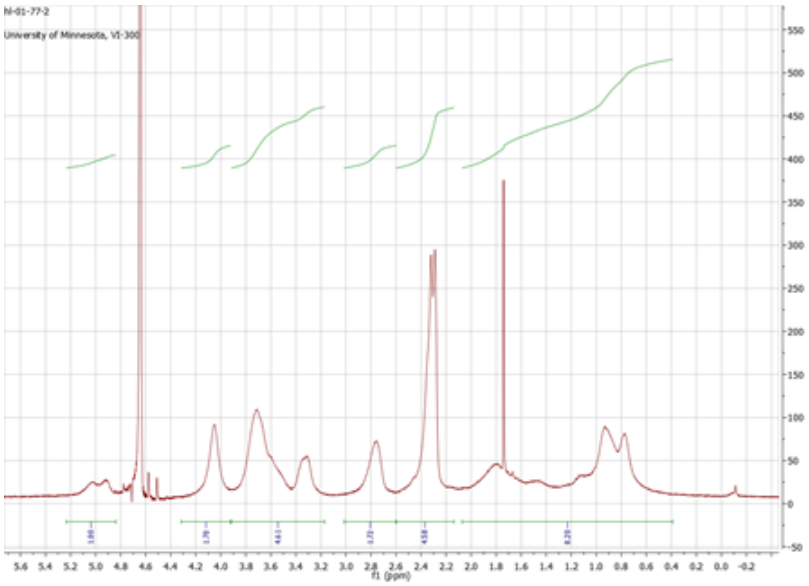

Figure 7.8. NMR spectrum of P(MAG$_{56}$-*b*-PDMAEMT$_{53}$).

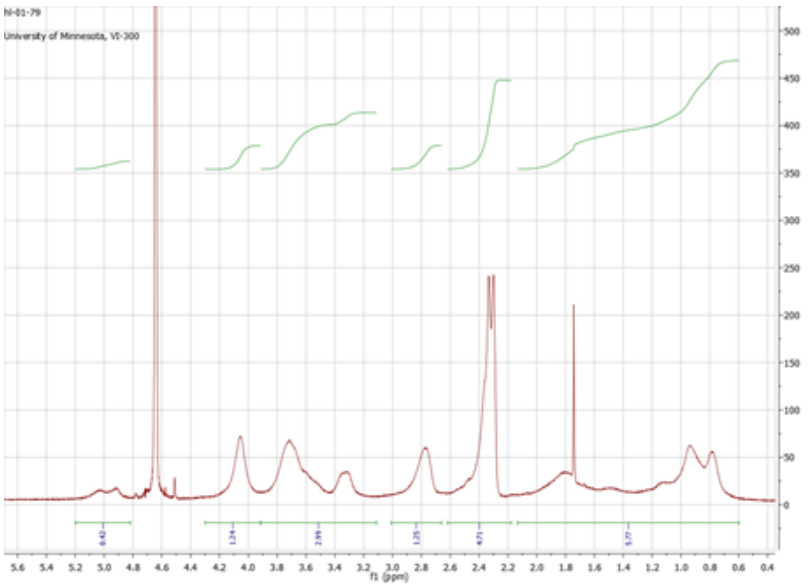

Figure 7.9. NMR spectrum of P(MAG$_{56}$-*b*-PDMAEMT$_{71}$).

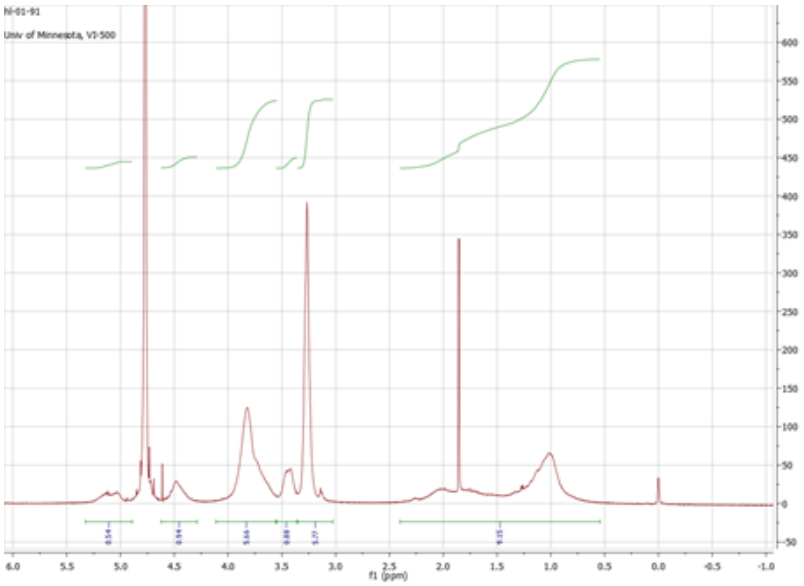

Figure 7.10. NMR spectrum of P(MAG$_{57}$-*b*-PDMAEMT$_{33}$).

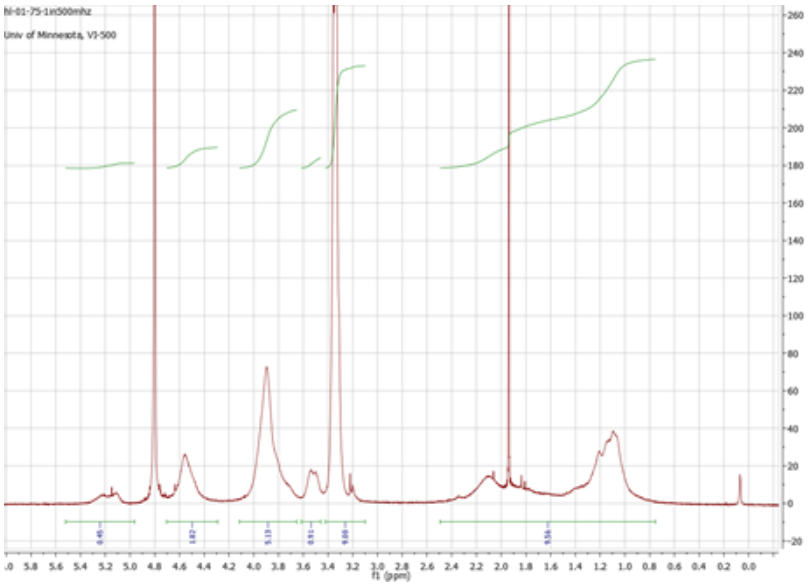

Figure 7.11. NMR spectrum of P(MAG$_{57}$-*b*-PDMAEMT$_{48}$).

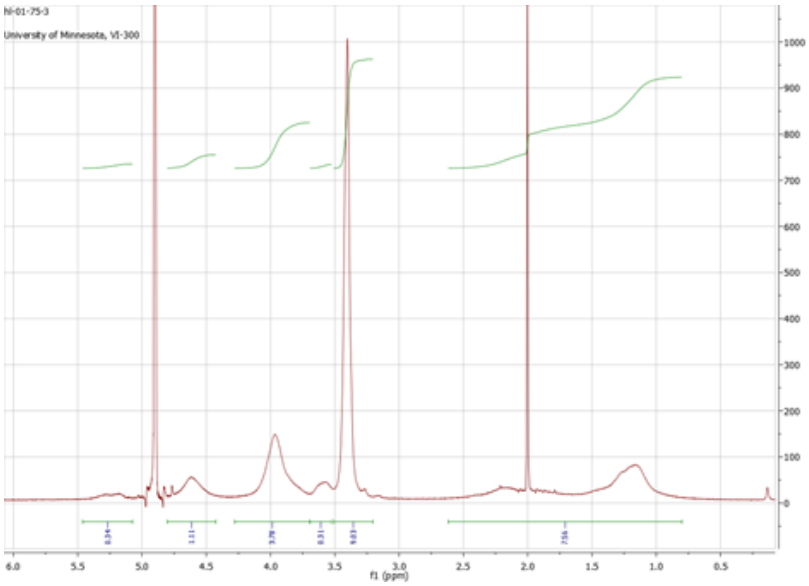

Figure 7.12. NMR spectrum of P(MAG$_{57}$-*b*-PDMAEMT$_{72}$).

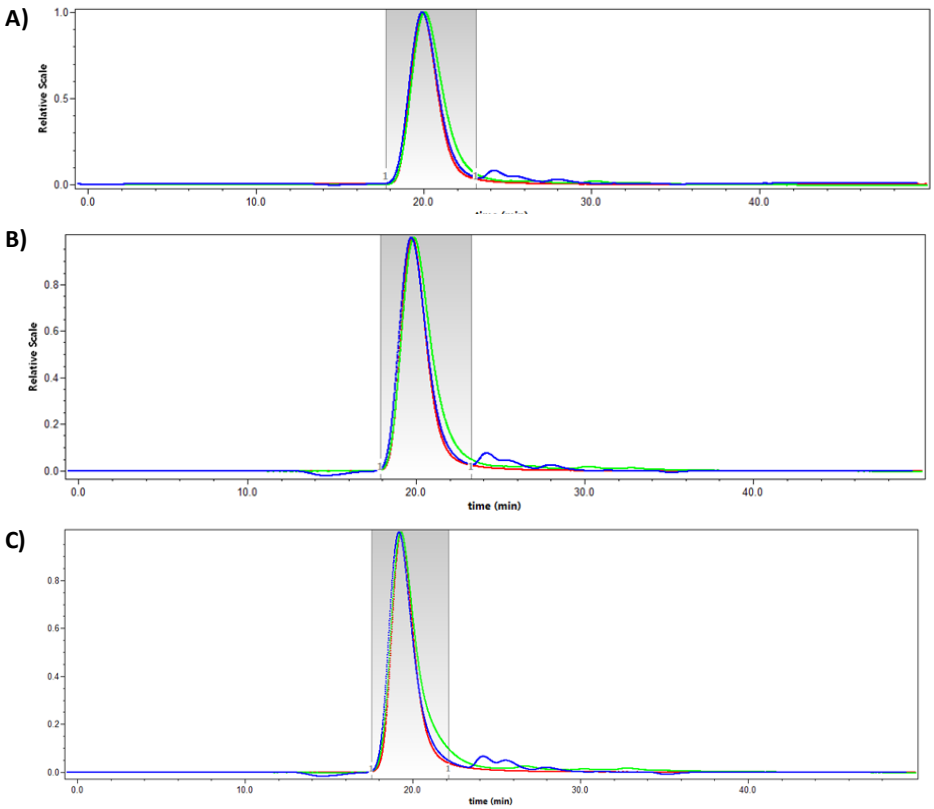

Figure 7.13. P(MAG-*b*-MAEMt)-1, -2, and -3.

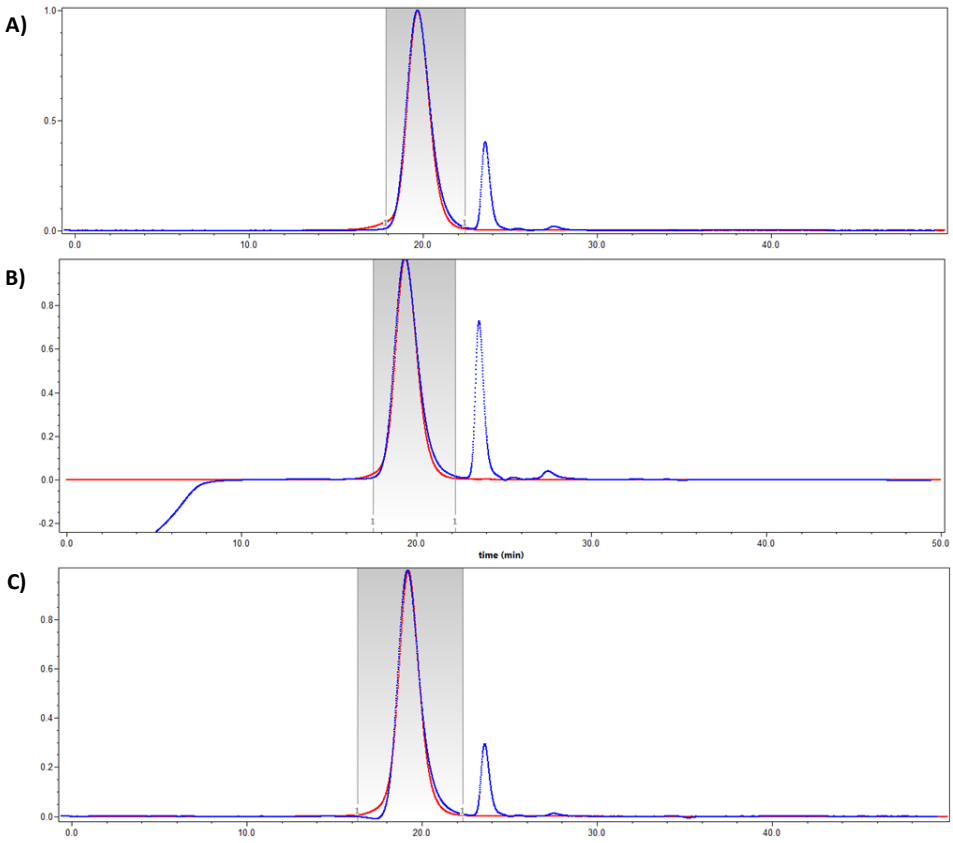

Figure 7.14. P(MAG-*b*-DMAEMt)-1, -2, and -3.

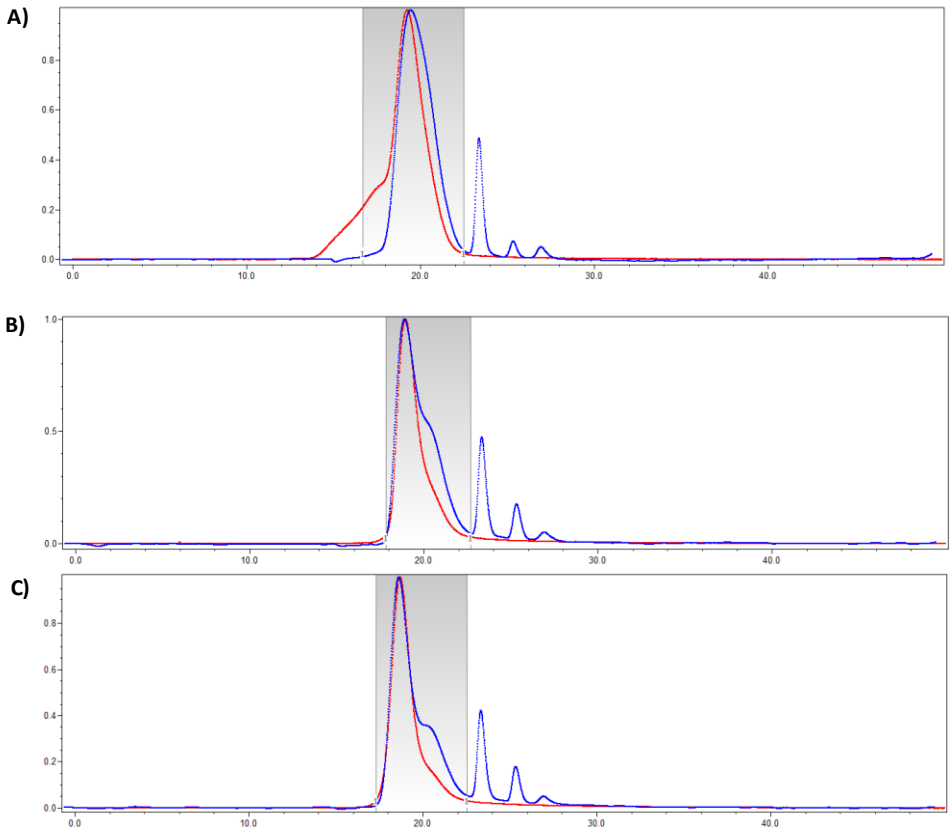

Figure 7.15. P(MAG-*b*-TMAEMt)-1, -2, and -3.

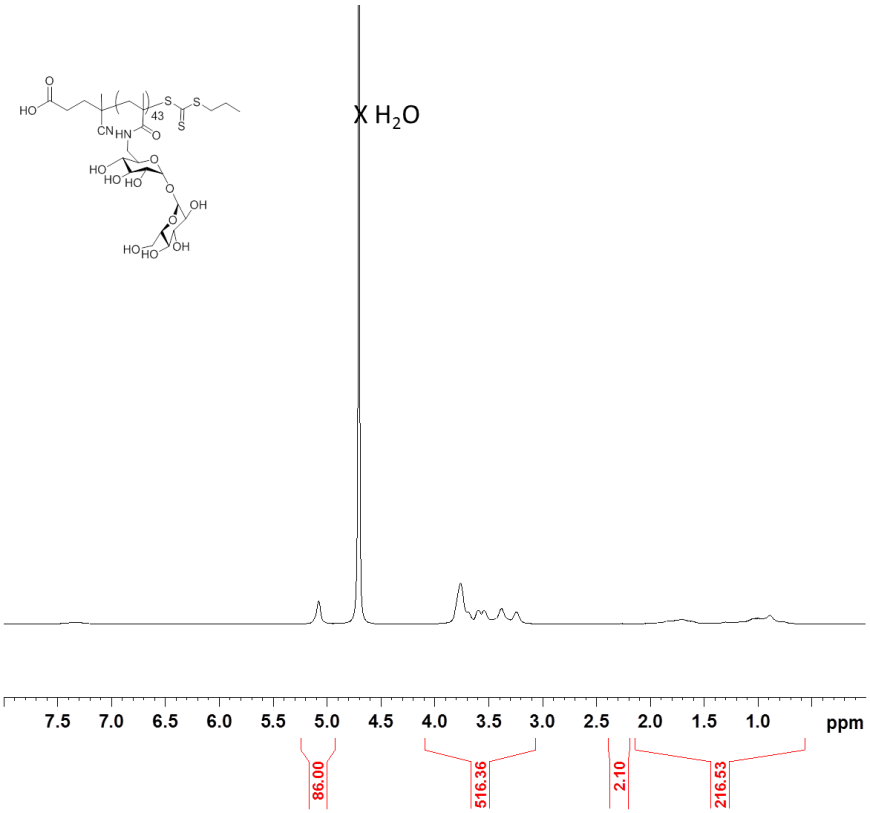

Figure 7.16. ^{1}H NMR spectrum (500 MHz, D_2O) of $P(MAT)_{43}$. δ ppm: 5.26 – 4.96 (bs, 86H), 4.00 – 3.04 (m, 516H), 2.35 – 2.21 (bs, 2H), 1.79 – 0.61 (m, 217H).

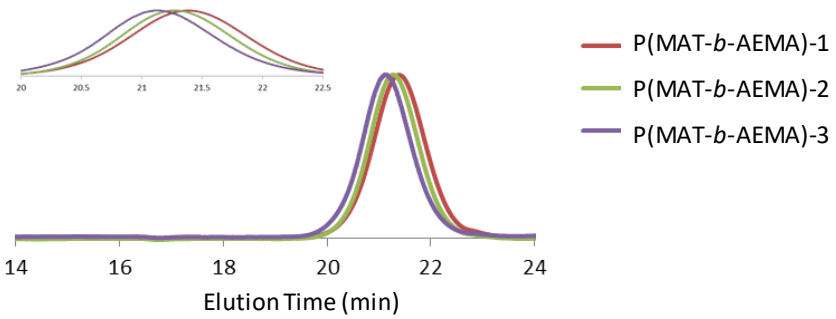

Figure 7.17. SEC traces of P(MAT-*b*-AEMA) series of polymer. Lower retention time indicates higher molecular weight. SEC conditions: eluent = 1.0 wt% acetic acid/0.1 M Na2SO4; flow rate = 0.4 mL/min; light scattering detector λ = 662 nm; refractometer λ = 658 nm.

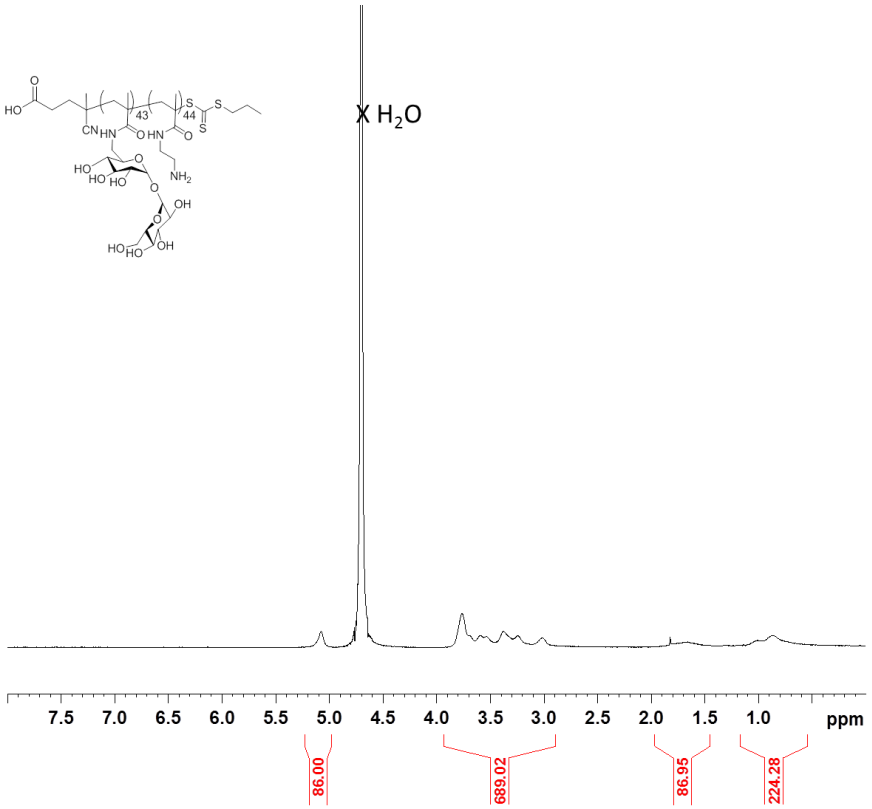

Figure 7.18. ^{1}H NMR spectrum (500 MHz, D_2O) of P(MAT-*b*-AEMA)-1. δ ppm: 5.18 – 4.97 (bs, 86H), 3.94 – 2.94 (m, 600H), 2.03-1.49 (m, 64H), 1.16 – 0.66 (m, 192H).

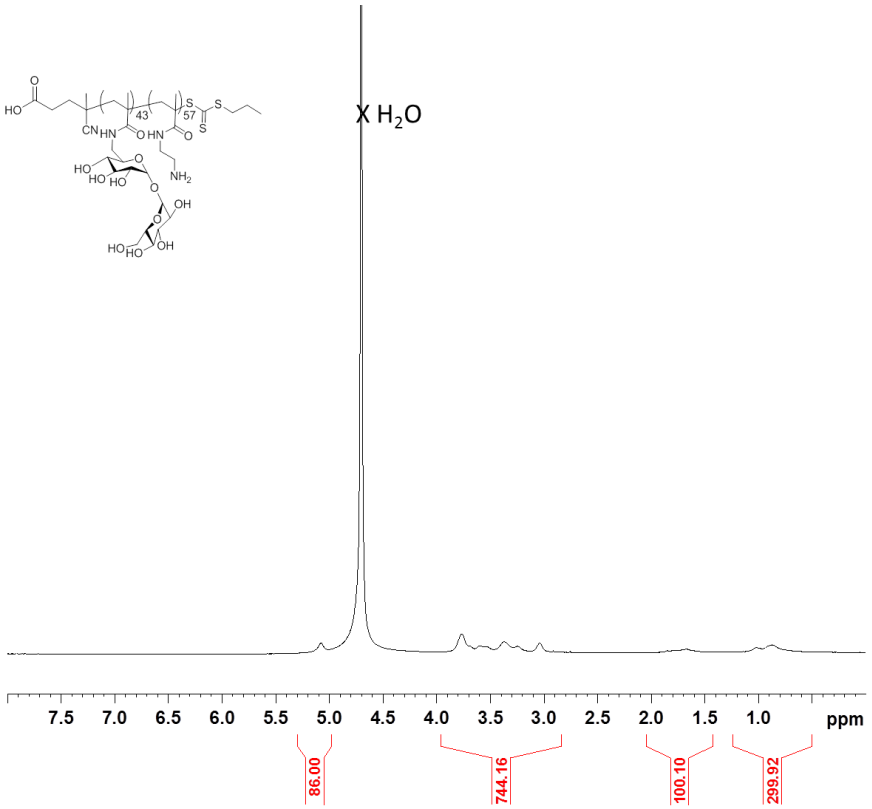

Figure 7.19. ^{1}H NMR spectrum (500 MHz, D_2O) of P(MAT-*b*-AEMA)-2. δ ppm: 5.18 – 4.97 (bs, 86H), 3.94 – 2.94 (m, 689H), 2.03-1.49 (m, 87H), 1.16 – 0.66 (m, 224H).

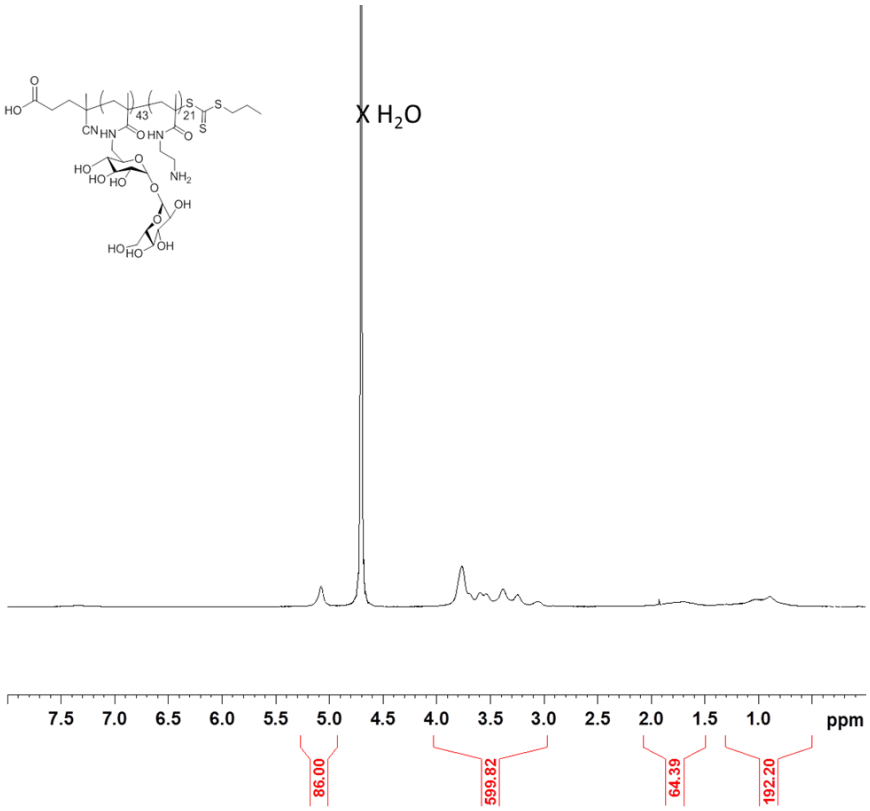

Figure 7.20. ^{1}H NMR spectrum (500 MHz, D_2O) of P(MAT-*b*-AEMA)-3. δ ppm: 5.18 – 4.97 (bs, 86H), 3.94 – 2.94 (m, 744H), 2.03-1.49 (m, 100H), 1.16 – 0.66 (m, 300H).

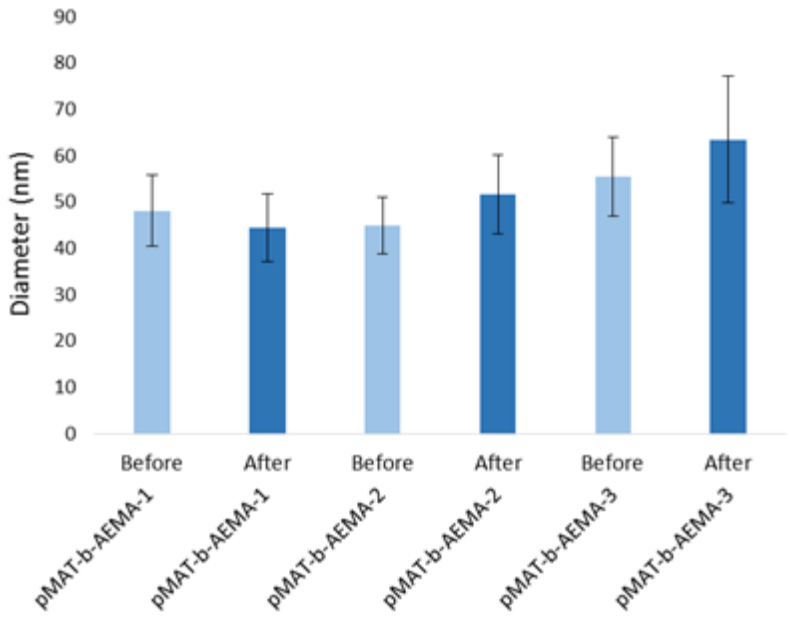

Figure 7.21. ImageJ TEM analysis

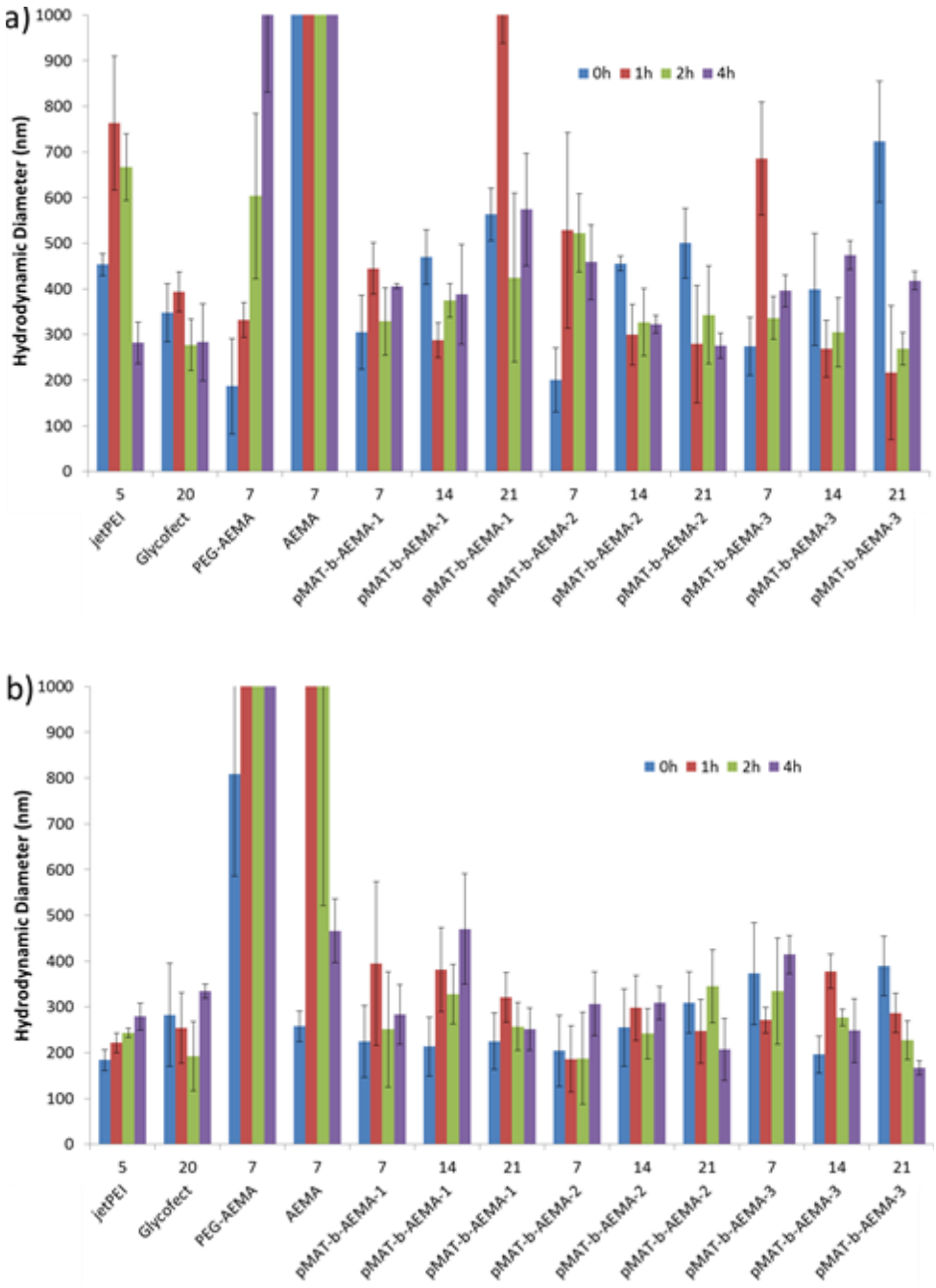

Figure 7.22. DLS in DMEM after lyophilization

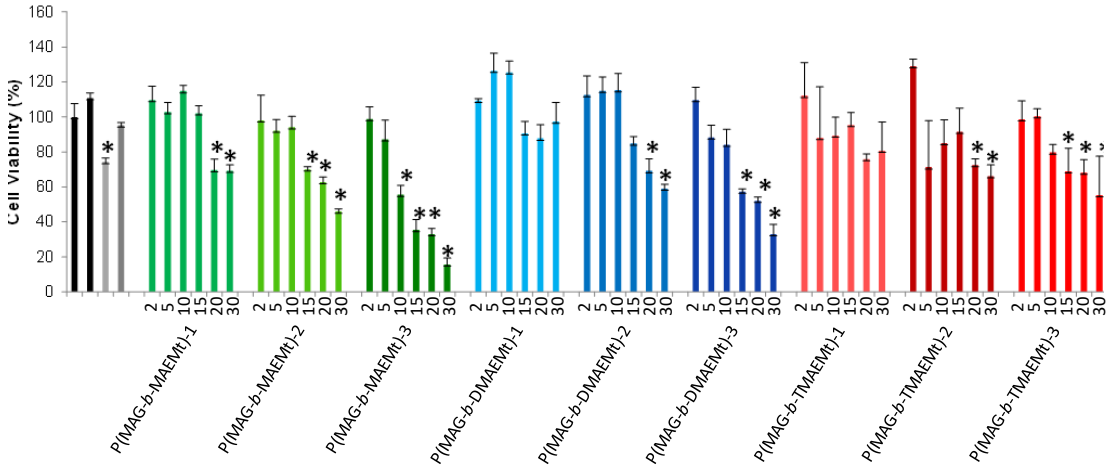

Figure 7.23. HepG2 cell viability in OptiMEM.

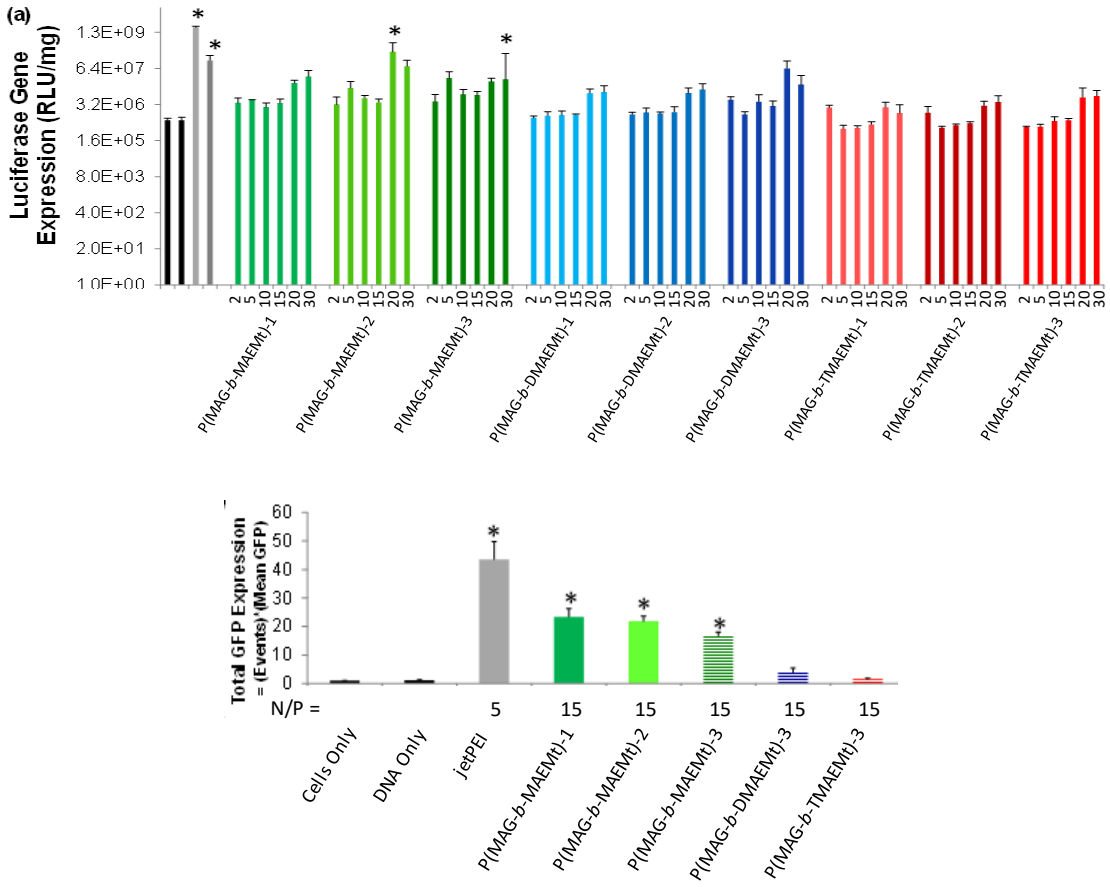

Figure 7.24. HepG2 gene expression in OptiMEM. A) Luciferase protein expression. B) GFP expression.

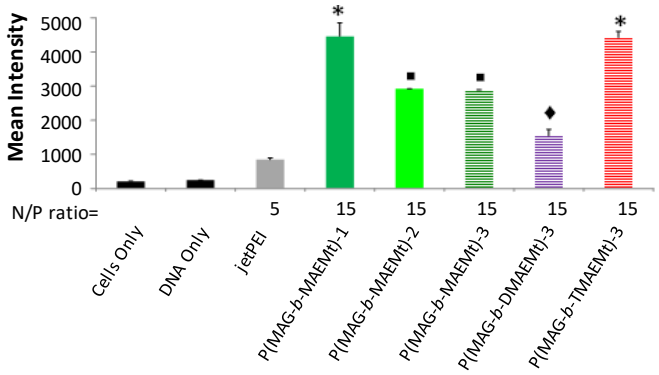

Figure 7.25. HepG2 cell uptake in OptiMEM.

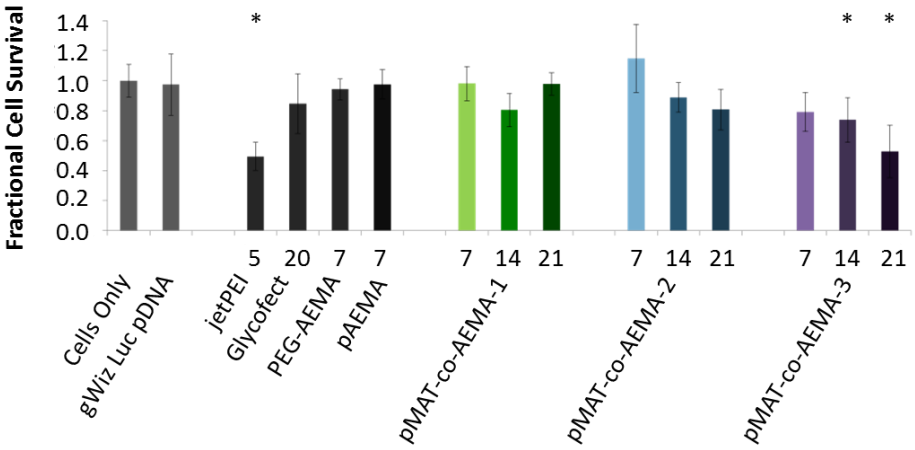

Figure 7.26. Cell survival MTT Assay following incubation of cells with pMAT-co-AEMA (-1, -2, and -3) polyplexes for 48 h in DMEM containing 10% FBS with U87 cells. The numbers on the x-axis represent the N/P ratio of polyplex formulation for each respective polymer. All results are normalized to a sample containing cells that underwent no treatment and were allowed to proliferate normally for 48 h in DMEM containing 10% FBS. All experiments were performed in triplicate with error bars marking the standard deviation. Samples that were found to be statistically different from cells only survival were marked with an * (according to Student's t-test with p = 0.05).

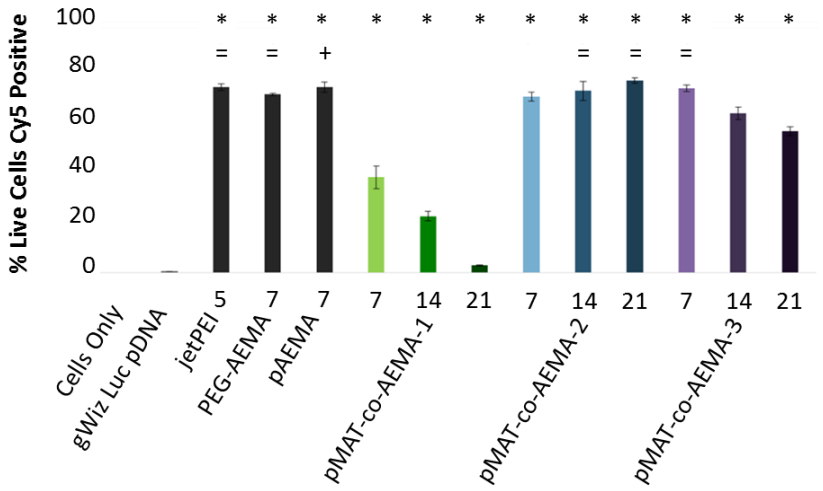

Figure 7.27. Cellular internalization of pMAT-co-AEMA polyplexes formed with Cy5-labeled pDNA and incubated with cells for 4 h in DMEM containing 10% FBS in U87 cells. The numbers on the x-axis represent the N/P ratio of polyplex formulation for each respective polymer. All experiments were performed in triplicate, where the error bars indicate standard deviation. All samples that were found to be statistically different from DNA only uptake were marked with an *. Samples that were found to be significantly higher than the positive control jetPEI are marked with a +, and samples found to be statistically equivalent to jetPEI are marked with a = (according to Student's t-test with p = 0.05).

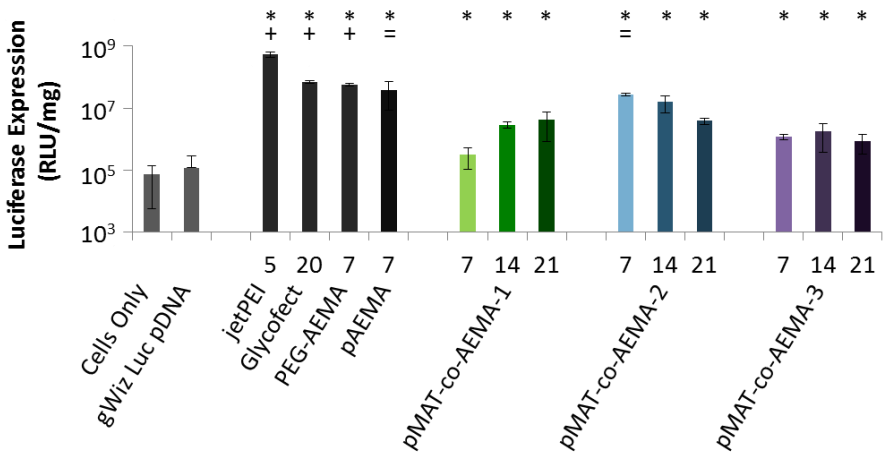

Figure 7.28. Luminescence of cell lysate following addition of luciferin in U87 cells. Cells were incubated with the polyplex formulations for 4 h in DMEM containing 10% FBS followed by an additional 48 h to allow for protein expression. The numbers on the x-axis represent the N/P ratio of polyplex formulation for each respective polymer. All experiments were performed in triplicate with error bars showing standard deviation. All samples that were found to be statistically different from cells only luciferase expression were marked with an *. Samples that were found to be significantly higher than the positive control pAEMA are marked with a +, and samples found to be statistically equivalent to pAEMA are marked with an = (according to Student's t-test with p = 0.05).

7.3.2 Chapter 3 Figures

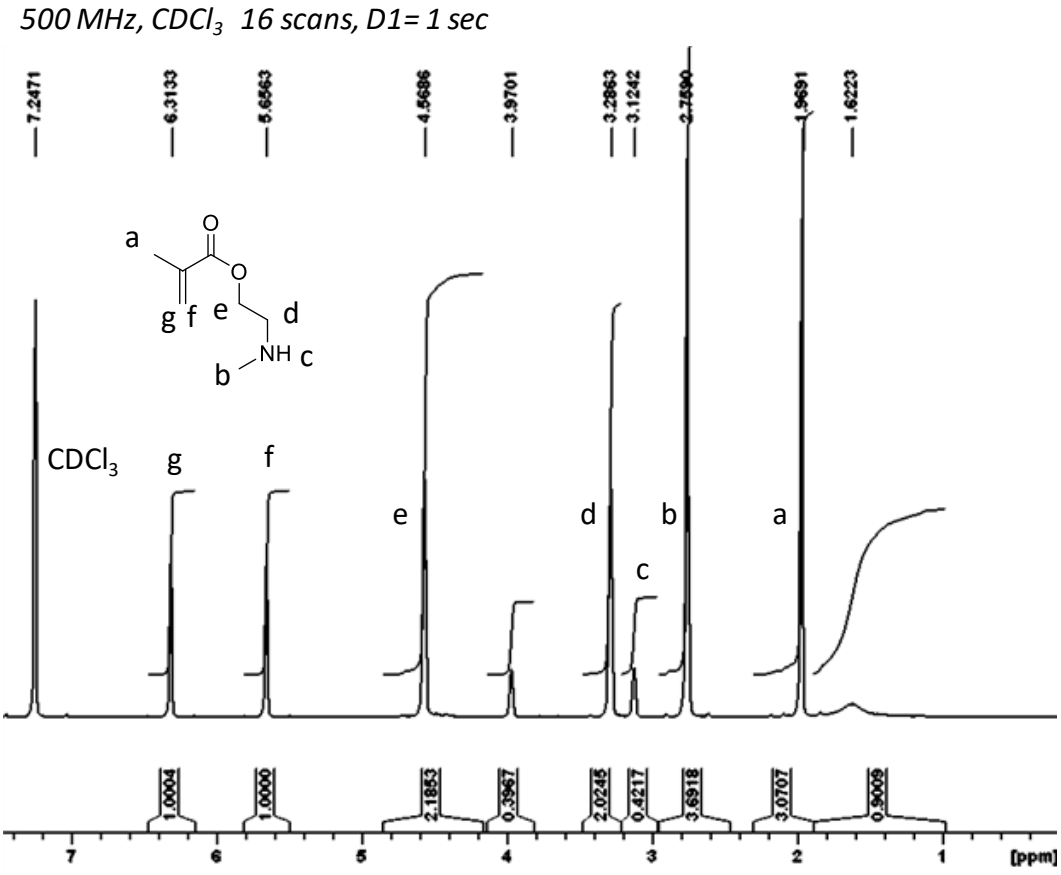

Figure 7.29. ^{1}H NMR of MAEMt monomer.

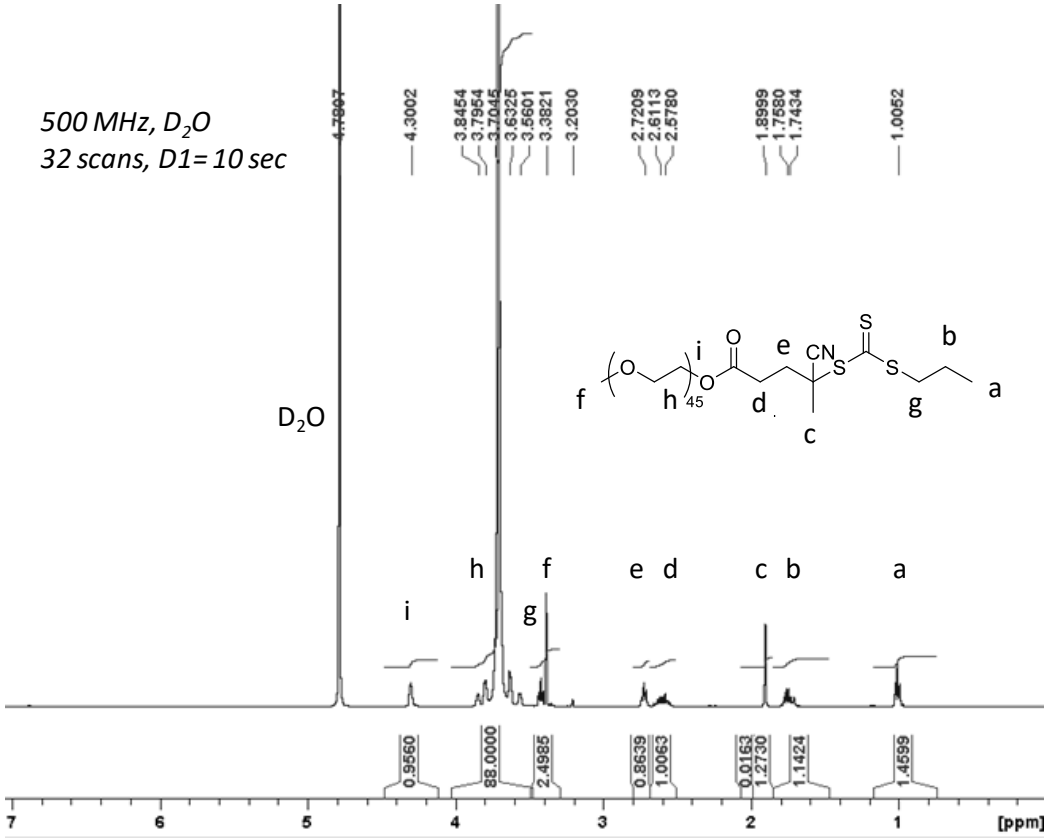

Figure 7.30. ^{1}H NMR of the PEG macroCTA.

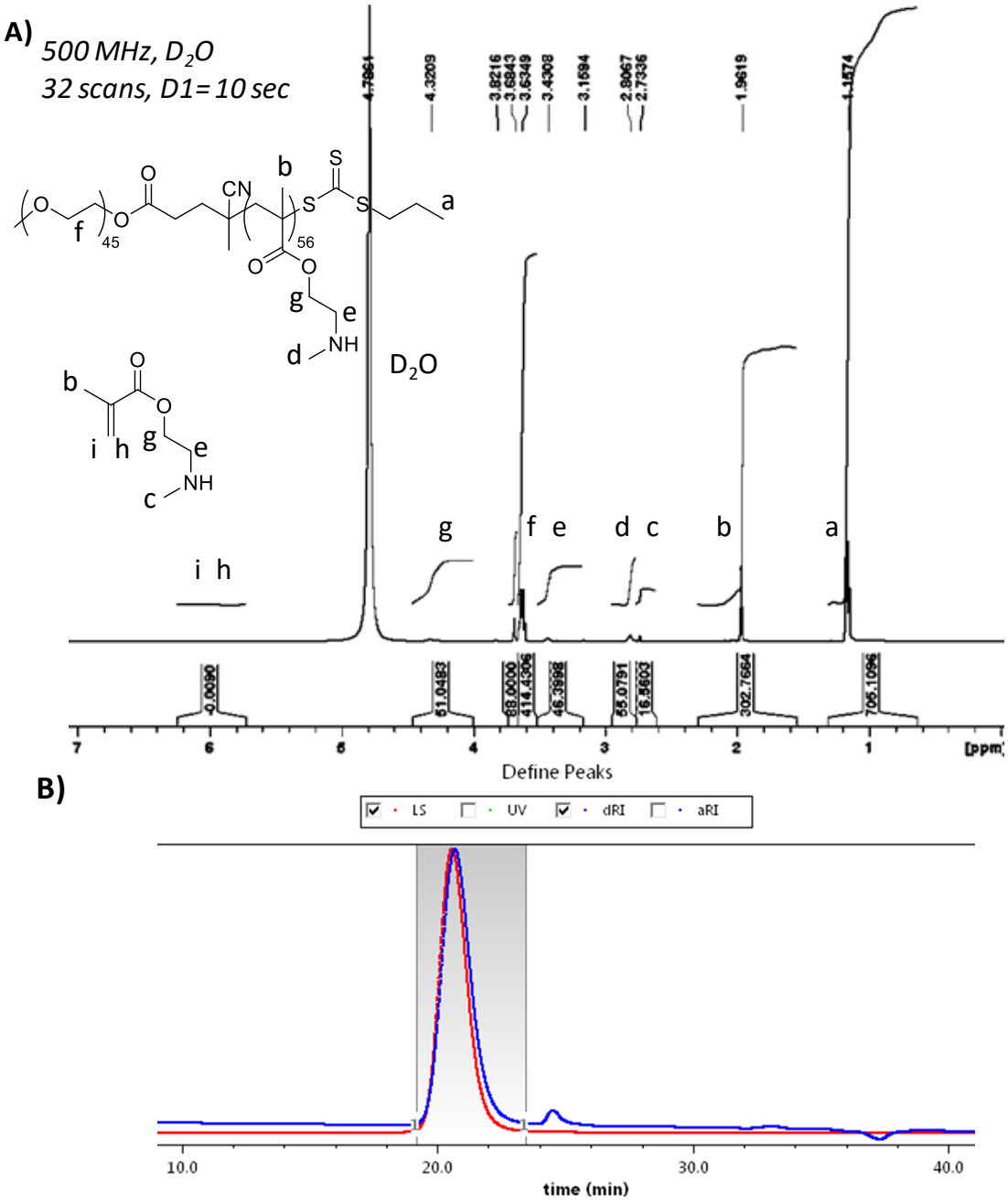

Figure 7.31. (A) ^{1}H NMR and (B) SEC traces (Red trace: light scattering; blue trace: refractive index) of P(EG-*b*-MAEMt).

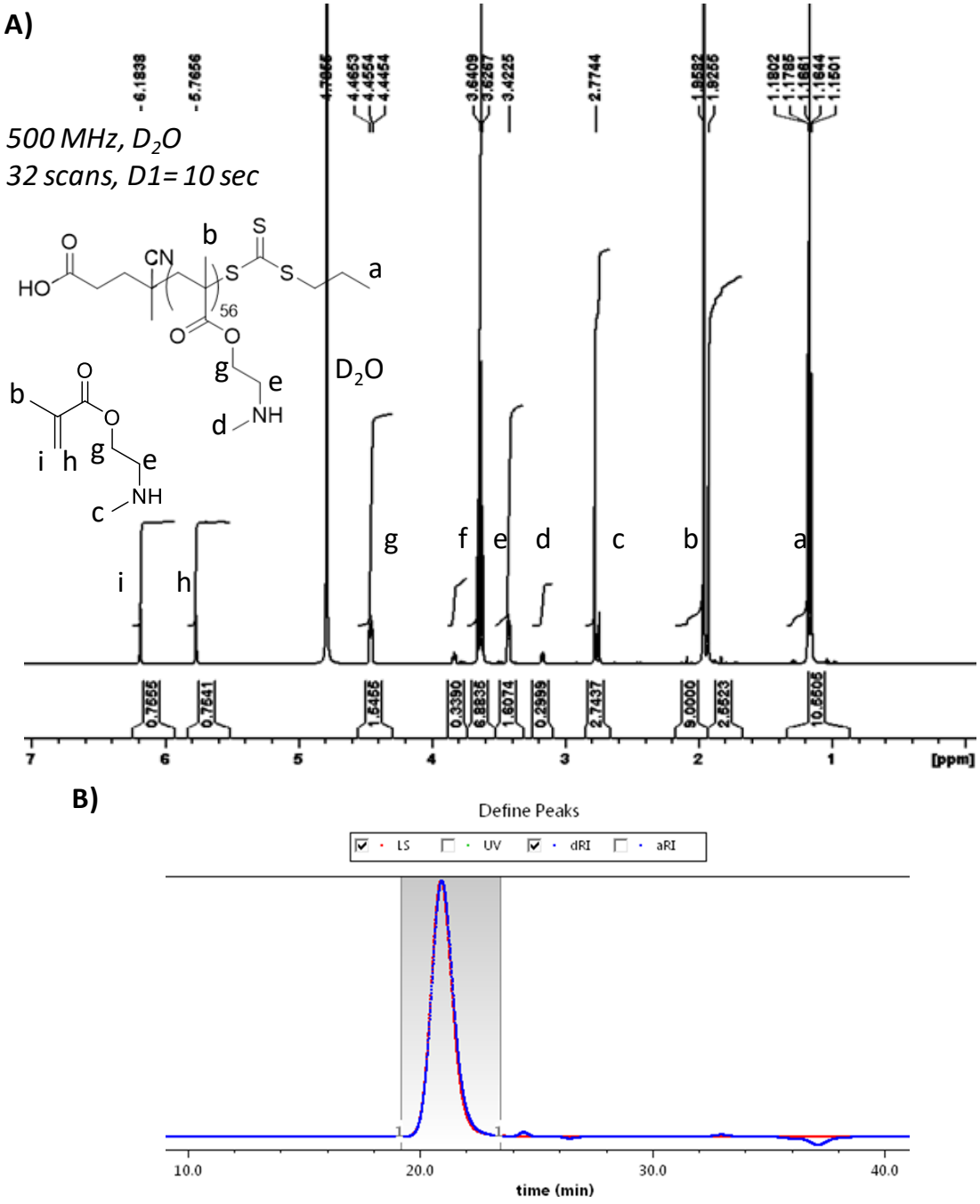

Figure 7.32. (A) ^{1}H NMR and (B) SEC traces (Red trace: light scattering; blue trace: refractive index) of P(MAEMt).

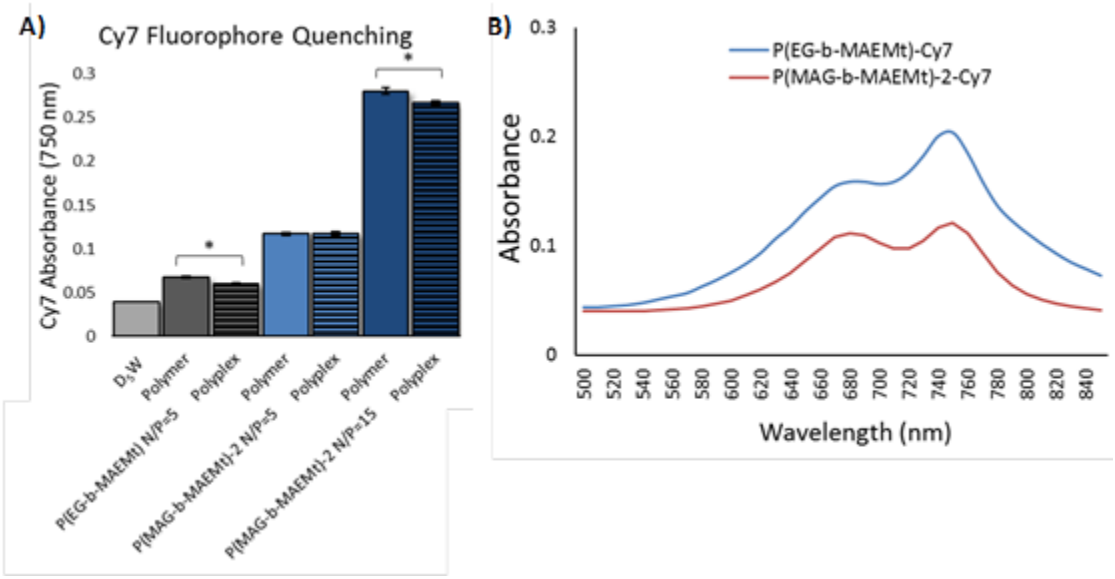

Figure 7.33. Cy7 fluorophore tagging results. (A) Cy7-tagged sample absorbance comparing free Cy7-polymer to complexed Cy7-polymer. (B) Cy7 absorbance spectra for the two Cy7-labeled polymers in water. The degree of polymer tagging was determined using the peak absorbance at λ = 750 nm.

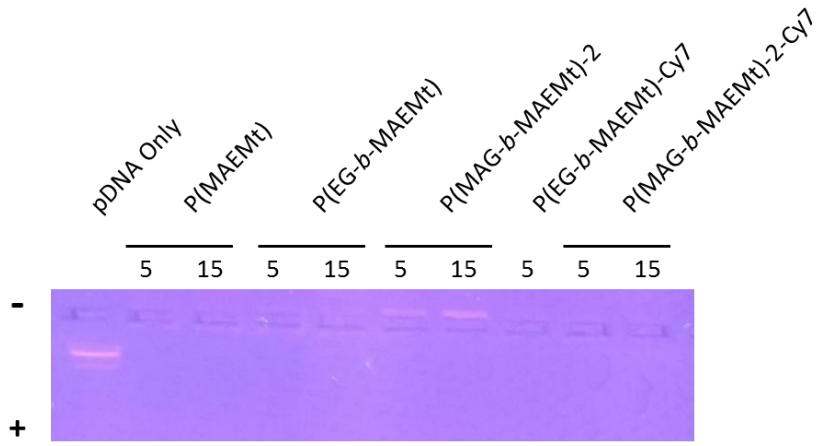

Figure 7.34. Gel electrophoresis of polyplex formulations with new polymers and with all polymers used in animal studies. All experimental polymers fully bound the plasmid DNA at N/P = 5.

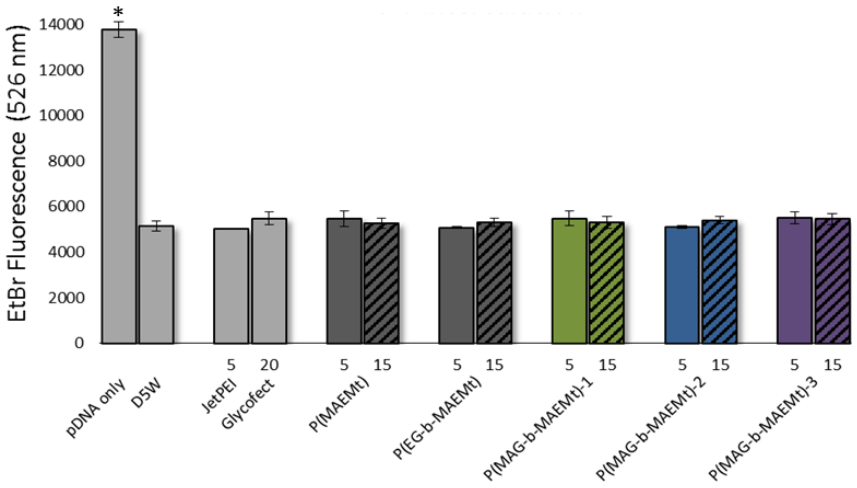

Figure 7.35. EtBr intercalation polyplex stability study. All polyplex samples prevented EtBr intercalation into pDNA cargo as compared to a pDNA only positive control. Each fluorescent sample was measured in triplicate and samples that significantly differed from the D_5W negative control were marked with an asterisk (Student's t test $p < 0.05$).

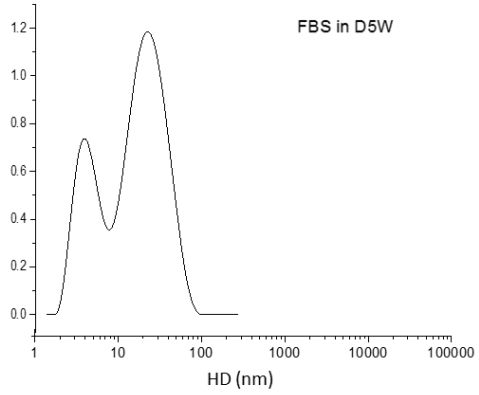

Figure 7.36. DLS correlation function of FBS only transformed by REPES analysis. Timepoints taken after addition of FBS solution. The x-axis is the hydrodynamic diameter (HD) in nm, and the y-axis is unitless intensity.

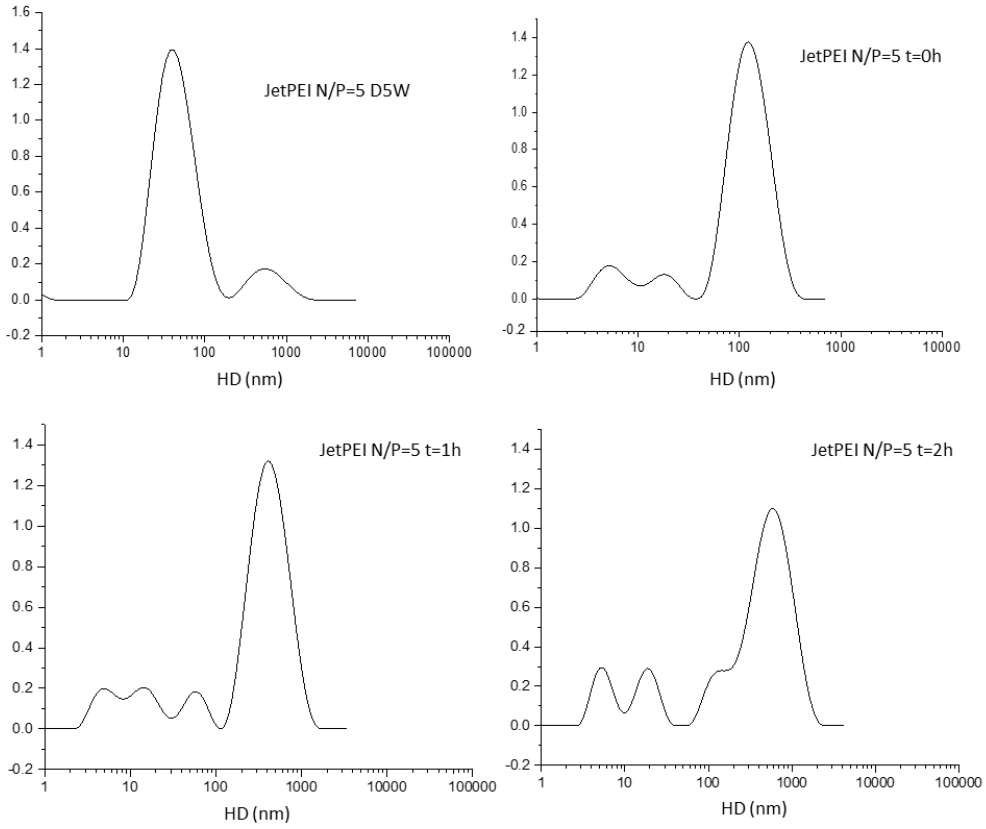

Figure 7.37. DLS correlation function of FBS only transformed by REPES analysis. Timepoints taken after addition of FBS solution. The x-axis is the hydrodynamic diameter (HD) in nm, and the y-axis is unitless intensity.

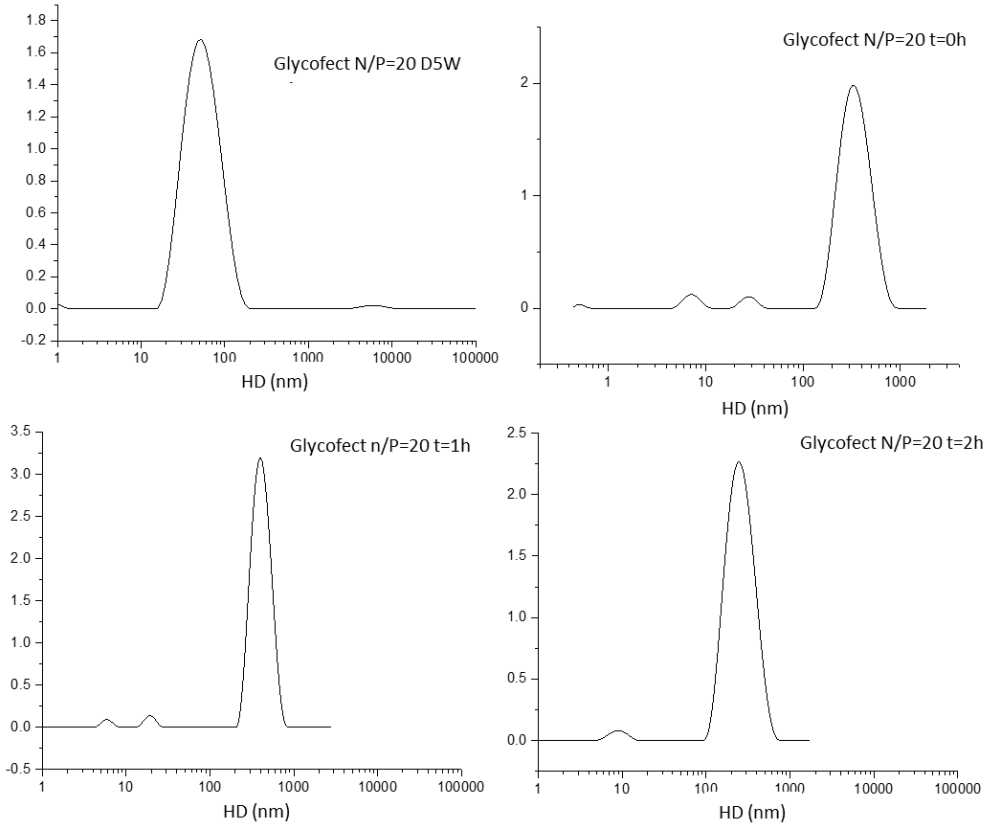

Figure 7.38. DLS correlation function of FBS only transformed by REPES analysis. Timepoints taken after addition of FBS solution. The x-axis is the hydrodynamic diameter (HD) in nm, and the y-axis is unitless intensity.

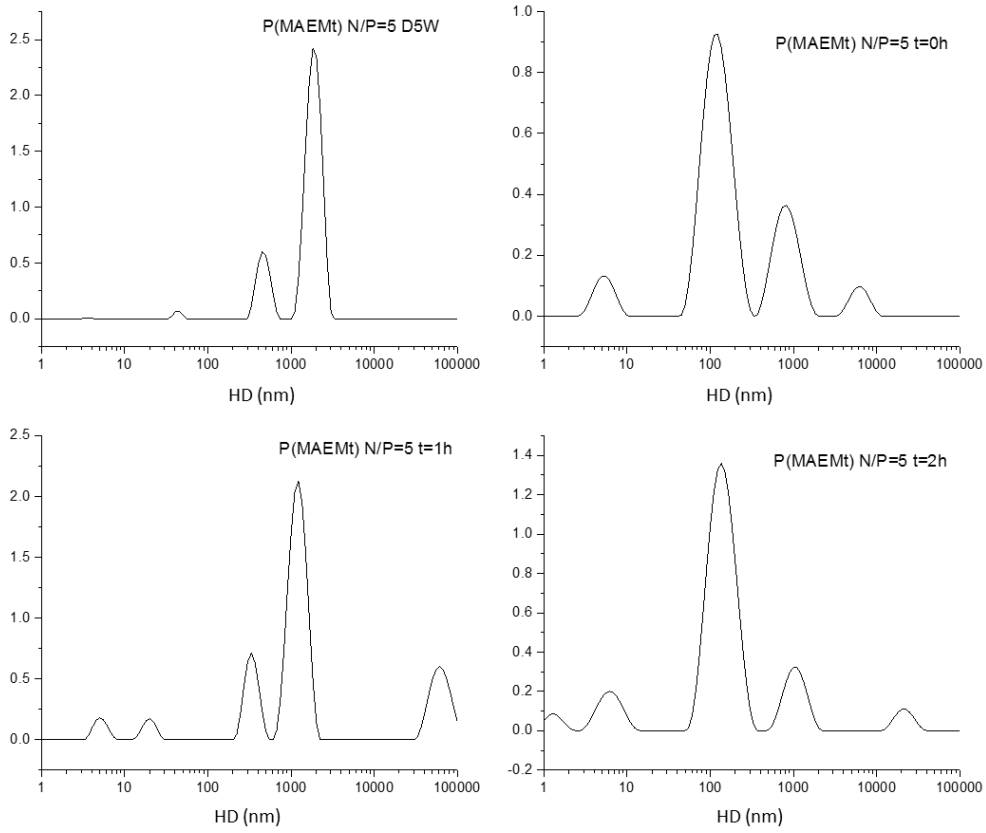

Figure 7.39. DLS correlation function of FBS only transformed by REPES analysis. Timepoints taken after addition of FBS solution. The x-axis is the hydrodynamic diameter (DH) in nm, and the y-axis is unitless intensity.

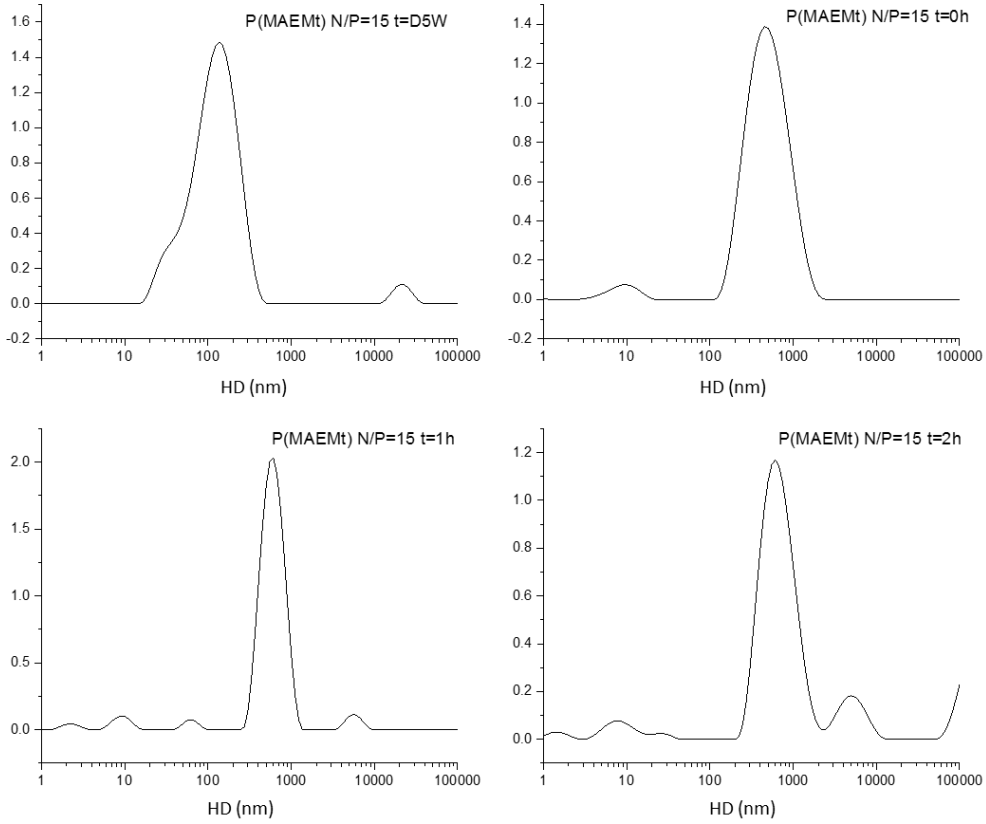

Figure 7.40. DLS correlation function of FBS only transformed by REPES analysis. Timepoints taken after addition of FBS solution. The x-axis is the hydrodynamic diameter (HD) in nm, and the y-axis is unitless intensity.

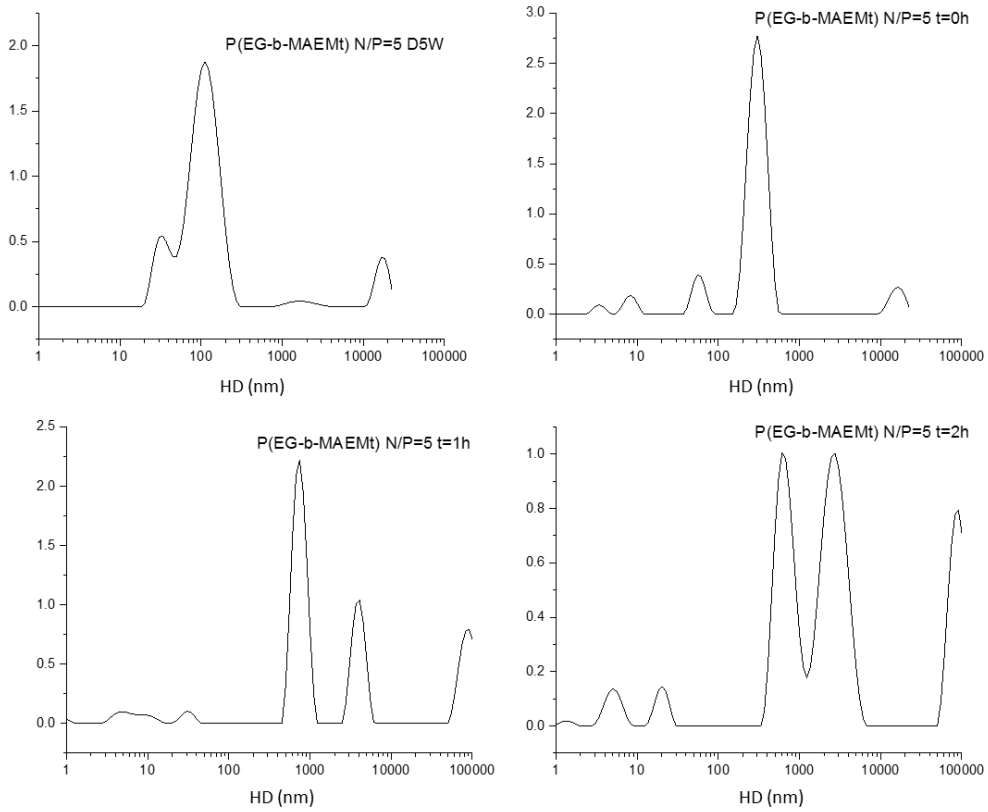

Figure 7.41. DLS correlation function of FBS only transformed by REPES analysis. Timepoints taken after addition of FBS solution. The x-axis is the hydrodynamic diameter (HD) in nm, and the y-axis is unitless intensity.

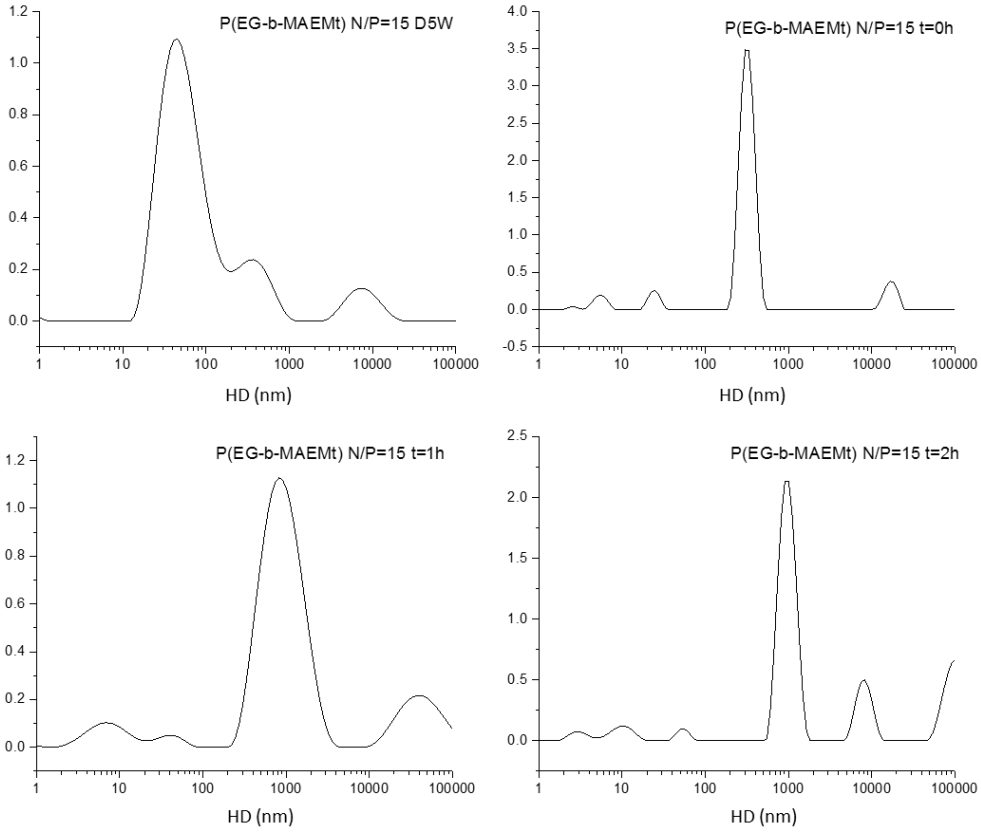

Figure 7.42. DLS correlation function of FBS only transformed by REPES analysis. Timepoints taken after addition of FBS solution. The x-axis is the hydrodynamic diameter (HD) in nm, and the y-axis is unitless intensity.

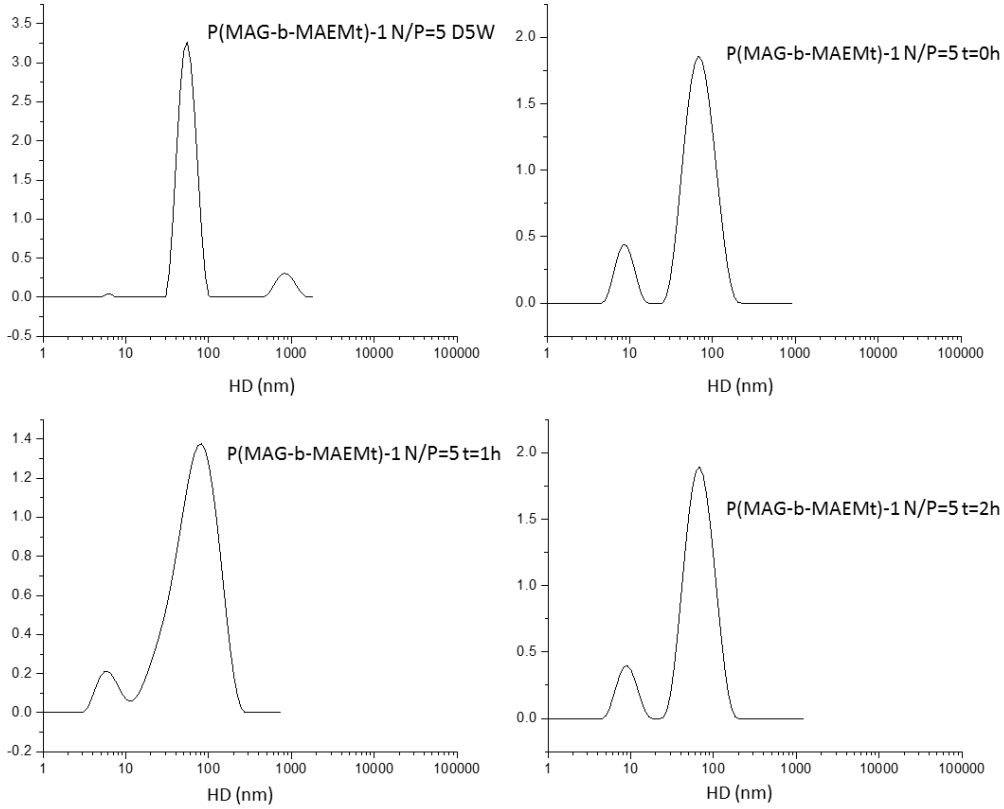

Figure 7.43. DLS correlation function of FBS only transformed by REPES analysis. Timepoints taken after addition of FBS solution. The x-axis is the hydrodynamic diameter (HD) in nm, and the y-axis is unitless intensity.

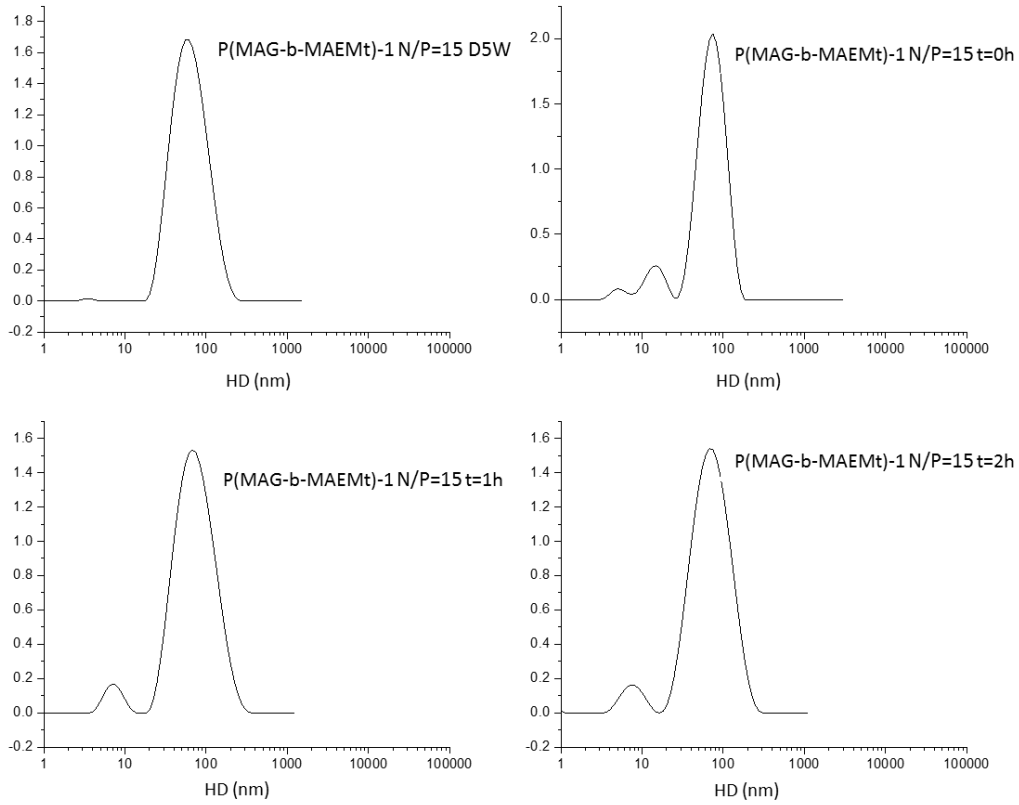

Figure 7.44. DLS correlation function of FBS only transformed by REPES analysis. Timepoints taken after addition of FBS solution. The x-axis is the hydrodynamic diameter (HD) in nm, and the y-axis is unitless intensity.

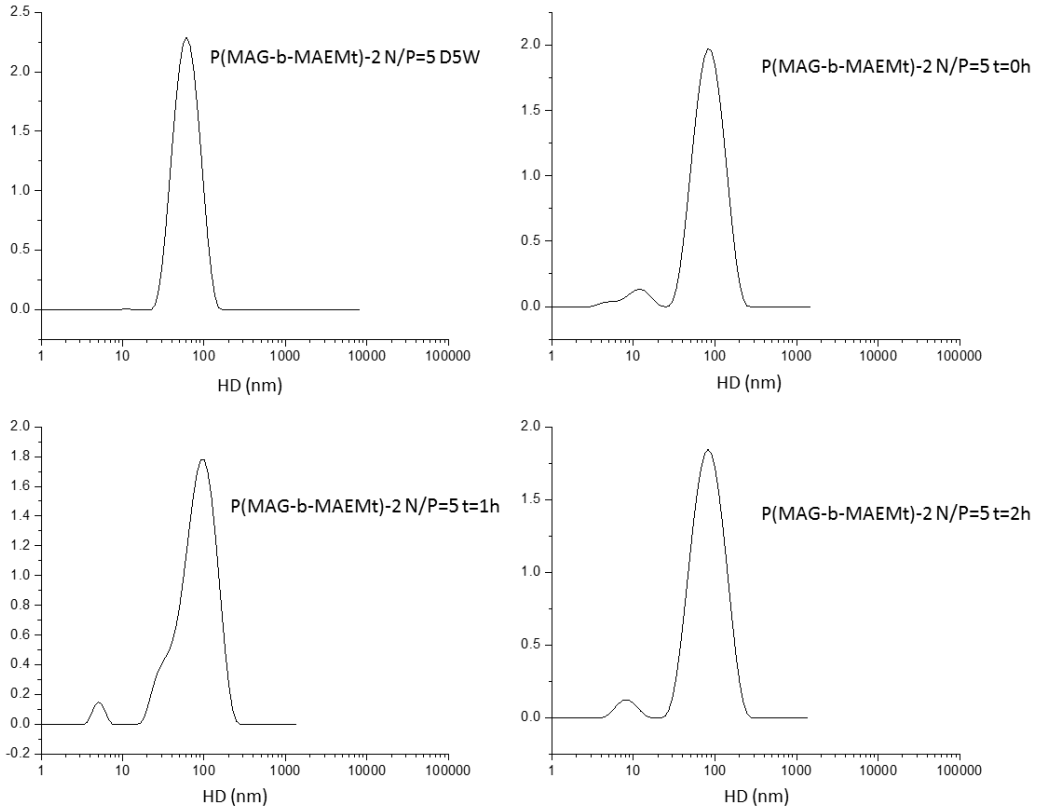

Figure 7.45. DLS correlation function of FBS only transformed by REPES analysis. Timepoints taken after addition of FBS solution. The x-axis is the hydrodynamic diameter (HD) in nm, and the y-axis is unitless intensity.

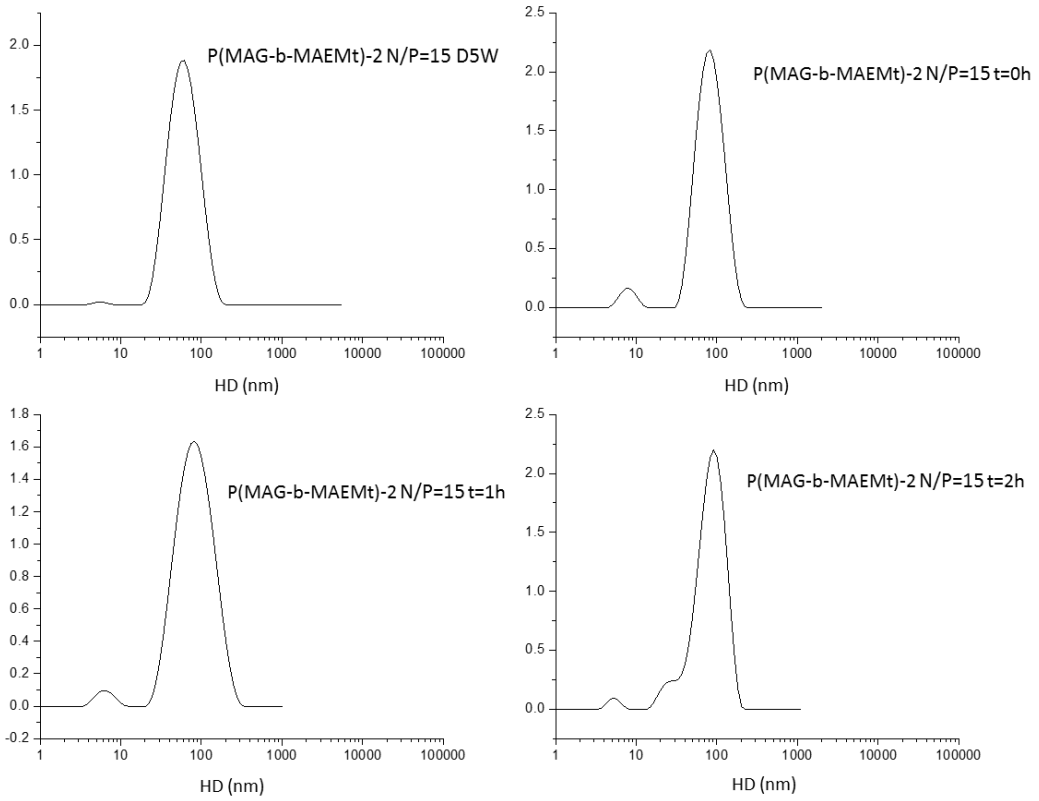

Figure 7.46. DLS correlation function of FBS only transformed by REPES analysis. Timepoints taken after addition of FBS solution. The x-axis is the hydrodynamic diameter (HD) in nm, and the y-axis is unitless intensity.

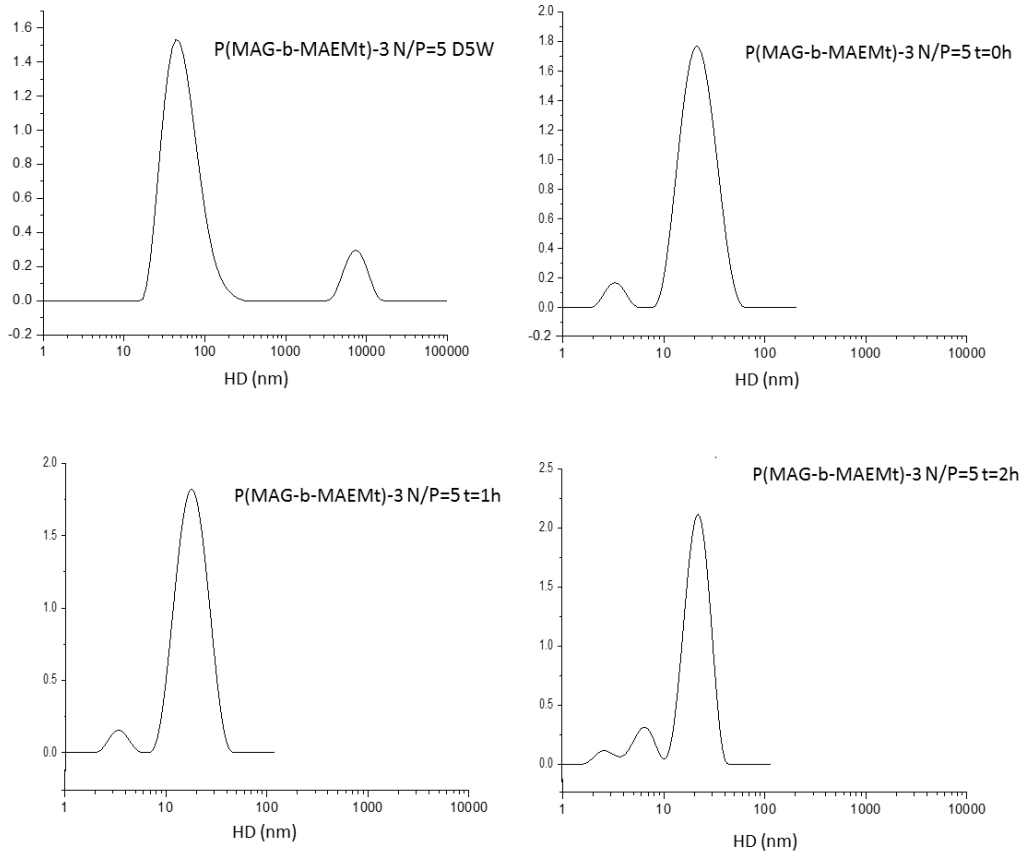

Figure 7.47. DLS correlation function of FBS only transformed by REPES analysis. Timepoints taken after addition of FBS solution. The x-axis is the hydrodynamic diameter (HD) in nm, and the y-axis is unitless intensity.

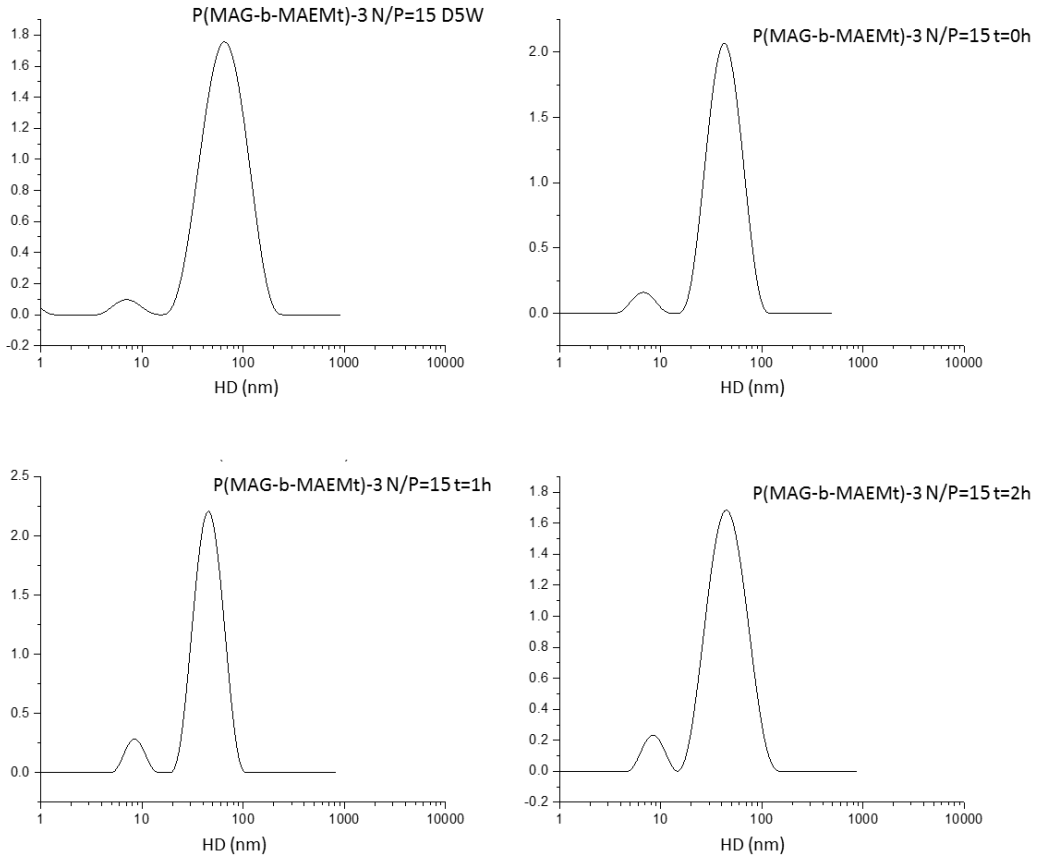

Figure 7.48. DLS correlation function of FBS only transformed by REPES analysis. Timepoints taken after addition of FBS solution. The x-axis is the hydrodynamic diameter (HD) in nm, and the y-axis is unitless intensity.

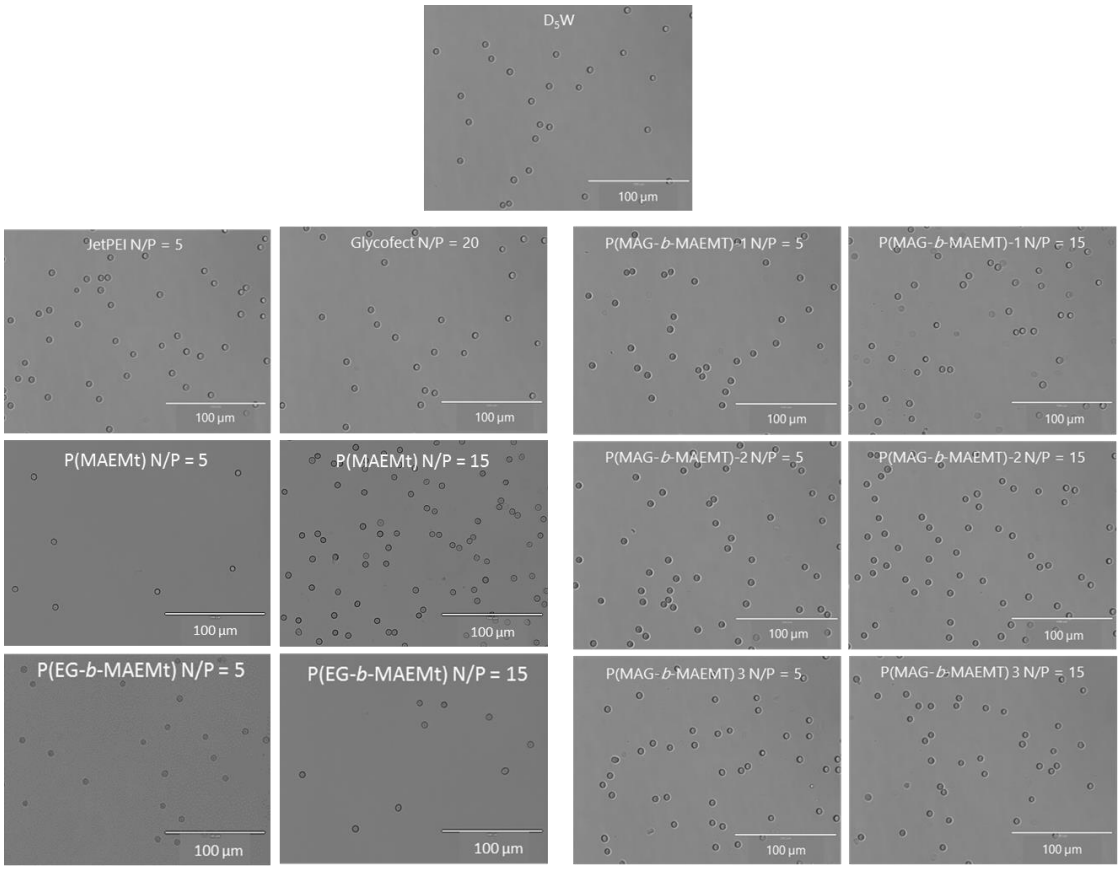

Figure 7.49. Representative DIC microscopy images at 20x magnification.

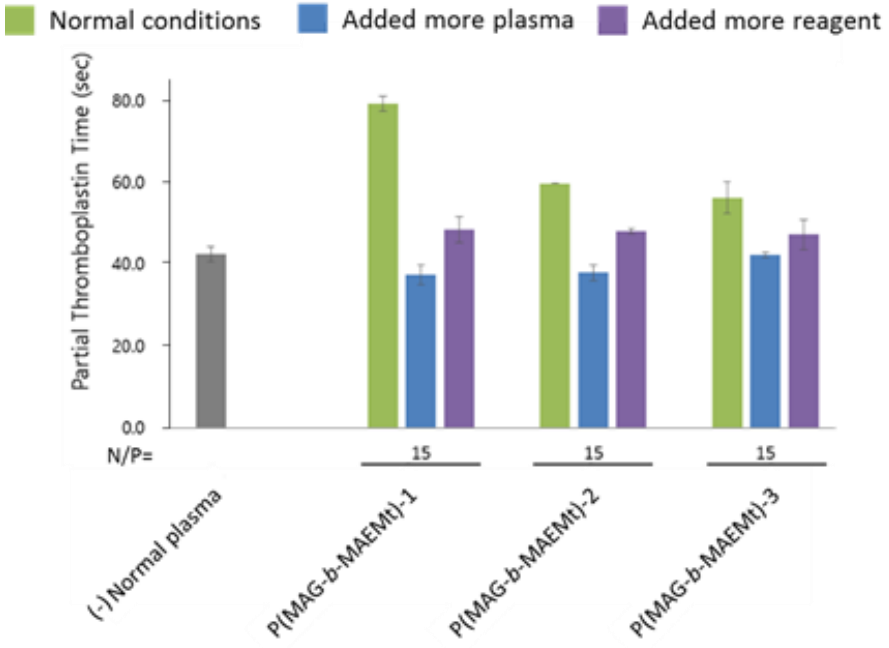

Figure 7.50. Coagulation times in seconds for human platelet poor plasma (PPP) only compared to PPP incubated with polyplexes at N/P=15 for 1 h. The green bars show results when testing with normal aPTT assay conditions. The purple bars are the results when 50% by volume PPP (150 additional µL) was added to the test tube during the assay, and the blue bars are the coagulation times when twice as much reagent was used.

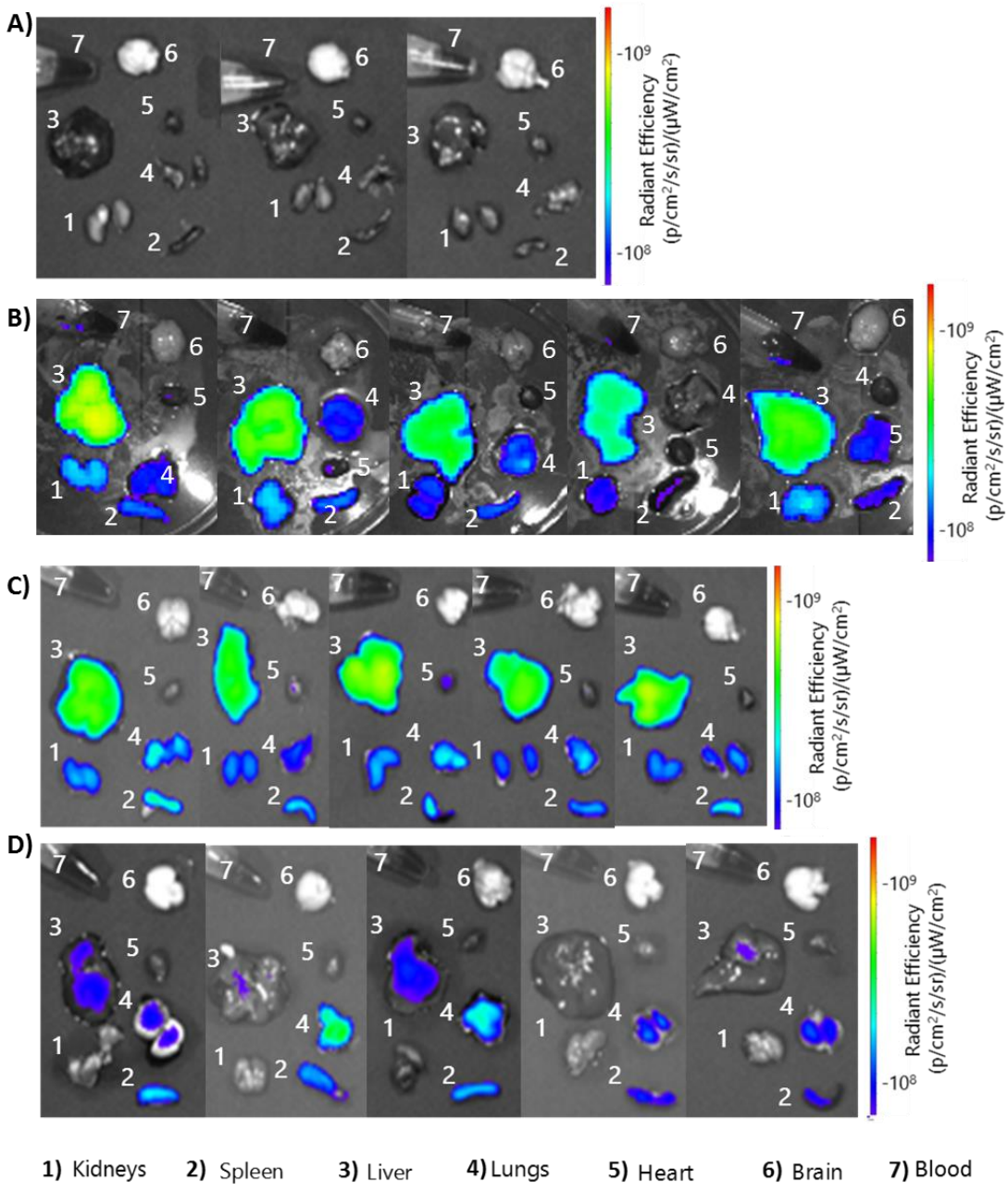

Figure 7.51. Fluorescent organ images after D_5W or polyplex injection. (A) D_5W only. (B) PEG-*b*-MAEMT-Cy7 N/P=5. (C) P(MAG-*b*-MAEMT)-2-Cy7 N/P=5. (D) P(MAG-*b*-MAEMT)-2-Cy7 N/P=15.

7.3.3 Chapter 4 Figures

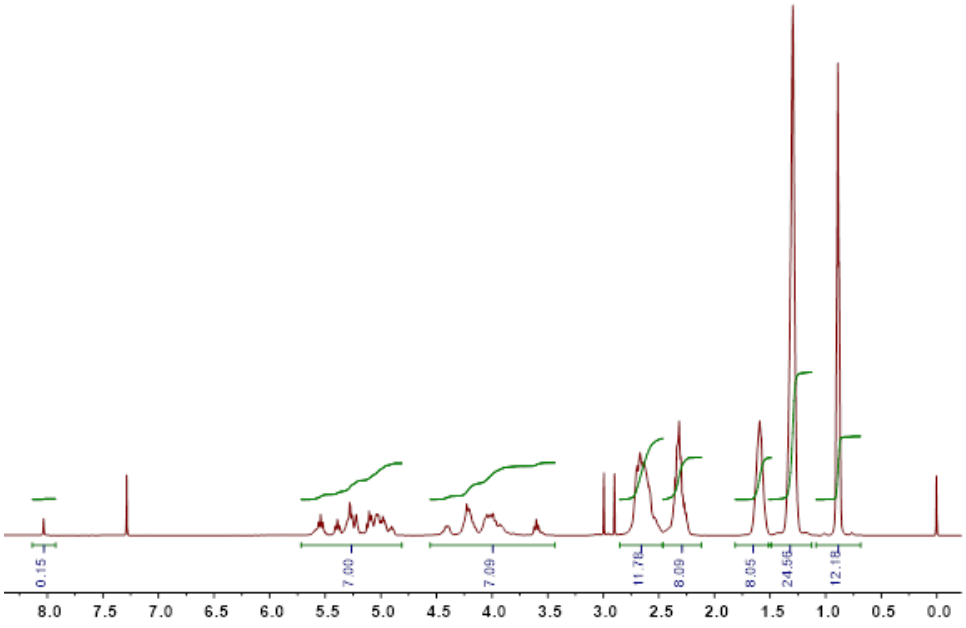

Figure 7.52. ^{1}H NMR of TR4HP3SA.

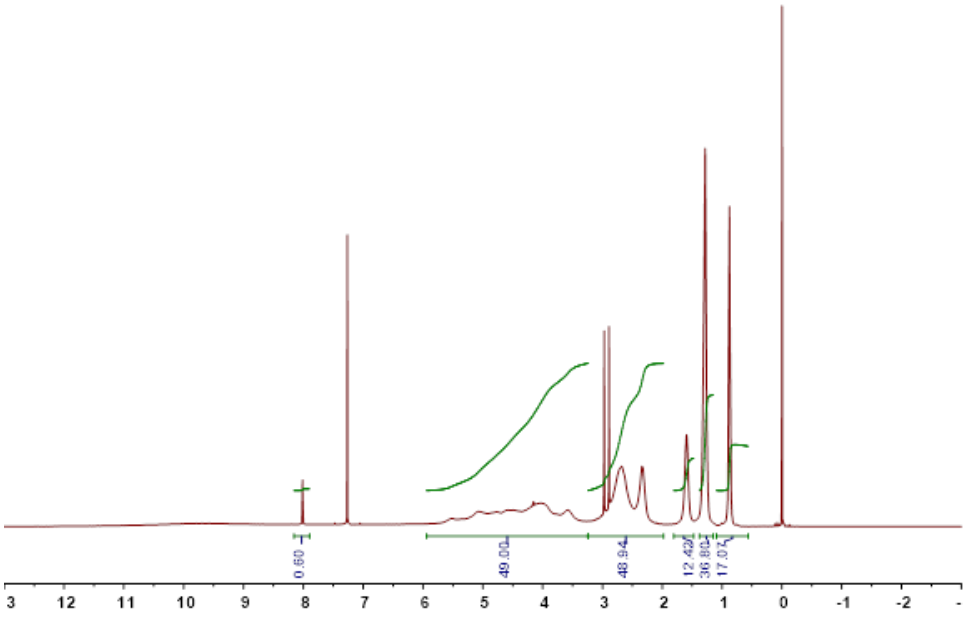

Figure 7.53. ^{1}H NMR of CD6HP8SA.

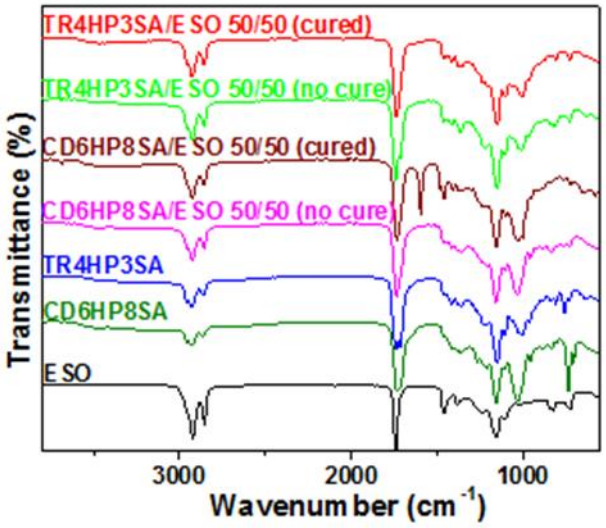

Figure 7.54. FT-IR spectra of TR4HP3SA, CD6HP8SA, ESO, TR4HP3SA/ESO (50/50), CD6HP8SA/ESO (50/50) before and after cure.

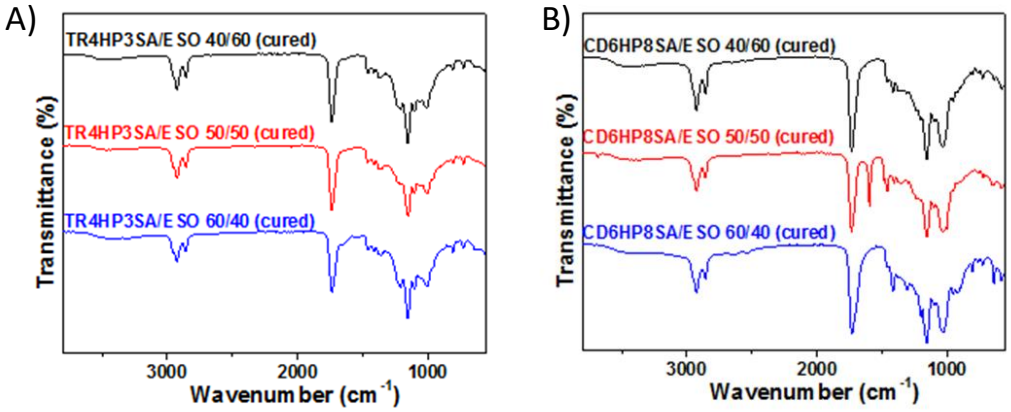

Figure 7.55. FT-IR spectra of cured A) TR4HP3SA/ESO and B) CD6HP8SA/ESO at different ratios.

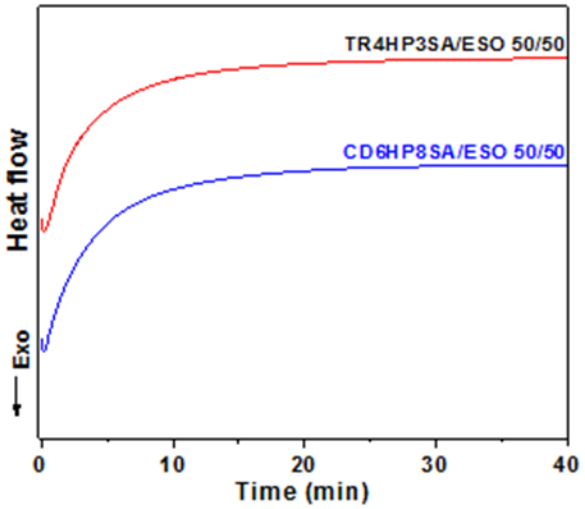

Figure 7.56. The isothermal DSC curves for TR4HP3SA/ESO (50/50) at 165 °C and CD6HP8SA/ESO (50/50) at 165 °C under nitrogen.

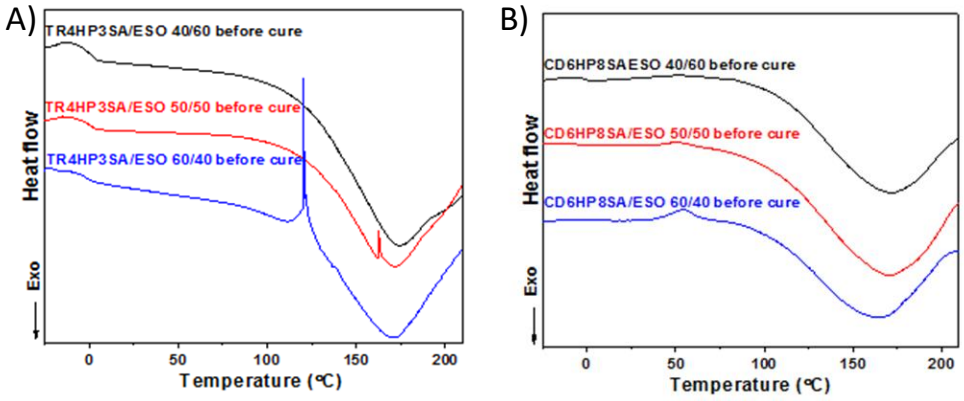

Figure 7.57. DSC curing thermograms of A) TR4HP3SA/ESO and B) CD6HP8SA/ESO at different ratios under nitrogen, 5 °C min^{-1}.

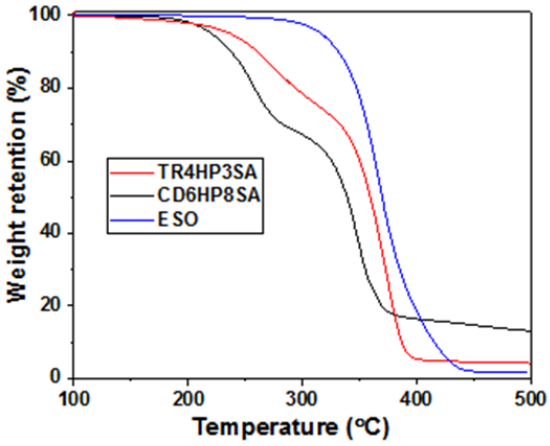

Figure 7.58. TGA curves for hardeners TR4HP3SA, CD6HP8SA and ESO with heating rate of 10 °C min^{-1} under nitrogen.

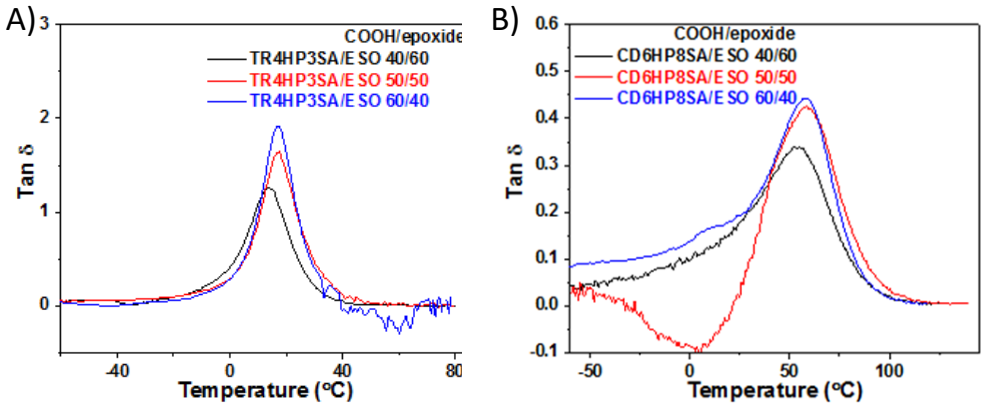

Figure 7.59. Tan δ curve versus temperature for cured A) TR4HP3HA/ESO and B) CD6NP8SA at different ratios by DMA.

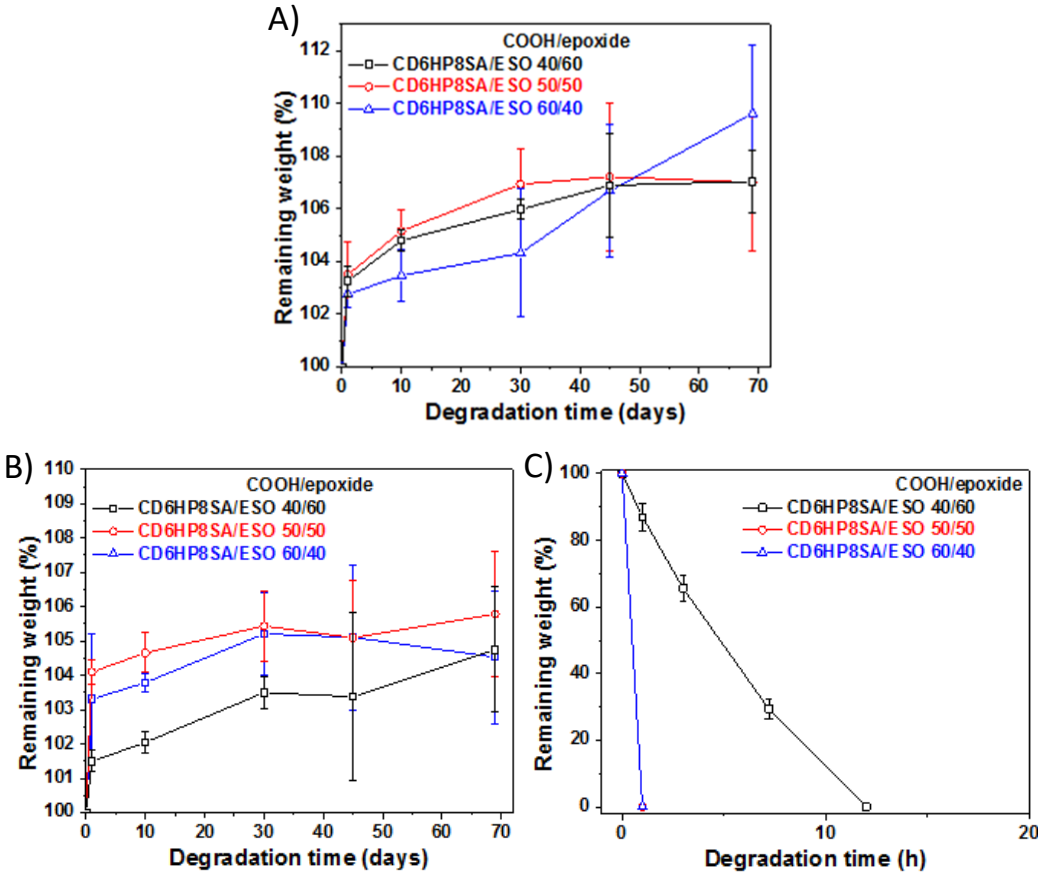

Figure 7.60. Hydrolytic degradation profile of cured CD6HP8SA/ESO at different ratios in A) water, B) 1 M HCl, and C) 1M NaOH. The error bars represent the standard deviation from the mean of 3 measurements.

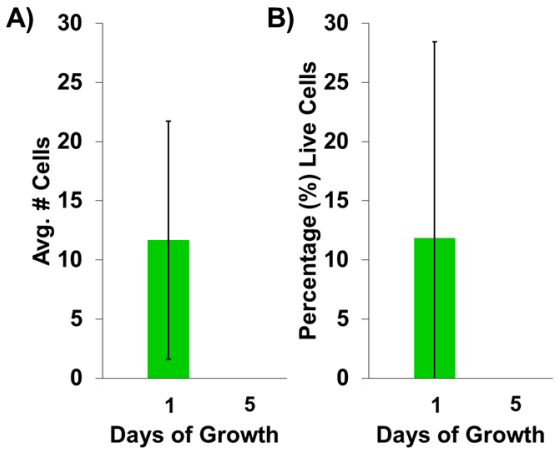

Figure 7.61. (A) Average number of cells and (B) the percentage of those cells that are alive adhered to the TR4HP3SA/ESO 50/50 film by flow cytometry at day 1 and day 5 culturing. N=3 for each assay, and the error bars represent the standard deviation from the mean. No samples were statistically different ($p<0.05$) according to Student's t-test.

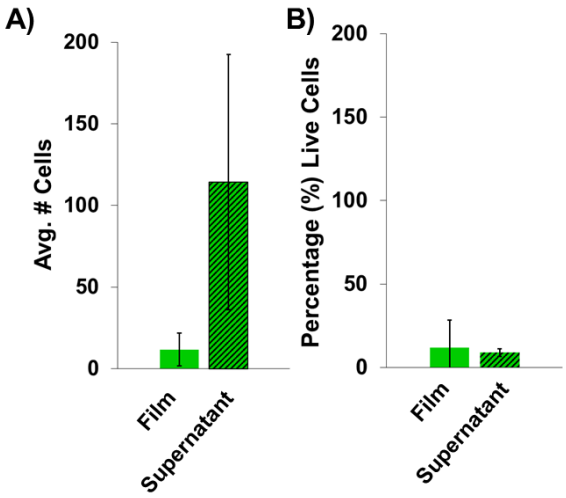

Figure 7.62. (A) Average number of live cells and (B) percentage of live cells adhered to the TR4HP3SA/ESO 50/50 film and in the supernatant above the film by flow cytometry after 24 h culturing. N=3 for each assay, and the error bars represent the standard deviation from the mean. No samples were statistically different ($p < 0.05$) according to Student's t-test on the polymer film and in the supernatant after 24 h.

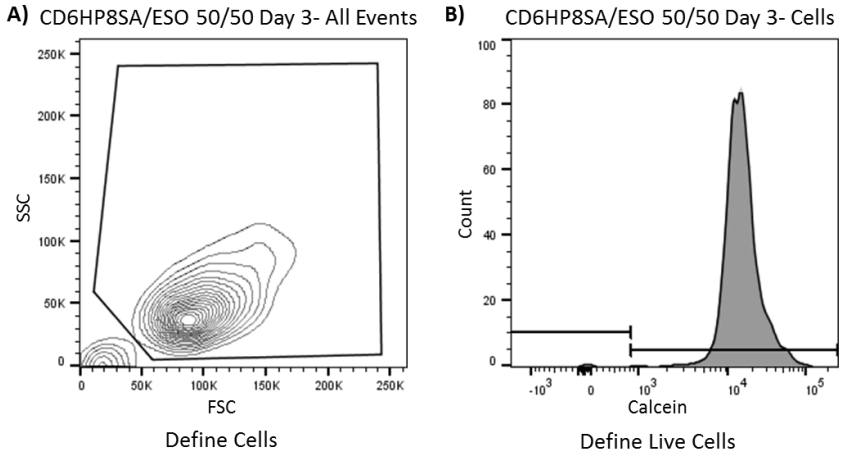

Figure 7.63. Gating parameters applied to all flow cytometry samples, shown using representative sample CD6HP8/ESO 50/50 on day 3 of cell culture. A) All flow cytometry events gated to capture cell count data. B) Data from cell count gate replotted as histogram to define live cells as indicated by expression of calcein.

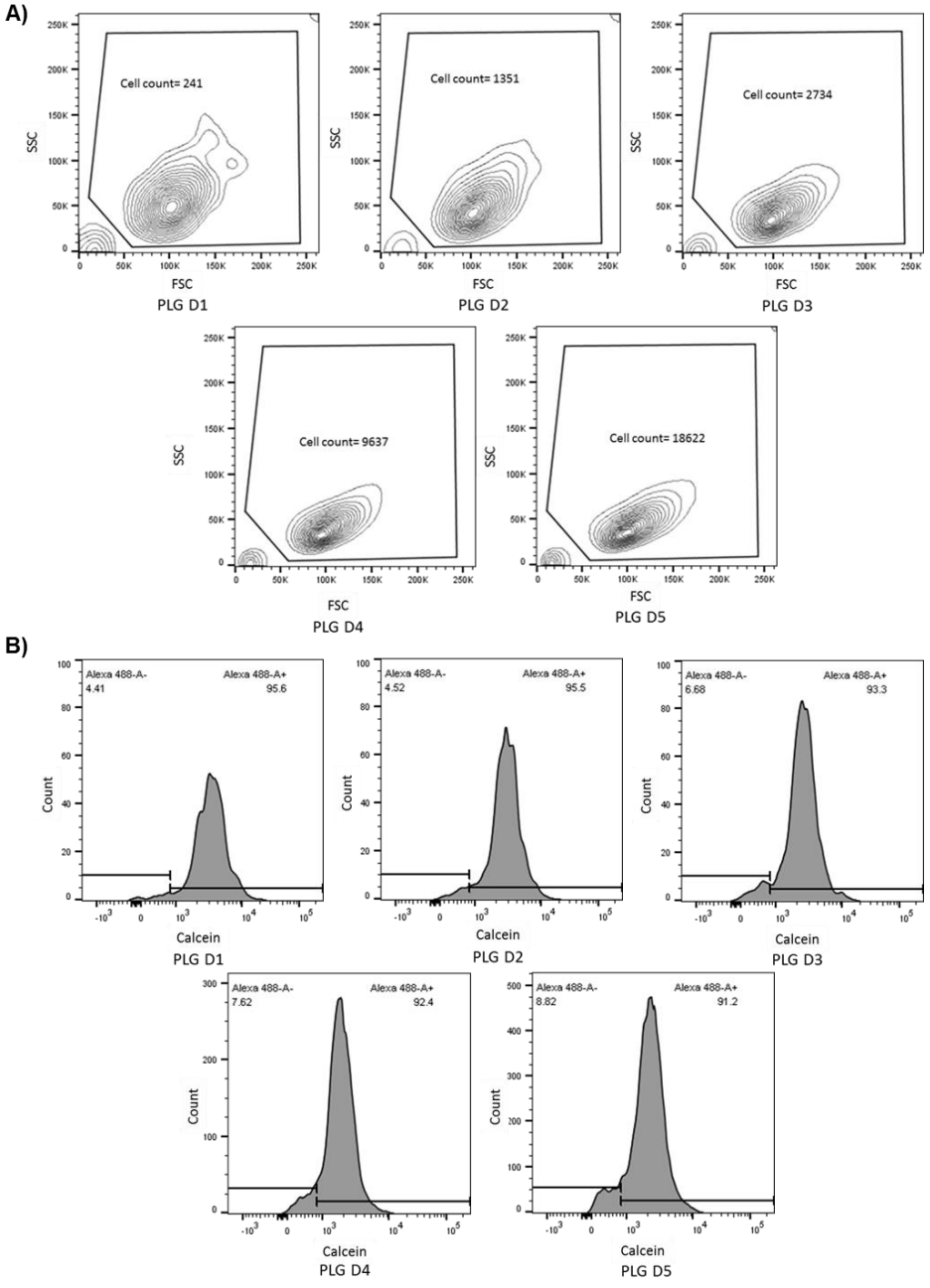

Figure 7.64. Representative raw flow cytometry data of cells grown on PLG from Day 1 - Day 5. A) Total number of cells counted. B) Percentage of those cells that are alive as determined by calcein staining.

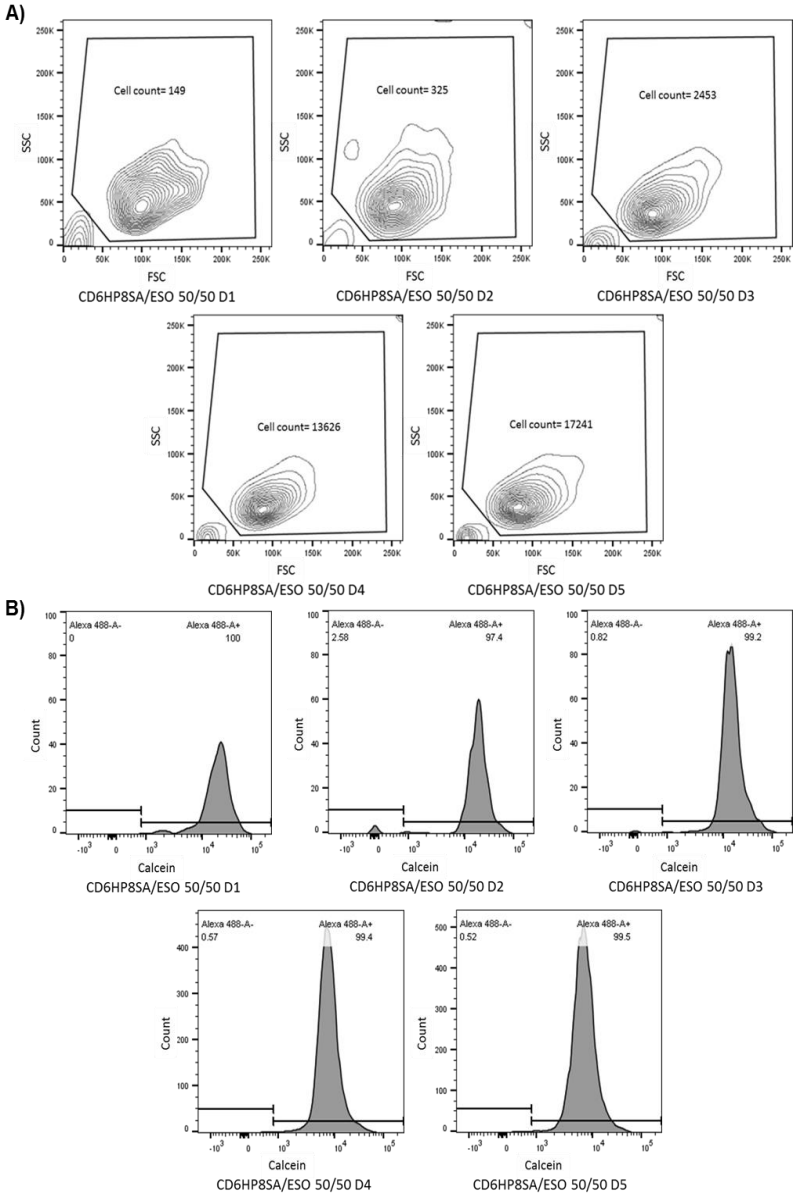

Figure 7.65. Representative raw flow cytometry data of cells grown on CD6HP8SA/ESO 50/50 from Day 1 - Day 5. A) Total number of cells counted. B) Percentage of those cells that are alive as determined by calcein staining.

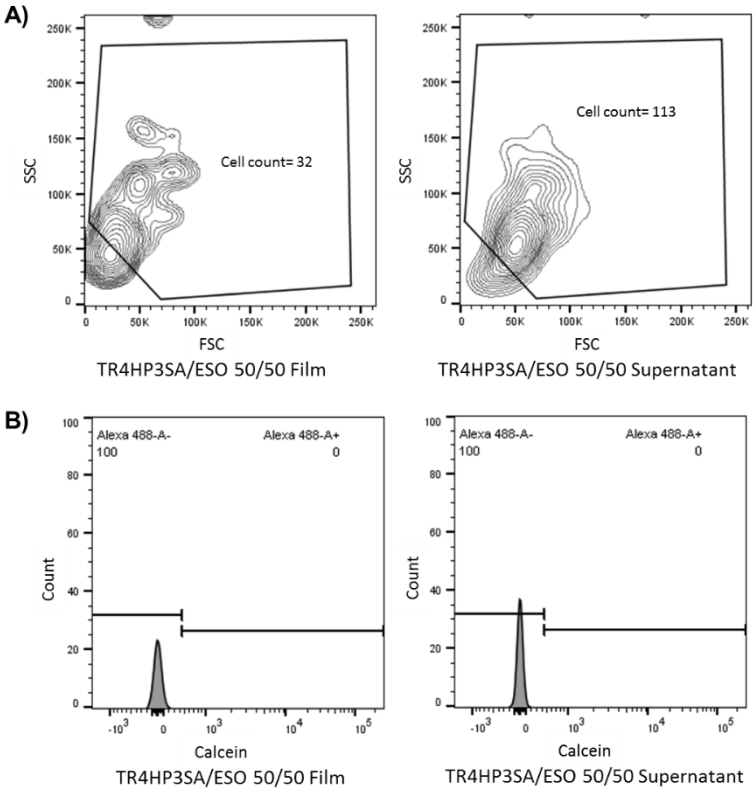

Figure 7.66. Representative raw flow cytometry data of cells from either the TR4HP3SA film or from the supernatant above the film collected after 24 hours (or one day) of growth. A) Total number of cells counted. B) Percentage of those cells that are alive as determined by calcein staining.

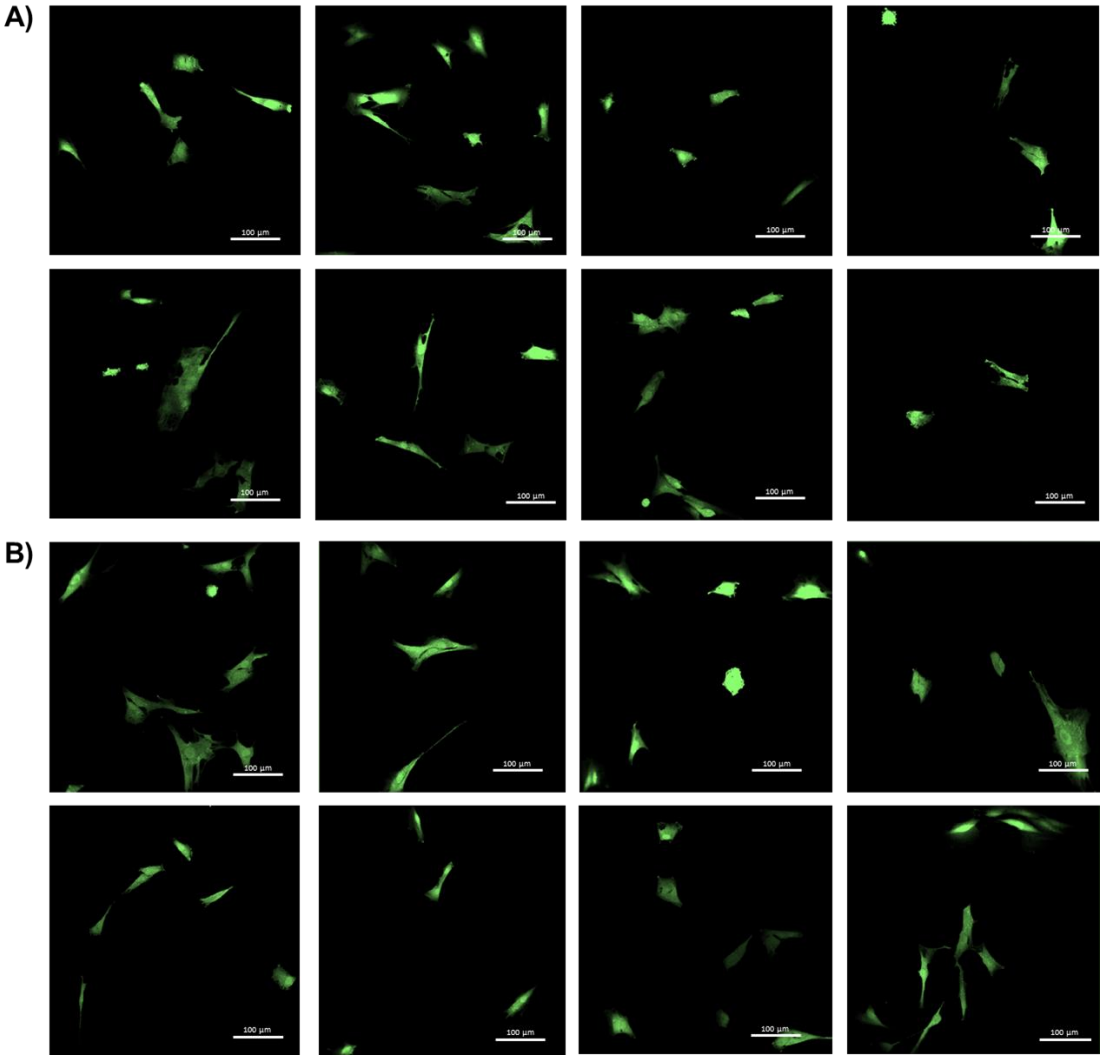

Figure 7.67. Representative confocal micrographs of cells expressing calcein (λ= 515 nm) after 24 h growth on films. A) Cells on PLG. B) Cells on CD6HP8SA/ESO 50/50. Scale bar represents 100 µm.

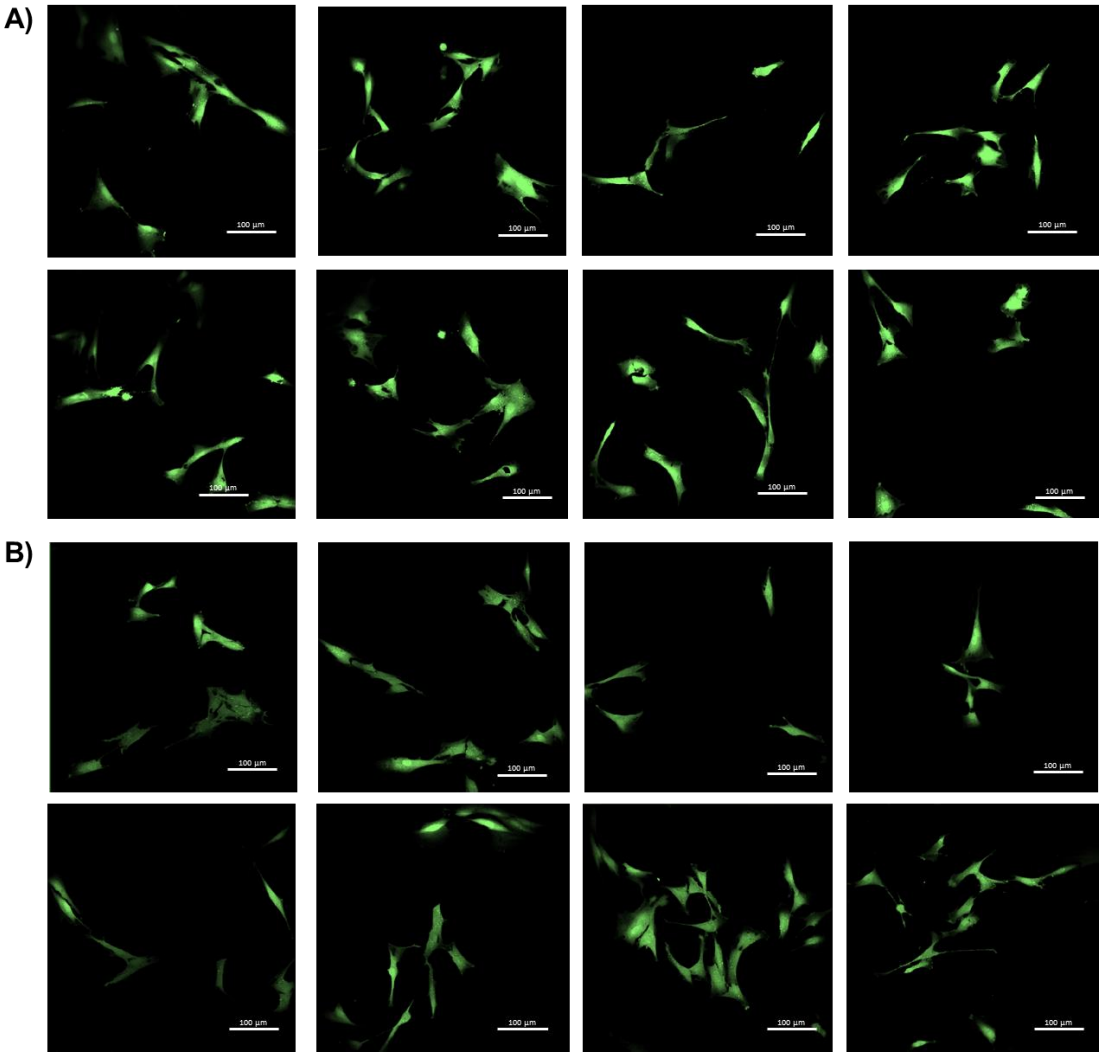

Figure 7.68. Representative confocal micrographs of cells expressing calcein (λ= 515 nm) after 48 h growth on films. A) Cells on PLG. B) Cells on CD6HP8SA/ESO 50/50. Scale bar represents 100 µm.

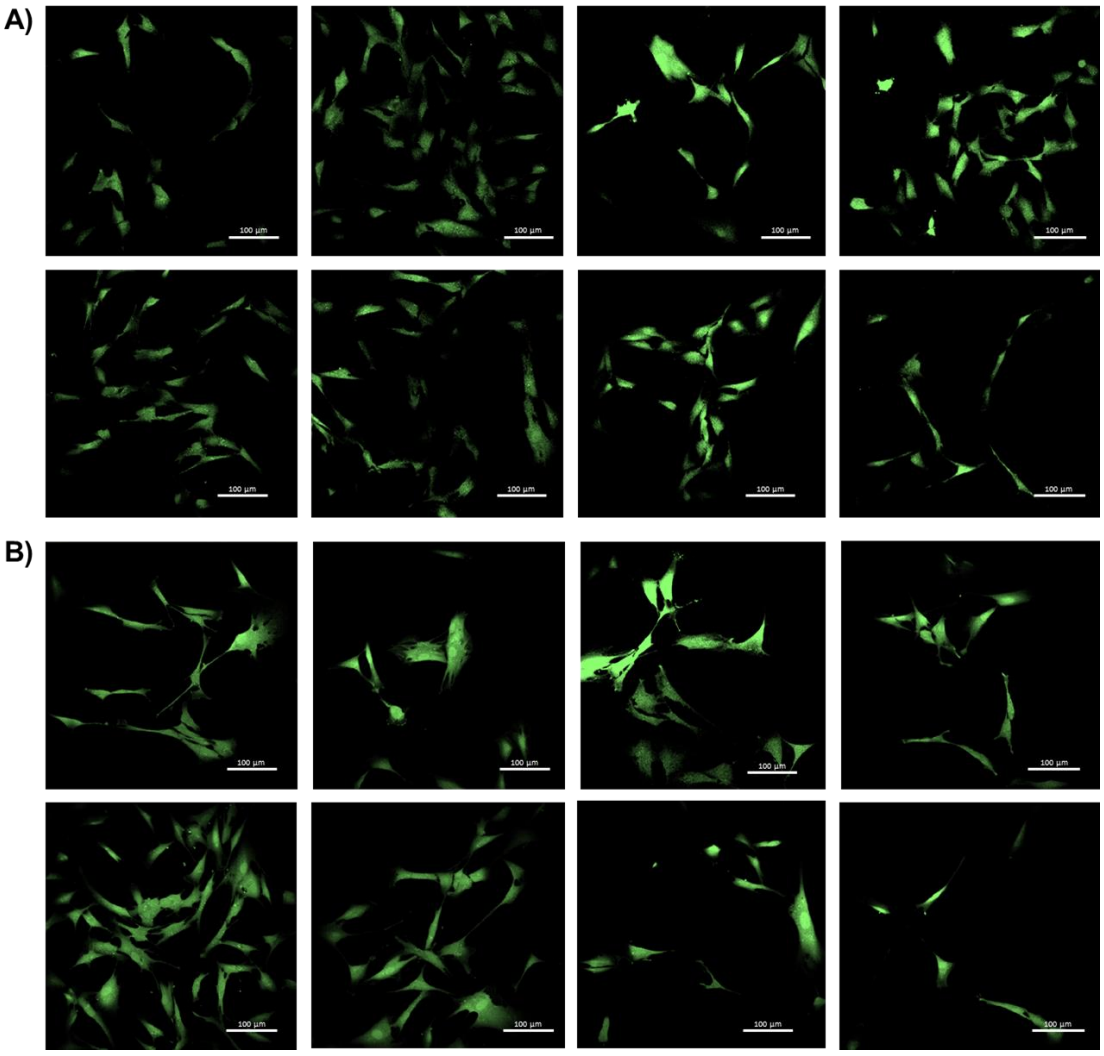

Figure 7.69. Representative confocal micrographs of cells expressing calcein (λ= 515 nm) after 72 h growth on films. A) Cells on PLG. B) Cells on CD6HP8SA/ESO 50/50. Scale bar represents 100 µm.

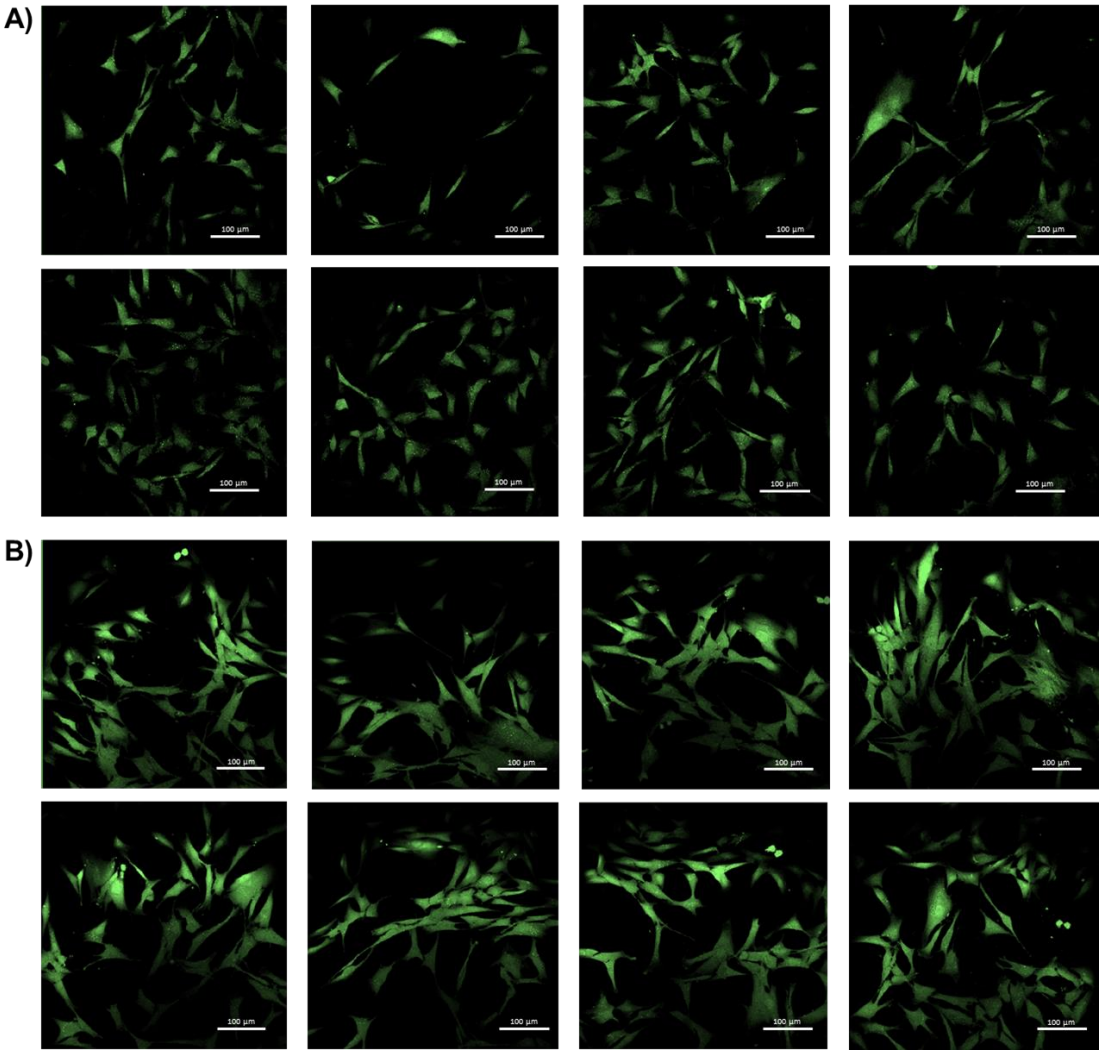

Figure 7.70. Representative confocal micrographs of cells expressing calcein (λ= 515 nm) after 96 h growth on films. A) Cells on PLG. B) Cells on CD6HP8SA/ESO 50/50. Scale bar represents 100 µm.

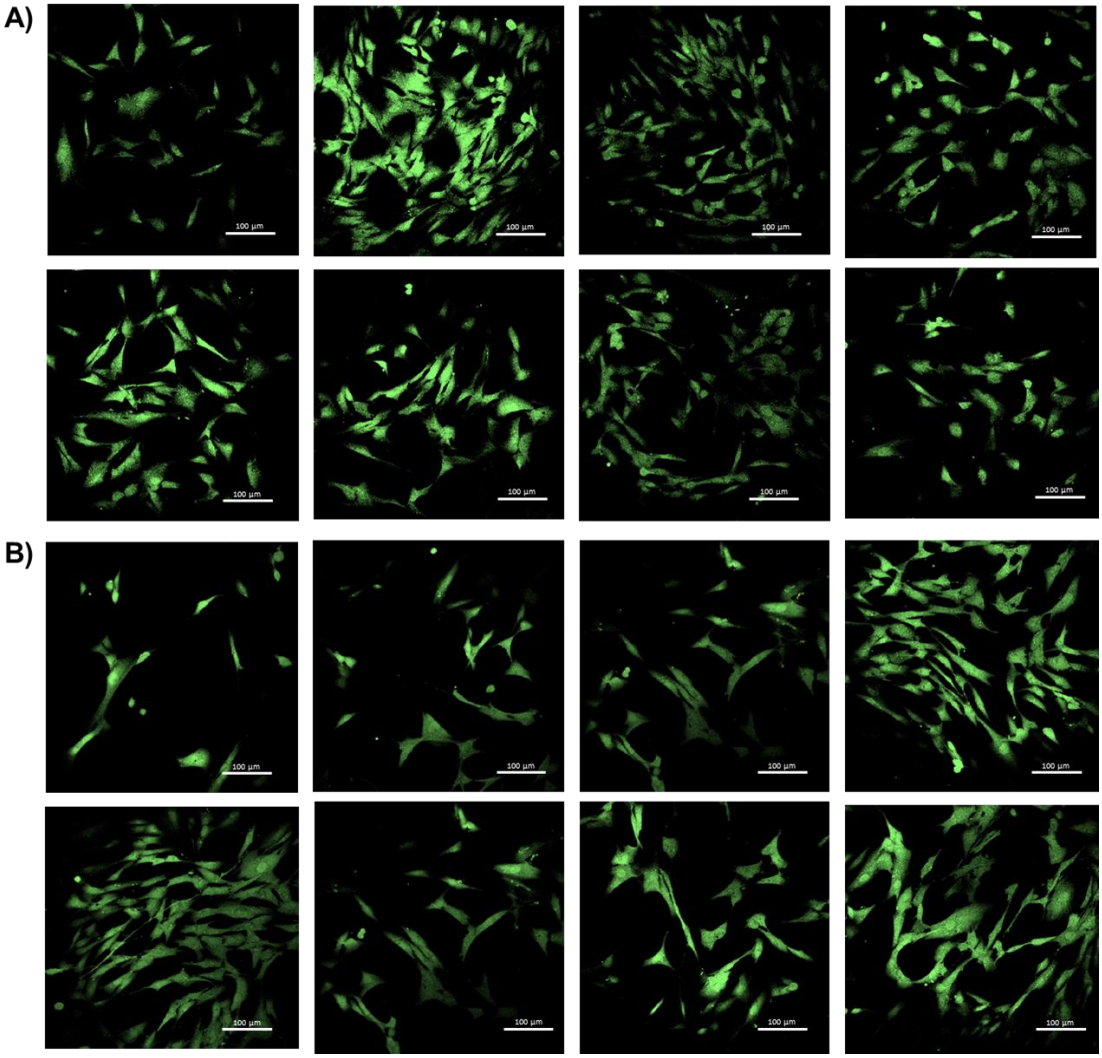

Figure 7.71. Representative confocal micrographs of cells expressing calcein (λ= 515 nm) after 120 h growth on films. A) Cells on PLG. B) Cells on CD6HP8SA/ESO 50/50. Scale bar represents 100 µm.